CONTRACT NO. NAS 3-2533

NAS NO.CR54159
GE NO. 64SD892

N66-10713
C. 54159

RESEARCH ON SPACECRAFT AND POWERPLANT INTEGRATION PROBLEMS

SPACECRAFT ANALYSIS
TOPICAL REPORT

Prepared for:
TECHNICAL MANAGEMENT
NASA-LEWIS RESEARCH CENTER
NUCLEAR POWER TECHNOLOGY BRANCH

JULY 24, 1964

GENERAL ELECTRIC
MISSILE AND SPACE DIVISION

CONTRACT NO. NAS 3-2533

NAS NO. CR54159
GE NO. 64SD892

RESEARCH ON SPACECRAFT AND POWERPLANT INTEGRATION PROBLEMS

SPACECRAFT ANALYSIS TOPICAL REPORT

Prepared for:
TECHNICAL MANAGEMENT
NASA-LEWIS RESEARCH CENTER
NUCLEAR POWER TECHNOLOGY BRANCH
ROBERT DENINGTON

Prepared By: J. W. Larson, Systems Engineer

Approved By: T. F. Widmer, Program Manager

Approved By: E. Ray, Manager - Advanced Nuclear Systems Engineering

GENERAL ELECTRIC
MISSILE AND SPACE DIVISION
Valley Forge Space Technology Center
P.O. Box 8555 • Philadelphia 1, Penna.

ACKNOWLEDGEMENTS

The author gratefully acknowledges the excellent cooperation and assistance of the following during the performance of the contract and the preparation of this document:

Thermionic Powerplant
R. Cohen

Electrical System
J. Bowen

Space Vehicle Design
K. Hagen

Turboelectric Powerplant
A. Schnacke

Mission Analysis
H. Brown

TABLE OF CONTENTS

Section		Page
1	INTRODUCTION	1-1
2	SUMMARY	2-1
	A. Guidelines to Overall Spacecraft Design	2-2
	1. Missions Attainable	2-2
	2. Powerplant Size	2-2
	3. Booster	2-2
	4. Spacecraft Size	2-3
	5. Trip Time	2-3
	6. Coast Time	2-3
	7. In-Flight Power Reduction	2-3
	8. Segmentation and Redundancy	2-4
	B. Guidelines to Spacecraft Component Design	2-4
	1. Radiator Configuration	2-4
	2. Type of Heat Rejection System	2-4
	3. Radiator Circulation Fluid	2-4
	4. Reactor and Shield	2-5
	5. Radiator Materials	2-5
	6. Radiator Deployment	2-5
	7. Radiator Launch Dynamics	2-5
	8. Startup	2-6
	9. Power Regulation	2-6
	10. Power Conditioning	2-6
	11. Transmission Lines	2-6
	12. Thrustors	2-7
3	MISSION REQUIREMENTS	3-1
	A. Powerplant Size	3-1
	B. Correction for In-Flight Power Reduction	3-6
	C. Reliability and Redundancy	3-10
4	SPACECRAFT CONFIGURATIONS	4-1
	A. Configuration Selection	4-1
	1. General Arrangement	4-3
	2. Launch Vehicle Considerations	4-7
	3. Heat Rejection Radiators	4-10

TABLE OF CONTENTS (Continued)

Section		Page
	a. Matrix Weight Comparison	4-10
	b. Fluid Circuit Arrangement	4-13
	c. Structural Considerations	4-16
	4. Vehicle Configuration Summation	4-22
	B. Vehicle Descriptions	4-23
	1. 1.2 MWe Turboelectric Vehicle	4-24
	a. Fixed Versus Folding Design	4-24
	b. Redundance Considerations	4-24
	c. Fixed Conical Design Description	4-25
	d. Folding Conical (Clamshell) Design	4-36
	e. Start-up, Checkout, and Preheat	4-42
	2. 4800 KWe Turboelectric Vehicle	4-45
	3. 1.0 MWe Thermionic Vehicle	4-46
5	RADIATOR ANALYSIS	5-1
	A. The Meteoroid Hazard	5-1
	1. Armor Criterion	5-2
	2. Bumper Effectiveness	5-8
	B. Mechanical Design	5-10
	1. Building Block Approach	5-10
	2. Matrix Joint	5-12
	C. Radiator Design Characteristics	5-18
	D. Structural Design Analysis	5-21
	1. Structural Loads	5-25
	2. Combined Load Analysis	5-30
6	TURBOELECTRIC POWERPLANT	6-1
	A. Reactor	6-1
	B. Power Generator	6-1
	1. General Description of 1200 KWe Powerplant	6-2
	a. Heat Balance	6-2
	b. General Arrangement	6-4
	c. Power Regulation Concept	6-9
	d. Startup	6-13
	2. General Description of 4.8 MWe Powerplant	6-16
	3. Turbogenerator	6-16

TABLE OF CONTENTS (Continued)

Section		Page
	4. Heat Transfer Components	6-29
	a. Boiler	6-29
	b. Condenser	6-30
	C. Shield	6-37
7	THERMIONIC REACTOR SYSTEMS	7-1
	A. System Specifications	7-1
	1. Pumps and Working Fluids	7-1
	2. Powerplant System Temperatures	7-3
	B. Reactor and Shielding	7-8
	1. Reactor Characteristics	7-8
	2. Shield Weights	7-12
8	ELECTRICAL SYSTEMS	8-1
	A. Configuration Study	8-1
	B. Electrical and Thermal Power Profiles	8-12
	C. Electrical System Components	8-24
9	ELECTRIC THRUSTORS	9-1

LIST OF ILLUSTRATIONS

Figure		Page
3-1	Booster Selection at a Powerplant Specific Weight of 30 Lbs/Kw ...	3-5
3-2	Central Angle Variation with Time for Two Typical Planetary Rendezvous Missions	3-9
3-3	Influence of Operating Time on Reliability	3-12
3-4	Probability of No More Than One Failure in Two Parallel Systems	3-14
3-5	Probability of No More Than One Failure in Four Parallel Systems	3-14
3-6	Probability of No More Than One Failure in Four Parallel Systems Accounting for Size Effects	3-16
4-1	Nuclear Electric Spacecraft Functional Block Diagram	4-2
4-2	Spacecraft Functional Block Grouping Diagrams	4-5
4-3	Saturn S-IV-B Booster Stage Payload Limitations	4-8
4-4	Saturn S-II Booster Stage Payload Limitations	4-9
4-5	Comparison of Fixed Radiator Arrangements	4-11
4-6	Effects of Fin Bumper on Tube Armor	4-12
4-7	Panel Specific Weights for Different View Factors	4-12
4-8	Matrix Weight versus Effective Radiating Area	4-13
4-9	Circumferential Radiator Tube Effects	4-15
4-10	Axial Flow and Temperature Profiles	4-16
4-11	Comparison of Separate and Integrated Radiator Structural Approaches	4-17
4-12	Radiator Structure Comparison	4-19
4-13	Conical Configuration Matrix Dynamic Buckling Analysis	4-19
4-14	Cruciform Configuration Booster Adapter	4-20
4-15	Cruciform and Conical Total Radiator Weight Comparison	4-21
4-16	1.2 MW Fixed Conical Vehicle - Launch Configuration	4-27
4-17	1.2 MW Fixed Conical Vehicle - Deployed Configuration	4-29
4-18	Comparable Approaches for Axial Tube Multiple Loop Designs	4-31
4-19	Feed and Return Line Arrangement - 1.2 MW Fixed Conical Vehicle	4-32
4-20	1.2 MW Folding Vehicle - Launch Configuration	4-37
4-21	1.2 MW Folding Vehicle - Deployed Configuration	4-39
4-22	Launch Configuration of the 4.8 MWe Turboelectric Vehicle	4-47
4-23	Deployed Configuration of the 4.8 MWe Turboelectric Vehicle	4-49
4-24	Launch Configuration of the 1 MWe Thermionic Vehicle	4-51
4-25	Deployed Configuration of the 1 MWe Thermionic Vehicle	4-53

LIST OF ILLUSTRATIONS (Continued)

Figure		Page
5-1	Room Temperature Meteoroid Armor Thickness for Aluminum and Stainless Steel (10,000 Hours)	5-4
5-2	Room Temperature Meteoroid Armor Thickness for Copper and Beryllium (10,000 Hours)	5-5
5-3	Room Temperature Meteoroid Armor Thickness for Titanium and Columbium (10,000 Hours)	5-6
5-4	Armor Thickness Correction Factor to Account for Temperature	5-7
5-5	Vulnerable Area Contribution of Headers and Feeds	5-8
5-6	Meteoroid Bumper Criterion	5-10
5-7	Coefficient at Thermal Expansion of Beryllium and Inconel 700	5-11
5-8	Manufacturing Sequence of Basic Matrix Panels	5-13
5-9	Fabrication Techniques	5-15
5-10	Header Detail	5-16
5-11	Feed Line — Header Joint Detail	5-17
5-12	Thermal Joint Details	5-19
5-13	Weight Distribution for the 1.2 MWe Turboelectric Fixed Configuration Vehicle	5-26
5-14	Normal Pressure and Circumferential Distribution for the 1.2 MWe Turboelectric Fixed Configuration Vehicle	5-27
5-15	Shear Moment and Axial Load Distribution for the 1.2 MWe Turboelectric Fixed Configuration Vehicle	5-29
5-16	Loading and Stress versus Length for the 1.2 MWe Turboelectric Vehicle	5-31
6-1	Heat Balance for the 1.2 MWe Turboelectric Powerplant	6-3
6-2	1.2 MW Power Unit	6-5
6-3	General Arrangement of 1.2 MWe Power Plant with Four Turbogenerators	6-11
6-4	Conceptual View of Powerplant Controls	6-14
6-5	300 KVA Turbogenerator with 14.5 Diameter Generator Rotor	6-17
6-6	600 KVA Turbogenerator with 18-inch Diameter Generator Rotor	6-19
6-7	600 KVA Turbogenerator with 20.5-inch Diameter Generator Rotor	6-21
6-8	1.2 MW Turbogenerator	6-23
6-9	1.2 MW Turbogenerator Power Unit	6-25
6-10	7.6 MWt Boiler, Design "A"	6-31
6-11	1.9 MWt Boiler, Design "B"	6-33
6-12	6.2 MWt Condenser, Design "A"	6-35
6-13	6.2 MWt Condenser, Design "B"	6-38

LIST OF ILLUSTRATIONS (Continued)

Figure		Page
6-14	Gamma and Neutron Threshold Radiation Tolerance	6-41
6-15	Dimensions of Shield and Separation Distances	6-43
7-1	Heat Balance for the 1 MWe Thermionic Powerplant	7-1
7-2	Heat Exchanger Weights	7-5
7-3	Heat Exchanger Δ P Versus Reactor Discharge Temperature	7-5
7-4	Cutaway Views of Straight Tube Heat Exchanger	7-6
7-5	Primary Loop Piping Weight and Pressure Drop	7-7
7-6	Optimization of Primary Loop Pipe Size	7-7
7-7	Reactor Hydraulic Characteristics	7-9
7-8	Optimization of Heat Exchanger ΔT	7-9
7-9	Shield Weight Parameters	7-12
8-1	Electrical System for the 1.2 MWe Turboelectric Vehicle	8-3
8-2	Electrical System for the 1 MWe Thermionic Vehicle	8-5
8-3	Typical Electric Engine Power Conditioning Schematic	8-7
8-4	Typical Powerplant Module for 1 MW Paralleled Generator System	8-9
8-5	Weight of 500 KVA, 98.0% Efficient Transformer as a Function of Frequency and Coolant Temperature	8-27
8-6	Weight of 500 KVA, 98.5% Efficient Transformer as a Function of Frequency and Coolant Temperature	8-27
8-7	Weight of 500 KVA, 99.0% Efficient Transformer as a Function of Frequency and Coolant Temperature	8-28
8-8	Weight of 500 KVA, 99.5% Efficient Transformer as a Function of Frequency and Coolant Temperature	8-28
8-9	Basic Rectifier Circuit	8-29
9-1	Arc-Jet Engine Thermodynamic Efficiency	9-2
9-2	Thermo-Ionic Accelerator	9-3
9-3	Efficiency of Candidate Thrustors	9-5

LIST OF TABLES

Table		Page
3-1	Payload Requirements Summary	3-3
3-2	Summary of Navigator Results	3-7
4-1	Characteristics of Selected Spacecraft and Powerplant Combinations	4-1
4-2	1.2 MWe Turboelectric Vehicle Weight Summary	4-34
4-3	1.2 MWe Turboelectric Vehicle Primary Radiator Weight Breakdown	4-35
4-4	Comparison of Fixed and Folding Conical Primary Radiator Weights	4-41
4-5	Weight Summary for the 4.8 MWe Turboelectric Vehicle	4-55
4-6	1 MWe Thermionic Vehicle Weight Summary	4-58
5-1	Summary of 1200 KWe Turboelectric Vehicle Radiator Parameters	5-22
5-2	Summary of 4800 KWe Turboelectric Vehicle Primary Radiator Parameters	5-23
5-3	Summary of 1 MWe Thermionic Primary Radiator Parameters	5-24
6-1	Electrical Generation System Containment Vessel Assembly Weights	6-8
6-2	Electrical Generation System Weight Tabulation	6-10
6-3	Turbogenerator Design Data	6-27
6-4	7.6 MWt Boiler Design Data	6-34
6-5	6.2 MWt Condenser Design Data	6-37
6-6	Shield Dimensions and Weights for 1.2 MWe Turboelectric Powerplant	6-45
7-1	1 MWe Net Thermionic Reactor Reference Design	7-11
8-1	Comparison of use of Semiconductors and High Temperature Tubes in Thermionic Dc-Dc Converters	8-13
8-2	Conductor Details - 1.2 MW Turboelectric Vehicle	8-14
8-3	Conductor Details - 1 MW Thermionic Vehicle	8-14
8-4	Powerplant Electrical Load Requirements for the 1.2 MWe Turboelectric Vehicle	8-15
8-5	Cooling Load Requirements for the 1.2 MWe Turboelectric Vehicle	8-17
8-6	Electrical Loads Requirements for the 1 MWe Thermionic Vehicle	8-19
8-7	Cooling Loads Estimates for the 1 MWe Thermionic Vehicle	8-21
8-8	Summary of Weight and Dissipation of Turbogenerator and Thermionic Systems	8-25

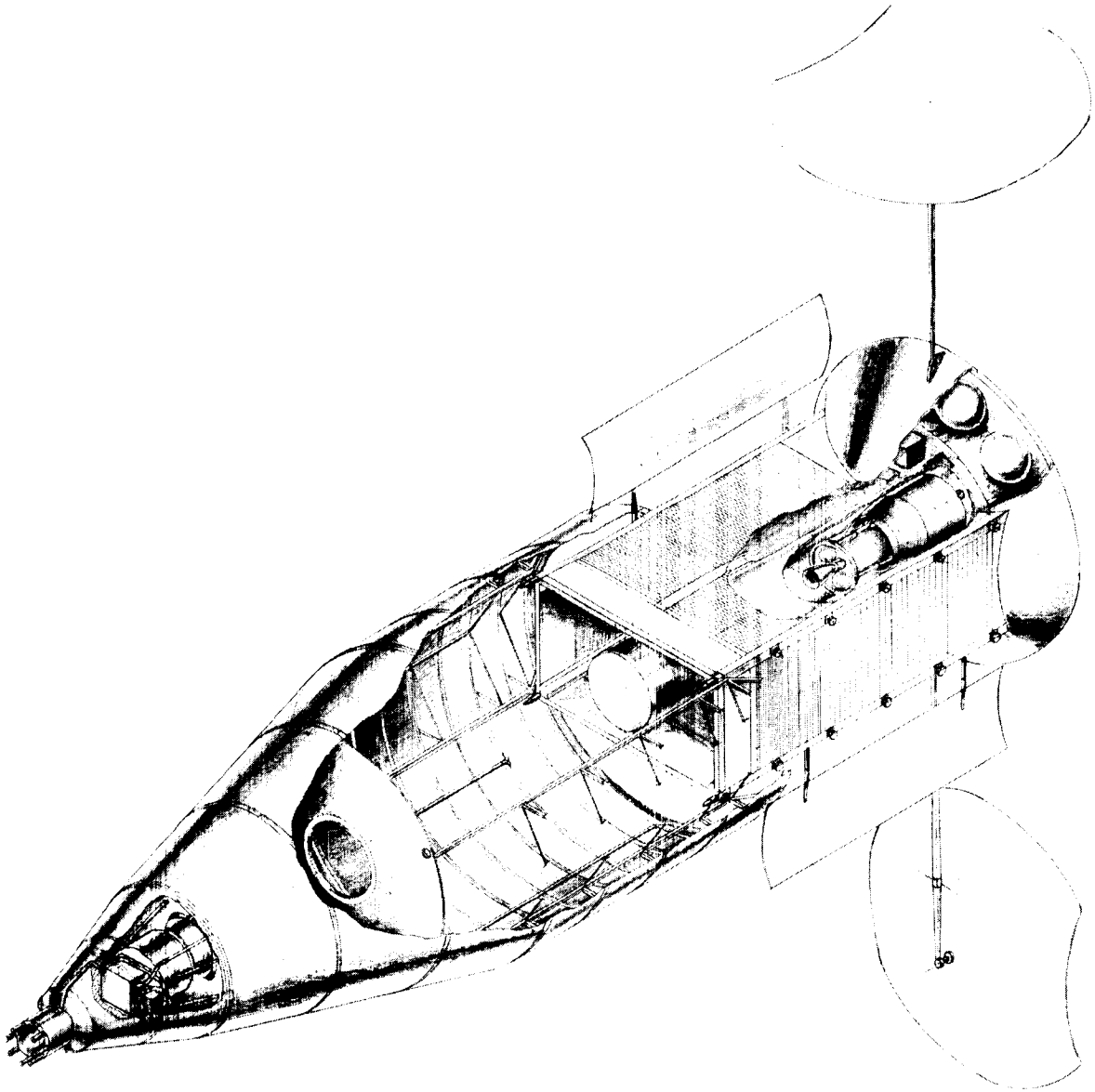

Frontispiece - 1200 KWe Turboelectric Powered Space Vehicle for Unmanned Scientific Probe Missions

1. INTRODUCTION

This topical report presents the results of spacecraft studies carried out by GE-MSD during the 14 months of Contract NAS3-2533, Research on Spacecraft and Powerplant Integration Problems. Four reports have previously been issued under this contract. These are:

1. 63SD760, First Quarterly Report, 26 April to 26 July, 1963;
2. 63SD886, Second Quarterly Report, 26 July to 26 Oct., 1963;
3. 64SD505, Mission Analysis Topical Report, Feb. 26, 1964; and
4. 64SD700, Third and Fourth Quarterly Report, 26 October 1963 to 26 April, 1964.

The mission analysis studies were presented in Report 64SD505 and summarized the results of the first 8 months of this effort, including that published in the first and second quarterly reports. This Spacecraft Analysis Topical Report summarizes the results of all the quarterly reports in addition to providing additional information as necessary to clarify and complete the discussion of the spacecraft studies. Many of the details are not repeated and the interested reader is referred to these past reports.

This program was initiated by General Electric Missile and Space Division under contract to the NASA Lewis Research Center. The program objective is to determine requirements for the nuclear-electric power generating systems required in the NASA unmanned scientific probe missions throughout the solar system, which are beyond the capabilities of presently envisioned chemical rocket propelled vehicles. Missions which can be performed by chemical propulsion were not investigated.

In addition, attention was limited to the presently envisioned Saturn class of launch vehicles under development, without consideration of uprating the potential of these vehicles. Finally, two types of nuclear powerplant were considered, namely, the advanced Rankine cycle turboelectric powerplant (which received the major attention) and the in-core thermionic powerplant.

Since the objective of this study is the determination of spacecraft and powerplant integration problems, complete detailed and rigorous systems optimization analyses have not been conducted. The optimization that has been performed, was limited primarily to radiator geometry. However, it is not expected that the performance of mathematical optimization would significantly reduce the powerplant weight below that tabulated in this report. A number of restraints have been identified for realistic flight radiators, which account for a major portion of the powerplant weight, leading to the conclusion that the estimates of weights and performance herein stand a reasonable chance of fulfillment, provided the assumed technological developments are achieved.

2. SUMMARY

Spacecraft and power generating system designs were investigated to determine the component and subsystem requirements and further research and development areas necessary to provide a capability for unmanned scientific exploration of the solar system. Power generation systems included both nuclear Rankine cycle and nuclear in-core thermionic powerplants. The Rankine cycle system was based on a powerplant technology level consistent with the original SNAP-50 design objectives as of contract initiation. The design conditions for both Rankine cycle and thermionic systems were specified by the Technical Management at NASA-Lewis.

Mission requirements were established for those unmanned missions which are marginal for, or beyond the capability of, chemical and solid core nuclear rocket propelled space vehicles. These missions included close approach solar probes, high inclination out-of-ecliptic probes, and orbiters for Mercury and the outer planets (beyond Mars).

Sample spacecraft and powerplant designs have been prepared. However, it is somewhat difficult to make direct comparisons between different powerplant types because many of the key components are not sufficiently advanced in development. Rigorous system optimization has not been conducted but key problem areas have been identified that would likely escape a purely parametric analysis. It is not believed that detailed component specifications can be established at this time. One particular reason is that an item such as required powerplant specific weight is related to trip time and the applicable tradeoff cannot yet be established.

General guide lines or ground rules that have been identified are listed below. These are divided into two categories:

1. Those arising from the mission analysis affecting the overall spacecraft and power system, and

2. Those pertaining to the design and proper functioning of particular components and subsystems.

A. GUIDELINES TO OVERALL SPACECRAFT DESIGN

1. Missions Attainable

An electric propulsion system at 30 lb/kwe with a two year propulsion life is capable of performing the following scientific exploratory missions:

- Solar probe
- Out-of-ecliptic probes approaching 65° inclination
- Mercury orbiter
- Small payload Jupiter orbiter
- Small payload Saturn orbiter

Additional accomplishments require lower powerplant specific weight and/or longer propulsion life.

2. Powerplant Size

The powerplant weight is the sizing parameter of interest for a nuclear electric propelled spacecraft. This weight, including shield, radiators, reactor, electrical generation system and power conditioning equipment, tends to optimize at approximately 30 percent of the gross weight of the spacecraft for the case where the payload is only a small fractional part.

3. Booster

The three stage Saturn V booster configuration is compatible with the nuclear electric spacecraft and is preferred for almost all missions because its use leads to a minimum trip time.

4. Spacecraft Size

Off-loading the Saturn V allows boost beyond escape of a small nuclear-electric propelled spacecraft. For many missions involving small payloads, the trip time only slightly increased relative to the larger, escape launched spacecraft. As a result, a small size spacecraft and nuclear powerplant can be used. Assuming nuclear powerplants of 30 lb/KWe, the required electric power level is in the range of 300 KW to 1 MW.

5. Trip Time

Estimates of trip times ranged from 170 to 2400 days, depending upon the mission and the powerplant specific weight. For many of the missions a one percent increase in allowable propulsion time yielded an allowable powerplant specific weight increase of three percent. Thus, the powerplant specific weight requirement could be significantly relaxed by increasing propulsion time.

6. Coast Time

The trajectory analysis was conducted assuming constant thrust propulsion. As a consequence a sizeable coast time, on the order of 40 percent of the trip time, occurs. Complete powerplant shutdown is possible but may not be desirable for this period of time. Auxiliary power is needed for electronic equipment and for maintaining liquid-metal circuits above the freezing point. The best solution appears to be lowering reactor temperature to achieve a part-load powerplant operation, which reduces rate of reactor burnup and powerplant wear. Also, auxiliary thrusters can be operated to provide attitude and orientation control, and trajectory corrections.

7. In-Flight Power Reduction

The trajectory is dependent on the thrust/weight versus time profile. Alternate trajectories can be pursued if the thrust reduces early in the mission, i.e., prior to

the coasting period. In general, however, the thrust needs to be maintained, and this can be accomplished by using either variable specific impulse thrusters or supplementary low specific impulse thrusters to be switched on at the expense of higher propellant consumption.

8. Segmentation and Redundancy

Reliability requirements are too severe for the mission success to be dependent on no component failures occurring, particularly since the environmental conditions are not fully established. Segmentation of radiators becomes an essential requirement to guard against meteoroids as well as tube structure failures. Multiple power conversion loops should also be considered with one loop being redundant. The use of multiple reactors and staging of powerplants has not been considered.

B. GUIDELINES TO SPACECRAFT COMPONENT DESIGNS

1. Radiator Configuration

The conical-cylindrical radiator configuration is positively preferred over flat panel type of radiators because of the launch loading. Using this configuration, up to 5 megawatts (electric) of Rankine cycle powerplant can be packaged on a two-stage Saturn V booster without need for deployment or folding of radiator panels.

2. Type of Heat Rejection System

Multiple liquid metal circuits should be used to transport heat of condensation from a compact condenser to a space radiator, rather than to directly condense the working fluid in the space radiator, in the case of the Rankine cycle system.

3. Radiator Circulation Fluid

The use of lithium in the radiators should be avoided because of its high freezing temperature (~350°F) and corrosiveness. Lithium requires refractory metal alloys

for containment, and large size radiator structures would be difficult to construct of these materials. Either sodium or NaK are satisfactory and can be contained by stainless steel or Hastalloy.

4. Reactor and Shield

Neither reactor fuel burnup limitations (Rankine system), nor converter power density capabilities (thermionic system) are well established. These parameters have a strong leverage (through core diameters.) on both reactor and shield weight.

5. Radiator Materials

The use of beryllium has been assumed for the Rankine cycle systems. The behavior of this material, and others, under hypervelocity impact has only been superficially explored. Further analytic effort should be directed towards the use of alternate materials such as steel and copper. Using Beryllium as the radiator material, radiator weights range between 7.5 and 9.5 lbs KWe in the megawatt power sizes.

6. Radiator Deployment

Only one satisfactory solution for radiator deployment was found. This method was to split the conical-cylindrical radiator longitudinally and use bellows piping to accommodate bending of the liquid metal lines across the joint.

7. Radiator Launch Dynamics

A significant system problem has been identified as a result of the dynamic response analysis of the various radiators. The results of this work show the expected dynamic acceleration input to the reactor and turbomachinery to be in the order of 16-38 g's, (zero to peak) where the input at the booster interface is 1 g. Although these results depend on the somewhat nebulous damping assumptions, the lower value represents the result obtained using an optimistically high damping level.

If these results are representative, and present evidence indicates that they are, either they should be included in the design requirements of the associated equipment or studies should be made to identify control measures. In view of the massive plumbing involved, vibration isolation may be extremely difficult to achieve.

8. Startup

Fully automated startup with an idle capability is required. In addition, a shutdown and restart capability may be desirable to allow some repair during initial orbital operation in the event of an early malfunction.

9. Power Regulation

Many different electrical loads are contained in a spacecraft. These may be switched on and off at command, and lead to a sudden change of powerplant loading. Thus, a proper power regulation and control system is needed for the nuclear powerplant.

10. Power Conditioning

The generation of low voltage electrical power leads to the need for power conditioning equipment near the generator to raise this voltage to a satisfactory level for transmission. For the Rankine cycle, the transformer is mounted near the generator, and for the thermionic system, almost the entire power conditioning is located near the generator.

11. Transmission lines

Skin effect is important for high frequency transmission in large diameter busbars. The selected frequency of 2000 cps and 10 to 20 KV, which yields small line diameters, is safely removed from the skin effect situation.

12. Thrustors

For most missions, the required specific impulse falls in the range of 2500 to 6200 seconds. Thus, development of ion engines should be directed towards achieving high efficiency and low specific weight in this low specific impulse range.

3. MISSION REQUIREMENTS

A. POWERPLANT SIZE

The mission studies were conducted to provide requirements for the nuclear electric propulsion system. (The results were published in GE Document 64SD505.) From these studies, a good approximation of the optimum powerplant size for any particular mission involving small payload fractions was found to be that which comprised 30 percent of the gross weight of the space vehicle at the start of nuclear-electric propulsion, the remaining weight consisting of payload, propellant, tankage, structures, and controls. Specification of the powerplant specific weight, which is technology dependent, and the scientific payload, yields a mathematical relationship between the electric power rating and propulsion time requirement. From this relationship the electric power rating can be selected to minimize propulsion time.

The scientific missions were selected to provide an overall representation of target planets, planetary terminal orbits, and scientific payloads. These payloads included scientific sensors, mapping radar, TV cameras, communications equipment for relaying the observations back to Earth, and landing vehicles for the minor planets and satellites of the major planets. A summary of these payloads is presented in Table 3-1 for each of the selected missions.

The propulsion time requirement for accomplishing the scientific probe missions was found to generally exceed the 10,000-hour life goal of the present advanced Rankine cycle powerplant program. Minimizing propulsion time requirements became a major objective of the mission studies. It was found that the use of the Saturn V launch vehicle was preferable for all missions for this reason. When the payload was large (i.e., above 20,000 pounds) a two-stage-chemical version of the Saturn V was preferable. This placed a 240,000-pound gross weight nuclear-electric space vehicle in a 300 nautical mile orbit. For small payloads, a three stage Saturn V is desirable. This booster launches a nuclear-electric space vehicle of 90,000 pounds, or less, to beyond

escape. Boost beyond escape is accomplished by aft-loading rather than modification of the S4B stage propellant tankage. Thus, a large variety of spacecraft sizes can be launched by the Saturn V.

The powerplant specific weight turned out to have less influence on mission performance than propulsion time limits. Increased propulsion time yields a lower characteristic velocity for the heliocentric phase of the mission, such that a 1 percent increase in propulsion time could achieve the same change in mission performance as a 3 percent decrease in powerplant specific weight.

Powerplant specific weights have been estimated to be between 20 and 38 lb/kwe (shielded) in the powerplant and space vehicle studies. Mission propulsion time requirements are tabulated in Figure 3-1 for each of the selected missions and Saturn V launch vehicle combinations. An optimum size nuclear-electric propulsion vehicle, which minimizes propulsion time requirements, exists for each of the missions. However, particular powerplant sizes can accomplish most of the missions at the penalty of some increased propulsion time. A chart containing an overall summary of the results of the mission studies is presented in Table 3-2. Here the electrical power rating, and specific impulse of the thrusters, are itemized for each of the missions as a function of powerplant specific weight.

From these studies, it appears that the range of nuclear powerplant sizes of interest for the unmanned probe missions is between 300 Kwe and 1 Mwe. The use of a 300 Kwe nuclear powerplant yields a space vehicle of 28,000 pounds gross weight, which can be launched by a Saturn IB into a 300 nautical mile orbit, as well as by a Saturn V to beyond escape. The 1 Mwe size powerplant by itself weighs less than 28,000 pounds and could be launched separately into Earth orbit by a Saturn IB for experimental purposes.

TABLE 3-1. PAYLOAD REQUIREMENTS SUMMARY

Missions	Landing Capsule Weights (No.)							Mapping Radar		Basic Sensors, TV Cameras, & Low Power Radar	Communications System					Payload Cooling System		Totals	
	Planetary Landers	Satellite Landers						Wide Sweep Mapper (16KW in)	High Resolution Mapper (140KW in)		Total Payload Information Bandwidth Cycles/Sec	Transmitter Output Power (KW)	XMTR WT (lbs)	Antenna WT (lbs)	Weight of Computers, Recorders, RCVRS, etc. (No.)	Heat Rejected (KWT)	Payload Radiator Weight	Peak Payload Power Input* (KW)	Total Payload Weight (lbs)
		Io	Europa	Ganymede	Callisto	Titan	Triton												
Solar Probe (83°)	—	—	—	—	—	—	—	—	—	525	10^3	30	1700	350	125	90	500	123	3200
Out of Ecliptic Probe	—	—	—	—	—	—	—	—	—	525	5×10^3	.05	—	350	125	—	—	3	1000
Mercury Orbiter I	—	—	—	—	—	—	—	2000	—	430	5×10^5	4	240	350	125	24	135	33	3280
Mercury Orbiter II	5900 (2 Capsules)	—	—	—	—	—	—	2000	—	430	5×10^5	4	240	700	125	24	135	33	9530
Asteroids	—	—	—	—	—	—	—	2000	—	430	5×10^5	40	2300	350	125	132	740	177	5945
Jupiter Orbiter I	—	—	—	—	2210	—	—	2000	—	430	5×10^5	95	5500	700	125	297	1665	397	12,630
Jupiter Orbiter II	—	2280	1935	2770	2210	—	—	2000	7500	430	5×10^5	95	5500	700	125	415	2320	537	27,770
Jupiter Orbiter III	10,000	2280	1935	2770	2210	—	—	2000	7500	430	5×10^5	95	5500	700	125	415	2320	537	37,770
Saturn Orbiter I	—	—	—	—	—	2670	—	2000	—	430	10^5	50	3000	700	125	162	910	217	9835
Saturn Orbiter II	2,850	—	—	—	—	2670	—	2000	7500	430	10^5	50	3000	700	125	279	1560	357	20,835
Uranus Orbiter	1,285	—	—	—	—	—	—	2000	—	430	2×10^3	4	240	700	125	24	135	33	4915
Neptune Orbiter	2,200	—	—	—	—	—	2670	2000	—	430	2×10^3	9	540	700	125	39	220	53	8885
Pluto Orbiter	3,730	—	—	—	—	—	—	2000	—	430	2×10^3	14	900	700	125	42	235	73	8120

*Note - Actual peak power to payload will probably be reduced below these values by alternating the operation of radar and communications transmitters; radar data is to be stored and played back at reduced rate.

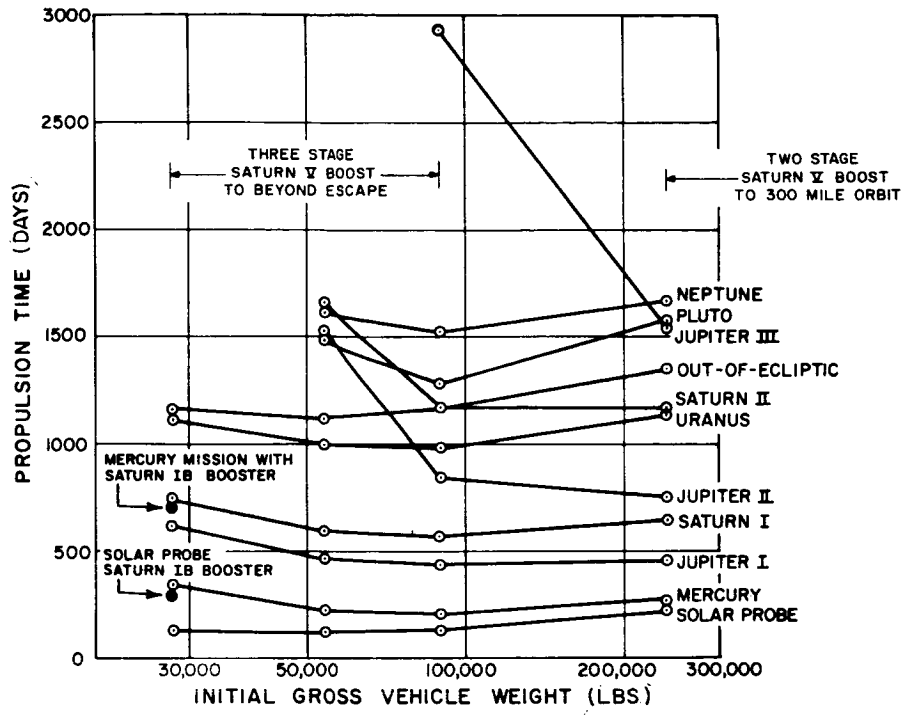

Figure 3-1. Booster Selection at a Powerplant Specific Weight of 30 Lbs/Kw

Four of the missions can be achieved with a Saturn IB-300 Kw system within the propulsion time that would appear to be a reasonable objective for the nuclear powerplant and space vehicle. These missions are:

- Solar Probe
- Mercury Orbiter
- Jupiter orbiter with small payload
- Saturn orbiter with small payload

The larger payload missions, outer planet orbiters, and out-of-ecliptic probes require at least three years of travel.

B. CORRECTION FOR IN-FLIGHT POWER REDUCTION

Powerplant and propulsion system requirements have been based upon the use of optimum thrust-time schedules for the heliocentric sun-centered phase of each of the planetary orbiter missions. Associated with each planetary mission-heliocentric trip time combination, are corresponding values of launch date, heliocentric central angle (angle between spacecraft and orbit perigee position vectors), planetary arrival date, and a heliocentric total impulse requirement (thrust-time integral). Any unscheduled power reduction after the initiation of the heliocentric propulsion phase would, therefore, result in an inability to complete the planetary rendezvous, unless some type of compensating adjustment is made to the thrust-time schedule. Preliminary investigations have been conducted in order to identify the nature of the compensating changes required.

Figure 3-2 illustrates the heliocentric central angle variation with trip time for typical Jupiter and Neptune trajectories. Corresponding characteristics for Saturn, Uranus, and Pluto trajectories would lie between these curves. The major portion of the central angle change occurs during the initial heliocentric propulsion period. The change during the second propulsion period is small. This leads to the conclusion that no significant change in the central angle variation can be achieved during this second propulsion period. The arrival date is tied to the arrival central angle by the planetary ephemerides. Thus, the arrival date and the heliocentric trip-time must be maintained at their nominal values after initiation of the coast phase. The thrust-time schedule can be modified to compensate reduction of power only during the first propulsion period.

The remaining alternative in the case of unscheduled power reduction is the reduction of specific impulse to maintain the required thrust level for the remainder of the mission. The lower specific impulse yields a higher propellant consumption rate.

In the event of a reduction of electrical power forcing a corresponding reduction of specific impulse during the critical heliocentric trajectory, the excess propellant utilized can be partially compensated for during the planetocentric phase of propulsion.

TABLE 3-2. SUMMARY OF NAVIGATOR RESULTS

Mission	Powerplant Specific Weight-lbs/Kw	Power KW	Trip Time Days	Propulsion Time Days	Initial Gross Weight-lbs	Specific Impulse sec	Thrust-Weight Ratio $(10)^{-4}$	Payload lbs	Terminal Radius miles	Propellant lbs	Characteristic Velocity, ft/sec			
											Total	Geocentric	Heliocentric	Planetocentric
1. Solar Probe (0.05 AU)	10	840	170	40	28,000	2,500	3.51	3,300	---	13,550	53,000	--	53,000	---
	20	420	260	80	28,000	2,500	1.75	3,300	---	13,550	53,000	--	53,000	---
	30	280	330	120	28,000	2,500	1.17	3,300	---	13,550	53,000	--	53,000	---
2. Mercury	10	2,700	90	70	90,000	3,600	2.95	9,530	2,000	44,600	79,000	0	69,000	10,000
	20	1,350	170	140	90,000	3,600	1.47	9,530	2,000	44,600	79,000	0	69,000	10,000
	30	900	230	210	90,000	3,600	0.98	9,530	2,000	44,600	79,000	0	69,000	10,000
3. Jupiter I	10	2,700	410	270	90,000	7,200	1.43	12,630	1,170,000	41,500	143,000	0	123,000	20,000
	20	1,350	560	370	90,000	5,900	0.86	12,630	1,170,000	41,500	117,000	0	97,000	20,000
	30	900	640	440	90,000	5,300	0.65	12,630	1,170,000	41,500	105,000	0	85,000	20,000
4. Jupiter II	10	7,200	580	360	240,000	8,400	1.31	27,770	262,000	116,700	180,000	23,000	107,000	50,000
	20	3,600	800	580	240,000	7,500	0.72	27,770	262,000	116,700	161,000	23,000	88,000	50,000
	30	2,400	990	740	240,000	6,900	0.52	27,770	262,000	116,700	148,000	23,000	75,000	50,000
5. Jupiter III	10	7,200	860	730	240,000	12,300	0.92	37,770	50,000	106,600	232,000	23,000	79,000	130,000
	20	3,600	1,460	1,210	240,000	11,600	0.48	37,770	50,000	106 600	219,000	23,000	66,000	130,000
	30	2,400	1,930	1,500	240,000	11,000	0.34	37,770	50,000	106,600	208,000	23,000	55,000	130,000
6. Saturn I	10	2,700	660	390	90,000	8,800	1.24	9,835	760,000	44,300	192,000	0	180,000	12,000
	20	1,350	840	520	90,000	6,900	0.78	9,835	760,000	44,300	150,000	0	138,000	12,000
	30	900	990	600	90,000	6,200	0.57	9,835	760,000	44,300	135,000	0	123,000	12,000
7. Saturn II	10	7,200	910	650	240,000	11,500	0.97	20,835	44,000	123,000	265,000	23,000	172,000	70,000
	20	3,600	1,300	920	240,000	10,500	0.53	20,835	44,000	123,000	242,000	23,000	149,000	70,000
	30	2,400	1,610	1,150	240,000	8,800	0.42	20,835	44,000	123,000	203,000	23,000	110,000	70,000
8. Uranus	10	2,700	950	680	90,000	11,800	0.95	4,915	20,000	137,500	322,000	0	282,000	40,000
	20	1,350	1,300	860	90,000	10,200	0.55	4,915	20,000	137,500	279,000	0	239,000	40,000
	30	900	1,580	990	90,000	8,500	0.43	4,915	20,000	137,500	232,000	0	192,000	40,000
9. Neptune	10	2,700	1,760	1,040	90,000	15,000	0.76	8,885	20,000	45,200	337,000	0	289,000	48,000
	20	1,350	2,150	1,360	90,000	11,900	0.47	8,885	20,000	45,200	267,000	0	219,000	48,000
	30	900	2,400	1,510	90,000	10,500	0.35	8,885	20,000	45,200	236,000	0	188,000	48,000
10. Pluto	10	2,700	1,430	960	90,000	14,200	0.80	8,120	5,000	45,900	325,000	0	307,000	18,000
	20	1,350	1,870	1,230	90,000	11,500	0.49	8,120	5,000	45,900	263,000	0	245,000	18,000
	30	900	2,140	1,380	90,000	9,700	0.38	8,120	5,000	45,900	222,000	0	204,000	18,000
11. Out-of-Ecliptic (83°)	10	1,620	350	350	54,000	8,500	1.64	1,000	---	31,500	239,000	--	239,000	---
	20	810	700	730	54,000	8,500	0.82	1,000	---	31,500	239,000	--	239,000	---
	30	540	1,050	1,110	54,000	8,500	0.55	1,000	---	31,500	239,000	--	239,000	---

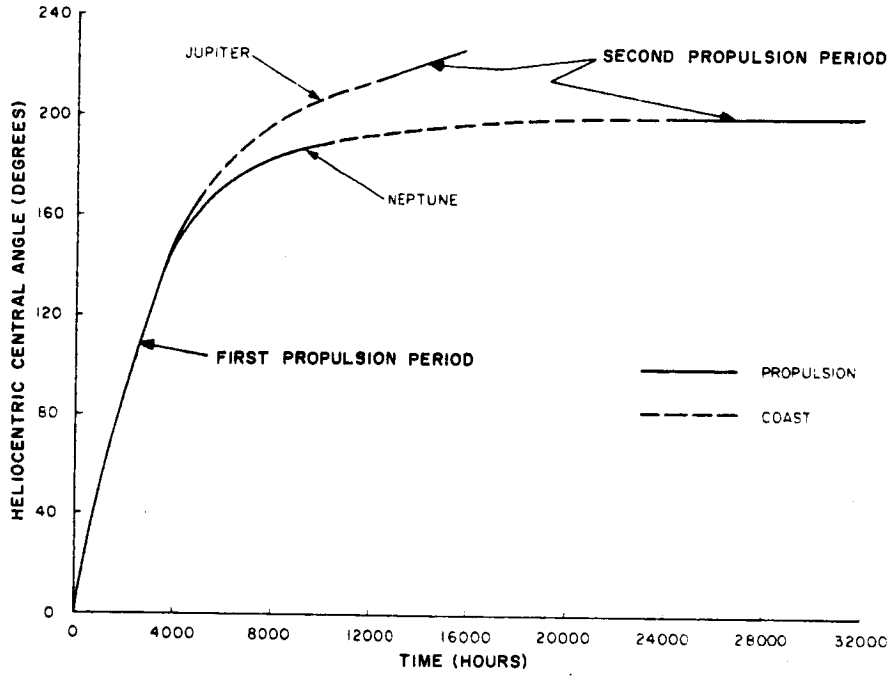

Figure 3-2. Central Angle Variation with Time for Two Typical Planetary Rendezvous Missions

After planetary capture has been achieved, the specific impulse, powerplant electrical output, and quantity of remaining propellant determine the terminal planetary orbit and the remaining time of propulsion. Increasing the specific impulse during this portion of the trip leads to a lower terminal altitude at the expense of increased propulsion time. Thus, a proper evaluation of the condition of the powerplant needs to be made after achieving planetary capture before selecting the terminal altitude and required specific impulse.

In the case of the mission designated Jupiter III in Table 3-2, 60 percent of the total required characteristic velocity occurs during the planetocentric phase (for 30 lb/KWe powerplant specific weight). As a result, the critical heliocentric phase is only 770 days out of 1930 days. This turns out to be an easier mission than journeying to Uranus, which requires 1580 days (1310 days for heliocentric portion of the trajectory).

An additional degree of freedom, which can be utilized after partial loss of power, is to abandon a portion of the payload such as a lander vehicle. However, this reduces the mission effectiveness and has to be balanced against the alternative of increasing the target terminal altitude.

The loss of power can also be tolerated by initially providing extra propellant in place of payload. All of those approaches are contingent on powerplant and spacecraft design in which failures lead to only partial reduction of available power.

C. RELIABILITY AND REDUNDANCY

The probability of mission success is dependent both on the proper functioning of space vehicle equipment and the flexibility of the space vehicle to accommodate loss of power and equipment without sacrificing mission goals. Although component reliability is stressed during the development program for each item of equipment, the space vehicle contains such a large number of components that vehicle reliability can be unacceptable with what would appear to be reasonably reliable equipment. The probability of successful vehicle operation is equal to the combined product of the probabilities of success for all prime components. Thus, a space vehicle containing eight prime components with reliabilities of 90 percent each, will have an overall reliability of 43 percent. (A prime reliability component is defined as one whose loss leads to mission failure.)

The number of prime reliability components is reduced by employing multiple components or redundancy, which leads to only a partial reduction in power and/or mission capability in the event of a component failure. A point of diminishing returns can be reached, if significant weight penalties are produced by the redundant equipment.

In the case of the radiator, where the failure rate is proportional to vulnerable tube and header area, a large amount of segmentation is advantageous. The failure of a tube by puncture or cracking results in loss of one radiator circuit, and that corresponding fraction of the total radiator area. If eight radiator segments are provided,

loss of one segment reduces useful radiator surface by 12.5 percent. The loss of electrical power would be approximately the same, unless extra segments were provided.

The issue of powerplant system redundancy can be placed in better perspective by first pursuing a few mathematical exercises. The assumption generally used is that the reliability is the inverse exponential

$$R = e^{-at},$$

where

R = probability of survival or reliability,

a = failure rate,

t = operating time.

If we want to compare reliabilities of species with the identical failure rate, a, but for different operating times, we find that

$$R_1^{1/t_1} = R_2^{1/t_2} = \text{constant},$$

or

$$R_2 = R_1^n$$

where

$$n = t_2/t_1$$

This relationship is plotted in Figure 3-3 for several values of n. The species can be either components or systems comprising groups of components.

The significance of this graph is as follows. Suppose it is decided that redundancy is to be provided for a particular process in the powerplant. The additional components will undoubtedly result in an increase in powerplant specific weight. For the case of

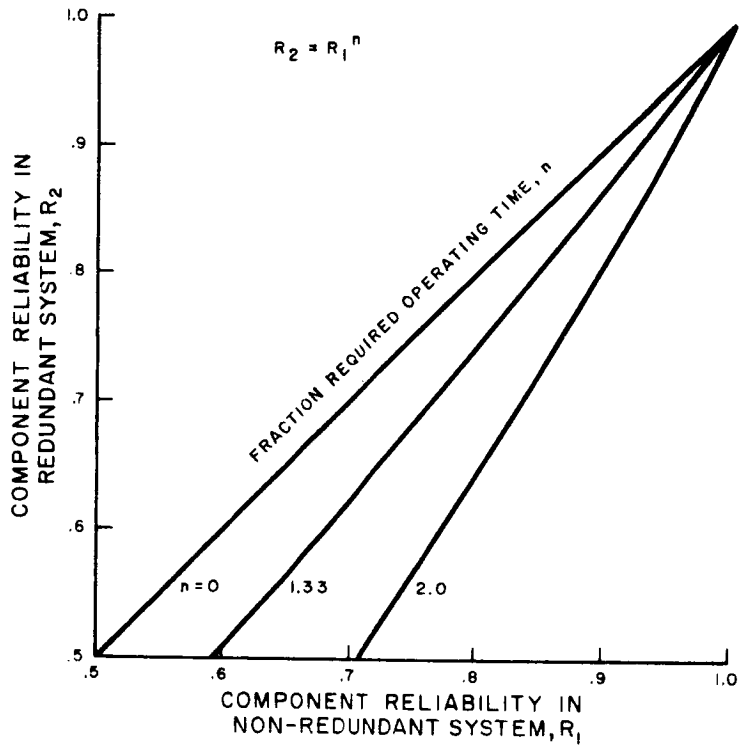

Figure 3-3. Influence of Operating Time on Reliability

nuclear electric propulsion, it can be shown that increased specific weight is compensated for by operating the powerplant during a proportionally longer time. As a result, the reliability of each segment of the process decreases according to the relationship shown in Figure 3-3, where r is the non-redundant process reliability, R is the redundant system reliability and n is the ratio of required operating time of the redundant to non-redundant system.

To continue this logic, let us assume that two systems are provided to perform a particular process and each system is capable of carrying the full load. Then, if r is the reliability of each system for operating time t, the probability of at least one system surviving is

$$R = 1 - (1-r^n)^2,$$

where n is ratio of redundant to non-redundant system operating time. This equation, which is plotted in Figure 3-4, is based on the assumption that operating duplicate systems in parallel does not introduce additional failure modes of significant value. If the redundant system represented a complete powerplant, it is conceivable that specific weight, and thus operating time, could double. This value is the n-2 line in Figure 3-4.

When the reliability of each system is greater than 0.90, a sizable reduction in mission failure rate is achieved by using a redundant system as shown in Figure 3-4. However, if system reliability is basically low and redundancy results in a sizable increase in operating time, the advantage of the redundant system vanishes.

Let us take, as a second case, the situation where four systems are provided with three required to successfully complete the mission. With r denoting the non-redundant system reliability, the redundant system reliability is

$$R = r^{3n} (4-3r^{n})$$

where n is the ratio of operating times. This function is plotted in Figure 3-5. The conclusion here is that the redundant system can have quite poor reliability relative to a non-redundant system.

Before applying the logic of this analysis to the selection of powerplant arrangements, there are a number of other considerations to be discussed. One consideration is the availability of developed components of particular sizes. Available hardware items will generally have an edge in reliability because of operating experience. It would be easier to improve existing components than to begin development of new size equipment.

Another consideration is the influence of size on component reliability. It might occur that a 200-kilowatt heat exchanger has double the failure rate of a 100-kilowatt heat exchanger. In the larger size unit, twice the number of welded tube to header joints could exist, each a possible cause of failure. Also, the smaller heat exchanger would

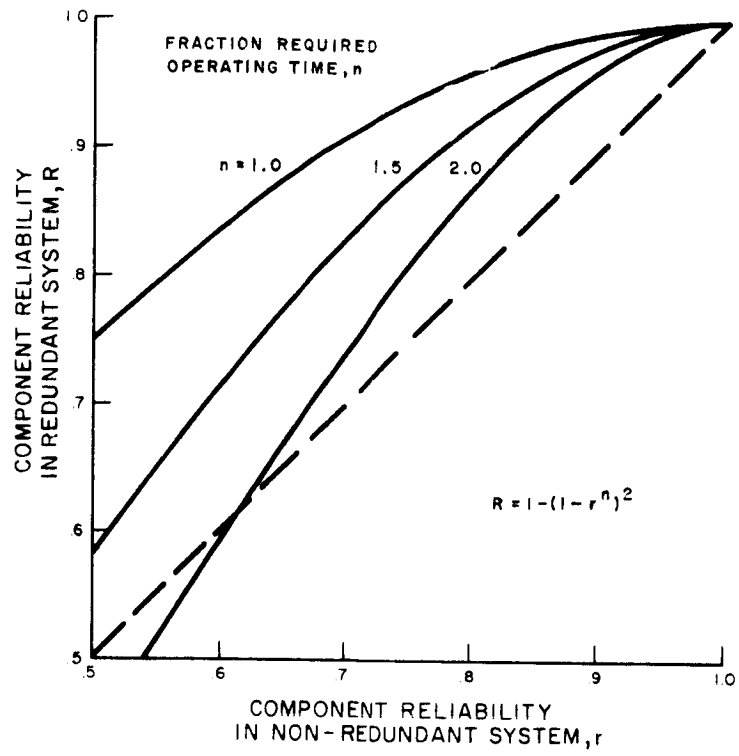

Figure 3-4. Probability of No More Than One Failure in Two Parallel Systems

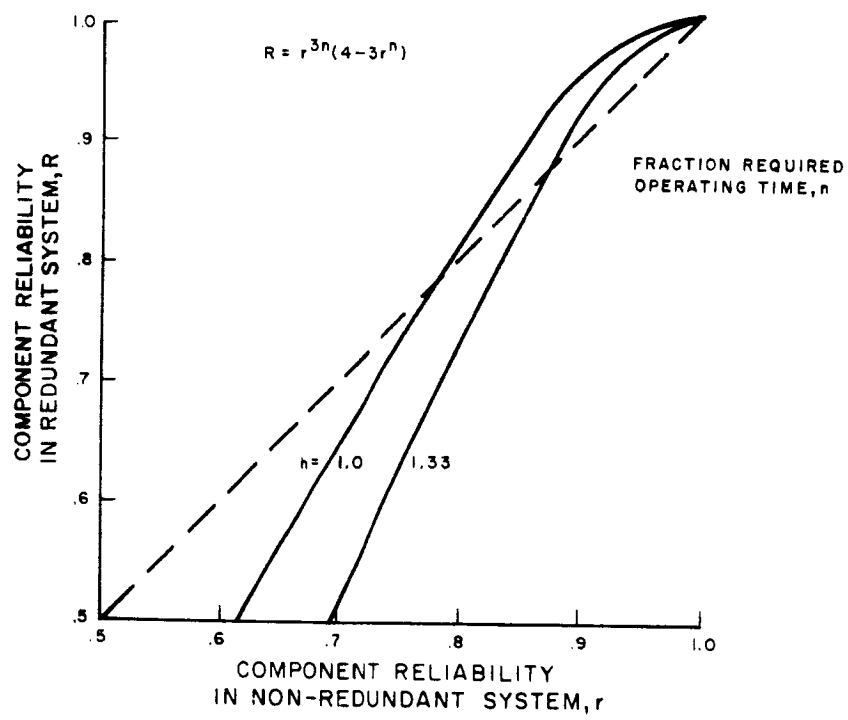

Figure 3-5. Probability of No More Than One Failure in Four Parallel Systems

be easier to test, resulting in more test hours of operation yielding higher perfection of design. This latter argument would also be true of rotating machinery.

A second mathematical analysis can be made accounting for the influence of component size on reliability. Let us assume that failure rate is proportional to component, or system, size. In the case where two systems are provided, each system is of the same size as the non-redundant system and the results shown in Figure 3-4 still apply. For the case of four systems with three required, the overall reliability expression is

$$R = r^n (4-3r^{n/3}).$$

This expression is plotted in Figure 3-6 and the conclusions from Figures 3-5 are reversed. Redundancy is now shown to yield a marked decrease in mission failure. Figures 3-5 and 3-6 show limiting situations with the real solution somewhere in between.

These types of analyses can be carried out to many more examples. The mathematical analysis does not by itself provide an answer to particular questions such as, "How many turbogenerators are to be used in nuclear space powerplants?"

One general conclusion we may make is that greatly improved reliability is achieved through redundancy when the basic system or component failure rates are less than 10 percent. Typical improvements such as raising reliability from 0.90 to 0.99 are important for missions where survival is important such as for manned spacecraft. This is not necessarily true for missions where the payloads are scientific instrument packages. These missions could be attempted before such high system reliabilities are demonstrated.

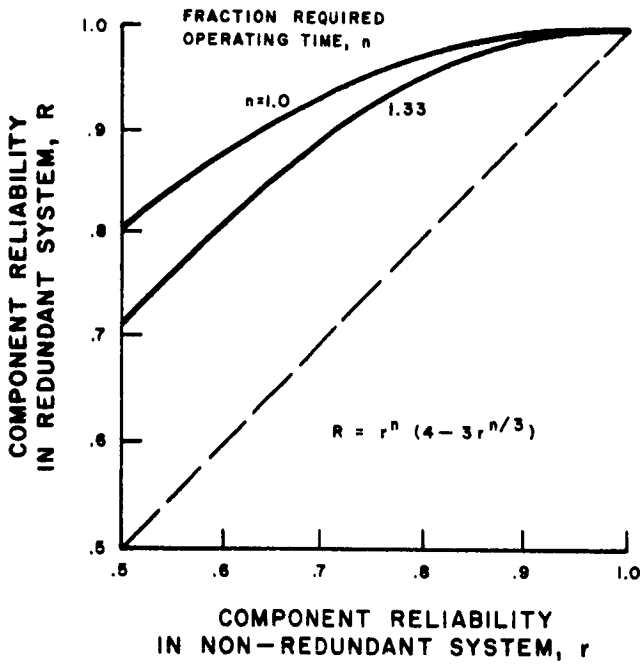

Figure 3-6. Probability of No More Than One Failure in Four Parallel Systems Accounting for Size Effects

4. SPACECRAFT CONFIGURATIONS

Mission analyses performed during the early stages of this study established that several different-sized nuclear-electric-propelled space vehicles would be considered for accomplishing unmanned exploration of the solar system. These sizes would be consistent with both two and three stage chemical versions of the Saturn V Booster, which yields the options of initiating nuclear-electric-propulsion at low Earth orbit, escape, or beyond escape trajectories. In addition, the use of both turboelectric and thermionic electric powerplants were to be considered. To accomplish these objectives, six particular spacecraft and powerplant combinations were originally selected for preliminary design study, which were later reduced to three cases containing most of the unique types of problems. The principal characteristics of these selections are listed in Table 4-1.

TABLE 4-1. CHARACTERISTICS OF SELECTED SPACECRAFT AND POWERPLANT COMBINATIONS

Booster Stages	3	2	3
Booster Cutoff	Escape	Orbital	Escape
Spacecraft Weight*, lb	88,500	234,000	88,500
Powerplant Output, Kwe	1,200	4,800	1,000
Powerplant Weight, lb	25,054	95,050	38,040
Propellant Weight, lb	44,080	89,000	33,350
Type of Powerplant	Turboelectric	Turboelectric	Thermionic

*At Start of Electrical Propulsion

A. CONFIGURATION SELECTION

To arrive at a practicable nuclear electric spacecraft configuration, it is necessary to examine the major elements of the power plant system as they relate to the spacecraft as a whole. The schematic diagram of Figure 4-1 identifies these elements and shows

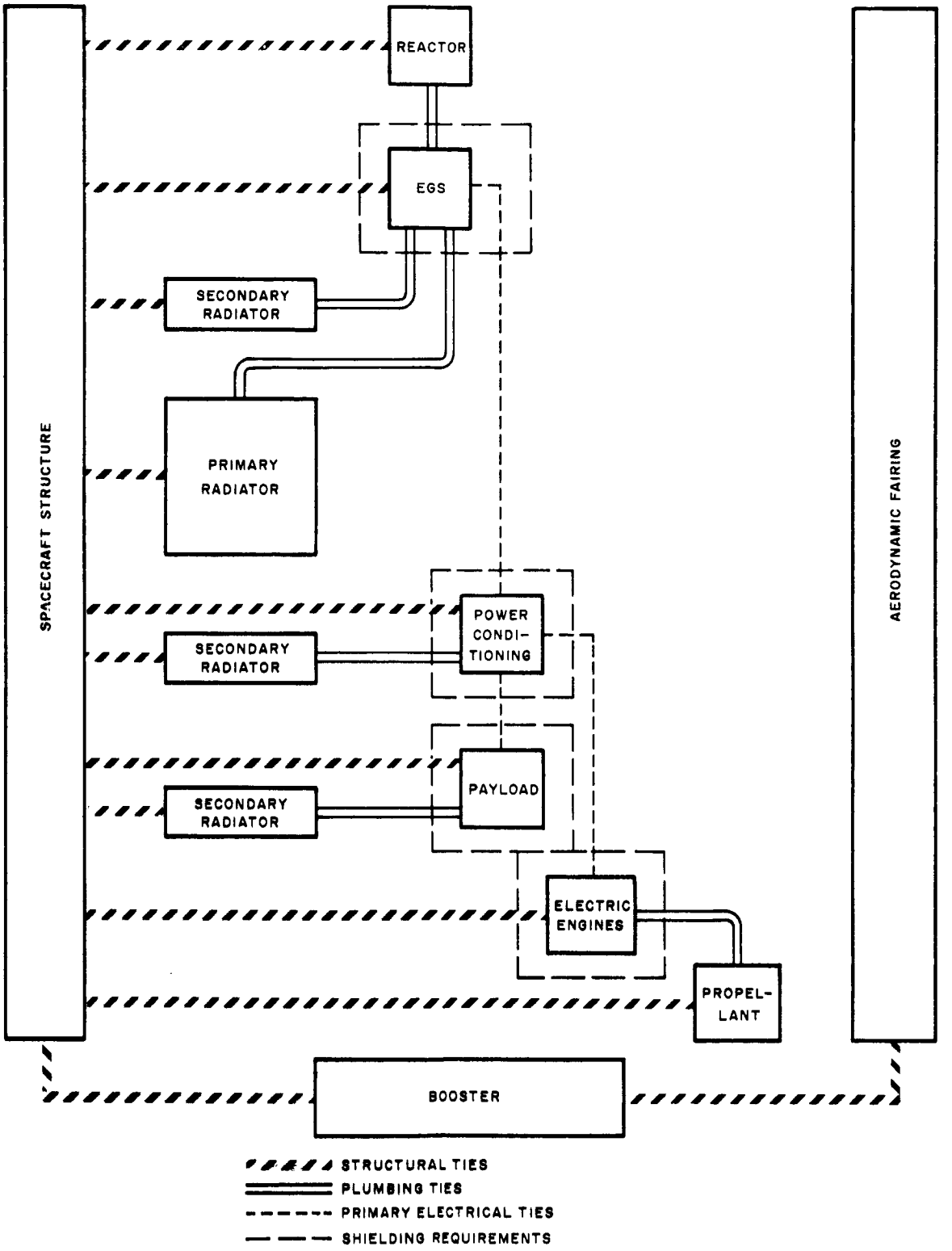

Figure 4-1. Nuclear Electric Spacecraft Functional Block Diagram

the functional integration in terms of mechanical, piping, and major electrical connections. In addition, the requirement for nuclear radiation shielding is indicated by dashed lines surrounding the appropriate "black boxes."

1. General Arrangement

Since the reactor is generally the smallest major component on the spacecraft, preliminary designs have consistently shown that the nuclear radiation shield is best used to shield the reactor from the spacecraft rather than individually shielding the sensitive components. This conclusion is further emphasized when the effects of radiation scatter from insensitive structures such as the radiators are considered. It is also found that the magnitude of the shield shadow cone angle is a major parameter affecting shield weight; hence, the reactor should be located at an extreme position on the spacecraft, and the sensitive equipment should be incorporated in a generally linear arrangement behind the shield. To a lesser extent, it is also desirable to follow this approach with the radiators to minimize scatter shielding requirements.

The next natural constraint relating the system elements is the plumbing. The electric generating system (EGS in Figure 4-1) includes the boiler, turbogenerator, condenser, and associated accessories. It is connected by relatively massive fluid lines to the reactor, the primary radiator, and the EGS component cooling radiator. These piping connections draw these items together into an intimate and basically rigid mechanical assembly, with the EGS located close to the reactor to minimize top end heat losses. The only necessary power connections between the power conditioning system and the EGS are electrical, which is, in principle, a less mechanically rigid tie and permits this item and its radiator to be considered as a mechanically separable unit. Similarly, the payload with its cooling radiator and the electric engines with their propellant tanks can be thought of as separable modules. In summary then, the major elements of the system may be grouped in four loosely connected packages as illustrated in Figure 4-2a; and, if any deployment is required, it is preferable to restrict it to the interfaces between these packages.

In view of the large propellant weights, it is desirable to locate the engines near the booster interface to minimize launch load bending moments and the associated structural weight requirements. This also provides a clear path for the efflux of propellant. To minimize the nuclear radiation shielding requirements, it is also desirable to locate the payload and power conditioning at a maximum distance from the reactor. The arrangement illustrated in Figure 4-2a reflects these ideas.

Transmission lines at low voltage can involve huge cabling weights; therefore, it is important to consider placing the power conditioning at a location to fully capitalize on the use of high voltage transmission where high power must be transmitted over large distances on the spacecraft. For example, a one megawatt, 120 volt line to neutral, 50 feet long, 3 phase, electrical feeder system weighs about 1500 pounds and, because of a 50 kilowatt electrical system loss, increases the net powerplant weight by 2500 pounds over that of a 1200 volt line to neutral system. The alternative arrangement shown in Figure 4-2b shows how this idea could be applied. It will be noted that the shift of the power conditioning equipment shown has also involved a secondary radiator with a resulting increase in the length of the heavy feed line connections between the EGS and the primary radiator. An alternative to combat this effect is illustrated in Figure 4-2c. This arrangement also contrives to stack the radiators to give a smooth temperature transition from the hot end of the system to the coolest end, and it provides a mechanical separation interface which can place two of the secondary radiators on a deployable module. Inasmuch as secondary radiators can require large surface areas, this can be a significant feature.

To aid qualitative comparison of the three arrangements shown in Figure 4-2, the piping and transmission lines have been identified as either heavy or light, and the radiators have been identified by their relative temperature levels. The structural and aerodynamic shroud factors are not shown, as examination of their influence requires somewhat more than a schematic insight.

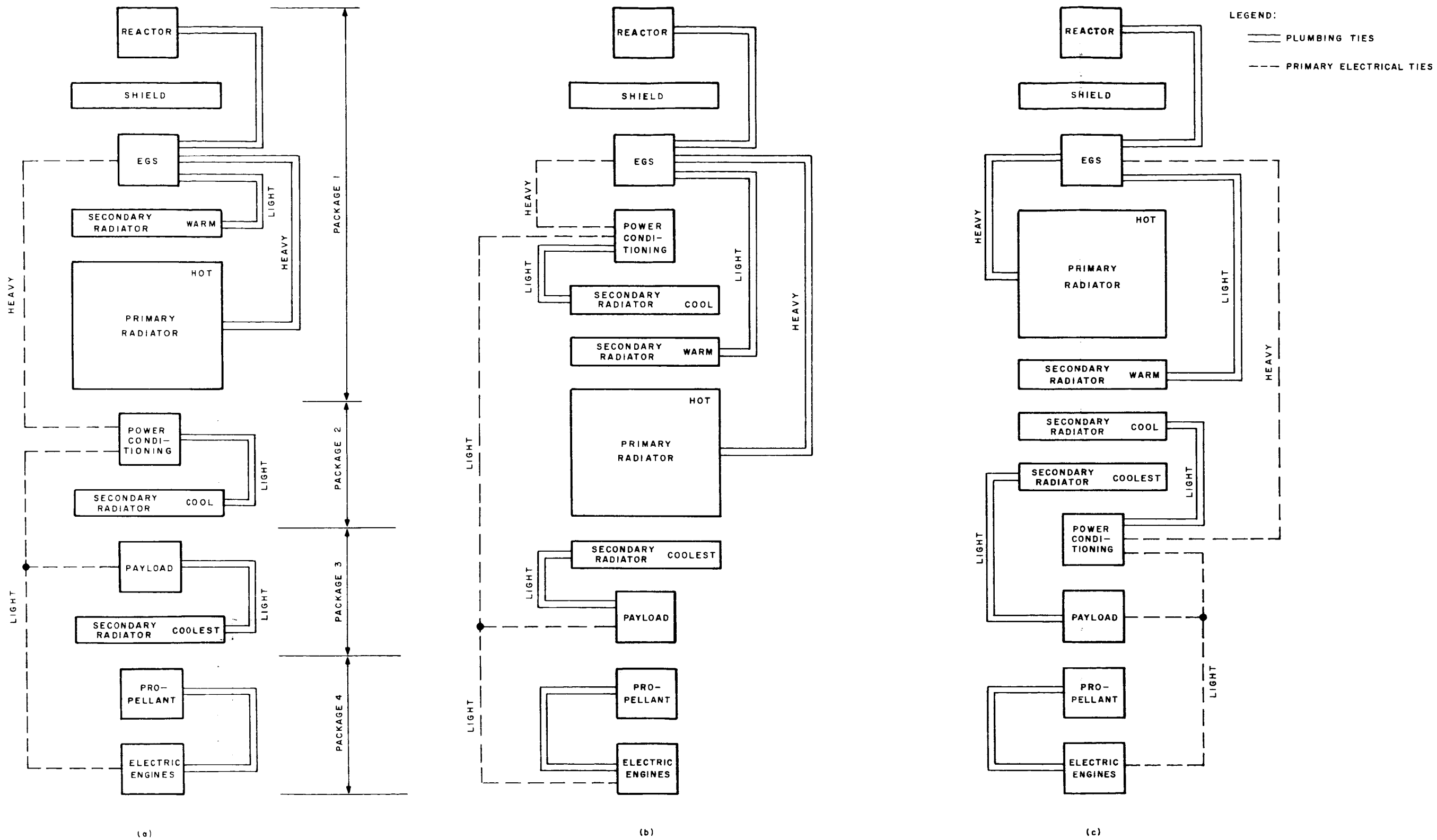

Figure 4-2. Spacecraft Functional Block Grouping Diagrams

2. Launch Vehicle Considerations

To accomplish the missions considered in this study, Saturn 1B, Saturn V (2 stage), and Saturn V (3 stage) have been identified as the boosters having the necessary payload capability. As related to the nuclear electric spacecraft configuration, the booster characteristics of major significance include limitations on center of gravity, payload fairing length and diameter, nose cone shape, center of pressure, and load distribution entering the booster structure.

Both Saturn 1B, and the escape version of Saturn V employ the 260-inch diameter S-IV-B as a final stage to which the spacecraft must be mated. Nevertheless, different shroud length and center of gravity restrictions exist for these two launch vehicles due to bending moment restrictions in the S-I first stage of Saturn IB. Figure 4-3 shows the maximum envelope for spacecraft launch configurations as recommended by NASA MSFC in a private correspondence (July 1963). Nose-cone angle can be varied a small amount from that shown, provided the length and center-of-gravity limits are properly adjusted. The Saturn V orbit launch vehicle has a diameter of 396 inches (S-II stage). A general guide in sizing payloads for this booster can be obtained by considering the RIFT and Apollo envelopes. Figure 4-4 shows the outline and center of gravity for both of these cases.

One other consideration relating to the launch vehicle is the aerodynamic shroud. As a rule of thumb, the loss of payload in orbit is approximately equal to 10 percent of the shroud weight, when it is ejected at first stage burnout. Although this is a fairly small penalty, for the Saturn class boosters the shrouds are very large as shown in Figures 4-3 and 4-4 and their weights will range in the tens of thousands of pounds. As a result, even a 10 percent penalty is a major item and there is a strong incentive to integrate the shroud load carrying function into the spacecraft design. In keeping with this line of reasoning, it is interesting to note that most current large spacecraft designs do not employ a separate aero shroud. This is true of Mercury, Gemini, Apollo, and the space station concepts.

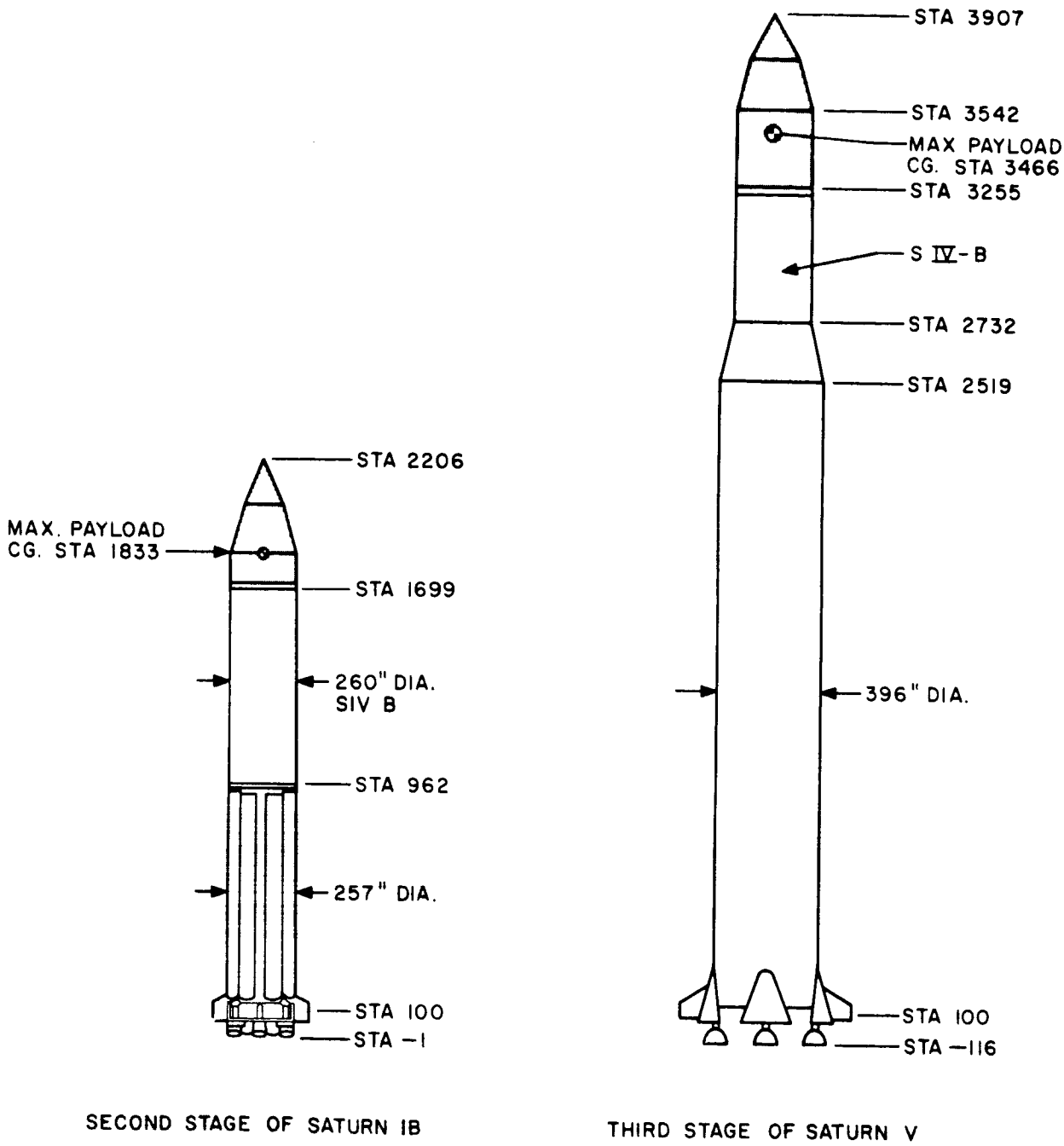

Figure 4-3. Saturn S-IV-B Booster Stage Payload Limitations

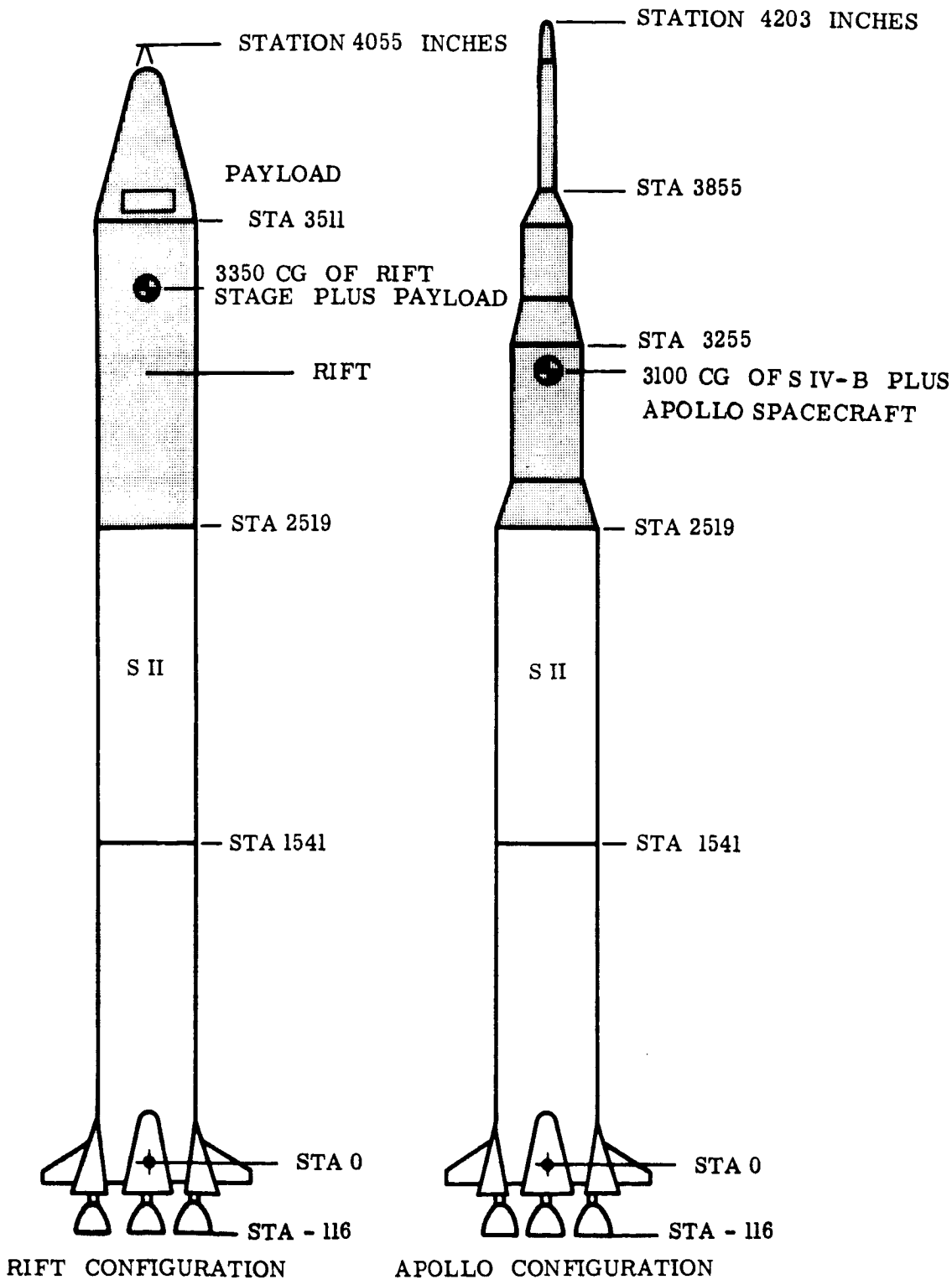

Figure 4-4. Saturn S-II Booster Stage Payload Limitations

3. Heat Rejection Radiators

The most dominant single factor in selecting a nuclear electric spacecraft configuration is the packaging of heat rejection radiators within the limited dimensional envelope of a booster fairing. Many designs have been proposed for solving the radiator packaging problem. Frequently, the approach has been to select a flat panel for the deployed configuration, and by means of various folds, reduce the radiator dimensions to fit a given booster shroud. In this way, maximum view factor is obtained, and panel area minimized. The disadvantages of this approach have been largely attributed to the reliability problems of actuation, deployment, and fluid transfer across the fold seams. For near term applications, the trend has therefore turned towards various fixed configurations. Practical arrangements may be obtained with cross-sections composed of radial or circumferential elements. The circumferential type is represented by the cone-cylinder combination, while the radial types could be of the flat panel, triform, or cruciform shape.

For such configurations are compared in Figure 4-5 on the basis of equal effective radiating area. Since radiator weight is related to panel area, the tabulated data shows why a high view factor appears desirable. The concurrent length increase detracts from this idea due to the associated increase in the weight of structure, fluid feed lines, electric cables, and other length-dependent spacecraft components. Within the confines of Figure 4-5, the triform stands out as a reasonable compromise between length and panel area, and this configuration has been employed in various system studies. Actually, a detailed look at the view-factor effect on the tube and fin matrix weight reveals a small difference between the four arrangements.

a. Matrix Weight Comparison

Two principal effects relate the radiator matrix weight to the view factor.

- As panel area is reduced, specific heat rejection capability must increase. To maintain an optimum thermal design this required larger tube diameters, closer tube spacing, and/or thicker fins resulting in a matrix specific weight (lbs/ft^2) increase.

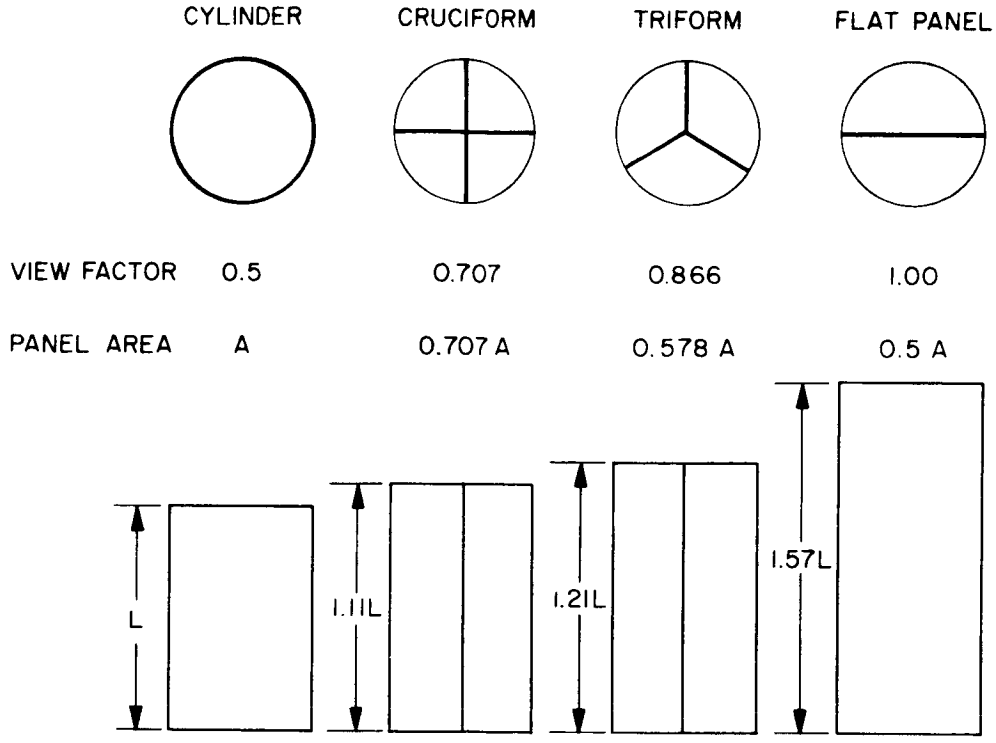

Figure 4-5. Comparison of Fixed Radiator Arrangements

- Cylindrical configurations can achieve a large reduction in armor weight on inward facing tube surfaces by capitalizing on the meteoroid bumper effect afforded by the fins.

Figure 4-6 illustrates the application of the self-shielding effect. To illustrate the comparative matrix weights of the various configurations of Figure 4-5, the results of a simplified study considering only radiator tubes and fins with aluminum construction are shown in Figure 4-7. Here the specific matrix weight is plotted against effective radiating area. The substantially reduced basic matrix weight of the cylindrical design is evident. When appropriate panel areas are applied to the specific matrix weight, the curves of Figure 4-8 result. Even the flat panel configuration with its unity-view factor is seen to be only slightly lighter than the cylindrical concept, the difference being considerably less than the anticipated structural weight penalty for a flat panel. Although done for fixed designs, the flatform, triform and cruciform results apply equally well to folding concepts of the same final cross-sections. Since

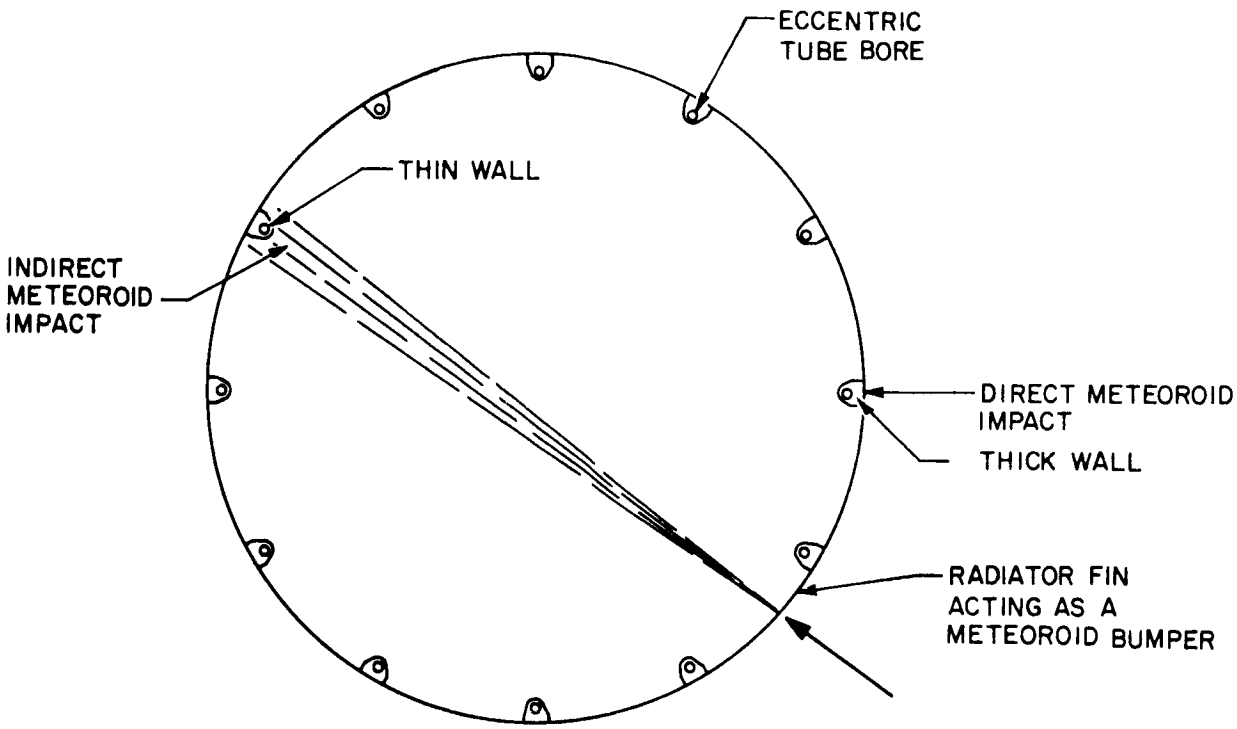

Figure 4-6. Effects of Fin Bumper on Tube Armor

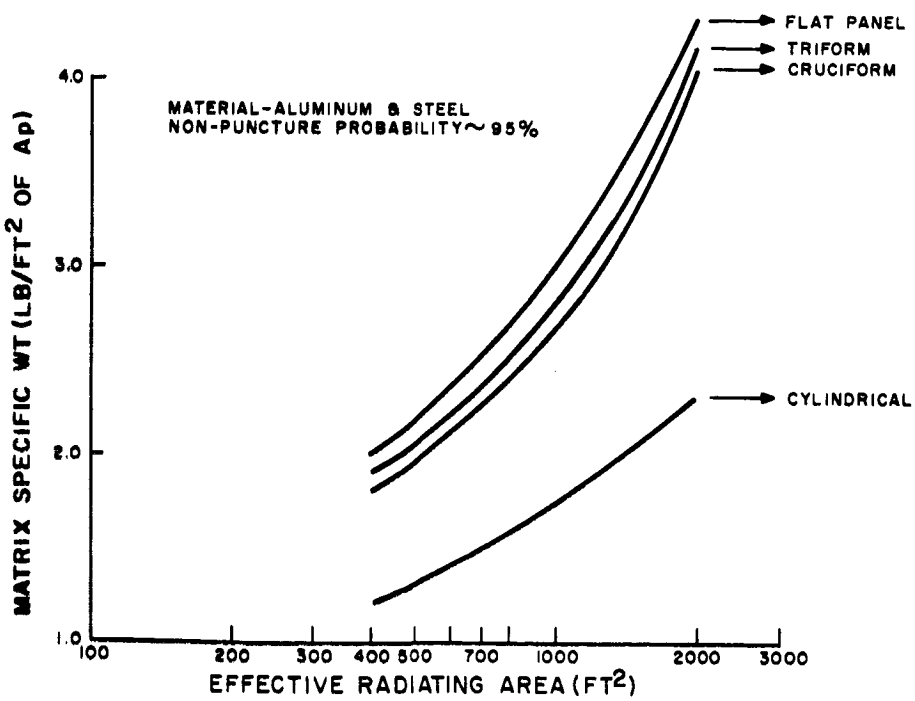

Figure 4-7. Panel Specific Weights for Different View Factors

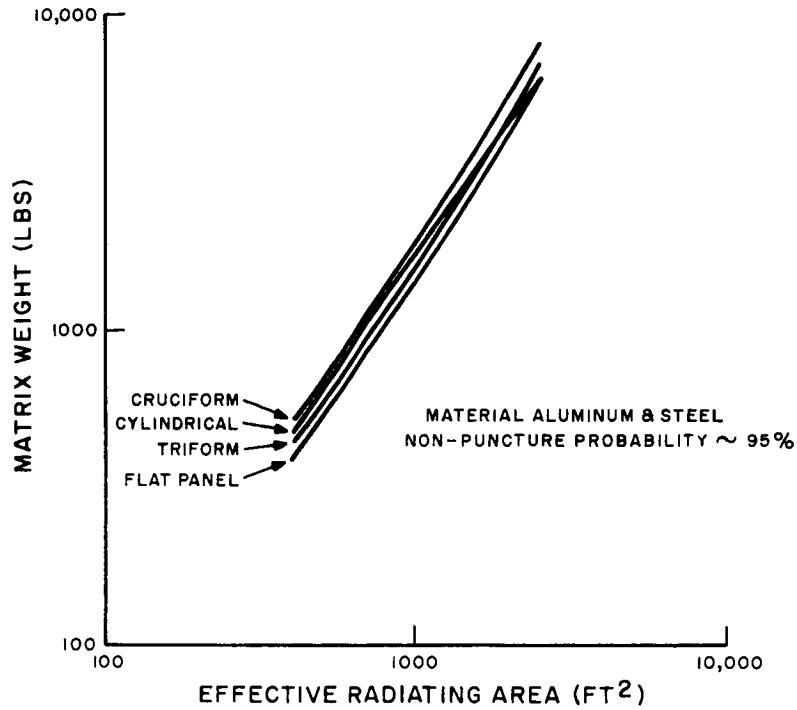

Figure 4-8. Matrix Weight versus Effective Radiating Area

folds entail significant weight, it is concluded that a fixed cylinder or conical design is fundamentally as light or lighter than any folding concept. Two effects not considered in these comparisons are shielding and structure.

b. Fluid Circuit Arrangements

Certain fundamental orthogonality relationships exist between the tubes, headers, feeds, and returns of any radiator. Since temperature gradients and differences occur among these members in a non-condensing radiator, there are apt to be thermal stress and stability problems. The flow path arrangement should be configured to minimize such problems.

Considering a conical configuration as an example, the radiator tubes can be arranged either longitudinally or circumferentially. With a circumferential arrangement, the temperature gradient along the tubes produces a differential thermal expansion pattern

which is highly unsymmetrical about the vehicle axis. If the tubes run halfway around the circumference, the vehicle experiences a bending moment tending to warp the longitudinal axis; for shorter tube lengths, the temperature gradient produces a cyclic thermal strain pattern around the axis. Both are illustrated in Figure 4-9. Without detailed analysis of a specific design, it is difficult to ascertain the effects of such a gradient; however, in a multi-loop radiator, should a panel be lost due to meteoroid puncture, an asymmetric moment is definitely produced on the vehicle which is generally undesirable both for flight control and structural reasons. On the conical portion of a radiator, a circumferential tube arrangement implies tubes of varying length in a given radiator loop which is not conducive to achieving desirable flow distribution. Finally, from a structural viewpoint, the circumferential arrangement places most of the fundamental radiator strength perpendicular to the primary loading direction. Since the longitudinal loads are of major concern, this approach implies the needed addition of many purely structural members to achieve an adequate mechanical design.

By running the tubes axially, the panel temperature drop is symmetrical about the configuration axis and follows a pattern as indicated in Figure 4-10. In this manner, differential thermal expansion produces an elongation of the whole radiator but no lateral warping. Local problems still exist due to the spanwise gradient on the fins, but these too are symmetrical. At the operating temperature, the fins can be designed so as to relieve themselves of stress resulting from this gradient by creep relaxation. The header arrangement shown provides alternate feed and return along the configuration axis, thereby eliminating temperature discontinuities. With this approach, each circumferential segment (bay) can be an individual loop. In the event of meteoroid puncture, a bay can "go dead" without producing asymmetric temperature distributions about the vehicle axis. From the structural viewpoint, the relative masses of material involved in the tube armor and header armor (or bumpers) is more naturally disposed to serve as stringers and rings respectively.

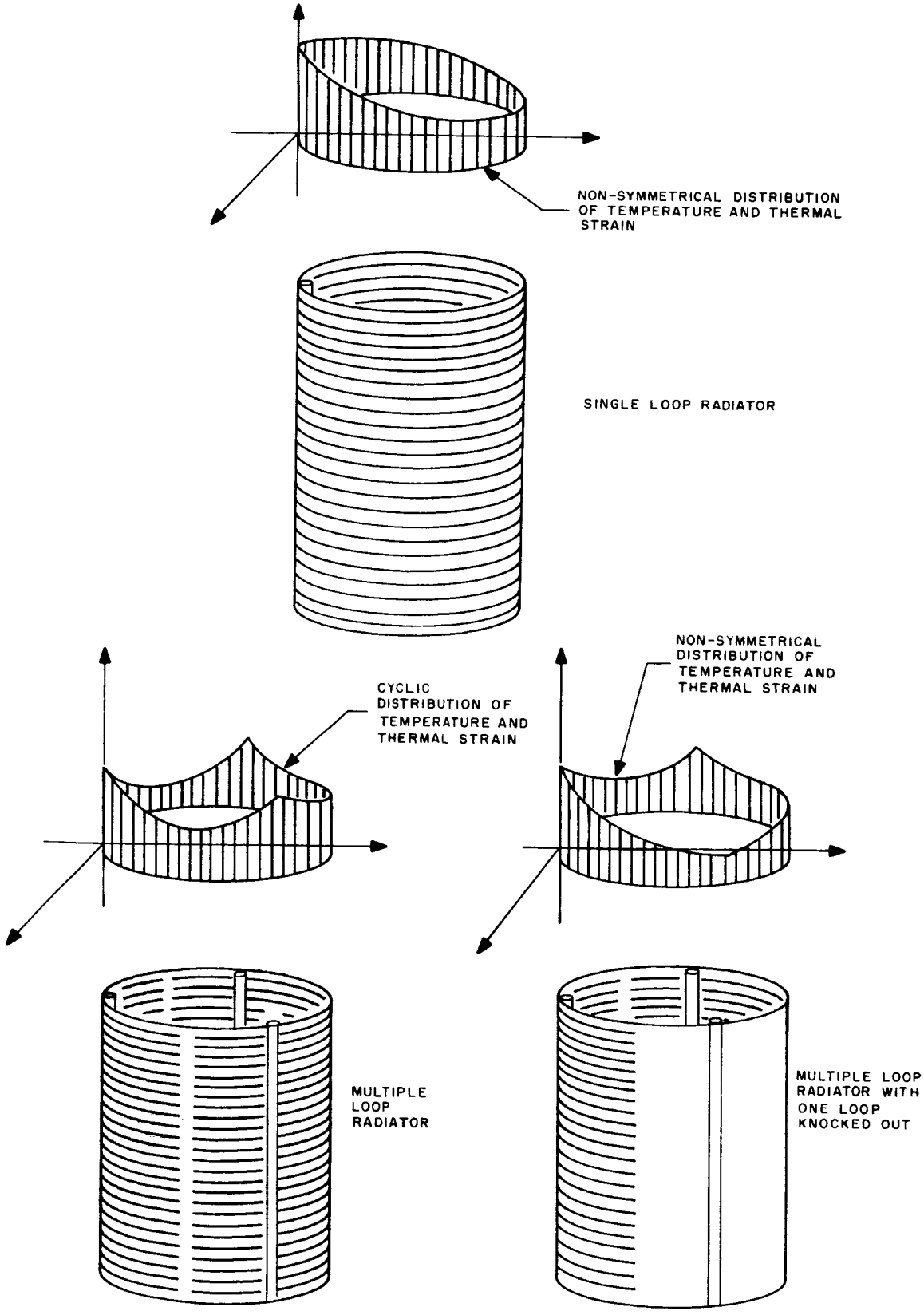

Figure 4-9. Circumferential Radiator Tube Effects

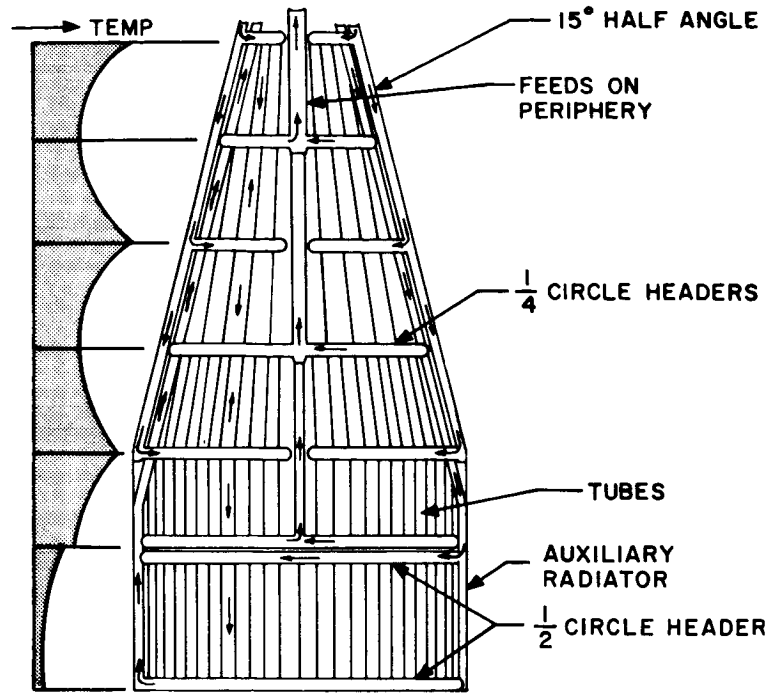

Figure 4-10. Axial Flow and Temperature Profiles

c. Structural Considerations

Foregoing discussions have presented arguments showing that thermal requirements and meteoroid self-shielding tend to offset view factor in the overall weight tradeoff. An additional factor in radiator weight analysis is the structure required to sustain mechanical integrity during the launch phase of flight. It is appropriate for the radiator matrix to serve as its own structure; in fact, it is difficult to conceive of a practical design where a large radiator is treated strictly as a passive component from a structural viewpoint. Figure 4-11 compares an integrated radiator structure with a separate radiator and structure; the most pertinent factor involved in the comparison is the structural nature of the fin/tube matrix itself.

As a result of the meteoroid armor, the tubes are quite stiff in bending and strong in pure compression along their axes. The fins partially stabilize the tubes against buckling and the armor or bumper meteoroid protection adds to the effective panel

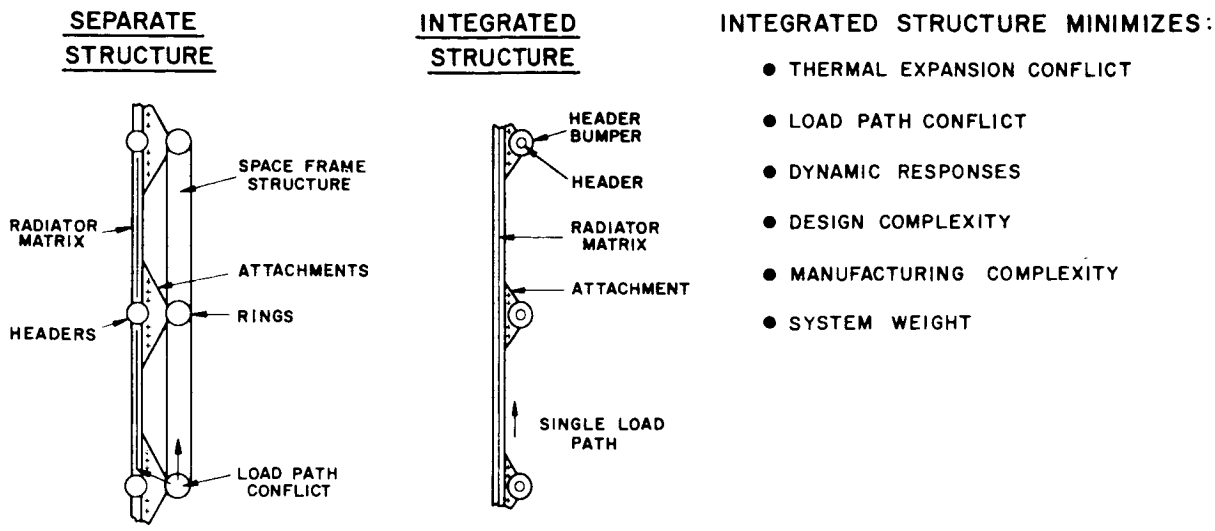

Figure 4-11. Comparison of Separate and Integrated Radiator Structural Approaches

stiffness. The overall matrix is also fairly heavy and requires strong attachments if it is to be supported from a separate structure. In order to ensure that the structure carries launch loads, it must be considerably stiffer in all loading directions than the radiator matrix. In view of the inherent stiffness of the latter, this requires an inordinately heavy structure. The only alternative is to segment the radiator axially and provide flexibility in the attachments to prevent the transmission of structural loads along the matrix. These approaches are inconsistent with the task of supporting the heavy matrix and controlling dynamic response.

In addition to the load-path conflict involved in the transmission of launch loads, there is also a thermal expansion conflict. With the fluid in direct contact with the radiator tubes, they will be hotter than the supporting structure. The differential expansion will stress both the structure and the matrix in proportion to their relative stiffness. To offset this effect, the structure would have to be very flexible, or contain numerous

expansion joints which again is totally inconsistent with its role as a structure. With the single load path shown in the figure for the integrated structure approach, both of these conflicts are avoided. In addition to these aspects, the added hardware involved in using a separate structure increases the number of dynamic responses that must be suitably controlled, increases the design complexity, and adds to the manufacturing processing and cost. Furthermore, an integrated structure minimizes the overall radiator and vehicle weight, unless the structure can be designed to be jettisoned after booster burnout. Using the radiator matrix as structure, the result is a semi-monocoque panel or shell. The fins act as the skin, the tubes function as longerons, and the headers act as stabilizing rings in conical designs and support beams in the radial element designs exemplified by the cruciform.

Comparative evaluation of structural requirements cannot be conveniently handled by parametric methods, and for this reason, mechanical design studies must be performed for specific radiator and vehicle combinations. However, a qualitative indication can be obtained from Figures 4-12 and 4-15 which show results of a design point study comparing a conical and cruciform configuration related to a SNAP-8 type of system. Dynamic conditions appear to be the more significant mode of loading, and auxiliary structure must be added to both radiator designs to supplement their own structural capabilities. In this respect, the cruciform is found to be the most deficient, and the main structural additions are compared in Figure 4-12. For the conical design, tube end stiffness and joint splice fittings are identified; these are also required in the cruciform. The only load carrying additions to the conical design are the auxiliary stiffening rings. These are needed to provide local stability of the matrix elements, and natural frequency isolation from the fundamental vehicle mode. As illustrated in Figure 4-13, increasing the ratio of the imposed compressive load on the matrix element to its critical buckling load, leads to a reduction of the panel natural frequency. Rings are required to adequately raise the critical buckling load such that the panel frequency is separated from the spacecraft fundamental; a typical design ratio would be $\sqrt{2}$.

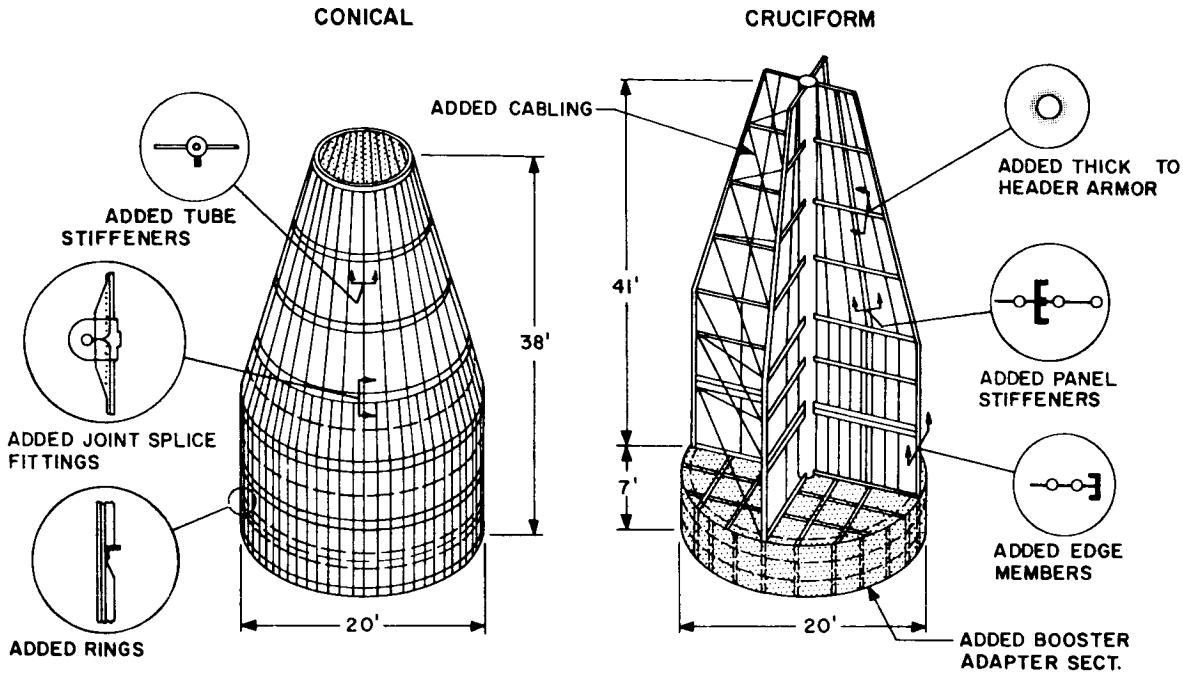

Figure 4-12. Radiator Structure Comparison

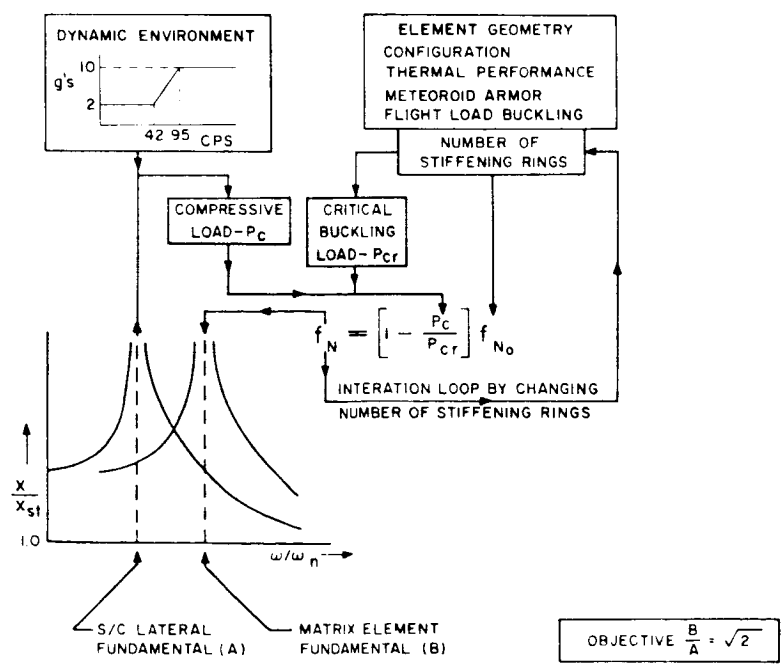

Figure 4-13. Conical Configuration Matrix Dynamic Buckling Analysis

Examination of the cruciform design reveals that it cannot really serve as its own structure. There is no convenient load path connecting the radiator to the booster mounting ring; this requires the addition of heavy edge members from which the matrix is essentially hung. The electrical generation system and reactor shield assembly could be supported on these edge members. In addition to transmitting axial loads, these edge members also stabilize the radial panel edges under overall bending. At the base of the cruciform design, the unit load coming out of the edge members is extremely high, and an adapter section is required to provide a uniform load distribution into the booster mounting ring. Figure 4-14 illustrates an adapter for Saturn IB and the degree of load equalization attained for typical extreme loading. With suitable tapering of the longitudinal stringers and circumferential gradation of the skin thickness as dictated by shear lag analysis, the concentrated load at the base of the cruciform edge member can be distributed to a uniform load having a 20 percent ripple with a 7-foot adapter length.

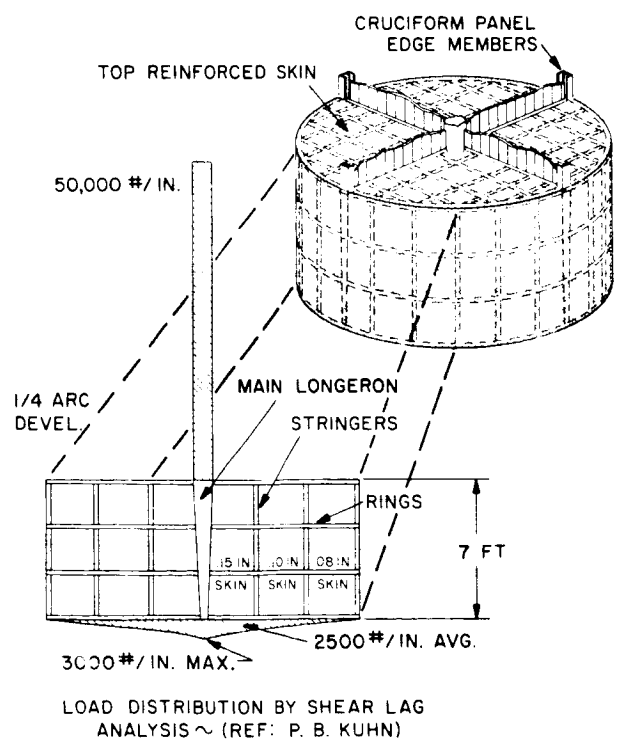

Figure 4-14. Cruciform Configuration Booster Adapter

The other major structural problems with the cruciform concern detuning of substructure natural frequencies from the fundamental system modes. To stiffen the radial panels, the header bumpers require thicker walls and larger diameters than would otherwise be needed for meteoroid protection. Figure 4-12 identifies this, and the cabling which can be added to provide simple support at the outboard ends of the header bumpers. Without the cabling, the header bumpers become excessively heavy; however, the problems of adequately achieving the cable rigging are considerable, due to the sensitivity of pre-tensioning to variations in temperature and geometry. In addition to raising the bending frequency of the radial members of the cruciform design, panel stiffeners are required to raise the natural frequencies of the individual flat panels between adjacent headers. The net result of all these structural additions is illustrated in Figure 4-15, which compares the weights of the two configurations based on 1300 square feet of total radiator area. Close similarity in the respective matrix weights reflects the findings presented in Figures 4-7 and 4-8, and the substantial structural difference is the net result of the features identified in Figure 4-12.

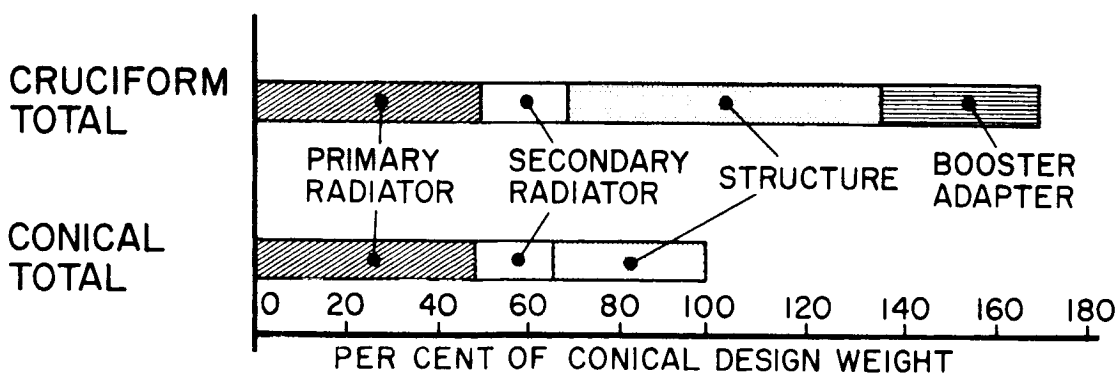

Figure 4-15. Cruciform and Conical Total Radiator Weight Comparison

4. Vehicle Configuration Summation

System studies of space nuclear powerplants consistently identify the radiator as the physically dominant component. Although its primary role is heat rejection for the power cycle, it is obviously not a mere adjunct to the spacecraft system. To adequately design a radiator to meet launch load as well as operational thermal requirements, it must be treated as a large structure. In so doing, by its very nature, it emerges as the basic spacecraft framework. Furthermore, the cylindrical-conical arrangement appears to be the most desirable. The meteoroid self-shielding effect shows that the basic matrix weight compares favorably with flat, tri-form, and cruciform radiators and the results of structural analysis identify a significant structural penalty for the cruciform design. By analogy, it may be reasonably deduced that the other radial element arrangements will have a similar structural comparison. The evidence heavily favors the conical arrangement as the lightest from an overall radiator weight viewpoint. A radical downward re-evaluation of the meteoroid hazard would not materially alter this conclusion since the structural considerations override the armor requirements as indicated by Figure 4-15.

In addition to the radiator weight optimization, the conical design concept has several system advantages. Since the inner surface is not contributing to the heat rejection function, almost anything can be done to it to meet general spacecraft needs. For example, coatings and insulation can be used to thermally decouple the primary radiator from the spacecraft components (including low-temperature radiators). Furthermore, by virtue of the circumferential distribution of the radiator matrix, maximum utilization of the booster payload envelope can be achieved for packaging payload, propulsion, and other spacecraft equipment. Apart from the need for auxiliary rings for stability, the conical radiator matrix is inherently over-designed from a structural viewpoint; it therefore has the capability to provide most of the load carrying requirements of the spacecraft in addition to meeting its own needs. In fact, analysis shows that it is structurally adaptable to also carry the aerodynamic loads associated with the booster shroud. On the basis of the reasoning presented here, the spacecraft

designs considered in this study utilize the fixed conical or cylindrical radiator configuration wherever possible, and folding radiators are only considered when booster packaging limitations are encountered. Furthermore, the primary radiator is employed as the outer shell, serving also as the aerodynamic shroud; and the payload/propulsion equipment is handled as a separate assembly housed within the primary radiator shell during launch. Beyond this, the configuration details are worked out in the specific vehicle designs to suit the demands of the particular system.

B. VEHICLE DESCRIPTIONS

The 1200°F operating temperature of the turbo-electric system radiator permits the use of beryllium as the primary construction material. Although it is recognized that many problems exist with the use of beryllium, the potential weight advantages stemming from its superior density and Young's Modulus characteristics make it very attractive. Therefore, for this study it was assumed that the theoretical meteoroid armor capabilities will be achieved and that the necessary shapes and fittings can be manufactured. The only concession made to the material's brittleness was in the detailed assembly concepts which employ simple geometries and fastening techniques geared to meet the known problems.

The 1200 KWe turboelectric powered spacecraft was considered to be of most general interest and, as a consequence, received the most detailed examination. The 4800 KWe turboelectric vehicle was then analyzed to determine the presence of any problems relating to either size or number of turbo-generators. Finally, the thermionic powered vehicle study was prepared, based on the use of a non-beryllium higher-temperature radiator to identify any unique problems associated with that selection. At the start of this program, the turboelectric powerplant sizes were selected at 1 MWe and 4.1 MWe. After preliminary designs and analysis were completed for the major components, system integration studies yielded a reduction of estimated pumping system and electrical system power losses, leading to an upgrading of the powerplants to

1200 KWe and 4800 KWe respectively. It was decided to retain the same major components and accept the power change rather than revise all the component calculations and design layouts.

1. 1.2 MWe Turboelectric Vehicle

To appreciate the reasoning behind the design of this nuclear electrical vehicle, it is pertinent to consider some of the design decisions, before presenting the vehicle decriptions.

a. Fixed Versus Folding Design

At the 1200 KWe power level, the optimum radiator area is somewhat greater than the envelope limits of the SATURN V (3 stage) booster payload. Actually, fin efficiency is a parameter which permits radiating area to be traded for weight. Therefore, by employing a fin efficiency in excess of 90%, a fixed conical configuration can be achieved. On the other hand, a folding configuration permits a lower fin efficiency to be used with the associated lighter weight matrix. Whether or not the complete spacecraft using a folding optimized radiator would be lighter than a fixed conical off-optimum radiator cannot be determined without a fairly detailed study of the respective problems. It was therefore decided to look at both. The folding configuration chosen was the so-called "clamshell" design which gives the structural and packaging advantages of the conical design during launch, and an improved view factor following deployment.

b. Redundancy Considerations

Since the conical configuration is already hard pressed to accomodate the basic radiator area requirements, conventional area redundancy is obviously out of the question. However, the folding clamshell is not so restricted. On this basis, added usefulness from the folding clamshell versus fixed conical comparison was identified with applying redundancy to the former, and this was used as a design ground rule. Specifically the folding design was given eight separate loops, one of which was redundant. With four

condensers in the EGS, the number of radiator loops is constrained to multiples of four. As the number of independent loops increase, the complexity of feed line piping and the associated weight rises, tending to defeat the advantages of redundancy. The selection of eight loops was based on judgement and does not necessarily constitute an optimum.

Aside from the application of redundancy, there are advantages to employing a multiplicity of independent radiator loops, even if no redundant area is provided. Doing this permits a step function deterioration of power with improved probability of obtaining part power. There is a weight penalty associated with the added plumbing complexity, but this was judged acceptable and the conical configuration was designed with eight independent fluid loops in the radiator.

One other aspect of redundancy which deserves mention is the possibility of using redundant tubes without redundant fins. This would permit redundancy to be applied to the conical design without incurring an area problem. There are also benefits in improved fin efficiency following puncture of one circuit. Use of this concept was not pursued as part of the studies reported herein.

c. Fixed Conical Design Description

Figure 4-16 shows the general arrangement of the fixed conical design as it would appear during the launch phase of flight. Since the radiator uses up almost all of the available payload envelope, there is no axial length available for packaging the payload and propulsion subsystems. The cavity within the radiator is readily adaptable to accommodate this packaging need, but the bulky communication antennas present a problem. By designing the entire payload and propulsion package as an integrated module, and deploying it after launch, erection of the antennas can be easily effected and the flight configuration appears as illustrated in Figure 4-17.

Packaged for boost, the total vehicle is a cylinder capped with a conic frustum. The maximum diameter is 260 inches and the overall length, including the ejectable aerodynamic nose cap, is 54.3 feet. Gross weight of the vehicle at launch is approximately

91,500 pounds, including 1500 pounds for the nose cap which covers the upper portion of the power system from station 3689 to 3907 as illustrated in Figure 4-16.

The reactor (7.6 MWt) and its radiation shield are mounted at the top of the vehicle taking full advantage of the conical shape of the payload envelope volume. All of the power generating components (including the super-heater, boilers, turbine, generator and condensers) are integrated within a single hermetically sealed shell which also houses the pumps for the reactor and primary radiator fluid loops. The installation of multiple turbogenerators does not significantly influence the system mechanical design using this integrated electrical generation system arrangement. As shown in Figure 4-16, the power package is mounted immediately below the shield and is enclosed by the powerplant and shield cooling secondary radiator which also serves as the mounting structure. This radiator provides 333 square feet of heat rejecting area and has an effective temperature of 600°F. The nuclear radiation shield is composed of a primary cone and a scatter ring.

The remainder of the external shell of the vehicle consists of primary radiator. As indicated above, it incorporates no area redundancy, but is divided into eight independent fluid loops such that failure of a single loop for any reason knocks out an average of only 12.5 percent of the system power capacity. Each fluid loop of the primary radiator is confined to a 360-degree segment or bay, which results in an average tube length of just under five feet. Short tubes require many headers with their associated bumpers and joint structure. One means of lengthening the tubes in this design would consist of splitting a bay into two 180-degree segments, each constituting one of the individual radiator loops. This was judged undesirable due to the dimensional instability of the vehicle axis that would result from failure of one of these 180° segments. Another more attractive solution to this problem was identified but not given detailed examination in this study. It consists of dividing each bay in half in such a way that alternate tubes are served by separate headers. For example, four bays can accomodate eight individual circuits while retaining thermal symmetry about the vehicle axis following a loop failure. This is illustrated in Figure 4-18. In addition to the possibilities

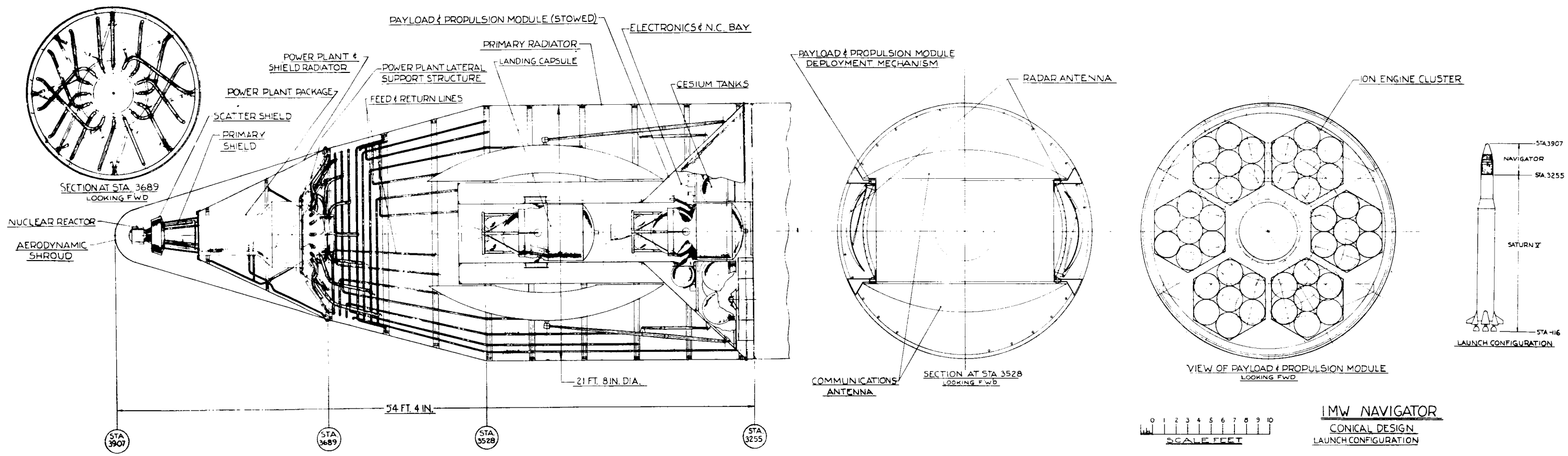

Figure 4-16. 1.2 MW Fixed Conical Vehicle - Launch Configuration

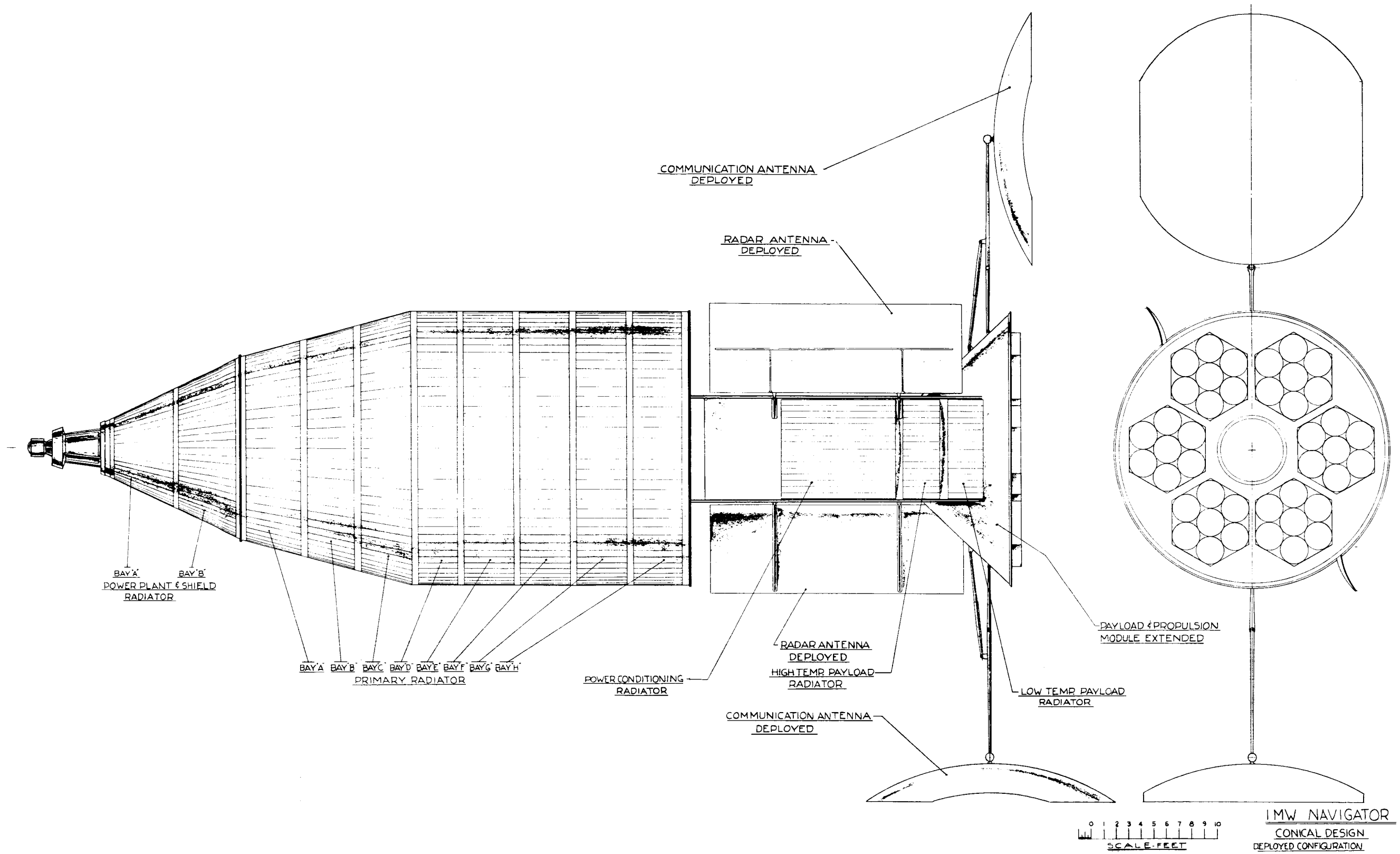

Figure 4-17. 1.2 MW Fixed Conical Vehicle - Deployed Configuration

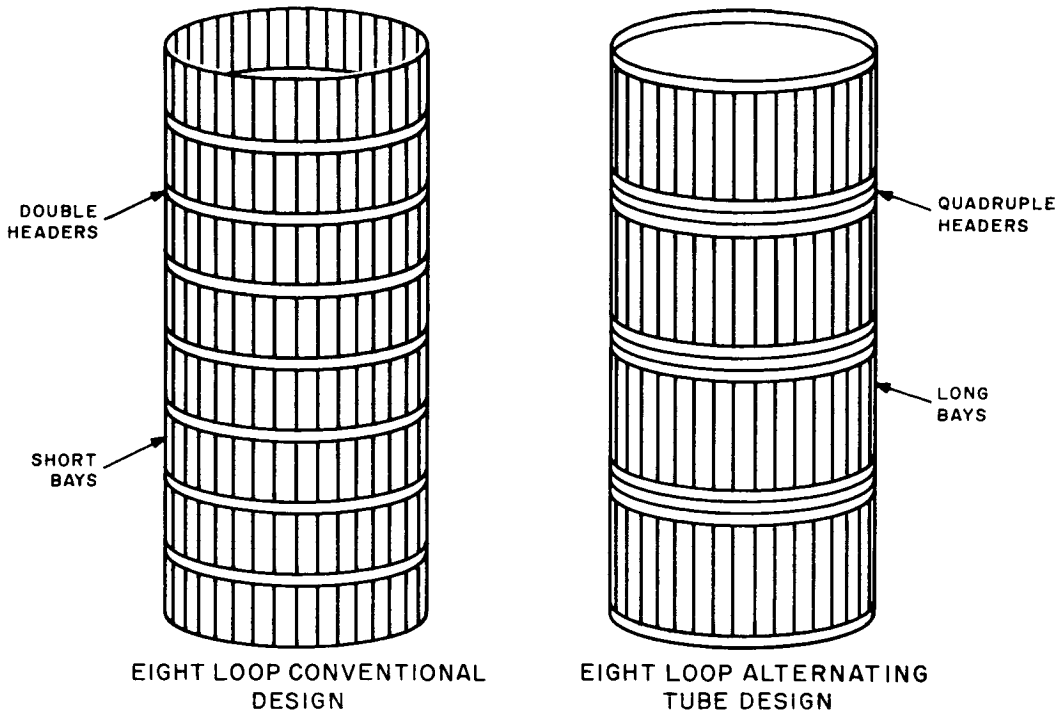

Figure 4-18. Comparable Approaches for Axial Tube Multiple Loop Designs

of weight savings in the headers, etc., this concept has the added feature of reducing the percent rate of degradation for a given number of independent loops. This results from the "dead" circuit functioning as additional fin for the associated "live" circuit.

Examination of differential thermal growth rates between the headers and the radiator matrix shell dictated that each bay of the primary radiator be subdivided into four 90-degree panels. Figure 4-19 illustrates the resulting feed and return line arrangement required to service each bay. The apparent complexity results from the practical need to structurally support these lines, and to provide flexibility to account for the differential thermal expansion between these lines and the radiator itself. Geometrical restrictions preclude the use of equal area primary loops; hence each primary bay on the conical portion, and one on the cylindrical section, each reject 720 kilowatts from 263 square feet of surface while each of the four remaining loops reject 832 kilowatts from 303 square feet. Condenser heat balance is maintained by pairing a large and small loop with each condenser.

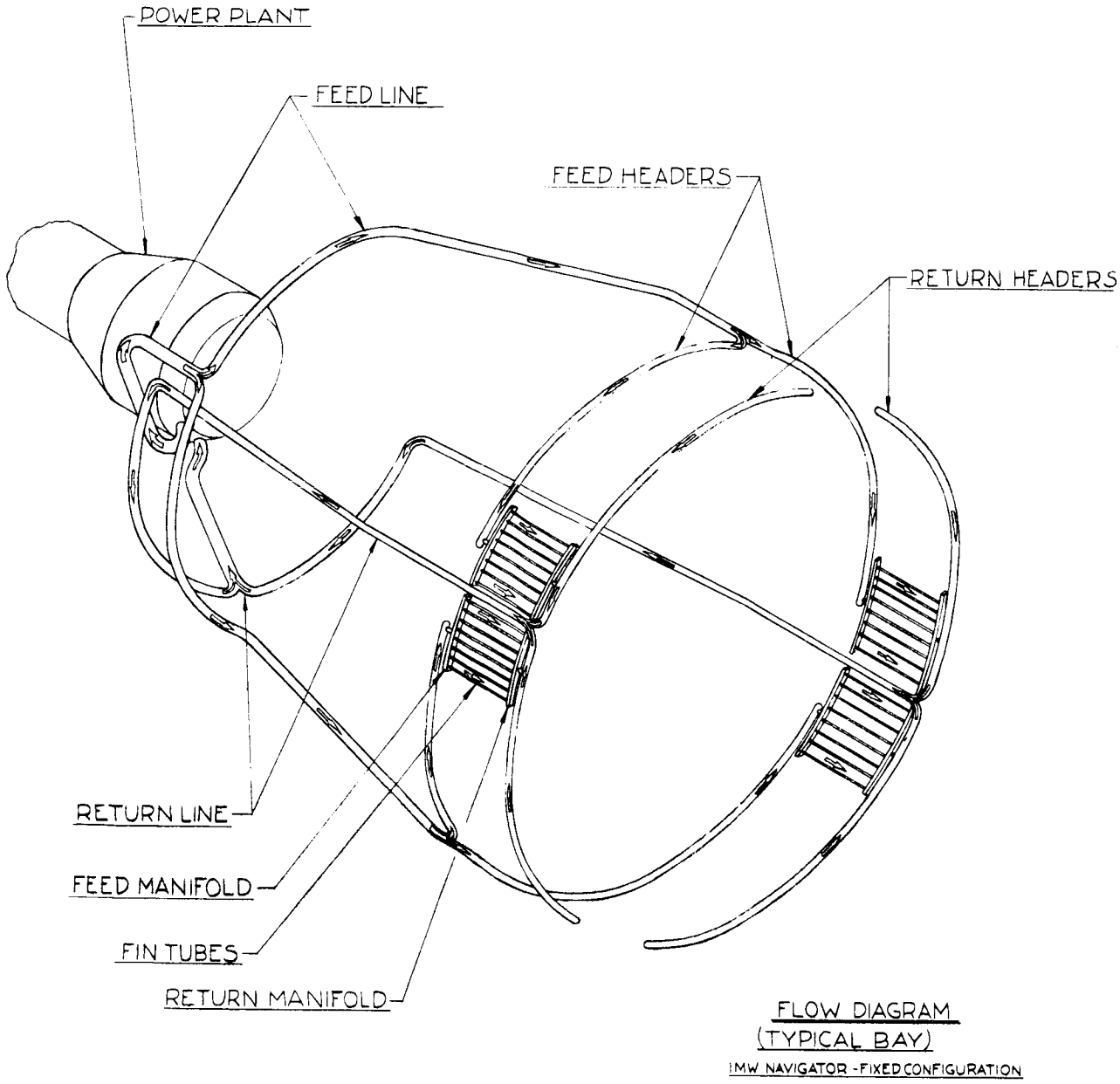

Figure 4-19. Feed and Return Line Arrangement - 1.2 MW Fixed Conical Vehicle

Payload systems, attitude control, and power conditioning equipment are packaged in the conical section of the deployable payload module. Two landing capsules, with umbilical connections for internal cooling and electrical connections, can be mounted in the central tube. This tube is insulated, and in critical areas, jacketed by an active cooling loop to maintain the temperatures required for biological experiments and chemical propellants. Depending upon mission requirements, one landing capsule may be eliminated in favor of other payload systems or higher propellant fractions.

Two modified 20-foot diameter rigid dish parabolic antennas are included for long range communications. The antennas are secured to the payload module during launch, and extended to operating positions by telescoping control arms after deployment of the module. Two rectangular radar mapping antennas have also been incorporated in the designs presented.

Electric engines are arranged in six clusters of seven modules each, and cluster gimbaling is provided to allow thrust vectoring. This engine arrangement affords 170 square feet of engine beam area without resorting to a deployable engine concept. Propellant storage tanks are located in the annular volume just forward of the ion engines.

With this modular arrangement, the deployment is achieved without the need for folding fluid lines, since the secondary radiators for both payload and power conditioning cooling are also incorporated into the deployable assembly. The only major powerplant connection crossing the deployment interface is the electrical supply from the generator to the power conditioning. An alternate arrangement could have placed the power conditioning on the primary structure but the area restrictions left insufficient room to accommodate the associated secondary radiator. A summary of the major vehicle weight items is furnished in Table 4-2 with a detailed breakdown of the radiator weights in Table 4-3.

TABLE 4-2. 1.2 MWe TURBOELECTRIC VEHICLE WEIGHT SUMMARY*

Powerplant	
Reactor & Primary System**	2,370
Turbomachinery	2,600
Boilers, Condensers, Pumps and Piping	3,440
Powerplant Containment Structure	1,360
Power Conditioning and Controls in EGS Assembly	1,730
Bus Bars and Rear Power Conditioning	694
Primary Radiators (2264 sq. ft.)	8,510
Secondary Radiators (477 sq. ft.)	950
	21,654 lbs
Shield	3,400 lbs
Propulsion System	
Thrustors	1,440
Propellant and Tankage	46,900
	48,340 lbs
Payload Systems***	
Landing Capsule	2,670
Mapping Radar	2,000
Sensors, TV and Radar Altimeter	430
Communications Transmitter	3,000
Antennas	700
Computers, Recorders and Receivers	125
Payload Cooling System	910
	9,835 lbs
Spacecraft	
Navigation, Guidance and Attitude Control	2,700
Payload Support Structure	980
Tank Support Structure	1,591
	5,271 lbs
Spacecraft Initial Flight Weight	88,500 lbs
Aerodynamic Nose Fairing	1,500 lbs
Start-up System	1,500 lbs
Spacecraft Weight on Booster	91,500 lbs

*Net electrical power to the electric thrustor power rectifier and space vehicle load is 1217 KWe, yielding an unshielded nuclear powerplant specific weight of 17.8 lb/KWe.

**Reactor and Shield based on a 12 inch diameter, 18 inch long reactor core.

***Payload weights are based on Saturn Orbiter I mission described in GE Document No. 64SD505 (Mission Analysis Topical Report).

TABLE 4-3. 1.2 MWe TURBOELECTRIC VEHICLE PRIMARY RADIATOR WEIGHT BREAKDOWN

Description	Weight (lbs)	
Inconel Tube Liners	455	
Beryllium Tube Armor	1530	
Beryllium Fins	1665	
Inconel Manifolds	178	
Matrix Dry Weight		3828
Inconel Headers	325	
Beryllium Header Bumpers	122	
Inconel Feeds and Returns	1535	
Plumbing Dry Weight		1982
Coolant in Tubes*	147	
Coolant in Manifolds*	221	
Coolant in Headers*	402	
Coolant in Feeds and Returns*	973	
Expansion Reservoir Coolant	280	
Total Coolant Weight		2023
Header Joint Splice Structure**	499	
Miscellaneous (Fasteners, Hard-points, etc.)	178	
Total Structural Weight		677
Total Primary Radiator Weight (2264 sq. ft.)		8510

*Coolant weights correspond to operating temperature
**This structure is associated with practical assembly

Note No structural additions are required to enable this primary radiator to carry the launch loads, or the aerodynamic loads normally associated with a fairing.

d. Folding Conical (Clamshell) Design

During launch, the folding conical design has a very similar appearance to the fixed conical design as can be seen by comparing Figures 4-16 and 4-20. The main differences lie in the feed-line arrangement and the special provisions associated with deployment. Packaged for boost the overall length is approximately 53 feet, including a short booster adapter section, and the gross weight is 91,500 pounds.

To provide increased radiating surface, the vehicle is split longitudinally and rotated about the hinge at the base of the cylindrical section. A second 180-degree rotation of the payload module, and extension of the antennas, completes the deployment sequence leading to the flight configuration as shown in Figure 4-21. When the deployment is effected, the reactor, shield, and power generation module remain on one half of the radiator, and the payload/propulsion module moves with the other half. After completion of deployment, a large separation distance is achieved between the reactor and the payload. This permits economies in shield weight due to both reduced thickness and reduced shadow angle.

Effective radiating area for the primary radiators of the folding configuration is over 3100 square feet as compared to 2264 square feet for the fixed conical vehicle. The radiator system is again segmented to allow eight fluid loops. However, in contrast to the fixed conical design, heat rejection capabilities are based on one loop being a redundant circuit. Each radiator loop is again confined to a single bay, but in this case they are 180-degree segments of arc and are divided into two 90-degree panels. The tube lengths are close to eight feet, which is more desirable than the short tubes of the fixed conical design. Feed lines from the power package run along the center line on the concave side of the radiator panels. Bays D and E are slightly larger than other primary bays to account for view-factor degradation by the feed line arrangement. Feed lines servicing primary Bays E through H must crossover the folding joint in the primary radiator. The helical joint concept illustrated accomplishes the fluid transfer by means of elastic deflection of the feed lines. This and other fluid joint concepts are discussed in detail in the Second Quarterly Report, GE document 63SD886.

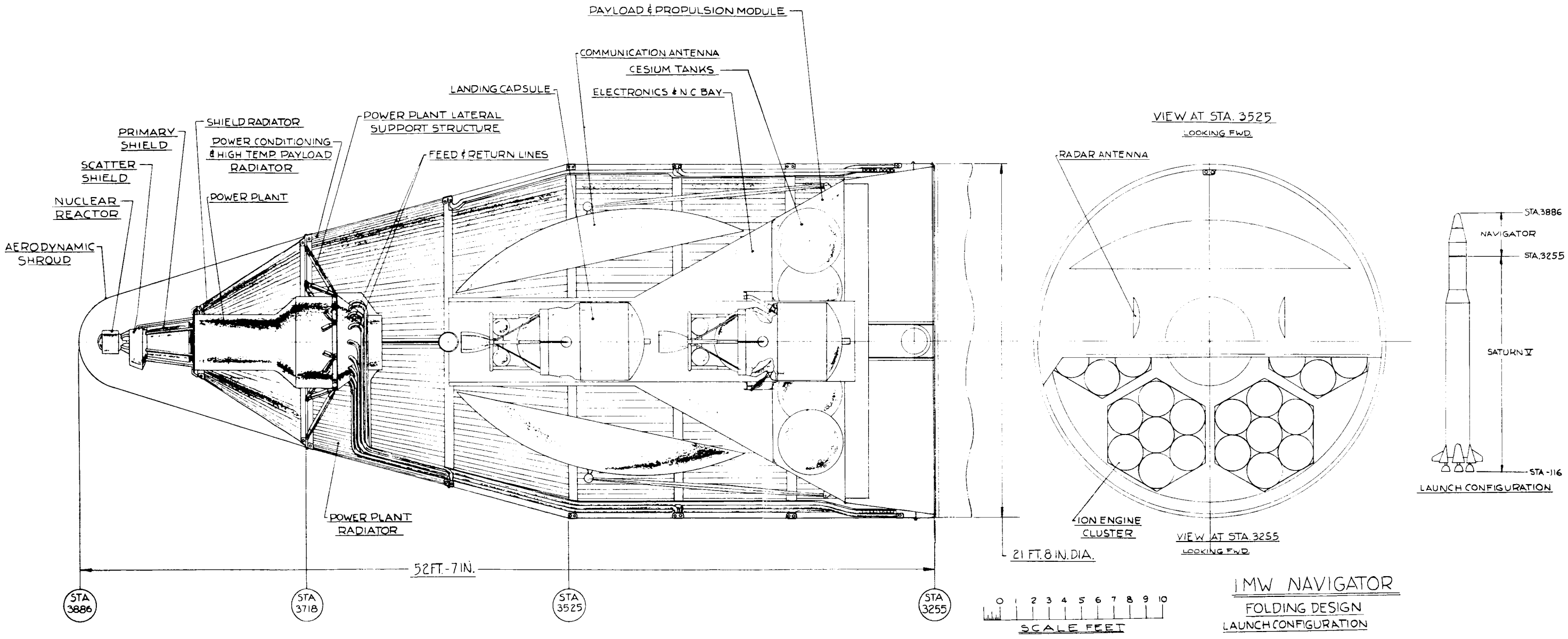

Figure 4-20. 1.2 MW Folding Vehicle - Launch Configuration

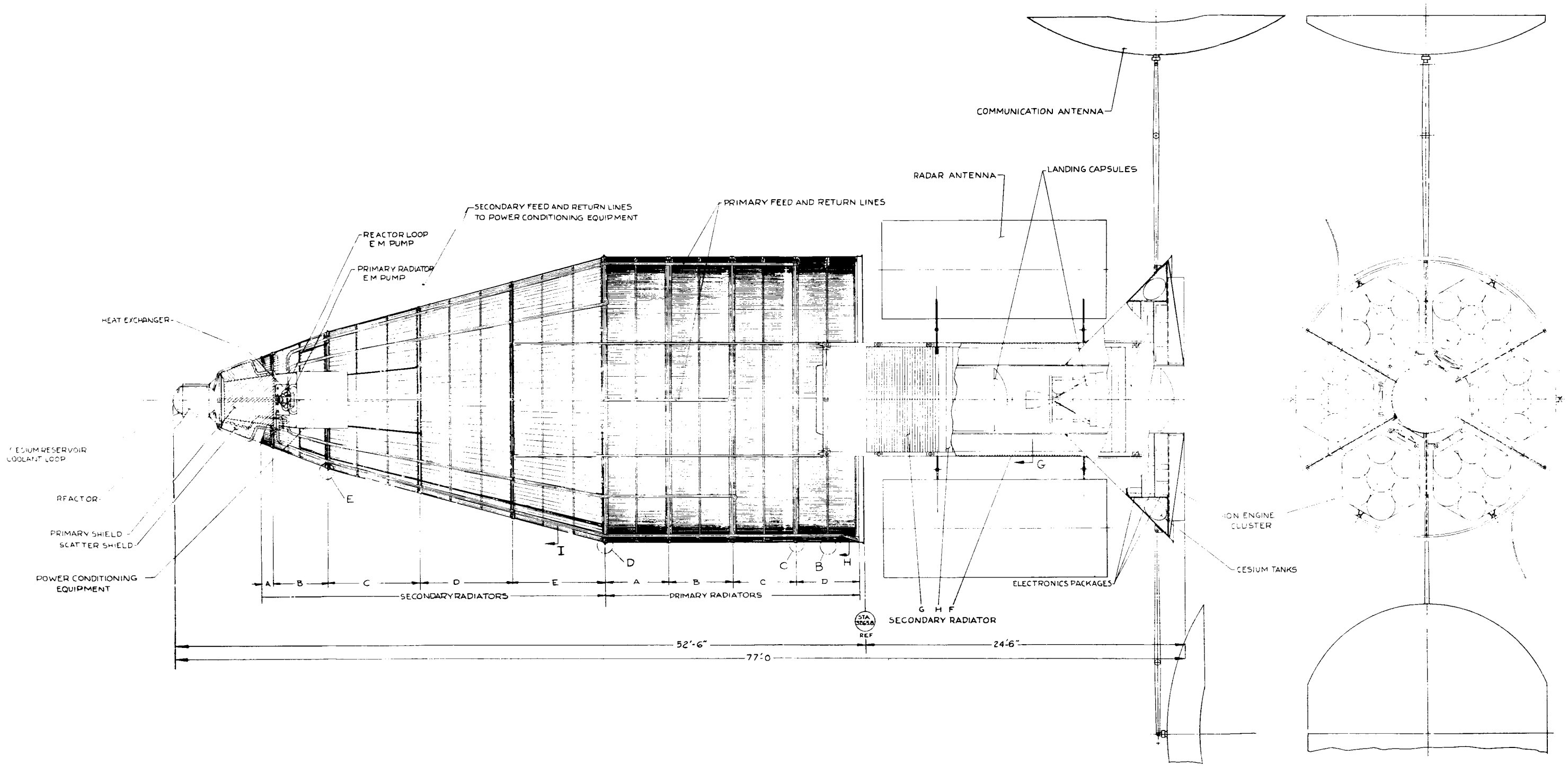

Figure 4-25. Deployed Configuration of the 1 MWe Thermionic Vehicle

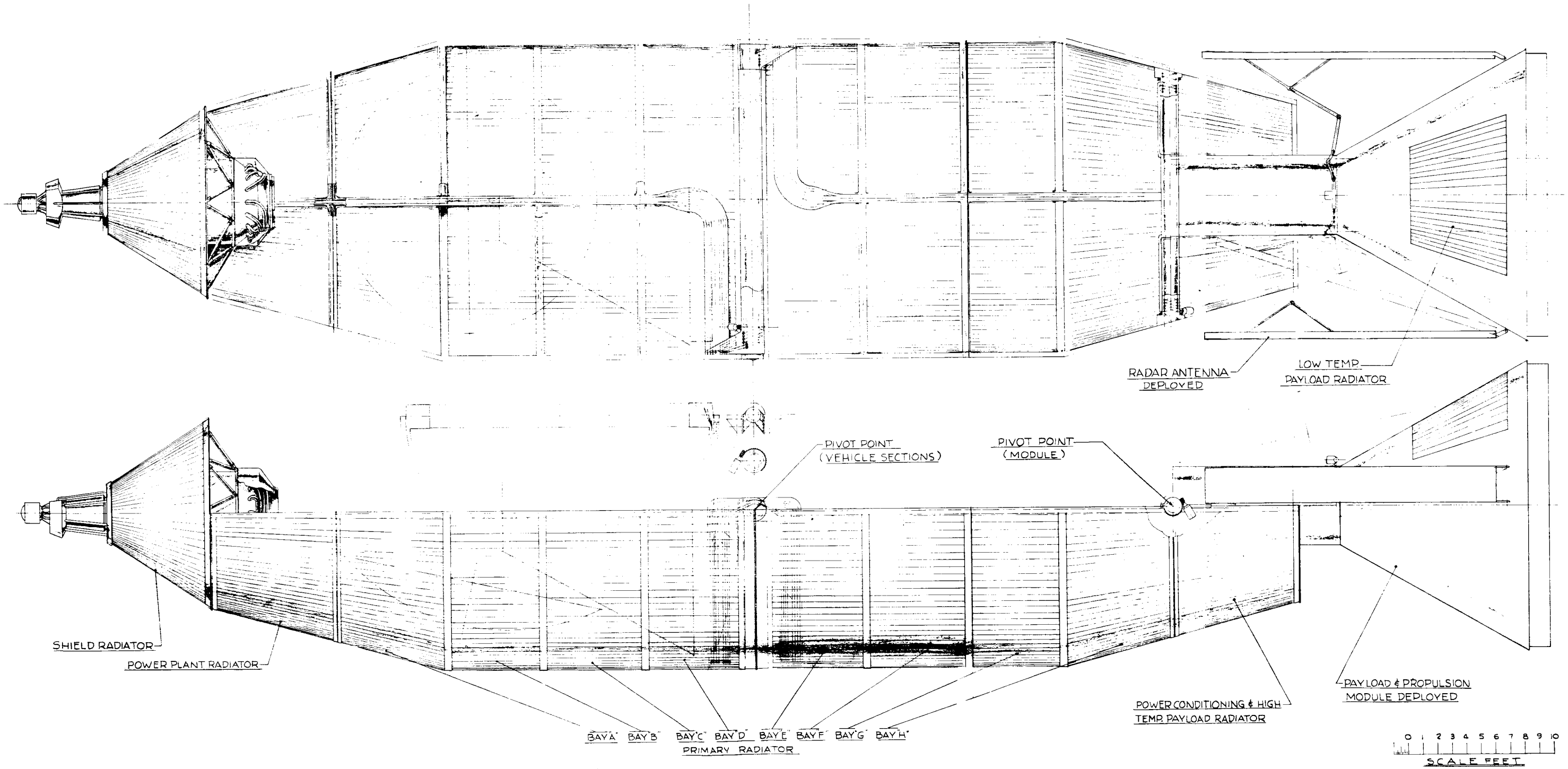

Figure 4-21. 1.2 MW Folding Vehicle - Deployed Configuration

The weight comparison between the fixed and folding conical designs was made fairly early in the program, concurrently with the identification of the magnitude of the NaK inventory and feed-line weights. Subsequent reiterations to better optimize and account for these factors were only applied to the fixed conical design; hence, the detailed weights in Table 4-3 do not permit a consistent comparison. Table 4-4 compares detailed weights for both designs on the earlier basis, and the conclusions drawn are not materially altered by subsequent work.

TABLE 4-4. COMPARISON OF FIXED AND FOLDING CONICAL PRIMARY RADIATOR WEIGHTS

Description	Folding Configuration Weight (lbs)	Fixed Configuration Weight (lbs) *
Fins and Tubes	2,980	3,210
Manifolds	220	180
Headers (excluding bumpers)	160	290
Feeds and Returns (including bumpers)	1,220	1,550
NaK Inventory	2,520	2,820
Header Bumpers (Structural)	800	620
Additional Structural Rings	170	180
Sub Total	8,070	8,850
Folding Joint Plumbing	270	---
Folding Joint NaK	960	---
Folding Joint Bumpers (Structure)	280	---
Actuators	50	---
Longitudinal Seam Joints	130	---
Total	9,760	8,850
Difference in System Weight		
Pump Work Penalty	580	
Effective Total	10,340	8,850
Radiator Area, sq. ft.	3,100	2,264

*Not Final Radiator Selection (See Table 4-3.)

As to be expected, the higher view factor, unrestricted area, and redundancy of the folding design yield a substantial weight saving in the basic radiator. The reduced weight of the fin-tube matrix permits corresponding savings in the headers, feeds, and fluid inventory. Since the header bumpers also serve as primary structural rings, they are identified separately; the lower weight for the conical design reflects the benefits of meteoroid self-shielding by the fins. Comparing the subtotals, a savings of roughly 9 percent can be claimed for the basic radiator of the folding design.

Examining the requirements of the folding joint identifies a heavy weight item and a controversial issue. Using a helical coil piping joint (see second quarterly report), which depends purely on elastic strain of smooth tubes for the desired flexibility, a total weight of nearly 1700 pounds is associated with the deployment feature. In addition to this, the large increase in system pressure drop associated with such a joint introduces a further penalty of 580 pounds, based on an assumed penalty rate of 25 pounds/kw. To reduce the weight of the joint, other concepts were examined. The imagination of the designer is the only limit to this pursuit, but it seems to be axiomatic that the weight varies inversely with the confidence in practical reliability being eventually achieved. For example, the use of bellows was examined and yields a weight saving of roughly 1100 pounds in the joint weight and 390 pounds in the pump-work penalty. Applying these changes to the results of Table 4-4 makes the two designs equal in weight. Because of the lower reliability of bellows, the choice of the fixed conical would still be made. In fact, if a fixed design is reasonably usable, it is probable that a folding alternative would have to show a very substantial weight advantage to justify its ultimate selection for a hardware program.

e. Start-up, Checkout, and Preheat

In Section 5-B of this report, some of the details of construction are considered, but even at this point it is clear that the radiator is a complex of plumbing for which high mechanical reliability will be difficult to achieve. During assembly of the entire spacecraft, there will be numerous opportunities to damage the integrity of the

radiator loops. This could take the form of bent tube connections, internal foreign material, leaks, etc. Whereas the compactness of the other powerplant components permits them to be more readily protected from handling damage, the radiator is inherently more vulnerable. A brief survey of the checkout and startup problems provides some general guidance in the procedures that will be required with a nuclear electric spacecraft.

Prevention of working fluid freeze-up prior to reactor activation is a major part of the system start-up problem; arguments for and against a liquid third loop radiator for the Rankine cycle are intimately tied with it. Two means are available for introducing the working fluid into the system:

- Store fluid in a reservoir, to be released into the system concurrent with reactor activation.
- Circulate the fluid through the system from the moment prelaunch charging is completed.

Where the turbine is concerned, the first approach must be used, and it is not difficult to imagine successfully vaporizing the fluid in the boiler and expanding it through the turbine. However, controlling the heat rejection side of the cycle to prevent freeze-up of the fluid front as it fills the system will require maintaining all the piping at a slightly elevated temperature. When the radiator is included in the circuit, this implies a complex and heavy system to achieve preheating in space, or to retain the energy of a prelaunch preheat.

With the second approach, heat can be continuously added to the circulating fluid to maintain its temperature sufficiently above the freezing point. The ready compromise afforded by the compact heat exchanger condenser and third-loop liquid radiator is evident. By maintaining the two-phase flow part of the cycle in a compact package, the problems of preheating are minimized and the reactor can potentially be used as the energy source. The radiator loop, using NaK as a working fluid, requires a minimum level of heat addition to maintain a temperature sufficiently above the freezing point.

With only a small mass relative to its surface area, the radiator is a very poor place to store heat, and high temperatures are needed to achieve any useful delay in freezing. This leads to very large insulation requirements. On the other hand, by circulating the fluid at low temperature and impeding heat rejection with a radiation barrier, a low heat flow rate can be readily achieved, and energy can be supplied to the fluid by a suitable compact heater. This approach can permit very long waiting periods for moderate energy expenditure. Maintaining an average radiator temperature of 200°F will result in approximately 50 watts per square foot heat rejection. A simple radiation barrier would reduce this by a factor of roughly 25, in which case the 2570 square feet of the conical design would reject only 5140 watts. Using a hydrogen-oxygen system as an energy source would require about 15 pounds/hour of mixture to provide both pumping power and thermal energy. In concept, the required radiation barrier can be quite light, since it can rest on the radiator and carry no loads.

With this radiator start-up approach in mind, it is now pertinent to retrace the prelaunch steps and see how they can enhance the achievement of a successful mission. Upon completion of the assembly of the flight powerplant, whose radiator is also the vehicle outer shell, various system checks would be made including leak checks of the radiator loops. To best achieve a good working radiator, purging and charging should be accomplished under well controlled conditions. It will require elevated temperatures and probably substantial flushing and chemical analysis to assure that impurity levels are within specifications. By doing this on the ground, any evidence of cold trapping, plugging, etc. will be detected and corrected. Following charging, it should be relatively easy to maintain sufficient flow and heat addition on the ground to prevent any plugging difficulties, and it will be possible to roughly check the radiator flow balance. If the spacecraft is installed on the booster with its radiator loop operating in this way, the start-up and mission success probability should be significantly enhanced.

2. 4800 KWe Turboelectric Vehicle

The 4.8 MWe turboelectric vehicle design study was based on the use of four of the 1.2 MWe electric generation system modules, and follows the same general philosophy as the 1.2 MWe vehicle. As illustrated in Figure 4-22, the configuration consists of two independent structural assemblies. Both of these are mounted at their bases to an adapter section that joins the vehicle to the SATURN S-II stage at Station 2537. This allows an 18-inch-long bay for the booster equipment package extending from Station 2519 to 2537.

The adapter section, spanning between Stations 2537 and 2555, supports the vehicle external shell, which consists of fourteen bays of cylindrical primary radiator (between Stations 2555 and 3536) and two additional conical primary radiator-bays (between Stations 3536 and 3684). Four bays of conical secondary radiator and one conical bay for the shield cooling loop radiator form the external shell from Station 3684 to Station 3879. From Station 3879 to Station 3981, a monocoque shell mounts the reactor and shield to the top of the radiator. In addition, the joint at Station 3879 also connects the aerodynamic shroud to the shield cooling loop radiator bay.

Due to the long length of this vehicle, fluid inventory and feed-line piping weights are reduced by mounting the power conversion units substantially below the reactor as shown in Figure 4-22. Cruciform box beams at Station 3398 support these four 1.2 MW net power unit modules, and the start-up system equipment, distributing the load to the external shell.

The internal structural assembly is a deployable unit which is contained within the radiator during launch, and telescopes to a position aft of the radiator as shown in Figure 4-23. It consists of a structural sandwich cylinder housing the landing capsules and their ejection gear, a conical structure segmented to provide mounting compartments for the payload electronics and hard points for launch storage of steerable dish antennas, and a toroidal ring structure on which the electric propulsion system is mounted. Deployment of this assembly is achieved by means of a

track and roller arrangement. The track beams used for roller guides on the deployable package also serve as mounting members for six flat panel radiators which provide cooling for the payload and power conditioning equipment.

The toroidal ring structure is divided into 52 cells, each containing an ellipsoidal cesium tank. This structure provides meteoroid protection for the tanks, and acts as an adapter reinforcement for the deployable package. Radial members connect the toroidal ring structure to the landing capsule dispenser tube, forming a structural foundation supporting the ion engine arrays. These engines are arranged in nine packages. One of these is stationary and mounted on the vehicle centerline, six are gimballed segments surrounding the stationary package, and two are deployable rectangular arrays. As a payload for the two stage SATURN V launch vehicle, the 4.8 MWe turboelectric spacecraft has an overall length of approximately 130 feet including the aerodynamic nose cap shroud, and a maximum diameter of 33 feet. The total weight at launch is 242,000 pounds, 2000 pounds of which is for the ejectable nose cap. Table 4-5 summarizes the spacecraft major subsystem weights.

3. 1.0 MWe Thermionic Vehicle

The launch configuration of the 1 MWe thermionic vehicle is shown in Figure 4-24. The spacecraft design is based on SCR power conditioning components and non-refractory metal radiators. The conclusions and design may differ under different assumptions. As shown, the spacecraft is 53.5 feet long and has a 260-inch to match the S-IVB stage of the SATURN V booster. The external shell formed by the powerplant radiators and the deployable payload and propulsion module are again designed as two structurally independent assemblies supported on the booster by a common mounting ring. The cylindrical primary radiator and conical secondary radiator support the reactor, nuclear radiation shield, and power conditioning equipment as illustrated in Figure 4-25. An adapter section joins the base of the primary radiator to the booster. Attachment to the bolt circle on the booster instrumentation package is made utilizing access provisions in the adapter section. Separation of the spacecraft takes place by explosive release of a V-band clamp holding flanges on the primary radiator and the top of the adapter section.

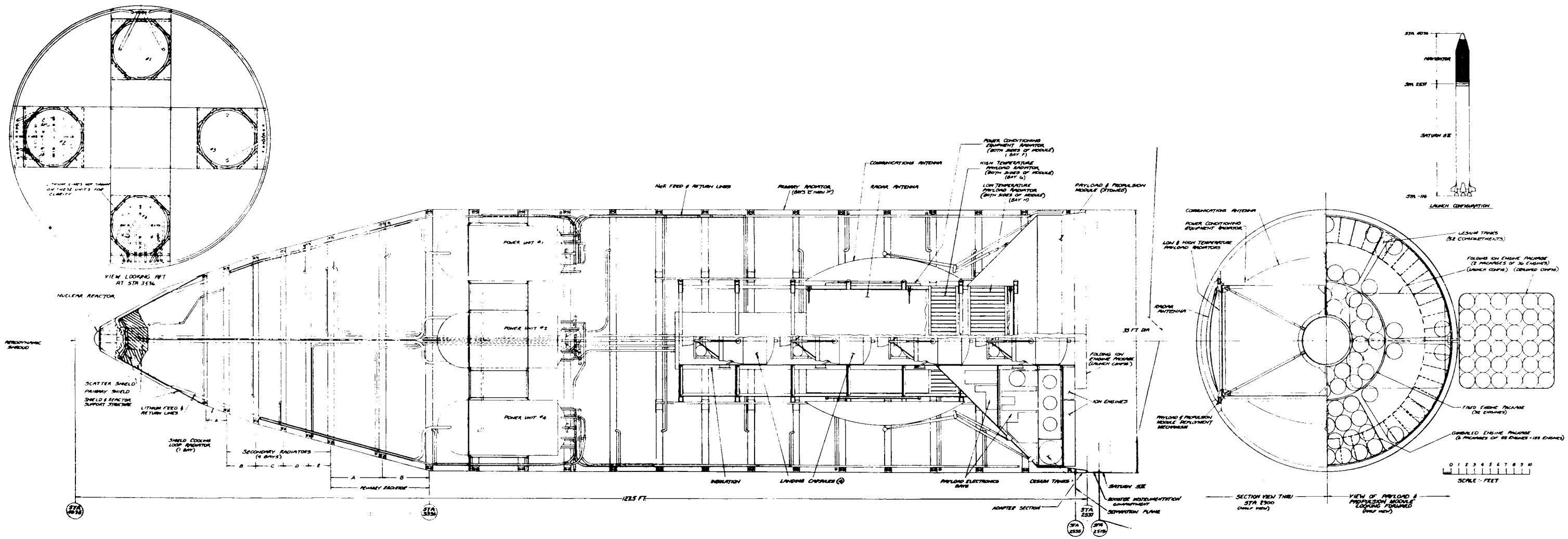

Figure 4-22. Launch Configuration of the 4.8 MWe Turboelectric Vehicle

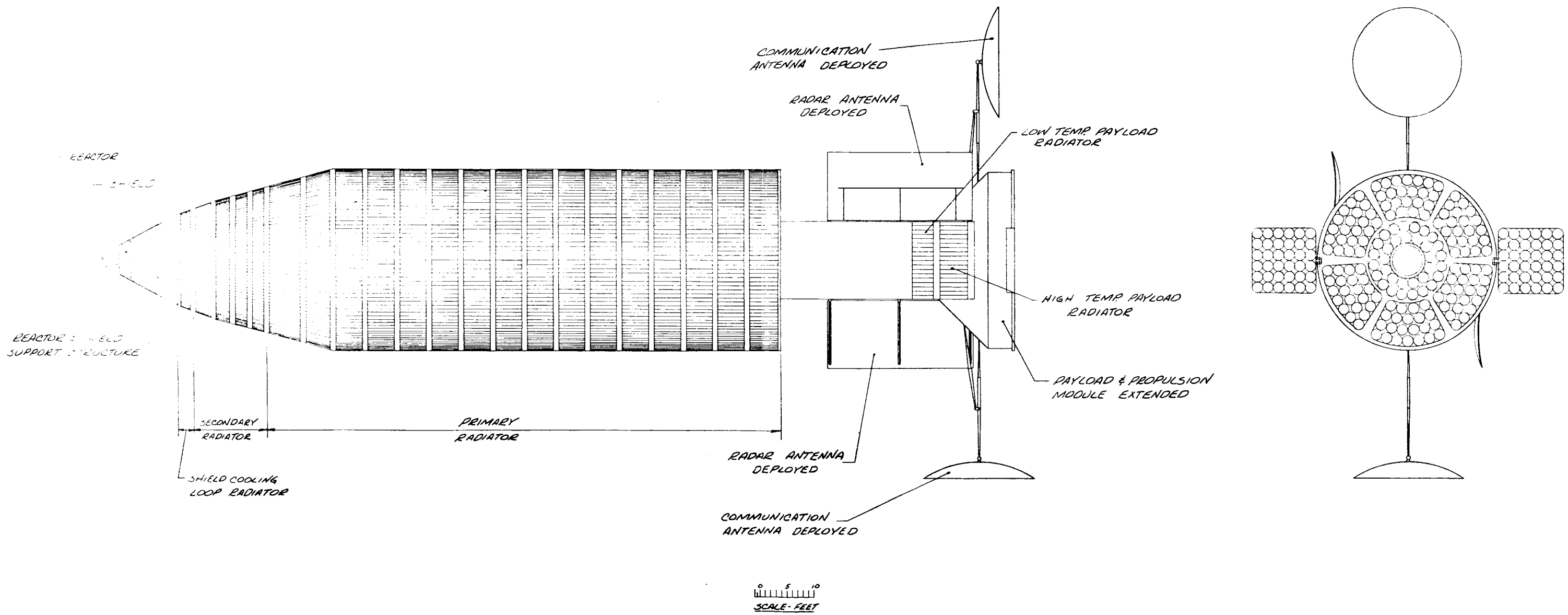

Figure 4-23. Deployed Configuration of the 4.8 MWe Turboelectric Vehicle

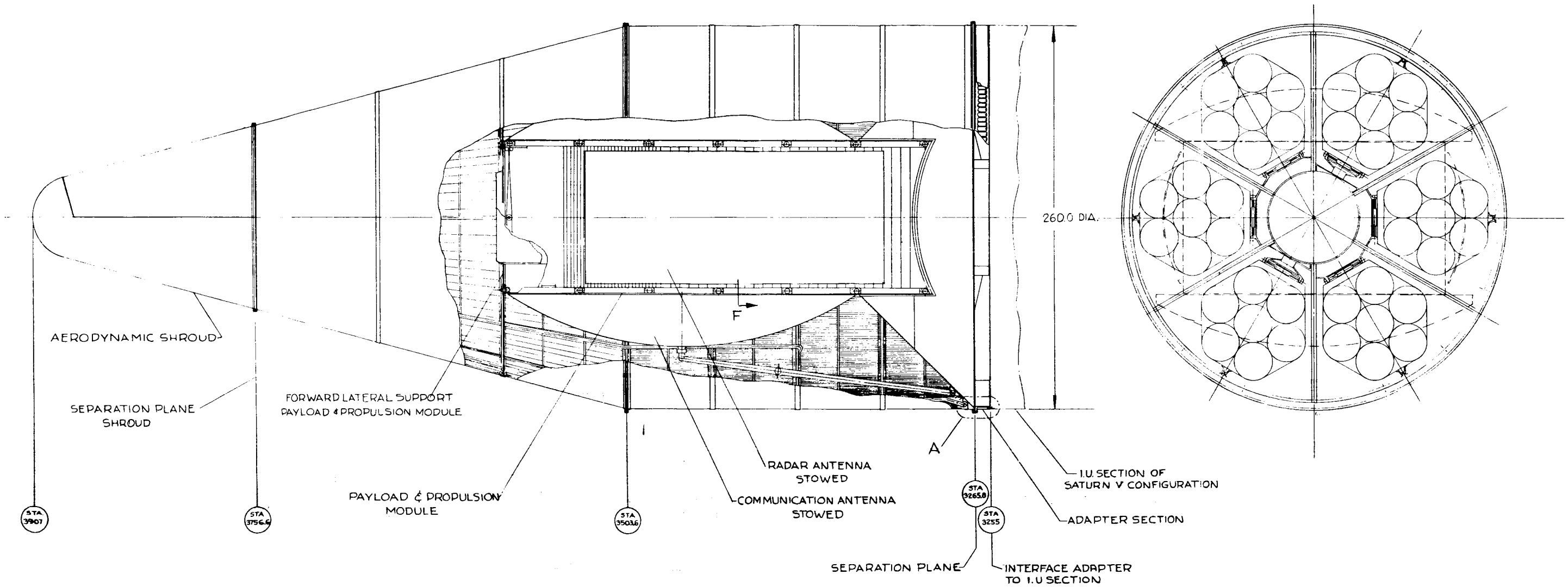

Figure 4-24. Launch Configuration of the 1 MWe Thermionic Vehicle

TABLE 4-5. WEIGHT SUMMARY FOR THE 4.8 MWe TURBOELECTRIC VEHICLE

Powerplant	
Reactor and Primary System	6,480
Turbomachinery	10,400
Boilers, Condensers, Pumps and Piping	13,760
Powerplant Containment Structure	5,440
Power Conditioning and Controls in EGS Assembly	6,920
Bus Bars and Rear Power Conditioning	2,776
Primary Radiator, (9600 sq. ft.)	37,410
Secondary Radiator, (1965 sq. ft.)	3,870
PCS Mounting Structure	1,000
	88,050 lbs
Shield	7,000 lbs
Propulsion System	
Thrustors	5,760
Propellant and Tankage	94,910
	100,670 lbs
Payload Systems**	
Landing Capsules (4)	9,195
Mapping Radar	2,000
High Resolution Radar	7,500
Sensors, TV and Radar Altimeter	430
Communications Transmitter	5,500
Antennas (2-20 Foot Dishes)	700
Computers, Recorders and Receivers	125
Payload Cooling System	2,320
	27,770 lbs
Spacecraft	
Navigation, Guidance and Attitude Control	4,800
Payload Support Structure	2,770
Task Support Structure	2,940
	10,510 lbs
Spacecraft Initial Flight Weight	234,000 lbs
Aerodynamic Nose Fairing	2,000 lbs
Start-up System	6,000 lbs
Spacecraft Weight on Booster	242,000 lbs

*Reactor and shield are based on an 18-inch diameter, 27-inch long, reactor core.
**The Payload Systems Weights are based on a Jupiter Orbiter II Mission described in "Mission Analysis Topical Report," GE Document No. 64SD505.

The payload and propulsion module is mounted within the primary radiator during launch, and extends 24.5 feet beyond the booster interface during flight. The extension of this module exposes additional secondary radiators to space, permits deployment of the communications and radar antennas, and increases the distance between the reactor and radiation sensitive payload equipment. The propulsion module has 36 ion engines mounted in steerable clusters of 6 each with their associated propellant tanks located at the base of the conical section. These tanks are mounted close to the booster interface to reduce bending moments, and close to the outer periphery to reduce the structural span to the outer shell.

Planetary landing capsules are tandem mounted on the axis of the deployable module in a sandwich structure launch tube. Payload equipment is mounted on the sandwich structure shelves which span between the launch tube and the conical section. Payload cooling fluid is circulated through the corrugated core of these equipment shelves. Radial webs are used to stiffen the shelves and the conical section. Surrounding the landing capsule launch tube, and mounting to the conical section, flat panel secondary radiators for payload and power conditioning cooling are arranged to form a rectangular box, the corners of which ride in the guide rails to effect deployment. Deployable radar and communications antennas mount to the external surface of the structural assembly formed by the conic section and rectangular box, and are stowed and snubbed against it during launch.

The primary radiator for the thermionic powerplant has a liquid-metal inlet temperature of 1800°F and an outlet temperature of 1562°F. The inlet temperature was selected to allow use of non-refractory metals in the radiator construction. The outlet temperature was selected by means of a weight optimization study. A limited number of materials are currently available with the capability to operate in this temperature range. Refractory metals such as columbium or molybdenum are the more obvious choices; however, the nickel and cobalt-base superalloys are also potentially applicable. Examination of the relative meteoroid penetration resistance identifies

molybdenum as the better choice with the superalloys (e.g., L605) and columbium alloys (e.g., Cb172 and Cb120) following in that order (see third quarterly report). In terms of high-temperature rupture strength, both molybdenum and columbium alloys are substantially superior to the superalloys.

In terms of fabrication and use, oxidation and welding embrittlement are particular problems with the refractories. In view of the apparent necessity for "field" assembly of a large radiator, the multiplicity of final welds and the associated final stress relieving treatment will present substantial difficulties in the manufacture of refractory metal radiators. Since the need for the higher strength properties is not clearly established at this time, it was elected to complete the thermionic vehicle design based on the use of L605 and the weight data reflects this choice. As a payload for the three-stage SATURN V booster, the 1 MWe thermionic vehicle has a total launch weight of 92,000 pounds, 2000 pounds of which is an allowance for the ejectable nose cap aerodynamic fairing. Table 4-6 summarizes the major elements making up the total spacecraft weight.

TABLE 4-6. 1 MWe THERMIONIC VEHICLE WEIGHT SUMMARY

Powerplant	
Reactor	3,100
Power Conditioning System (SCR's)*	8,935
Bus Bars	1,000
Heat Exchanger and Primary Loop Piping	825
Primary Radiators (1320 sq. ft.)	14,536
Secondary Radiators (2050 sq. ft.)	1,644
	30,040 lbs
Shield	8,000 lbs
Propulsion System	
Thrustors	1,200
Propellant and Tankage	34,350
	35,550 lbs
Payload Systems (Same as Table 4-2)	9,835 lbs
Spacecraft	
Navigation, Guidance and Attitude Control	2,700
Payload Support Structure	980
Booster Adapter	300
Task Support Structure	1,095
	5,075 lbs
Spacecraft Initial Flight Weight	88,500
Aerodynamic Nose Fairing	2,000
Start-Up System	1,500
Spacecraft Weight on Booster	92,000 lbs

*These power conditioning weights correspond to an ion engine system requiring high voltage. If low voltage DC arc jets are used, it may be possible to eliminate almost all power conditioning weights in the thermionic spacecraft.

5. RADIATOR ANALYSIS

In support of the spacecraft studies, detailed thermal analyses of the powerplant radiators for all three vehicles were completed and many of the mechanical design, fabrication, and structural analysis problems were examined in considerable depth. This section covers both the general aspects of this work and the specifics as they relate to the three vehicle designs.

A. THE METEOROID HAZARD

In the vacuum of space, one small puncture in the power generation system circuit would quickly deplete the cycle working fluid. Therefore, meteoroid damage protection is a primary reliability consideration in the design of space radiators. The more common designs consist of a fin and tube configuration which requires appropriate protection of each tube. Other concepts, such as the rotating disk and revolving belt, attempt to solve the meteoroid penetration problem by utilizing puncturable surfaces as the exposed heat rejection face.

Each concept to date, however, has other inherent disadvantages which make the basic fin and tube configuration the most feasible design. Several methods appear possible to circumvent or control the adverse effects of tube puncture resulting from meteoroid penetration.

- Shut-off valving can be employed to isolate an individual tube following puncture. Techniques to effect the closure and detect the punctures can be devised in concept, but this approach presents its own reliability problems due to the complexity of the implied system.
- Self sealants are, in principle, very attractive. Temperature limits and the high vacuum sublimation rates, however, are limiting factors in this approach.
- Thick armor is the most feasible approach but involves a substantial increase in the basic radiator weight. Armor thickness sizing requires an understanding of the environment and the mechanism of puncture; many uncertainties still exist in these areas, but much experimental and theoretical analysis has been expended and design criteria have been developed.

- The bumper concept as proposed by Whipple places a separate expendable surface between the environment and the vital surface. This approach requires substantially less weight than integral armor but can conflict with the thermal performance requirements of the radiator.
- Redundancy can be used in the form of excess radiator area to economize on required armor thickness at a given life and survival probability. This approach becomes attractive for very large systems.

1. Armor Criterion

Criteria used for the establishment of meteoroid armor thickness have varied widely as the store of information concerning this problem has grown. An up-to-date assessment of the meteoroid protection requirements for space radiators and a proposed method for calculating the required armor thickness was reported by Loeffler, Lieblein, and Clough of NASA-Lewis[1] in November 1962. Subsequent work by Whipple, Cook, and others at Harvard[2, 3] resulted in the modification of the values for meteoroid density, flux density, and flux distribution as presented by Loeffler et al. A combination of data contained in these references in addition to unpublished communications between NASA-Lewis and Whipple leads to the following equation for the required armor thickness,

$$t_a = 1.75\delta\left(\frac{\rho_p}{\rho_t}\right)^{\varphi}\left(\frac{\nu}{c}\right)^{\theta}\left(\frac{6}{\pi\rho_p}\right)^{1/3}\left(\frac{a\,Av\,T}{-\ln P_o}\right)^{1/3\beta}\left(\frac{2}{3\eta^{\theta}\,\beta+2}\right)^{1/3\beta}$$

where

t_a = required armor thickness, cm

ρ_p = assumed meteoroid density (0.44 g/cm^3)

ρ_t = density of vulnerable mat'l, g/cm^3

(1) ARS paper #2543-62 "Meteoroid Protection for Space Radiators" by I. J. Loeffler, S. Lieblein-NASA Lewis, Presented at Space Power Systems Conference, September 25, 1962.

(2) AAS paper: "On Meteoroids and Penetration" by F. L. Whipple, Presented at Interplanetary Missions Conference, January 15, 1963.

(3) "Luminance Efficiency of Iron and Stone" by A. C. Cook, L. C. Joechea, and R. E. McCrosky.

ν = assumed meteoroid velocity (9.84×10^4 ft/sec)

C = speed of sound in the vulnerable mat'l, ft/sec

a = assumed meteoroid flux density $\left(5.31 \times 10^{-11} \frac{gm^{\beta} \text{ particles}}{ft^2 \text{ - day}}\right)$

Av = vulnerable area, ft^2 (measured to O.D. of pipes and tubes)

T = time for which protection is desired, days

P_o = probability of no meteoroid penetration

($\delta = 2$, $\varphi = 1/2$, $\theta = 2/3$, $\eta = 1$, $\beta = 1.34$)

NOTE: 1.75 factor related required armor thickness to penetration depth

Incorporating the above data into the equation, converting to engineering units, and utilizing Young's Modulus in place of sonic velocity, a more compact form of the relationship becomes,

$$t_a = \frac{0.448}{\gamma\ 1/6\ E\ 1/3} \left(\frac{AT}{-\ln P_o}\right) 0.249$$

where

t_a = armor thickness, in.

γ = specific weight of vulnerable material, lbs/in^3

E = modulus of elasticity of vulnerable material, psi

A = vulnerable area, ft^2

T = time for which protection is desired, hr.

P_o = probability of no meteoroid penetration

This equation is presented graphically in Figures 5-1 through 5-3 for six radiator design materials of interest; values of armor thickness are related to total vulnerable area and no-puncture probability at room temperature for a 10,000-hour life. Actual operating temperature changes the material Young's Modulus, and hence, the required armor thickness. To account for this a correction factor is given in Figure 5-4 which relates the required armor thickness at temperature to the room temperature values.

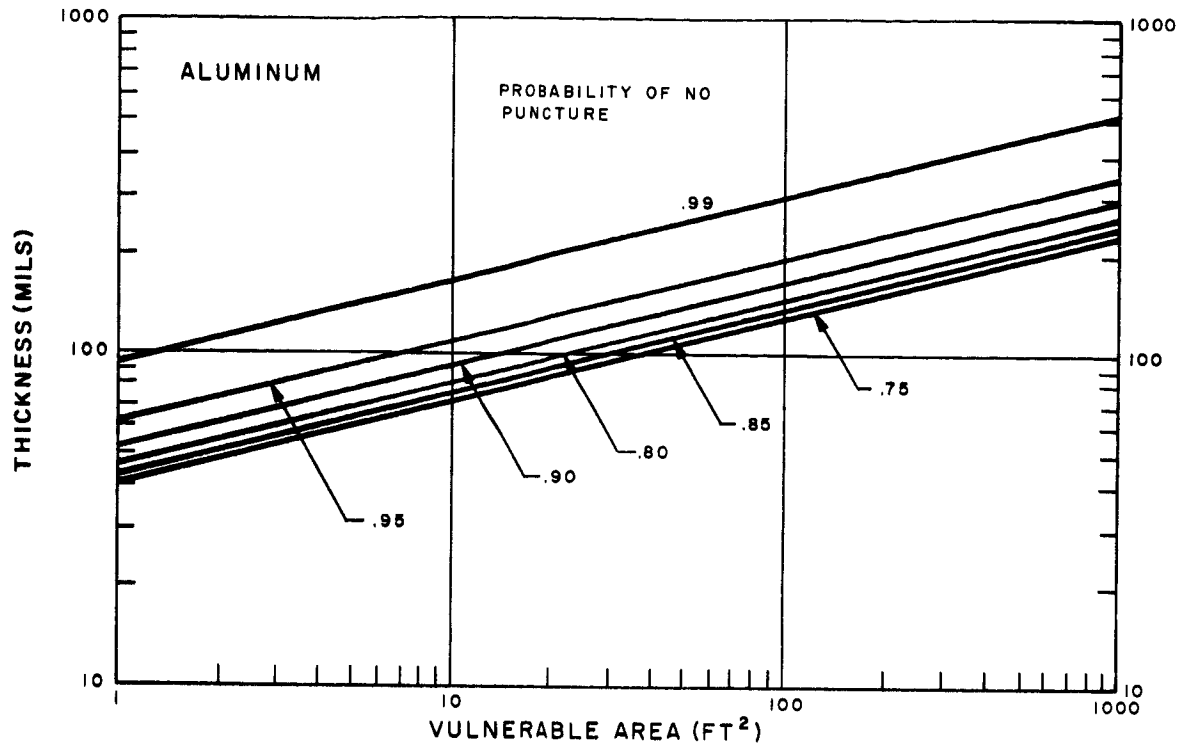

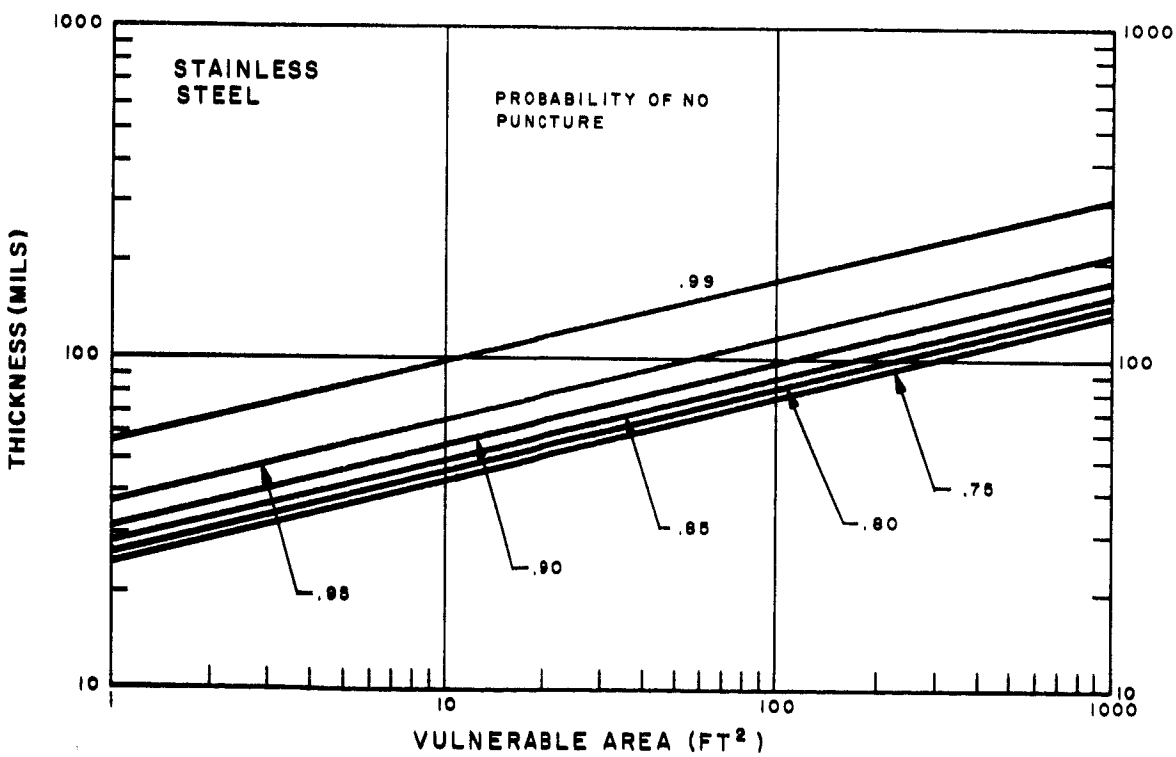

Figure 5-1. Room Temperature Meteoroid Armor Thickness for Aluminum and Stainless Steel (10,000 Hours)

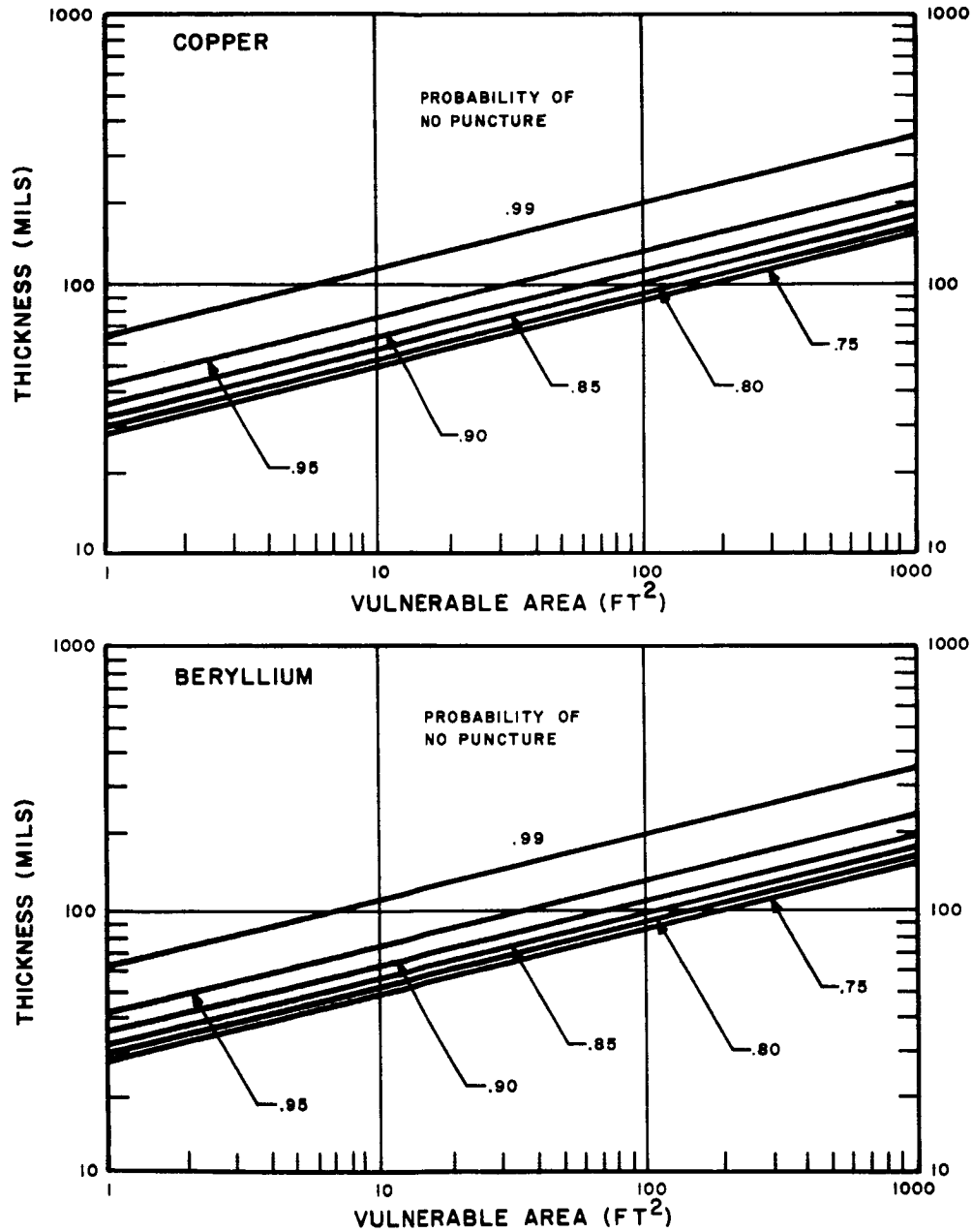

Figure 5-2. Room Temperature Meteoroid Armor Thickness for Copper and Beryllium (10,000 Hours)

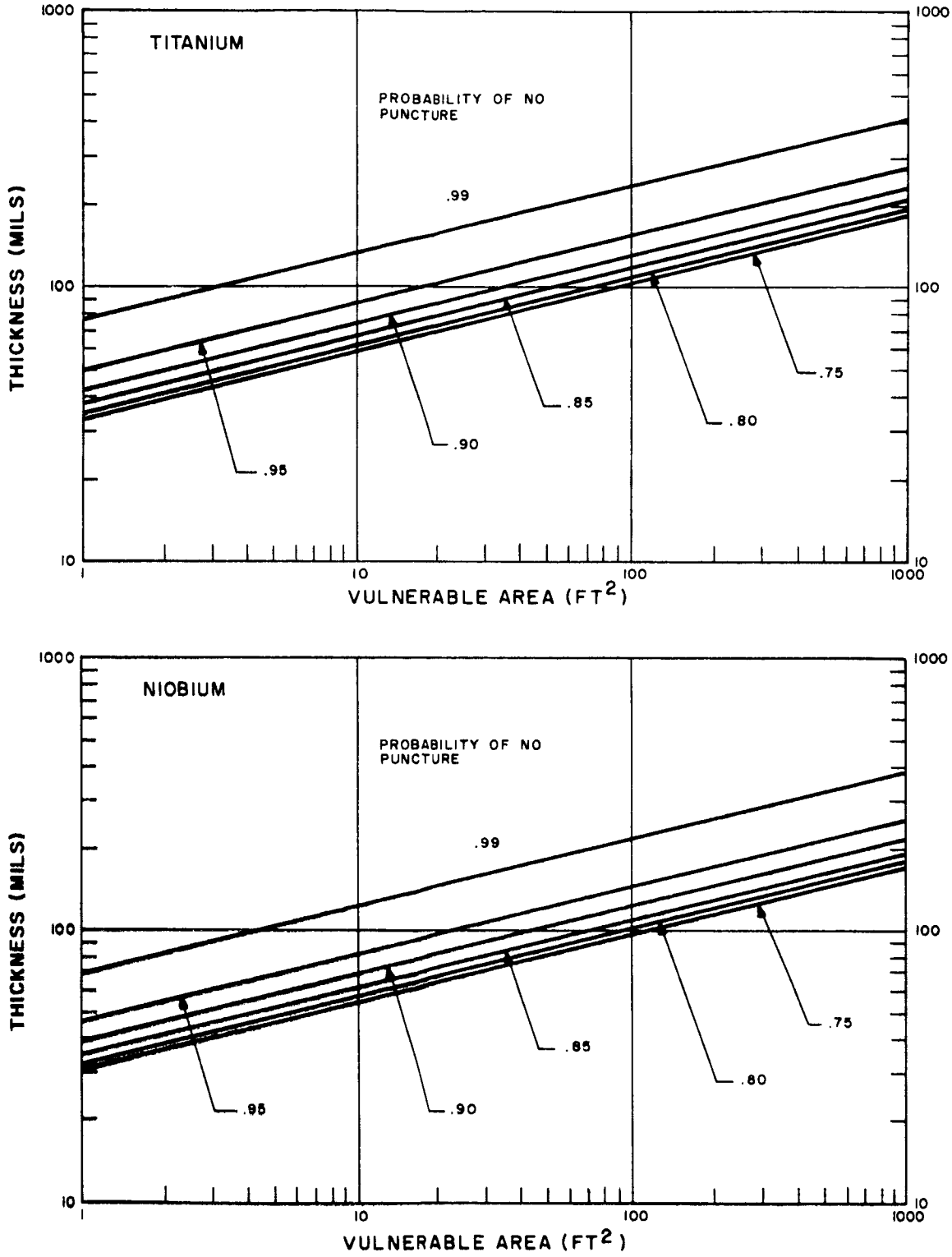

Figure 5-3. Room Temperature Meteoroid Armor Thickness for Titanium and Columbium (10,000 Hours)

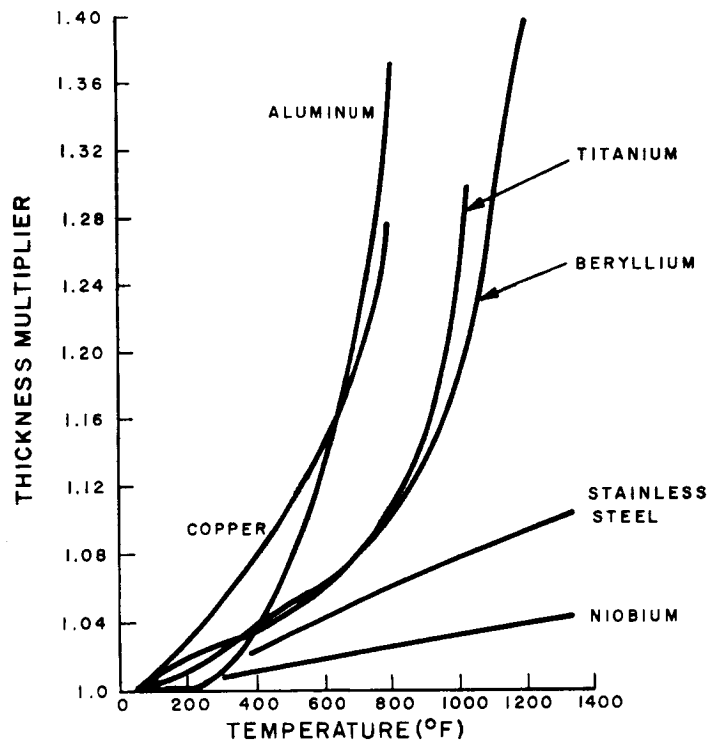

Figure 5-4. Armor Thickness Correction Factor to Account for Temperature

Consistent with NASA-Lewis recommendations, the vulnerable area of the tubes is defined as the external surface area of the armor. In computing the armor requirements for this study, the vulnerable area was taken as the total external surface area of all the tubes, headers and feeds in a given loop; the contribution of the associated condenser coil was not included since it is deeply buried in the integrated power module. The effect of including the vulnerable area of the headers and feeds is significant and increases as a direct function of the number of individual segments used in the radiator design. Figure 5-5 shows this for the radiator size associated with the 1.2 MWe turboelectric vehicle. The vulnerable area of the headers and feeds is plotted as a fraction of the total radiator tube liner surface area. It is noted that the headers contribute more than the feeds by roughly a factor of two and the total contribution for eight segments is roughly 0.75 times the total tube liner surface area. Inasmuch as the total tube vulnerable area based on the outer surface is three to five

Using the required integral armor thickness (t_a) as a reference quantity, wall thickness (t_w), bumper thickness (t_b), and spacing (s) may be related dimensionlessly as shown in Figure 5-6.

The points shown are test data (4) and the heavy line is curve fitted to these points. Variation with ($s/^t a$) is established by forcing an asymptote slightly beyond the line for $s/^t a = 2.5$ and adapting the mathematical relationship to conform to findings reported by Nysmith and Summers[5]. The asymptote provides a conservative limit on the function for large spacings since little is known of the parametric behavior in this region. In addition to its relationship to test data, this criterion follows a logical sequence from integral armor. Where the spacing is zero, the bumper and wall merge into a single member and their combined thickness should logically equal that of integral armor. Furthermore, at the extremes where either the bumper or the wall reduce to zero thickness, it is again logical for their combined thickness to reduce to the integral armor value. Figure 5-6 is seen to conform to these expectations. As shown, this criterion assumes the same material for the wall and bumper. To account for different materials, equivalent thicknesses may be used based on the general equation for armor thickness or the data shown in Figures 5-1 through 5-3.

In applying this criterion to a design, the first step is the determination of the required armor thickness by means of the armor criterion as though bumpers were not being used. Following this, the relative thicknesses of bumper and wall are determined using this reference armor thickness and Figure 5-6 as a basis. The vulnerable area is not considered to be altered by the use of a bumper, since damage to the bumper by a meteoroid which would not normally have impacted the wall is of secondary concern. In the normal context of a bumper as applied to the outer shell of a space station, for example, this vulnerable area philosophy would not be important; however, in the case

(4) Wallace, R.R. et al, "Effects of Hypervelocity Particles on Shielded Structures", ARS Journal, Vol 23, No. 8, 8/62, pp 1231-1237

(5) Nysmith, C. R. and Summers, J. L., "Preliminary Investigation of Impact on Multiple-Sheet Structures and an Evaluation of the Meteoroid Hazard to Space Vehicles", NASA TN D1039 9/61

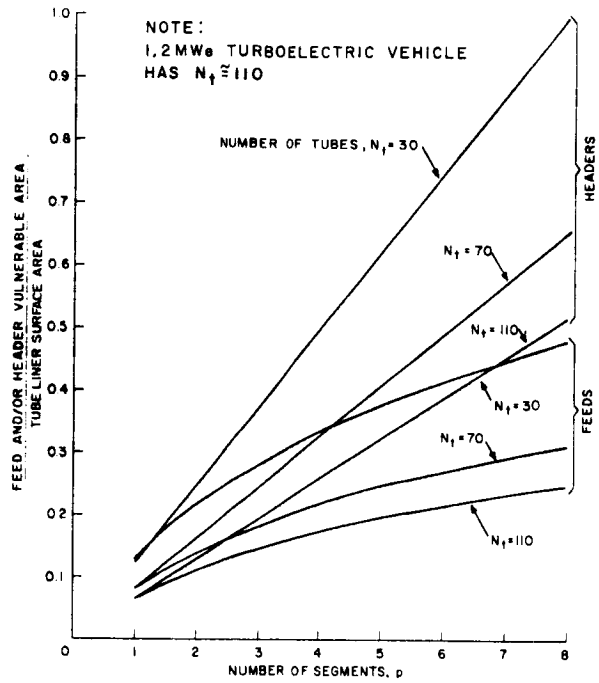

Figure 5-5. Vulnerable Area Contribution of Headers and Feeds

times the bore surface area, this 0.75 factor really corresponds to a true vulnerable area addition of approximately 15 to 25 percent.

2. Bumper Effectiveness

To protect radiator headers, feed lines, and in some cases, parts of the tubes themselves, it is desirable to use a meteoroid bumper instead of integral armor. Hypervelocity testing has shown that the combined thickness of bumper and tube wall may be as little as half the thickness of equivalent integral armor, depending on the spacing and relative thickness of the two. Neither theoretical nor experimental work has yet reached a sufficient level of sophistication to provide an equation relating these parameters. To meet the needs of preliminary design and digital computer analysis, a self consistent interim criterion based on limited test data and a simplified phenomenological model has been devised.

$$\frac{t_w}{t_a} = \frac{2}{\pi}\tan^{-1}\frac{2(1-t_b/t_a)}{\frac{t_b}{t_a}\left(2-\frac{t_b}{t_a}\right)\left[\frac{4}{3}+\frac{10.4(s/t_a)^2}{1+3.6(s/t_a)^2}\right]} - \frac{2(s/t_a)^2}{1+3.6(s/t_a)^2}\left(e^{-3.5\,t_b/t_a}\right)\sin 2\pi\frac{t_b}{t_a}$$

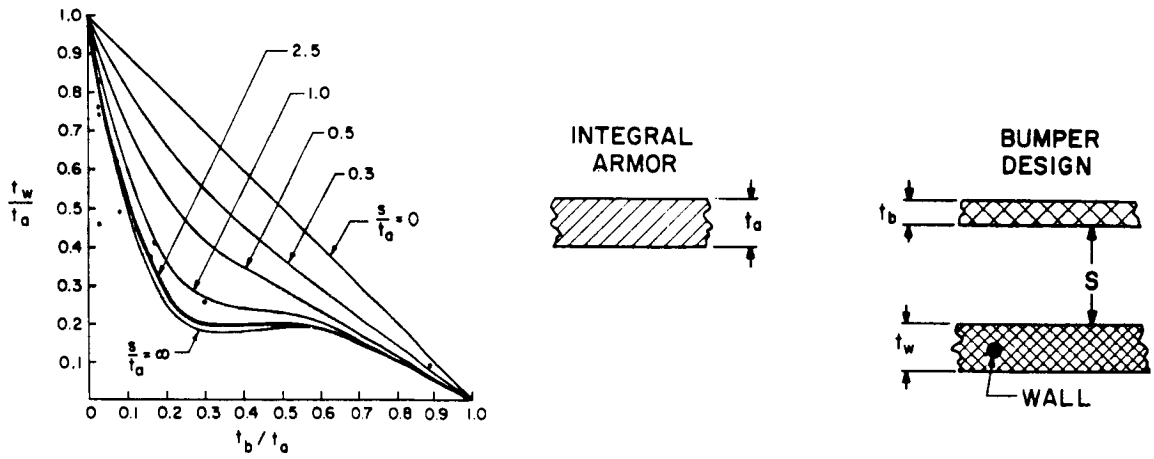

Figure 5-6. Meteoroid Bumper Criterion

of a radiator we are generally referring to the situation of a small diameter pipe (e.g., a two-inch diameter feed line) enclosed within a large diameter shell (e.g., a 260-inch diameter radiator).

B. MECHANICAL DESIGN

For the turboelectric vehicles, beryllium has already been identified as the primary material of construction. To meet the corrosive problems of NaK at 1200° F, Inconel 700 was selected for all surfaces exposed to the working fluid. This selection was made from a number of chemically suitable materials because of the favorable expansion coefficient related to beryllium. Figure 5-7 compares the values of these coefficients for temperatures ranging up to 1400° F. The importance of achieving a reasonable match is concerned with maintaining a thermal bond in the radiator tubes between the liner and armor, and minimizing the accumulation of dimensional differences due to expansion between headers and their meteoroid bumpers.

1. Building Block Approach

Recognizing the potential fastening problems involved with assembling a beryllium structure of this size, the construction concept is based on a building block approach

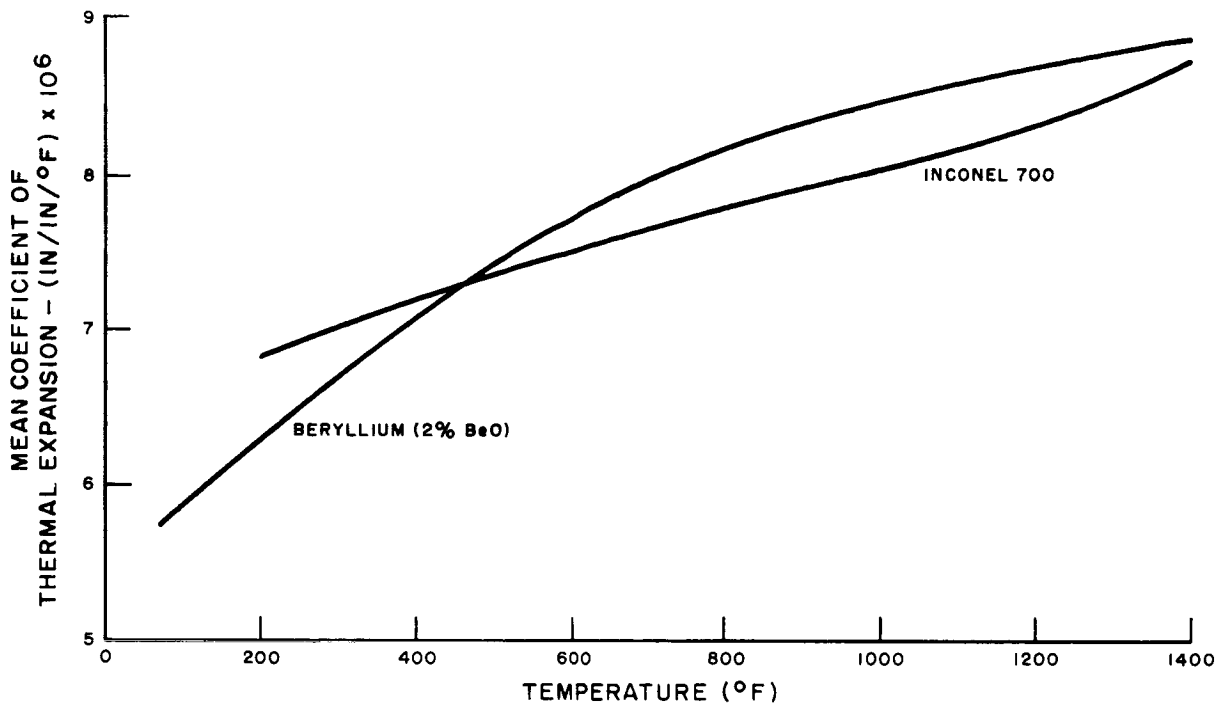

Figure 5-7. Coefficient at Thermal Expansion of Beryllium and Inconel 700

utilizing a basic matrix fin and tube panel subassembly. It consists of a number of beryllium tubes coextruded with Inconel liners, and brazed to a chemically milled fin plate. The ends of the tube liners are electron-beam welded to flow manifolds at each end of the panel which also incorporate stub pipes for connecting the panel into a radiator loop. A visualized manufacturing sequence is presented in Figure 5-8. First the coextruded tubes are brazed to pre-milled fin plates which are shaped to provide a thickened end section in order to shear lag the peak point loads of the tubes to a nearly uniform loading at the mounting interface. Following assembly of the tubes to the fin panel, an L-shaped manifold strip is e-beam welded to the tube liner stubs by means of a series of circular-end welds. A similar L-shaped manifold strip, having a manifold feed stub end welded into place, is then mated to the assembly by seam welding the two L-sections together thereby forming a manifold having a roughly square cross section. End caps complete the panel subassembly and it can be leak checked and

inspected, as a module of manageable proportions. Overall dimensions of a panel are typically 18 inches by 4 to 8 feet.

Using these panels, a radiator assembly sequence has been identified which lends itself to unsophisticated fixturing requirements, and prevents the build up of large tolerance accumulations. Figure 5-9 schematically illustrates the procedure. A header bumper ring assembly is laid horizontally with a second unit located vertically above it and held in reasonable alignment by suitable fixturing. The basic matrix panels are then introduced as shown and attached to the header bumper rings at each end by means of huck-lockbolts or Hi-lok fasteners. These are superior to rivets since the clamping pressure applied to the beryllium bumper is readily controlled; furthermore, pre-loading of the holes due to rivet expansion is eliminated.

In keeping with the use of Inconel for the flow path, the headers and feeds consist of thin-wall pipes of this material. On final assembly, the single pipe stubs on each manifold of the matrix panels are inductively brazed to a corresponding pipe stub on the circumferential header. By suitably designing these connections, they can be made to have sufficient elastic flexibility to account for both thermally induced and manufacturing tolerance dimensional mismatching without jeopardizing the integrity of the fluid connection. Header bumper cover plates complete the structural skin of the radiator and the meteoroid protection of the headers. This assembly approach applies to all the radiator designs considered. Some of the details vary to suit local conditions, but the basic modular, building block approach is common to all.

2. Matrix Joint

Figure 5-10 illustrates the appearance of a typical joint where the basic matrix panels are attached to the headers and the header bumper rings. The various elements of the concept are identified in the Figure and the lower right-hand end shows the scheme for splicing the free edges of adjacent matrix panels to each other using a splice plate. At discrete points around the circumference (generally two), the headers are joined

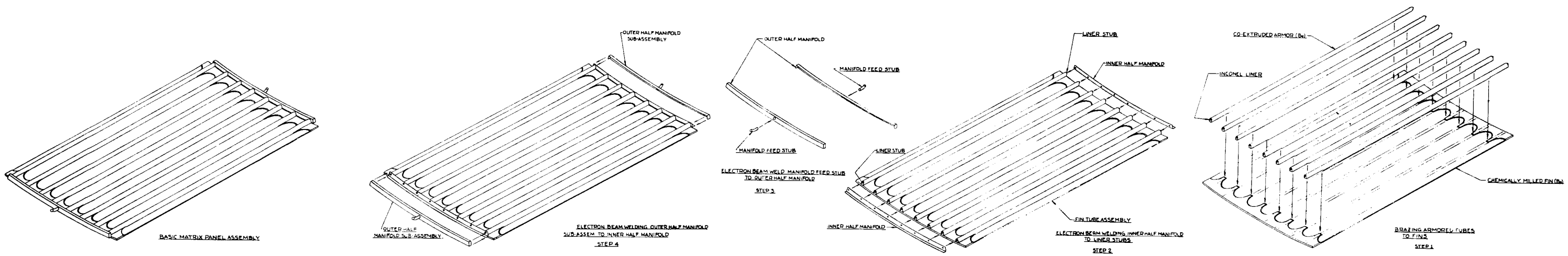

Figure 5-8. Manufacturing Sequence of Basic Matrix Panels

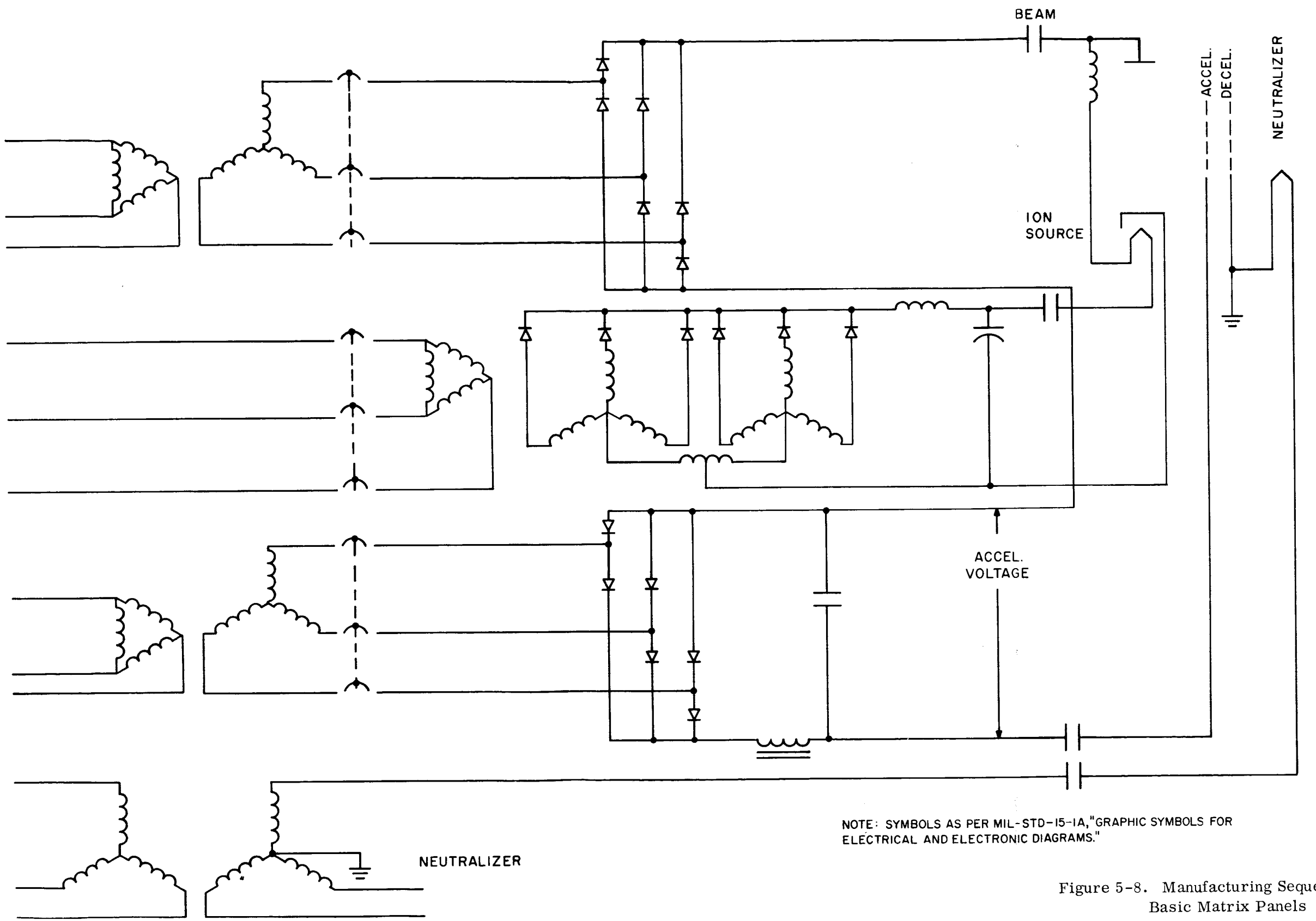

NOTE: SYMBOLS AS PER MIL-STD-15-1A, "GRAPHIC SYMBOLS FOR ELECTRICAL AND ELECTRONIC DIAGRAMS."

Figure 5-8. Manufacturing Sequence of Basic Matrix Panels

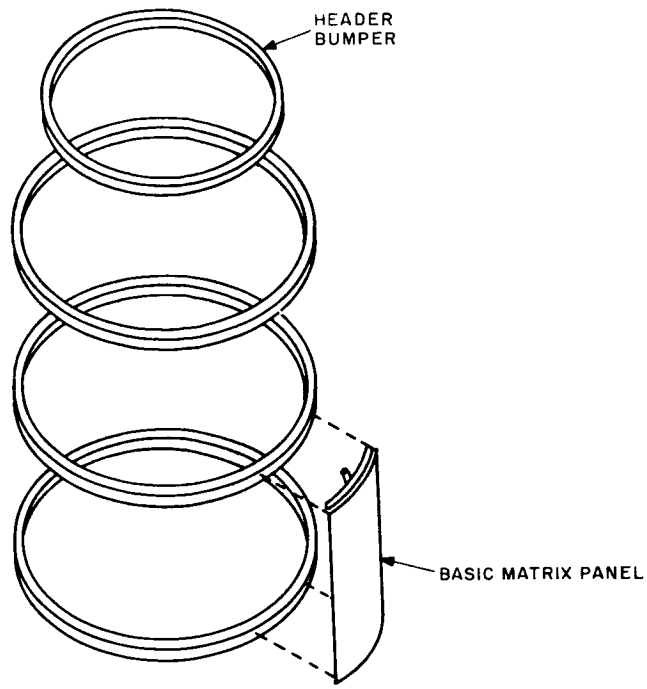

Figure 5-9. Fabrication Techniques

to a feed line, and a concept of this is shown in Figure 5-11. Upon assembly of the radiator structure, the feed and return headers are first inserted in the header bumper rings. The V-adapter tube section which connects the feed or return tube with the two 90-degree header arcs is installed as an integral part of the headers. It is able to pass through the header bumper by means of a cut-out hole which is shown covered by a plate in the drawing. This plate and the two stiffeners on both sides of the cut-out maintain the stiffness continuity of the header bumper and bumper stiffener combination. The feed and return lines are then welded to the V-adapters. The line supports take loads from the feed and return lines and transfer them to the header bumper and fin-tube combination. With the preceding parts in place, the basic radiator matrix panel previously described is attached to the header bumper ring in the usual manner.

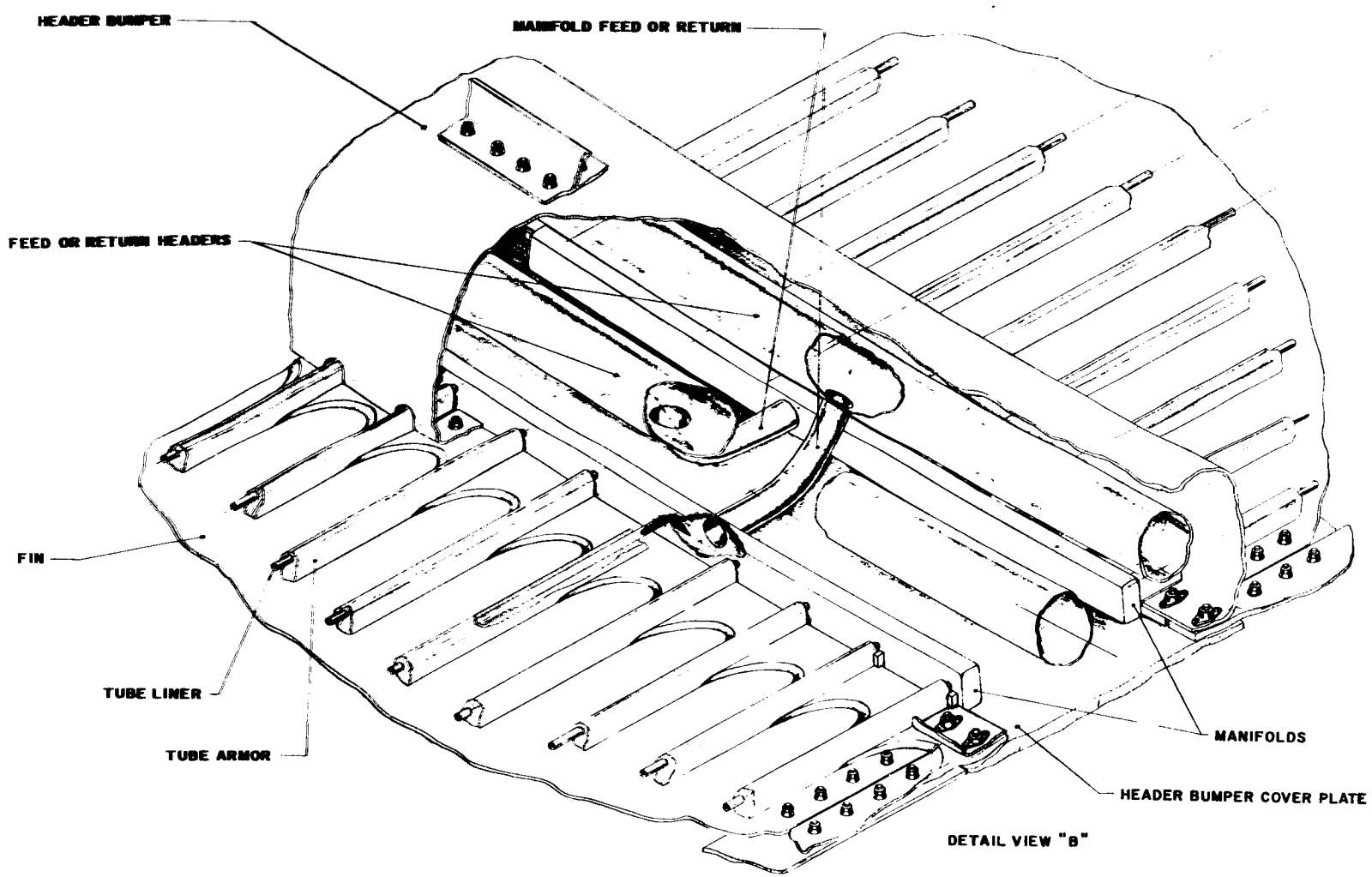

Figure 5-10. Header Detail

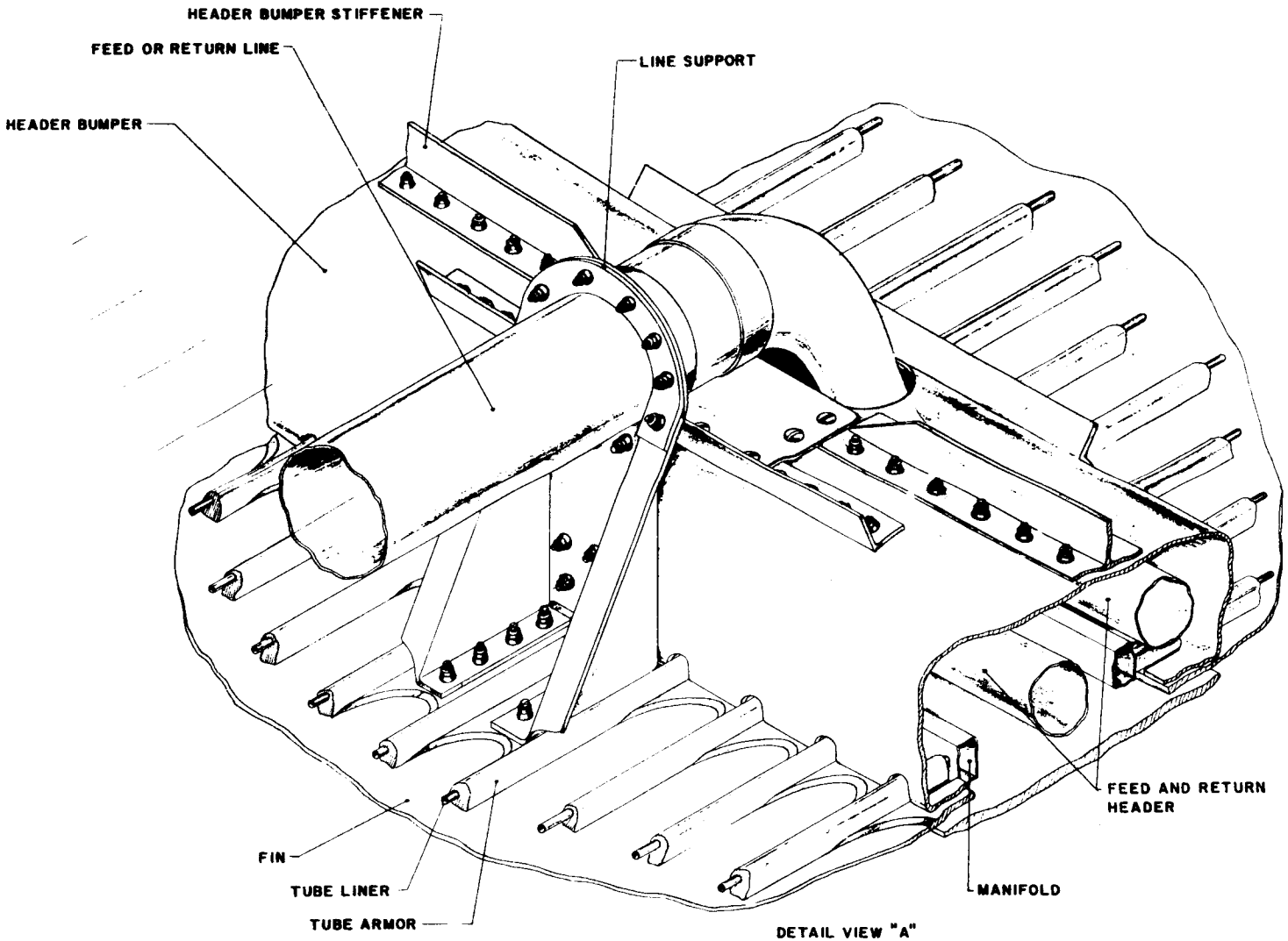

Figure 5-11. Feed Line — Header Joint Detail

In all three vehicle designs there are axial locations at which radiators of greatly differing temperatures are immediately adjacent to each other. Furthermore, they all incorporate an ejectable nose cap aerodynamic shroud. A structural joint conceived to cope with these problems concurrently in the 1200 KWe turboelectric vehicle design serves to illustrate a feasible approach; it is illustrated in Figure 5-12. A V-band clamp is used as a structural tie between the primary and secondary radiators and the aerodynamic shroud during boost. Upon release of the V-band and deployment of the fairing, the tie between secondary and primary radiators consists of the thermal expansion blocks shown in Figure 5-11. These blocks allow radial differential expansion between the 600°F secondary radiator and the 1200°F primary radiator at operating temperature. During the boost phase of flight it is anticipated that the radiators would both be at about 200°F. The secondary radiator base ring is a continuous structure which incorporates lug attachments for the powerplant lateral support members and the thermal expansion block receptacle. The ring also has an integral lip for V-band clamping and shear continuity. The lower secondary header is enclosed in a bumper ring and coverplate which attach to the base ring. The primary radiator end cover plate is a continuous ring structure incorporating a shear lip and V-band clamping to mate with the corresponding pieces on the secondary radiator. Located between the primary radiator end cover plate and the secondary radiator base ring is a multiple layer of insulation to minimize heat transfer between the two radiators. The shear lip is designed to permit free radial expansion of the primary radiator at operating temperature.

C. RADIATOR DESIGN CHARACTERISTICS

Weight optimization of the radiator system for the nuclear electric vehicle studies was accomplished with the aid of the GE Spartan III Radiator Analysis Computer Program. Input for this program includes thermal requirements, environmental factors, geometric design factors, physical property data, criteria for meteoroid protection, pressure drop, and heat transfer. The geometrical input can be any desired combination of configuration (flat panel, cylinder, cruciform, etc.), number of tubes per

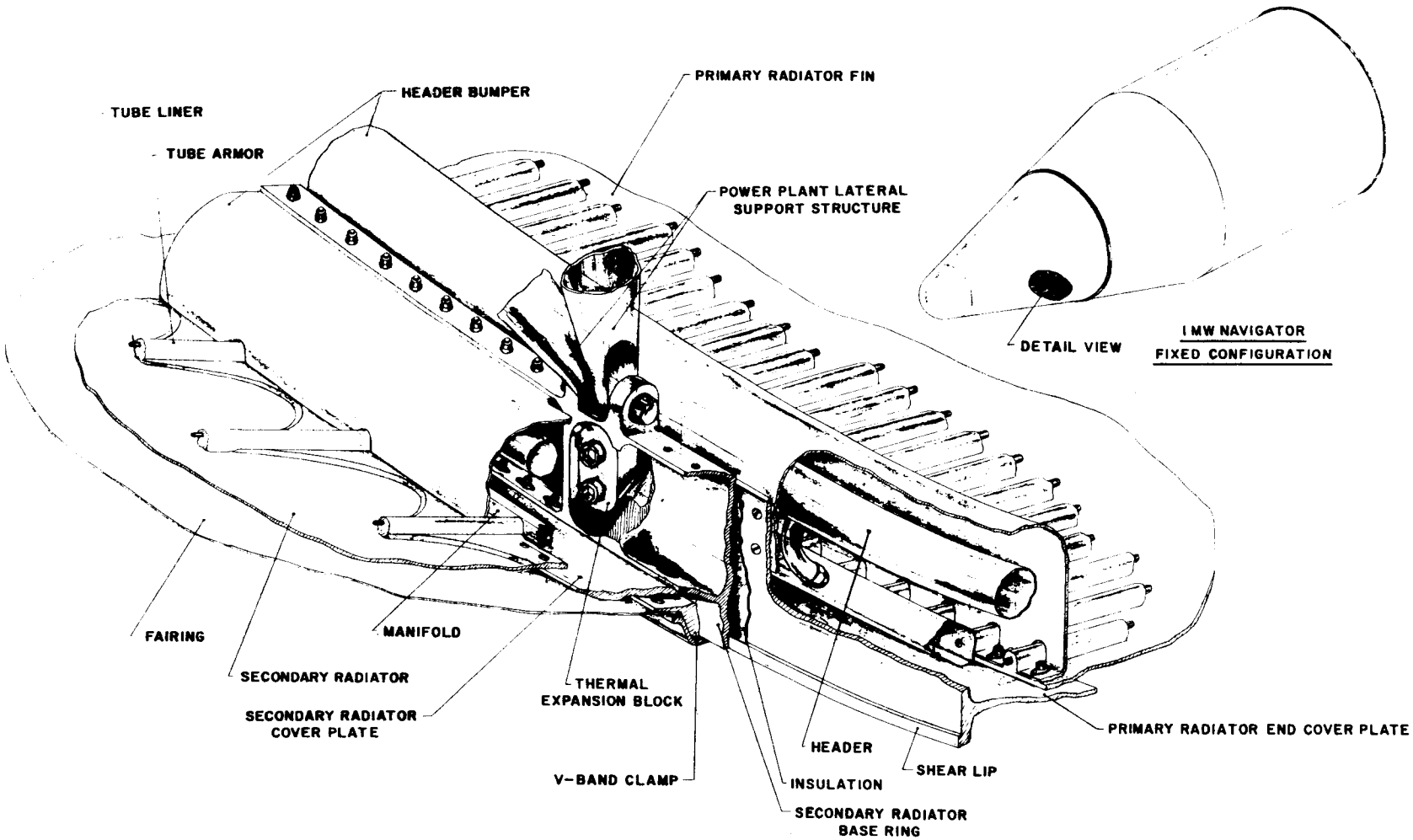

Figure 5-12. Thermal Joint Details

panel, tube inside diameter, and fin thickness. Variations in fin-tube design (such as offset or central fin tube), header shape, header location, and any reasonable series-parallel arrangement of feed and return lines can also be analyzed. The relationships for meteoroid armor requirements include allowances for bumper effects and are consistent with the meteoroid criteria described above. The output includes weights, areas, pressure drops, fluid pump work, and dependent geometric factors. Of these geometric factors, the length of the fin-tube elements is the major one used to satisfy the heat balance.

Although the designs do not incorporate redundant fluid loops, the concept of independent loops was used in all three vehicles, and the powerplant radiator systems (including both primaries and secondaries) were all based on a 95-percent probability of no puncture during a 10,000-hour mission. To capitalize on the meteoroid self-shielding effect of the fins, the tube cross sections are tailored to provide reduced armor thickness on the inward facing side. Headers of constant cross section are used in all three designs. Although a slight weight savings can be realized by employing constant velocity parabolic headers, it is questionable that the manufacturing problems involved could be justified. The problem of obtaining an even flow distribution in the radiator tubes has not been explored in great detail; however, all radiators presented have tube pressure drops at least 10 times greater than the header pressure drop. This criterion tends to ensure uniform flow distribution by inducing a plenum effect in the headers. Final designs undoubtedly will require flow model studies.

In the initial iterations on the 1200 KWe turboelectric vehicle radiators, the headers and feeds were sized to have an average flow velocity equal to that in the tubes. When the large quantities of NaK inventory were encountered in the feeds, it became clear that the optimization had to trade off the feed and header volume against system pump work. Since the feeds contained by far the major fraction of the NaK inventory, further optimization was directed mainly at them. The net result is that the constant diameter headers were sized to have a mean fluid velocity equal to that in the tubes,

and the feeds and returns were optimized to give minimum system weight. Summaries of the detailed design parameters for all three primary radiators are given in Tables 5-1 through 5-3.

D. STRUCTURAL DESIGN ANALYSIS

As treated in these studies all the radiators were first designed to perform their respective heat rejection functions. Other than the philosophy underlining the configuration arrangements, structural load carrying considerations did not influence the sizing of the tubes, fins or header bumpers. These were designed: 1) to meet reasonable fabrication requirements. For example, the header bumpers were sized mainly to contain the headers, permit standard pipe-bend radii in the connecting tubes from the matrix panels, and provide some room to permit assembly to be achieved. Header bumper cover plate thicknesses were established on the basis of the meteoroid bumper criterion and the local thickening at the ends of the fin plates was based on maintaining the same compressive area as the basic matrix. Clearly, the completed radiators do embody some structure at this point, but it is very difficult to separate and is largely related to the powerplant ground rules. For example, if the requirement for eight independent loops in the 1200 KWe turboelectric vehicle was reduced to four, some of the ancillary structural weight associated with the header bumper connections could be eliminated along with the reduction in segmentation. Following this line of reasoning to its logical conclusion, it is to be supposed that a lighter weight radiator would result if only one bay were utilized. This does not follow because of the pump work trade off associated with lengthening the tubes; however, it does serve to illustrate how these structural aspects also enter into the radiator optimization and their effect should be reflected all the way back to the matrix geometry optimization.

In addition to this ancillary structure, primary structure is also required to meet the launch load requirements. Due to the massive proportions of the matrix to meet the thermal and meteoroid puncture needs, stresses are generally low, and the main mode of structural failure is buckling. Control of this is largely a matter of providing rings

TABLE 5-1. SUMMARY OF 1200 KWe TURBOELECTRIC VEHICLE RADIATOR PARAMETERS

		PRIMARY									SECONDARY			PAYLOAD	
	UNIT	A	B	C	D	E	F	G	H	TOTAL	A	B	C	HT.	LT.
Heat Rejected	kw	720	720	720	720	832	832	832	832	6208	59.2	98.8	64	9	2
Area	ft^2	263	263	263	263	303	303	303	303	2264	125	207	145	45	46
Subsystem Wt.	lbs	699	787	827	864	1035	1045	1076	1083	7421	138	246	137	45	46
Inlet Temp.	°F	1250	1250	1250	1250	1250	1250	1250	1250	--	650	650	650	450	200
Fluid ΔT in Rad	°F	122	131	116	112	105	120	129	118	--	75	75	75	75	40
No. of Panels	-	4	4	4	4	4	4	4	4	--	2	2	4	4	4
No. of Tube/panel	-	80	101	109	113	105	115	121	112	--	32	56	9	9	6
Header Length	ft	12.4	14.4	16.2	17	17	17	17	17	--	11.17	18.66	4.0	4.0	4.0
Header ID	in.	1.13	1.28	1.32	1.35	1.30	1.36	1.40	1.34	--	.72	.95	.38	.38	.31
Header Wall Thk.	in.	.020	.020	.020	.020	.020	.020	.020	.020	--	.015	.015	.015	.015	.015
Tube Length	ft	5.08	4.34	3.83	3.64	4.24	4.23	4.24	4.24	--	5.44	5.37	9.06	2.73	2.81
Tube ID	in.	.180	.180	.180	.180	.180	.180	.180	.180	--	.18	.18	.18	.18	.18
Fin Thickness	in.	.080	.080	.080	.080	.080	.080	.080	.080	--	.06	.06	.05	.06	.05
Fin Length	in.	.77	.68	.72	.73	.80	.71	.67	.73	--	1.93	1.83	2.48	2.50	3.82
Basic Feed Line ID	in.	1.80	1.80	1.80	1.80	2.0	1.80	1.80	1.80	--	--	--	--	--	--
Feed Line Wall Thk.	in.	.068	.068	.068	.068	.068	.068	.068	.068	--	--	--	--	--	--
Radiator ΔP	psi	5.15	2.53	2.51	2.41	4.54	2.98	2.33	3.23	25.68	3.24	3.08	5.06	.19	Negl.
Feed Line ΔP	psi	8.17	8.06	10.99	12.85	12.86	17.94	16.00	20.30	107.2	--	--	--	--	--
Heat Exchanger ΔP	psi	2	2	2	2	2	2	2	2	16	--	--	--	--	--
Rad. Matrix Wt (Wet)	lbs	527	577	580	588	635	665	685	650	4913	136	242	126	44	37
Matrix (Dry) Wt	lbs	466	495	485	483	534	557	573	550	4143	127	218	120	42	35
Tubes	lbs	236	258	245	241	262	286	302	279	2109	46	80	50	13	10
Fins	lbs	196	194	192	192	223	223	223	223	1666	70	116	70	30	22
Headers	lbs	23	33	39	41	40	42	43	41	302	19	46	69	6	5
Armor	lbs	171	188	178	175	190	207	219	202	1530	39	71	40	12	10
Coolant (MATRIX)	lbs	61	82	95	105	101	108	112	106	770	9	23	41	2	2
Fin Efficiency	%	92	93	93	93	91	93	94	93	--	87	88	79	89	89
Feed & Return (Dry) Wt	lbs	104	127	151	173	237	235	243	265	1535	--	--	--	--	--
Total Coolant Wt.*	lbs	129	165	191	213	264	253	260	268	1743	9	24	6	2	2
Wt Coolant in Feeds*	lbs	68	83	96	108	163	145	148	162	973	--	--	--	--	--
Coolant Flow Rate	lbs/sec	27.3	25.4	28.7	29.7	36.6	32.1	29.8	32.6	--	3.56	5.95	3.85	.52	.05
Hydraulic Pump Power	kw	1.83	1.40	1.95	2.25	3.12	3.22	2.66	3.65	20.1	.045	.072	.219	Negl.	Negl.
Pump Efficiency	%	40	40	40	40	40	40	40	40	--	50	50	50	50	50
Coolant	-	NaK	NaK	NaK	NaK	NaK	NaK	NaK	NaK	--	NaK	NaK	NaK	NaK	Water

*Coolant weights correspond to operating temperatures

Survival Probability ~ 0.95 for 10,000 Hours

TABLE 5-2. SUMMARY OF 4800 KWe TURBOELECTRIC VEHICLE PRIMARY RADIATOR PARAMETERS

	UNIT	A	B	C-P	TOTAL
Heat Rejected	kw	1591	1591	1591	25456
Area	ft^2	600	600	600	9600
Subsystem Wt.	lbs	2031	2015	2088*	33278
Inlet Temp.	°F	1250	1250	1250	--
Fluid ΔT in Rad	°F	145	130	125	--
No. of Panels	--	2	2	2	--
No. of Tubes/Panel	--	280	300	310	--
Header Length	ft	44.1	49.3	51.8	--
Header ID	in.	2.13	2.20	2.24	--
Header Wall Thk.	in.	.030	.030	.030	--
Tube Length	ft.	6.43	5.70	5.41	--
Tube ID	in.	.180	.180	.180	--
Fin Thickness	in.	.120	.110	.120	--
Fin Length	in.	.75	.81	.81	--
Fin Efficiency	%	94.8	93.8	93.9	--
Basic Feed Line ID	in.	3.10	3.25	3.35	--
Feed Line Wall Thk.	in.	.030	.030	.030	--
Radiator ΔP	psi	11.67	11.89	11.82	189.64
Feed Line ΔP	psi	14.23	12.76	12.24*	198.35
Rad. Matrix Wt. (wet)	lbs	1631	1629	1646	26304
Wt. Coolant in Feeds	lbs	277	307	313*	4976
Total Coolant Wt.	lbs	501	588	594*	9405
Coolant Flow Rate	lbs/sec	50.0	55.8	58.0	--
Hydraulic Pump Power	kw	5.65	5.99	6.08*	96.76
Pump Efficiency	%	40	40	40	--
Coolant	--	NaK	NaK	NaK	--

Survival Probability ~ 0.95 for 10,000 Hours
*~ Denotes Average Value

along the cylindrical/conical shell. The header bumpers themselves provide for this function, and in a highly segmented radiator they may be sufficient. In general, it is found that some auxiliary rings must be added. They are quite light so this is not a major consideration; however, as the number of segments is decreased their number and size increases. These rings are fully classifiable as load carrying structure and

TABLE 5-3. SUMMARY OF 1 MWe THERMIONIC PRIMARY RADIATOR PARAMETERS

	UNIT	A	B	C	D	TOTAL
Heat Rejected	kw	1876	1876	1876	1876	8504
Area	ft^2	330	330	330	330	1320
Subsystem Wt	lbs	2751	2822	2844	2914	11331
Inlet Temp	°F	1800	1800	1800	1800	--
Fluid ΔT in Rad*	°F	238	238	238	238	--
No. of Panels	-	2	2	2	2	--
No. of Tubes/Panel	-	326	326	326	326	--
Header Length	ft	34	34	34	34	--
Header ID	in.	2.29	2.29	2.29	2.29	--
Header Wall Thk.	in.	.058	.058	.058	.058	--
Tube Length	ft	4.45	4.45	4.45	4.45	--
Tube ID	in.	.180	.180	.180	.180	--
Fin Thickness	in.	.070	.070	.070	.070	--
Fin Length	in.	.470	.470	.470	.470	--
Fin Efficiency	%	80.9	80.9	80.9	80.9	--
Basic Feed Line ID	in.	3.30	3.30	3.30	3.30	--
Feed Line Wall Thk	in.	.058	.058	.058	.058	--
Radiator ΔP	psi	2.10	2.10	2.10	2.10	8.40
Feed Line ΔP	psi	3.12	3.19	3.54	4.08	13.93
Heat Exchanger ΔP**	psi	1.0	1.0	1.0	1.0	4.00
Radiator Matrix Wt (Wet)	lbs	2637	2637	2637	2637	10548
Feed Line Wt (Wet)	lbs	308	332	354	423	1417
Wt Coolant in Feeds	lbs	156	168	176	214	714
Total Coolant Wt	lbs	330	350	358	396	1434
Coolant Flow Rate	lbs/sec	35.6	35.6	35.6	35.6	--
Hydraulic Pump Power	kw	1.055	1.067	1.126	1.216	4.464
Pump Efficiency	%	15	15	15	15	--
Coolant	-	NaK	NaK	NaK	NaK	--

Survival Probability - 0.95 for 10,000 Hours
* Optimized for System Using EM Pumps
** Assumed

are independent of the radiator performance function; it is quite apparent that working in conjunction with the radiator matrix, they represent a very effective way of acquiring a spacecraft structural frame. It is also clear that an optimum total system requires that they be included in the overall system weight trade-off; however, it is suspected that they have a relatively minor effect.

In a study such as this, it is obvious that a comprehensive structural analysis cannot be made. Not only is the basic environmental information insufficiently defined, but the proportionate information yield is not worth the major effort required. However, it is appropriate for the gross effects to be examined.

1. Structural Loads

During the launch trajectory the radiators described herein will experience varying histories of inertial, aerodynamic, and dynamic loading. Each will peak out of phase with the others and each has a very complex make-up. The basic load analysis in this study was directed at the 1200 KWe turboelectric vehicle. Determination of the axial distribution of mass identified the inertial loads; aerodynamic loading was determined by analyzing the external flow at the maximum dynamic pressure point in the launch trajectory, and a dynamic analysis of a simplified vehicle model under axial excitation provided the dynamic loads. Figure 5-13 shows a weight distribution for the 1200 KWe vehicle based on an early assessment of the design weights. Each of the spikes in the figure reflect the mass concentration associated with a header joint. Since the entire weight loading into the outer shell structure is in the vicinity of 25,000 pounds, a maximum axial inertial load at the base under 7 g's would be approximately 175,000 pounds.

The maximum aerodynamic loads associated with the launch trajectory were determined to occur at an altitude of 43,000 feet at which point the flight Mach number is 1.411. Under these conditions the dynamic pressure is found to be 749 lbs/ft.^{2}. An angle of attack of 7-1/2 degrees was assumed, and the resulting pressure distributions over the entire external surface of the vehicle shell determined as shown in Figure 5-14.

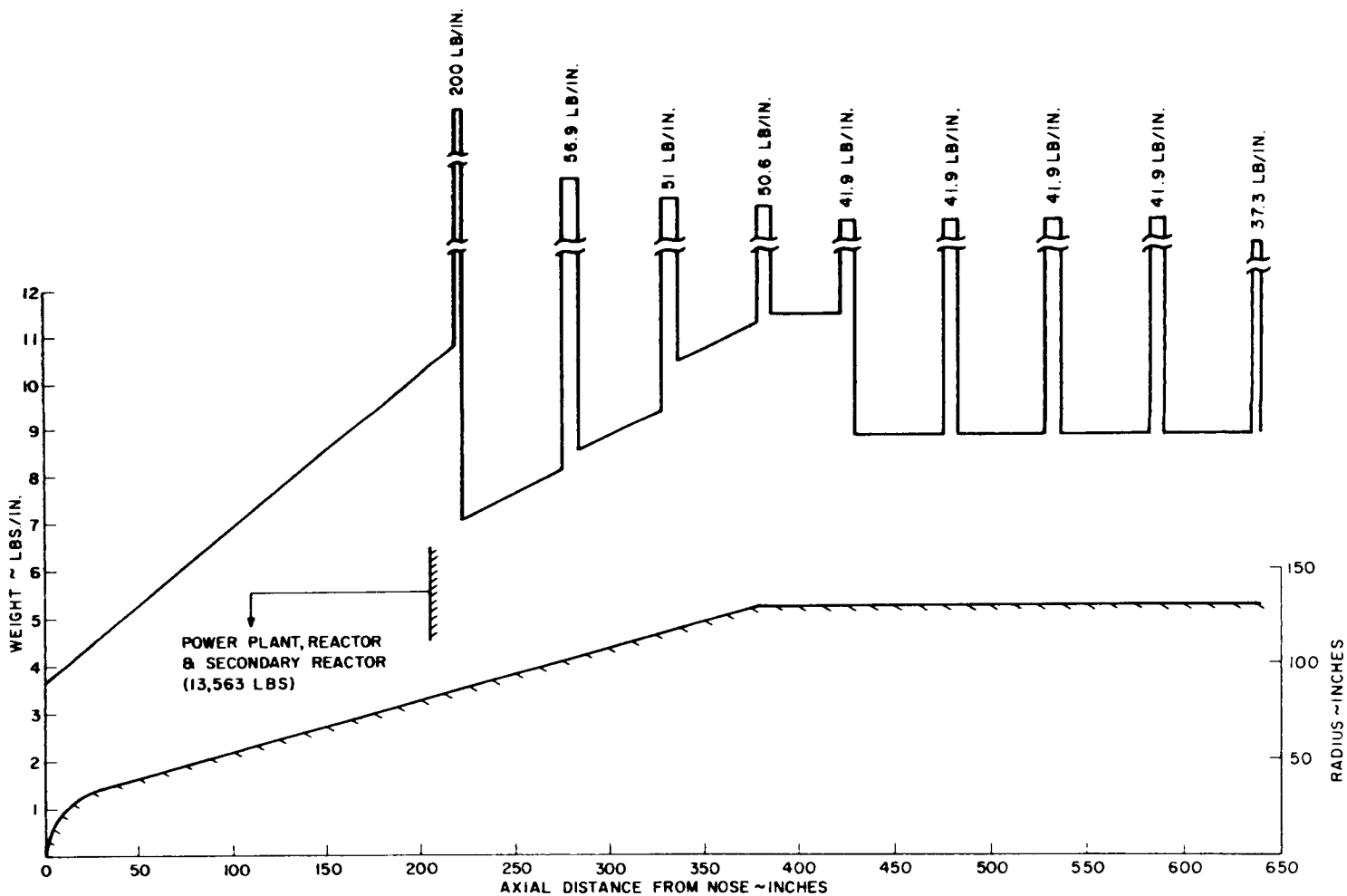

Figure 5-13. Weight Distribution for the 1.2 MWe Turboelectric Fixed Configuration Vehicle

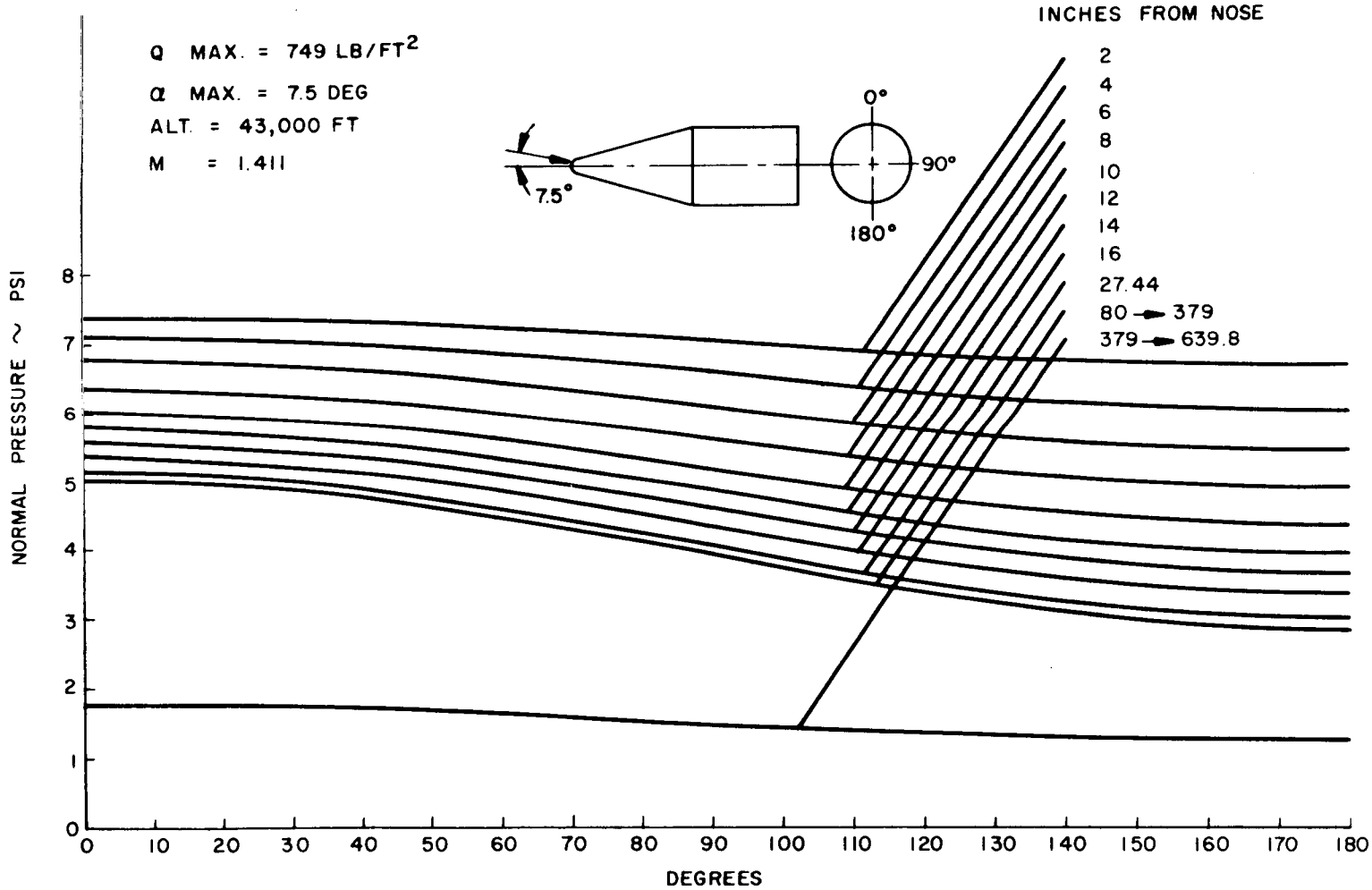

Figure 5-14. Normal Pressure and Circumferential Distribution for the 1.2 MWe Turboelectric Fixed Configuration Vehicle

Shear, axial, and moment loads resulting from this distribution were then determined. By way of comparison with the 7g axial inertia load cited above, this aerodynamic loading alone results in a total axial force at the base of the vehicle of about 210,000 pounds. For the purposes of this analysis, the aerodynamic loads at the point of maximum dynamic pressure were combined with inertial loads based on 2.11 g's of axial acceleration, 1.29 g's of lateral acceleration, and 2.56 radians per second of pitching angular acceleration. The net result, in terms of loading on the radiator, is summarized in Figure 5-15 which shows the distribution of axial, shear, and moment loading plotted against a profile of the spacecraft shape. The discontinuity in all three loads resulting from the inertia of the internal package made up of the reactor, shield, power system, and secondary radiator is clearly identifiable at the axial station at which the nose cap shroud is mounted (approximately 220 inches from the nose). It can also be noted how the low pressures on the cylindrical portion of the shell produce a very gradual increase in the axial load as a result of the 7-1/2 degree angle of attack.

Determination of the dynamic loading is very much a function of the assumption used for system damping. A 7-degree-of-freedom model was analyzed with three damping assumptions which were intended to represent two extremes, and a median estimate of the damping to be encountered. The result of the dynamic analysis is a set of curves giving the transmissibility of each mass in the system over a range of excitation frequencies. At any given frequency the booster input spectrum gives an input acceleration level. By applying the appropriate transmissibility of each of the lumped masses, its acceleration in gs can be determined. Knowing its mass, the forces acting on it can then readily be calculated. For any vibration mode but the first, the determination of net force at any point in the radiator requires a knowledge of the phase relationships between the masses. Since the results of the computer analysis of the seven degree of freedom model showed the peak forces to occur on all masses at the fundamental mode, the loads on the radiator are merely an accumulation of the inertial forces calculated at the fundamental frequency. For the model analyzed, the computer determined the peak forces; these were later corrected to reflect the weight changes associated with subsequent design interations. Based on the median modal damping assumption, the peak

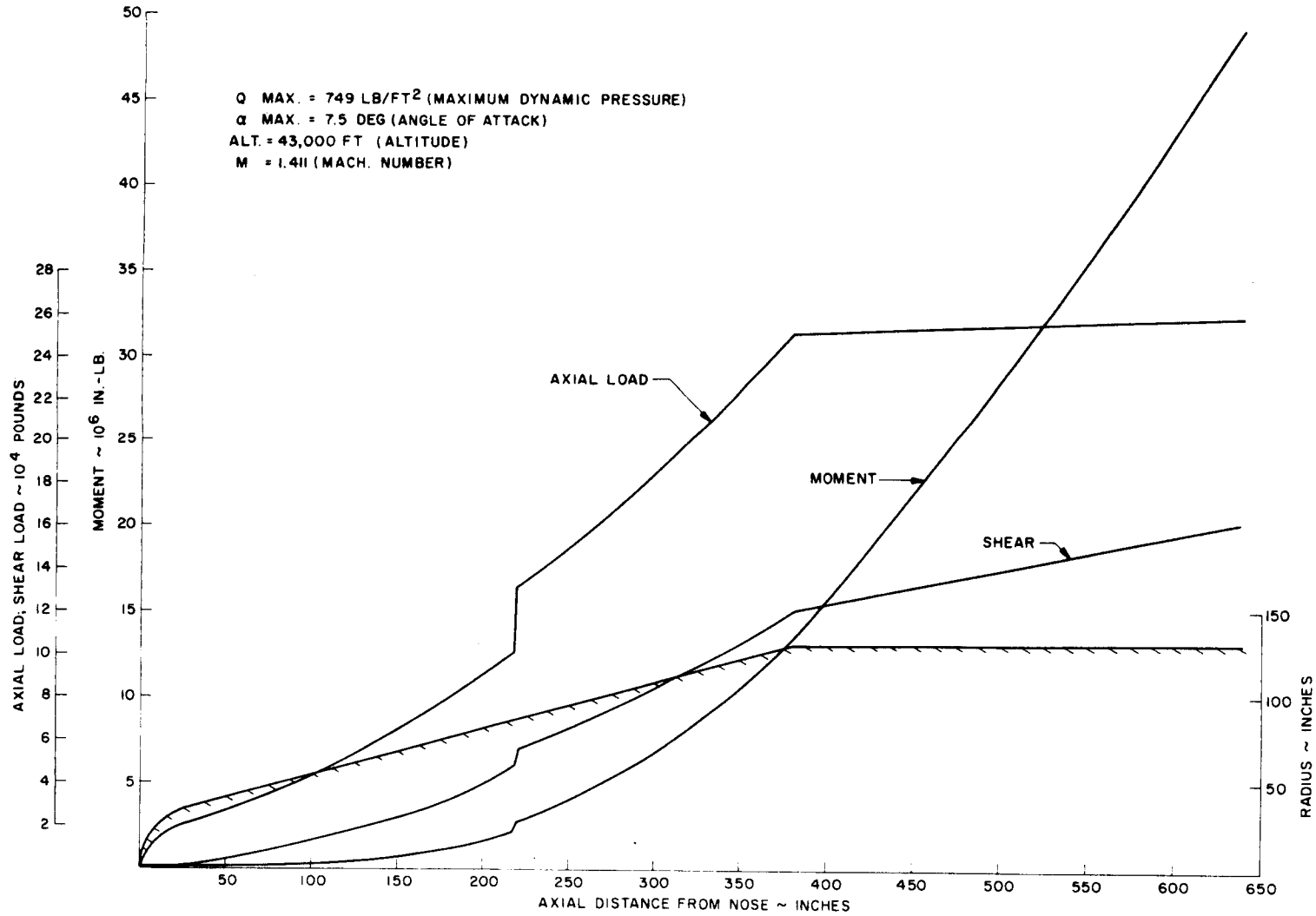

Figure 5-15. Shear Moment and Axial Load Distribution for the 1.2 MWe Turboelectric Fixed Configuration Vehicle

dynamic force at the base of the 1200 KWe radiator would be 384,300 pounds. Using the high and low damping extremes, this force would range from 275,000 pounds to 600,000 pounds. Clearly then, the dynamic loading appears to be the most severe of the three considered here.

Before considering the application of these loads to the radiator, there is an interesting point of concern associated with the dynamic analysis. According to the seven degree of freedom dynamic model of the 1200 KWe turboelectric vehicle, the dynamic acceleration levels to be expected at the reactor will range from about 16 g's to 38 g's depending upon the level of damping assumed. It is not clear at this point in time that control of these levels will be practically possible by means of vibration isolation techniques. Hence, further evaluation of this vibration consideration should be conducted since it has a major effect on establishing realistic vibration specifications for the reactor and other associated powerplant equipment.

2. Combined Load Analysis

As a result of the loading analysis outlined above, it was decided to consider the described aerodynamic and inertial load combination to act independently of the dynamic load. Furthermore, only the effects of these loads on general and local stability were examined. Figure 5-16 summarizes the combined load analysis for the 1200 KWe turboelectric vehicle and this figure is used as a basis for explaining the procedure. The curve identified as P_D identifies the computed axial load resulting from the dynamic excitation. It is seen to be a relatively constant load; this results from the concentrated mass of the reactor, shield, and power system located at the upper end of the structure. The curve identified as P_E is an equivalent axial load accounting for the combined effects of the axial and bending moment loads stemming from the aerodynamic and inertia load combination. This equivalent load is defined as:

$$P_E = P + \frac{2M}{1.3R}$$

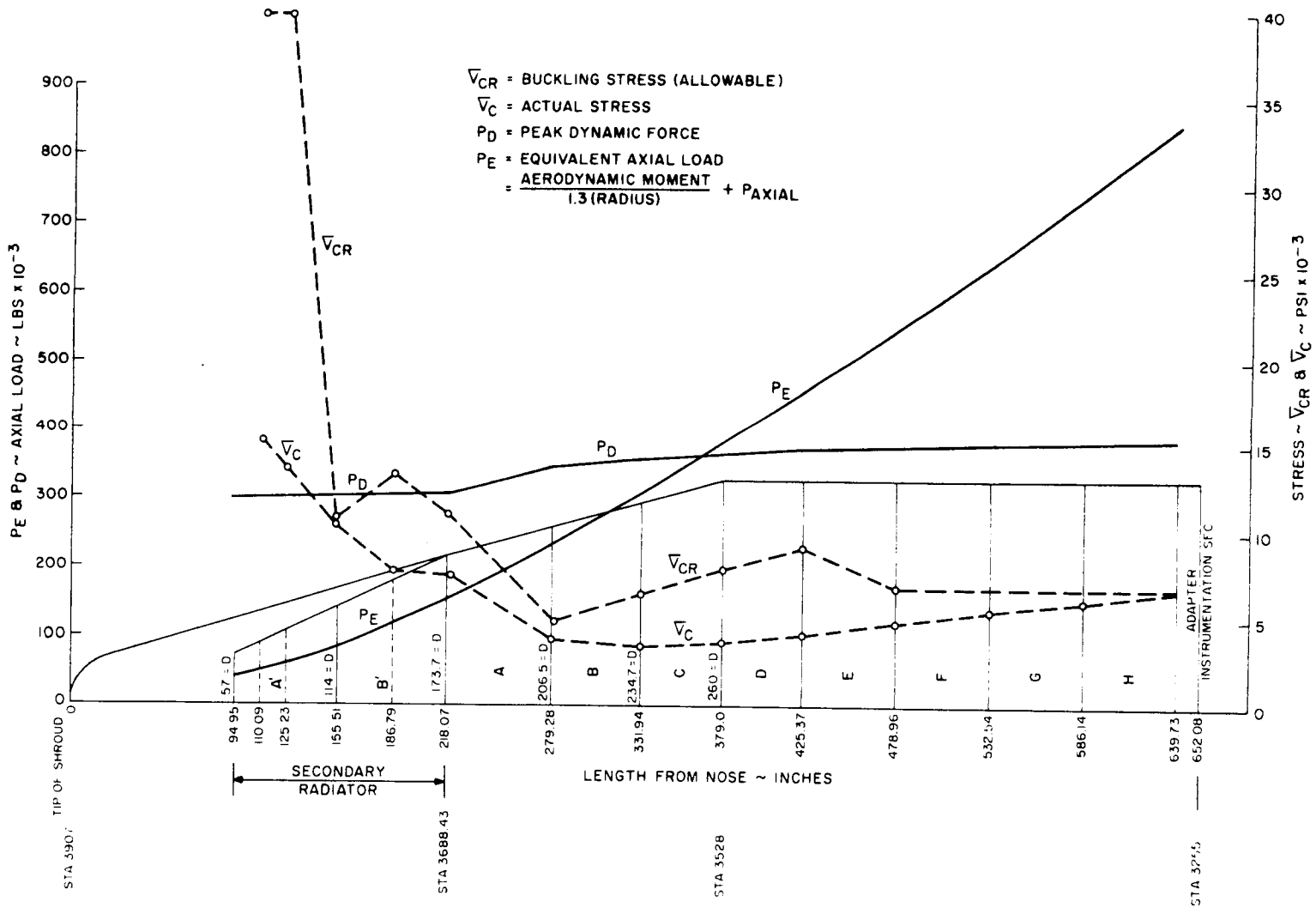

Figure 5-16. Loading and Stress versus Length for the 1.2 MWe Turboelectric Vehicle

where M and R are the binding moment and radiator radius; this equation is a standard device for treating the effects of combined loading in a buckling analysis. Comparing the curves for P_D and P_E, it is seen that the upper portion of the radiator is concerned more with the dynamic load, and the lower portion is concerned with the aerodynamic and inertial equivalent load.

Taking the complete radiator under the influence of these loads, it is first examined for general instability. Inasmuch as the header bumpers represent stiffening rings, their adequacy as is, is first checked. To assure general stability of the total shell they require a cross-sectional moment of inertia sufficient to meet the following criterion:

$$I_f = \frac{1.3\ C_f\ P_E\ D^3\ d}{4\ EL}$$

where D is the header bumper ring diameter, d is the axial spacing between the rings, C_f is a coefficient relating the analysis to test data, E is the material Young's Modulus, and L is the overall length of the shell. In the case of conical portions of the radiator, equivalent values are used for D, d, and L which convert the cone dimensions to those of an equivalent cylinder. In all three vehicle designs, the header bumper rings were found adequate to ensure general stability without additional beefing-up.

The next step in the analysis is concerned with buckling failure of the portions of the radiator between the header bumper rings. To accomplish this an individual tube fin element is examined by comparing its compressive stress and its critical buckling stress. The applied stress is merely the total appropriate axial load at the section divided by the total cross-sectional area of the radiator bay matrix. The critical buckling stress is given by

$$\sigma\ CR = \frac{C\ \pi^2\ EI}{AL^2}$$

In this case L is the equivalent spacing between the stiffening rings, I and A are the moment of inertia and cross-sectional area properties of the tube-fin element and c is

an empirical coefficient accounting for the type of end fixity to be assumed. In many cases the radiators were found to be insufficient when checked for this local instability, and auxiliary rings were added between the header rings to reduce the value of L in the equation.

In a case such as this, it is difficult to optimize the design. For example, adding one ring immediately reduces the σ_{CR} by a factor of four. If the initial discrepancy were only a factor of two, the solution of adding a ring is excessive. In a normal shell design the procedure would be to go back and reduce the I_f of the major rings (header bumpers in this case) consistent with the reduced ring spacing. Since other considerations influence the dimensions of these rings, full optimization is a complex task completely inconsistent with the scope of the present study.

In the case of the 1200 KWe turboelectric vehicle, Figure 5-16 shows the comparison of compressive stress and buckling stress along the entire length of the radiator. Rings were only required in the upper two bays and the large resultant margin clearly illustrates the problem of optimizing this buckling consideration. Similar analyses were completed for both the 4800 KWe turboelectric and the 1000 KWe thermionic vehicles. These were reported in the Third and Fourth Quarterly Report, GE Document No. 64SD700 and are therefore not repeated herein. As was mentioned before, these purely structural additions to the radiator are a small percentage of the total weight; however, it is apparent that careful optimization of the structural requirements with the radiator design might lead to appreciable savings. For example, by increasing the header pipe wall thickness, the bumper thickness could be reduced on the basis of the meteoroid bumper criterion. This would reduce the I_f of the header bumper rings and cause the auxiliary rings to be more effective. The net result could be a lighter weight overall design. As the depth of involvement in the detailed design of these radiators has increased, the desirability of incorporating some degree of structural analysis into the system optimization computer program has become increasingly apparent.

6. TURBOELECTRIC POWERPLANT

The powerplant discussions presented in the quarterly reports concentrated on details of particular component designs. In this topical report a broader perspective of the powerplant is presented to include discussion of power regulation and startup. Much of the details and discussion of the major components as previously published is omitted.

A. REACTOR

The assumed reactor provides lithium at about 2000°F to the boiler for vaporizing the potassium working fluid. This temperature and heat transfer medium requires refractory metal alloys in the construction of the reactor and the primary circuit. The reactor parameters of significance to the powerplant and space vehicle are the diameter and length of the radiation emitting volume, which establishes the size of the shielding. The weight of the shield can be expected to be several times that of the reactor, and will vary directly as the reactor cross-sectional area.

For use in this study, a reactor reflector outside diameter of 16 inches has been assumed for the 1.2 MWe size powerplant. The reactor is assumed to be shaped as a right circular cylinder with a 25-inch separation distance between the front plane of the active core and the front plane of the nuclear radiation shield. The sizing of the reactor for larger powers was accomplished by assuming constant power density and length to diameter ratio.

B. POWER GENERATOR

In the case of the Rankine cycle turboelectric powerplant, the power generator major components are boiler, turbogenerator, condenser and feed (or condensate) pump. The subsystems provide liquid metal circulation and pressurization. Reactors, shields, radiators, and power conditioning equipment are not included, except for that power conditioning equipment essential for operation of the power generator system components.

1. General Description of 1200 KWe Powerplant

a. Heat Balance

The design requirements for the powerplant components are illustrated by the heat balance and flow schematic presented in Figure 6-1. The selection of three major loops and 1850°F turbine inlet temperature was made by the Technical Manager at the NASA-Lewis Research Center for use in this study. The auxiliary circuits presented are one solution to component cooling and lubrication.

The use of a primary circuit to transport thermal energy generated in the reactor, to a separate boiler for the heat addition process of a Rankine cycle, separates nuclear problems from two-phase flow boiling problems. Lithium is selected as the heat transfer medium because of its low vapor pressure, excellent thermal conductivity, high specific heat and low nuclear activation properties.

The secondary circuit performs the two-phase Rankine cycle power conversion process. A simple four process circuit is selected, which consists of heat addition (boiler), expansion (turbine), heat rejection (condenser), and compression (pump). The alternatives of using complex Rankine cycles with reheat or turbine interstage bleed to preheat the boiler feed have not been considered. Potassium is selected as the working fluid because of its favorable vapor pressure in the required operating temperature range.

Tertiary circuits are provided to transport heat of condensation from the condenser to the radiator for rejection to space. A direct condensing radiator design is more sensitive to uncertainties in prediction of startup, heat transfer and probability of survival of meteoroid impact than an indirect heat rejection system. In addition, the use of tertiary circuits allows radiator segmentation which prevents a complete loss of power generation capability in the event of a meteoroid puncture or plumbing-system failure. NaK is selected over other liquid metals as the heat transfer medium to minimize the hazard of freezing during launch and prior to startup.

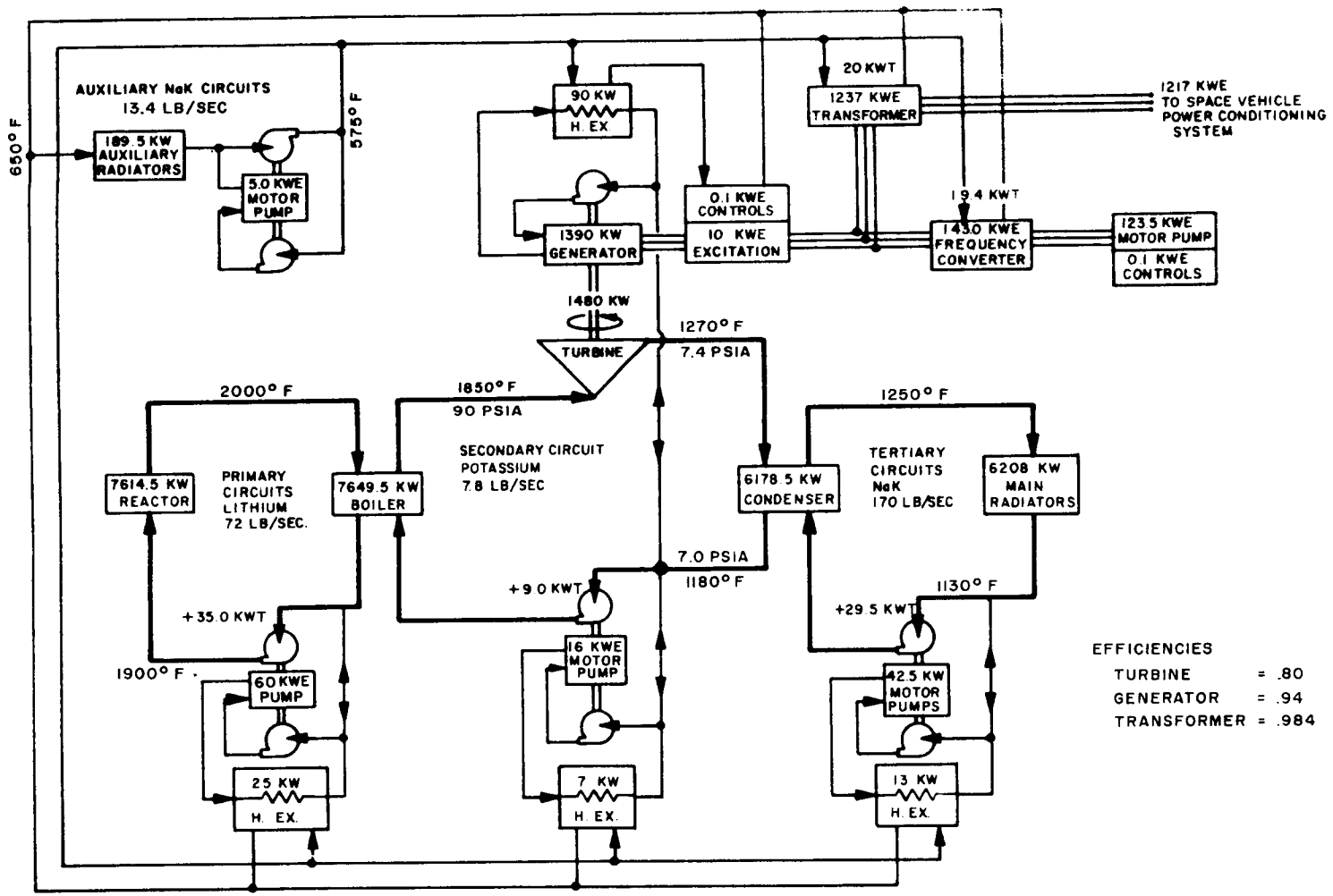

Figure 6-1. Heat Balance for the 1.2 MWe Turboelectric Powerplant

One or several auxiliary NaK circuits are provided to cool, either directly or indirectly, the electrical and rotating mechanical equipment. This equipment will have to be maintained at temperatures ranging between 150°F and 650°F, which are below that of the tertiary NaK circuits for the main radiators. Thus, auxiliary radiators are provided to achieve the required lower temperature environments, and the auxiliary NaK circuits are used to transport the waste heat away from the cooled equipment to the low temperature radiators.

In Figure 6-1, each rotating assembly is assumed to contain its own bearing lubrication pump and the lubricant is the liquid metal in the loop being serviced. Auxiliary heat exchangers are used for transfer of the waste heat from the rotating machine system into the auxiliary NaK circuits. This minimizes the vulnerability of the main liquid metal circuits to failure of fluid containment. Multiple auxiliary NaK circuits can be utilized to provide both redundancy and availability of different coolant temperatures.

b. General Arrangement

The flow schematic and heat balance described above can be transformed into a variety of general arrangements with many combinations of multiple major and auxiliary components. One typical arrangement is illustrated in Figure 6-2. In this power generator system layout, one turbogenerator is coupled to four boilers and four condensers. The heat rejection system consists of eight main radiator NaK circuits and two low temperature auxiliary NaK circuits. One of the auxiliary NaK circuits is maintained at a level of about 600°F and the other at about 200°F.

To provide convenient packaging, four boilers are used as an example in the design. These four boilers discharge wet potassium vapor into a single superheater, or dryer, located on the centerline of the power generator module immediately ahead of the turbine. This allows design of one type of heat exchanger to generate high quality vapor where nucleate boiling is dominant, and a second type to generate dry vapor

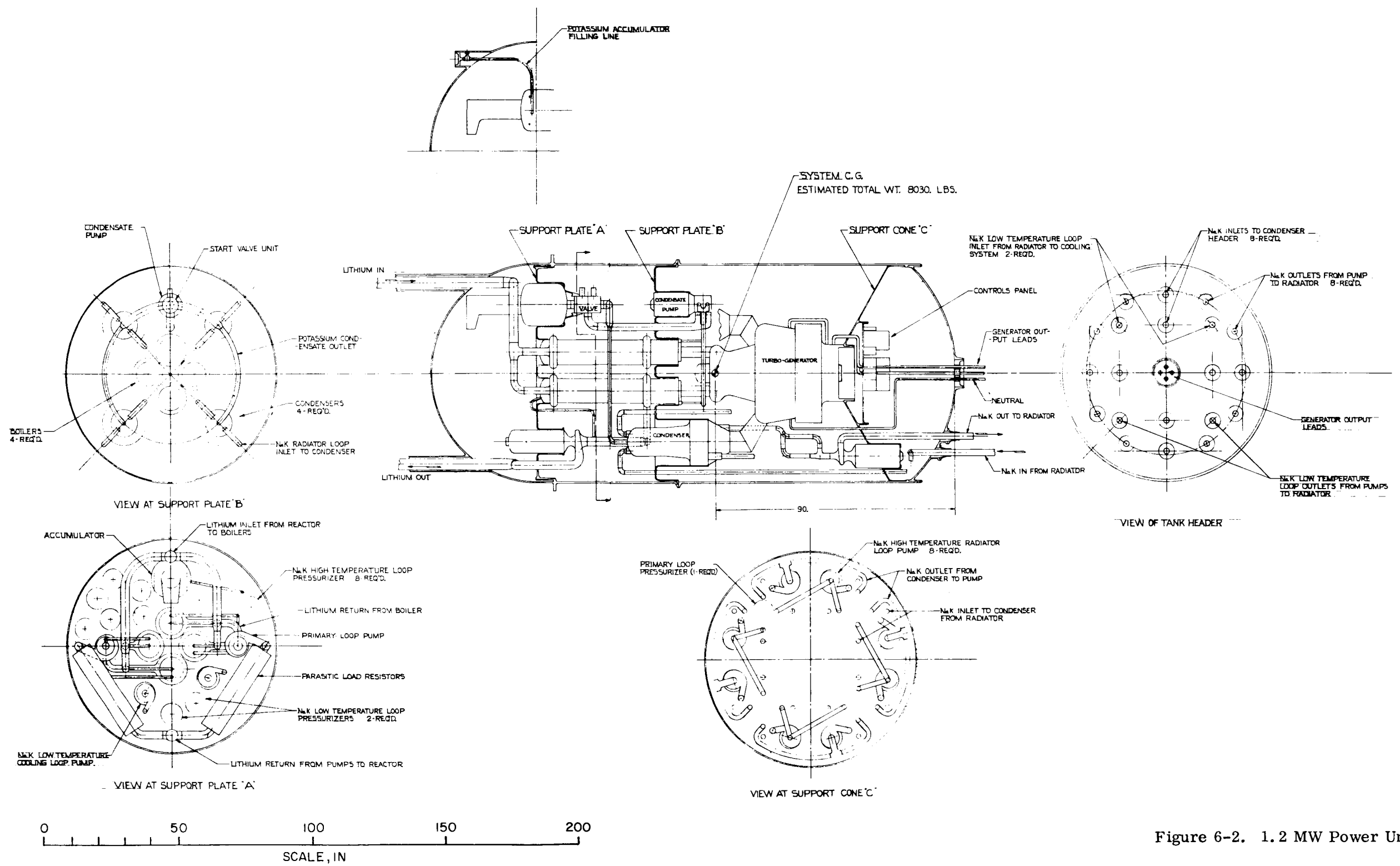

Figure 6-2. 1.2 MW Power Unit

where vapor film boiling occurs. The separation of these two heat transfer processes into two components also allows side-by-side placement of the boiler and dryer-superheater, thereby shortening the length of the potassium heating assembly.

Four condensers are used, also as an example, on the basis of packaging. In addition, the flow distribution discharging from the turbine is improved over that which would occur for a single condenser arrangement.

All of the liquid metal circulation pumps, except for those serving the power conditioning and payload equipment in the telescoping payload assembly, are located in the power generator containment vessel. Valves, pressurizers, accumulators, cold traps, and hot traps are also contained within the containment vessel. The use of this packaging approach allows manufacture and checkout of this equipment in a sealed and controlled environment and provides clean interfaces between the power generator, reactor and space vehicle radiators. This power generator module is a cylinder with hemispherical ends, 200 inches in length and 83 inches in diameter. The use of this containment vessel approach does introduce a weight penalty of 1360 pounds, but in its place other structural supports would have to be provided. The containment tank approach also simplifies the mounting of the power generator equipment in the space vehicle by utilizing the minimum number of attachment points.

Liquid metal circulation is provided by the use of motor driven centrifugal pumps. The pumps can not be designed to operate without cavitation at rotational speeds compatible with the generator output frequency of 2000 cps. As a consequence, a frequency converter is required to reduce the generator output frequency from 2000 cps, which was assumed for the study, to within the range of 100 to 400 cps which is satisfactory for the pump motor. It is believed that a satisfactory frequency converter concept has been identified, which has an additional feature of allowing variable output frequency. This scheme also permits control of condensate flow to the boiler by use of a variable speed pump, thereby eliminating the need for a flow control valve.

Estimated weight for this power generator module and its elements are listed in Table 6-1. The location of each component and resultant center of gravity is also provided.

TABLE 6-1. ELECTRICAL GENERATION SYSTEM CONTAINMENT VESSEL ASSEMBLY WEIGHTS

Item	Weight, lb Component	Weight, lb Subsystem
Primary System		370
Pumps (2)	360	
Pressurizer	10	
Turbogenerator		2600
Boilers, Condensers, Pumps and Piping		3440
Boilers	800	
Condensers	500	
Condensate Pump	150	
Potassium Piping and Valves	540	
Potassium Accumulator	250	
Main NaK Pumps (8)	880	
Aux. NaK Pumps (2)	120	
NaK Pressurizers (10)	100	
NaK Piping	100	
Powerplant Containment Structure		1360
Bulkhead "A"	120	
Bulkhead "B"	120	
Bulkhead "C"	120	
Containment Tank	1000	
Electrical System		400
Controls	150	
Pump Power Supply	50	
Parasitic Load Resistors	200	
Total Power Conversion Does Not Include Forward Power Conditioning Equipment (Located within Powerplant Containment Vessel)		8170 lb

An alternate design to the single turbogenerator power generator module is illustrated in Figure 6-3, where four turbogenerators are used. The structural integration of this package is simpler and involves less weight than that for the single turbogenerator. The boilers and turbogenerators are mounted on the central cylinder. The primary loop pumps and associated primary loop equipment are mounted on the reactor end bulkhead of the containment tank. Condensers, condensate pumps, high and low temperature radiator coolant pumps, start valves, and accumulators are mounted on the opposite end bulkhead. The outer shell of the tank is free of all equipment. Thus, the conversion system can be assembled on the open inner-cylinder-end bulkhead structure prior to putting on the outer shell. Table 6-2 lists the conversion system package weights. The reduction in weight results mainly from the improved structural configuration (elimination of heavy intermediate bulkheads) and from the assumption that the containment tank structure can make extensive use of titanium honeycomb construction, which leads to an estimated containment tank weight of 500 pounds.

c. Power Regulation Concept

The power generator needs to be controlled to follow variations of the electrical load without exceeding design tolerances on frequency and voltage. In addition, precautions need to be taken to protect the components of the power generator from unfavorable operating conditions. In particular, reactor and turbine temperatures need to be constrained, and either the potassium quality or the net positive suction head at various stages of the power cycle have to be limited. This is accomplished by installation of several feed-back controls in the power regulation systems.

One of these feed-back controls maintains the lithium temperature leaving the reactor within a selected tolerance of a scheduled temperature. The scheduled temperature should decrease below that of design point operation when the rated power is not being fully utilized. This approach has the advantage of reducing reactor, boiler and turbine materials temperatures, thereby prolonging structural life. In addition, the turbine inlet temperature tends to approach that of the reactor coolant discharge temperature as power output reduces, and the reactor outlet temperature reduction is necessary to prevent over-temperaturing the turbine.

TABLE 6-2. ELECTRICAL GENERATION SYSTEM WEIGHT TABULATION*
4-Turbogenerator Configuration

	Pounds
8 Radiator Pumps	880
Controls	150
Pump Power Supply	50
1 Primary Loop Pressurizer	10
4 Turbogenerators	2550
Piping	400
Containment Tank Structure	500
4 Condensers	500
4 Condensate Pumps	160
4 Boilers	800
4 Primary Loop Pumps	370
4 Accumulator-Valve Assemblies	250
2 Cooling Loop Pumps	120
4 Parasitic Load Resistors	200
10 Radiator and Auxiliary Cooling Loop Pressurizers	100
	7040

*Not used in Space Vehicle Layouts

The generator frequency is directly proportional to the turbine rotational speed and a feed-back control is necessary to maintain this frequency within specified limits. For this function either an electrical heat dump or a potassium flow control can be utilized. Probably the best scheme is to use a parasitic heat dump for rapid response, and a slower acting flow control to unload the parasitic heat dump. This flow control can be a throttle valve in any of the main potassium lines, a component bypass line with throttle valve, or a variable speed condensate pump. In the power generator design

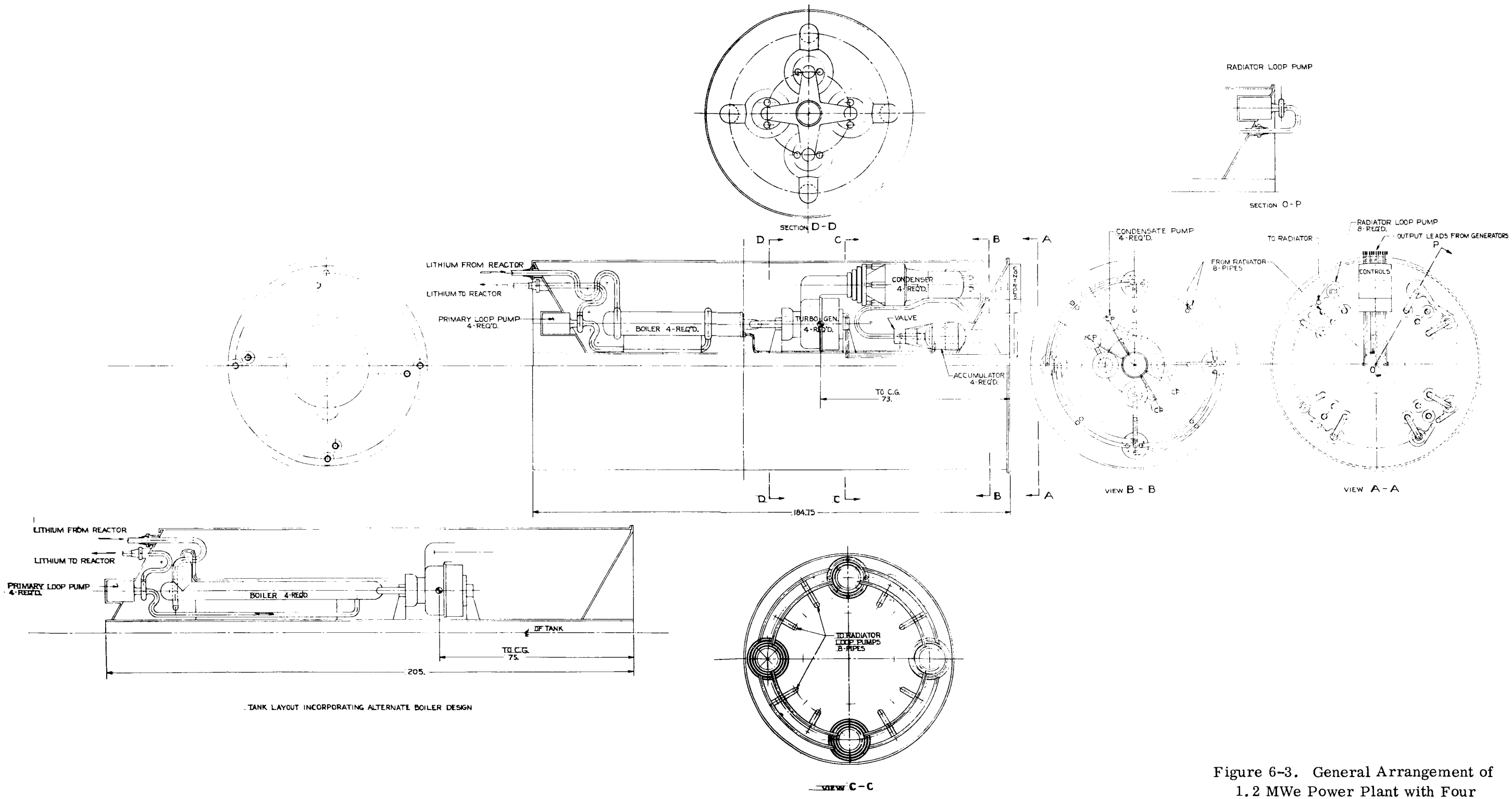

Figure 6-3. General Arrangement of 1.2 MWe Power Plant with Four Turbogenerators

presented above, the variable speed condensate pump was selected. This can be accomplished by either a variable slip coupling between motor and pump, or a variable frequency input to the motor. The frequency converter concept, also mentioned above, provides a variable frequency at command into the condensate pump motor.

An additional circuit may be necessary to control the potassium inventory in the power conversion loop. This is accomplished by a pressure regulating accumulator which functions to add or subtract potassium as required to maintain a scheduled pressure. The location for this device should be in the potassium circuit between the condenser and the condensate-feed pump.

The generator output voltage is determined by the amount of field excitation. This excitation can be varied to maintain generator voltage within design limits by the voltage regulator. However, the speed of response of this control must be slow compared to the turbine speed or frequency control in order that coupling interactions do not occur.

Overload of the power generator system may be prevented by automatic dropping of power load equipment in reverse order of priority. These dumped loads can include single thrustor units. As a result of component performance deterioration and radiator circuit loss, the maximum power generation capacity will tend to decrease with time. Thus, this situation needs monitoring to preserve the proper functioning of the powerplant. The schematic for the control system is presented in Figure 6-4.

d. Startup

The startup of a Rankine cycle turboelectric powerplant in a zero gravity space environment poses a major problem in control of the location of the liquid and vapor portions of the potassium circuit. To operate the circuit, the potassium pump needs to be filled with liquid. On the other hand, the presence of liquid in a rotating turbine may produce damage. During normal operation the dynamic processes provide the proper distribution of liquid and vapor throughout the circuit. However, during startup these dynamic forces are not yet present.

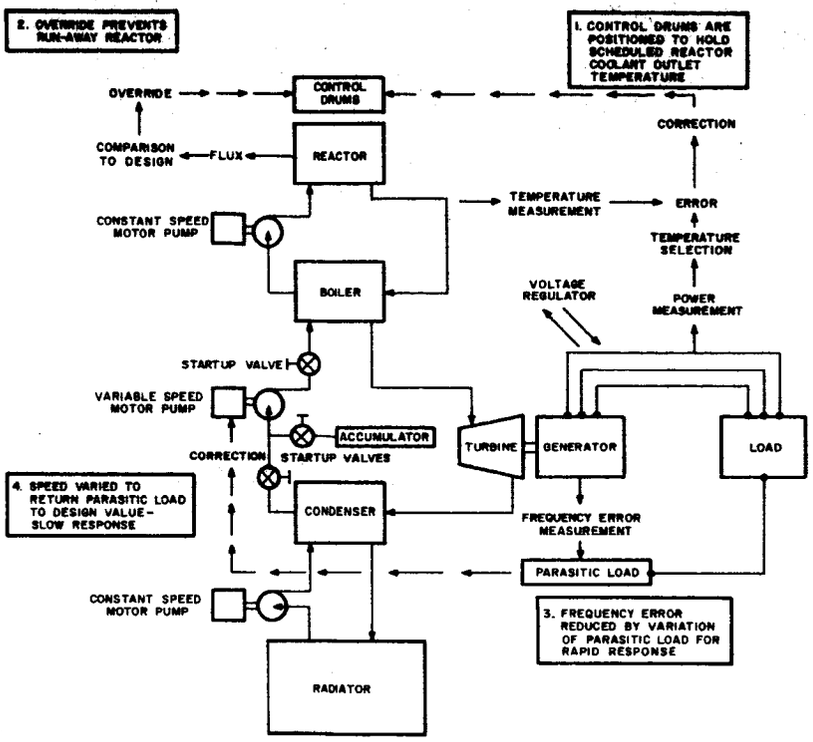

Figure 6-4. Conceptual View of Powerplant Controls

The control system schematic presented in Figure 6-4 also shows the valves and accumulator used in the startup operation. Valves are located so that the condensate-feed pump can be solid filled with potassium, allowing pump checkout before committing the powerplant to startup. The condenser exit valve could be a check valve, but a positive control actuated valve is preferable.

An example of a normal startup procedure consists of the following steps:

1. Confirm that the space vehicle is on a satisfactory trajectory to avoid unnecessary nuclear hazard.

2. Confirm that all liquid metal containment systems are sufficiently above the liquid metal freeze temperature.

3. Confirm that all single-phase liquid loops are filled and pumps are providing circulation.

4. **Bring reactor to zero power critical and maintain at selected temperature condition for normal no-electrical load operation.**

5. Close valve provided in pipe between condenser and potassium pressurizer.

6. Close valve provided between potassium condensate-feed pump and boiler.

7. Open valve connecting potassium storage tank with portion of potassium circuit between condenser exit valve and boiler inlet valve, thereby liquid filling potassium condensate-feed pump.

8. Start motoring potassium condensate-feed pump.

9. Crack open boiler inlet valve.

10. Open condenser exit valve as condenser pressure begins to exceed potassium condensate-feed pump inlet pressure.

11. Start potassium pressurizer control operation.

12. Start turbine speed control operation.

13. Start generator voltage control operation.

14. Open boiler inlet valve completely.

15. Start reactor power regulation control operation.

16. Transfer power generator system electrical loads from auxiliary power supply to main generator.

17. Checkout power generator system operation.

18. Add vehicle electrical loads as desired.

There are many details in the startup of a Rankine cycle powerplant to be perfected before satisfactory space environment operation can be established with automatic startup. The solutions to these problems may lead to ever increasing complexity of the powerplant.

To accomplish the first start, liquid potassium can be contained outside the working fluid loop and injected at a proper position and time in accordance with a scheduled sequenced and timed operation to develop the necessary dynamic forces for a controllable working fluid circuit. Shutdown and restart are desirable, as they provide flexibility. If restart of the powerplant can be accomplished it might allow manned repair in orbit and shutdown of the powerplant for periods of time when not in use, (coast period). The powerplant shutdown reduces radiation fields, which might allow access for repair and maintenance. This could be important during the initial stages of flight for the unmanned missions, if failures brought about by launch can be corrected.

2. General Description of 4.8 MWe Powerplant

The features described above for the 1200 KWe power generator system apply equally well to the 4800 KWe turboelectric powerplant installation. A layout for an integrated 4800 KWe power generation system has not been made for this study. Instead, the use of four 1200 KWe power generator modules of the type illustrated in Figure 6-2 was assumed for the space vehicle arrangement (shown in Figure 4-4). These four power generators operate from heat produced in a common reactor. The use of multiple reactors has not been studied.

3. Turbogenerator

Preliminary turbogenerator designs are presented in Figures 6-5 to 6-9, for 300, 600 and 1500 KVA capacities, which have been prepared to support powerplant layout studies of multiple turbogenerator power generation systems. Miscellaneous design data is listed in Table 6-3.

The turbine is a convential axial flow type with four to six stages. The generator selected is an axial-gap design, although a radial gap configuration could also be used.

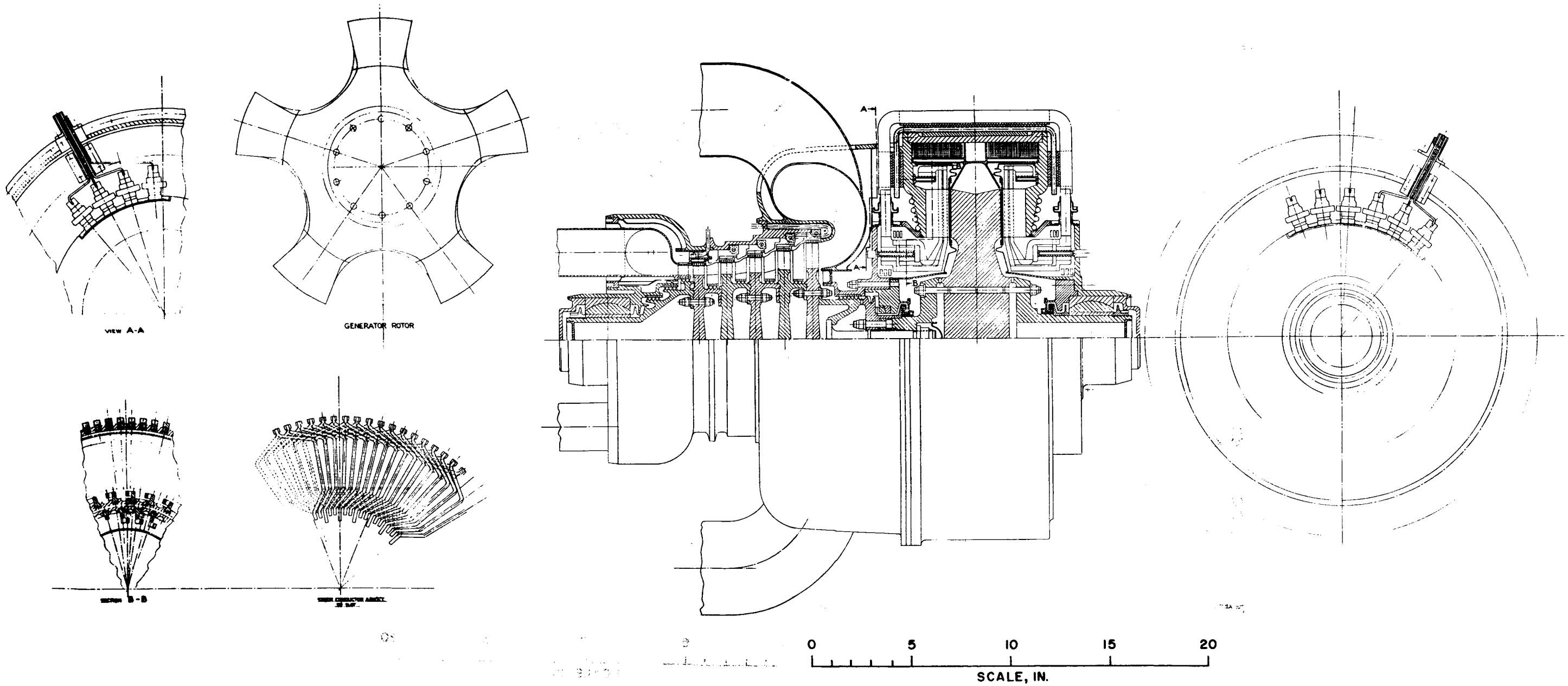

Figure 6-5. 300 KVA Turbogenerator with 14.5 Diameter Generator Rotor

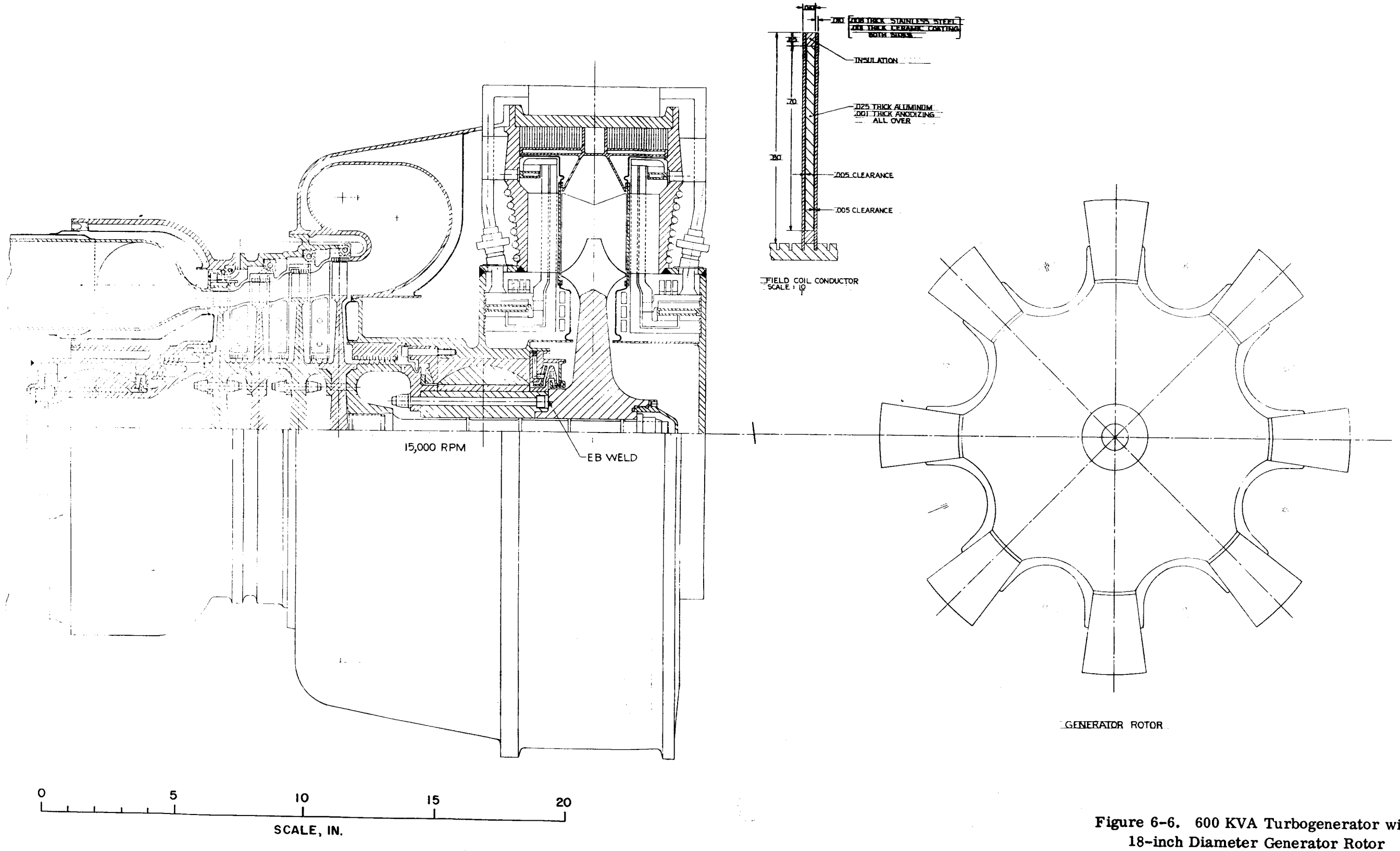

Figure 6-6. 600 KVA Turbogenerator with 18-inch Diameter Generator Rotor

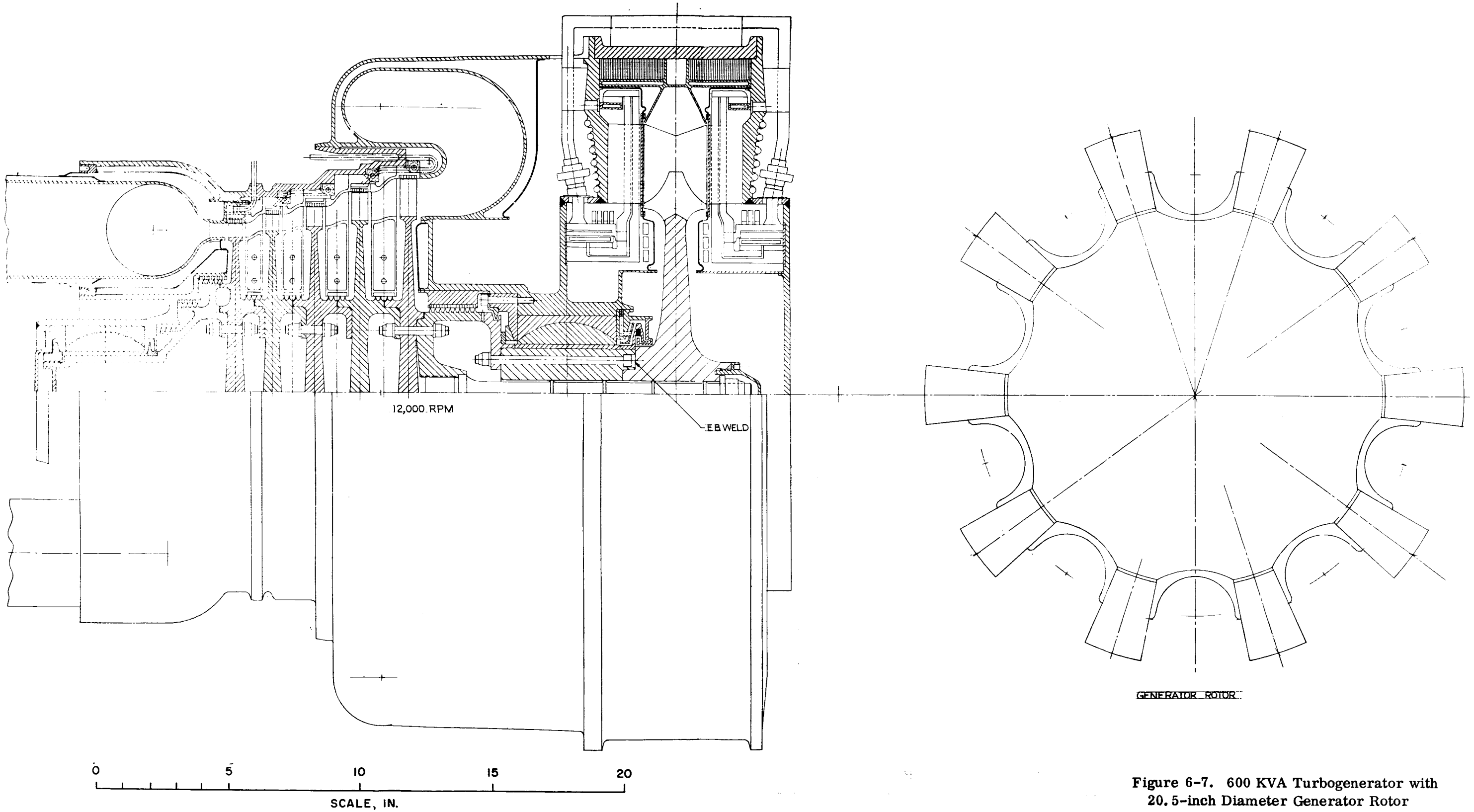

Figure 6-7. 600 KVA Turbogenerator with 20.5-inch Diameter Generator Rotor

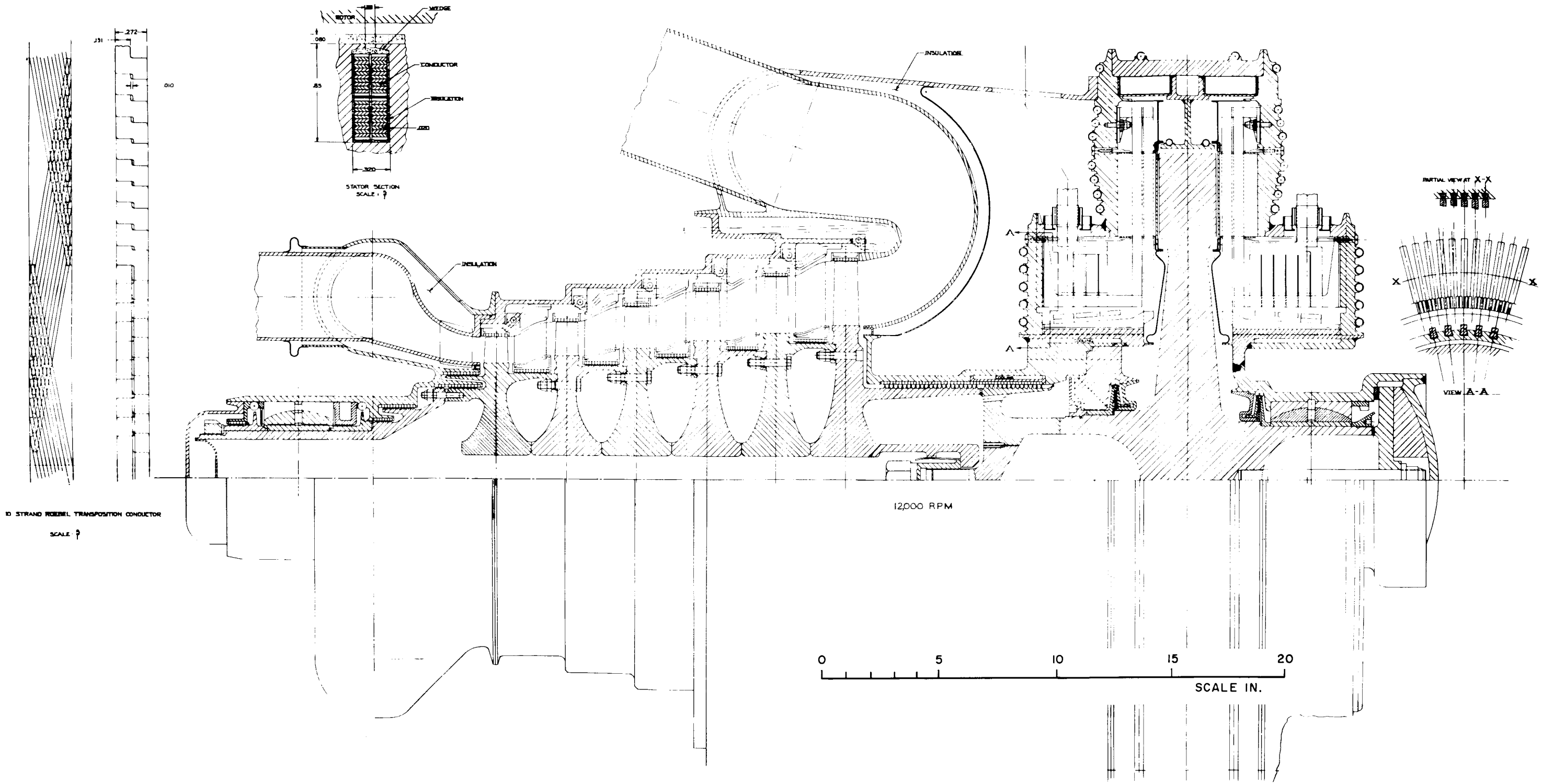

Figure 6-8. 1.2 MW Turbogenerator

TABLE 6-3. TURBOGENERATOR DESIGN DATA

Ref. Figure	6-5	6-6	6-7	6-8/9
Capacity, KVA	300	600	600	1500
Voltage	600/1040	600/1040	700/1212	120/208
Frequency, cps	2000	2000	2000	2000
Rotor Speed, RPM	24,000	15,000	12,000	12,000
Inlet Temperature, °F	1,850	1,850	1,850	1,850
Discharge Temperature, °F	1,290	1,340	1,340	1,250
No. of Stages	5	4	5	6
Stage Velocity Ratio	0.54	0.52	0.52	0.60
Bucket Root Stress, psi				
First Stage	5,700	4,700	4,000	6,000
Last Stage	23,800	13,000	12,000	25,000
Max. Wheel Stress, psi				
First Stage	17,000	16,000	15,000	25,000
Last Stage	37,000	25,000	30,000	48,000
Generator Tooth Root Stress, psi	85,000	65,000	55,000	60,000
Power Losses, KW				
Radial Bearings	15	16	14	10
Thrust Bearing	<1	< 1	1	20
Hydrodynamic Seals	6	2.5	3	15
Turbine Shaft Efficiency	0.77	0.80	0.81	0.80
Generator Efficiency	0.93	0.93	0.93	0.94
Weights, lb				
Turbine	265	360	525	1,000
Generator	375	450	600	1,600
Total	640	810	1,125	2,600
Rotor	160	160	260	500
Rotor Tooth Dimensions, in.				
O.D.	14.5	18	20.5	28
I.D.	10.0	12	14.5	21
No. of Rotor Teeth	5	8	10	10
No. of Poles	10	16	20	20

The axial gap inductor alternator is rigidly coupled to the turbine rotor and the assembly is supported on two liquid metal lubricated bearings. The salient features and advantages of this design approach are:

1. Integrated rotor design is based on two self-aligning liquid potassium radial bearings and on rigid turbine-generator coupling. The turbine rotor is designed for high flexural stiffness. This approach is compatible with angularly stiff mounting of the axial gap generator and offers the best possible solution to the problem of rotor mounting on liquid metal bearings. It avoids the use of spline couplings for which no adequate lubricant is available, and it avoids flexible couplings which are undesirable with synchronous machinery because of the torsional vibration (hunting) problem.
2. Hydrodynamic seals are employed for the maintenance of a controlled temperature liquid to vapor interface on both sides of the generator rotor space cavity. By this means the density of the vapor in the generator rotor space can be maintained sufficiently low that rotor windage is negligible and liquid accumulation is eliminated.
3. Alumina disc gap seals are used for isolation of the armature winding spaces from the rotor space vapor atmosphere. (The configuration can be modified to omit this seal for the case where alkali metal vapor is not present.)
4. Machine heat transfer in vacuum environment is improved:

   - The stator core and winding structure is divided into two sections, each having short slots. Each section has end windings, which are accessible to cooling by positive clamping to heat sink surfaces. This allows design for a conductor hot spot to coolant ΔT in the range of 100°F to 200°F by axially conducting heat along the conductor to the cooled end winding. Thus, heat transfer through the stack is not necessary. (The latter heat transfer path involves conduction across several metal to insulator interfaces having relatively large thermal resistances under vacuum conditions.)
   - The rotor configuration is an axially short wheel with magnetic poles attached to the outer periphery. Pole face losses generated in these teeth can be removed by: 1) radiation from the outer edge of the teeth and from the contiguous intertooth peripheral surfaces of the wheel to a cooled stationary surface enclosing the wheel, 2) radiation from the sides of the wheel to cooled stationary surfaces.
   - The axial interface between the stator core and the frame is a plane surface facilitating cooling of the core by conduction to the cooled frame.

- Conduction radially inward through the wheel to the cooled journal section of the shaft. Rotor cooling in this manner eliminates the need for circulation of liquid metal through the generator rotor.

5. The turbine rotor consists of a rabbetted and body-bound bolted assembly of discs with integrally machined buckets, interstage spacer-seal rings, end shaft tubes, and labyrinth seal rings. Material tentatively selected for the rotating parts is TZM molybdenum. Static parts are columbium - 1% zirconium alloy.

6. The two radial bearings are supported through spherical seats which permit free angular alignment of the bearings. The thrust bearing, which is located on the generator end of the shaft, is also mounted in a spherical seat so that it exerts no radial or angular restraint upon the rotor.

4. Heat Transfer Components

a. Boiler

A boiler design concept is illustrated in Figure 6-10. There are four identical once-through boiler units. Each unit incorporates a feed heater counterflow heat exchanger coil through which the feed liquid from the condensate pump is fed to the floating nucleate boiling tube header. The coil itself provides the necessary differential thermal expansion flexibility between shell and tubes. From the preheater coil, the feed liquid passes into the nucleate boiling tube header and into the nucleate boiling tubes. From these tubes, wet vapor at a quality of approximately 85 percent discharges into the end bell plenum and then undergoes a 180 degree turn into the dryer superheater duct inside the nucleate boiling tube annulus.

In the center of this duct is a bayonet tube full of heating fluid. Around this duct a spiral vane swirler is wrapped. Drying is accomplished through centrifuging of entrained drops onto the heated outer wall of the duct. A capillary structure on this hot wall promotes the retention of impinging drops until they can be boiled. Capillary structures are also employed in the swirler vane, bayonet tube and on the end bell wall. In the case of the vane the capillaries retain and feed impinging liquid to the contiguous heated surface where boiling can take place. The effectiveness of this

approach to drying wet vapor has been demonstrated in water tests at General Electric. It permits an order of magnitude higher drying section heat flux rates than are possible by the method of convective superheating of the vapor phase to boil off entrained drops within the stream. The pressure drop is also substantially less.

A compact L tube boiler has been designed as an alternate, using helical inserts to obtain dry vapor. The layout of this design is shown in Figure 6-11. Heat transfer performance has been based upon Dwyer's work for liquid flowing parallel to tube bundles. Proper insert design is expected to produce 100 percent quality at the mass flow rates selected with pressure drop values as described below. This design utilized 3/4-inch tubes with 0.063-inch wall thickness. The tube diameter and length have not been optimized but are selected on the basis of reasonable values for the helical inserts presently under study. The inlet region of the tubes would be orificed with a sharp edge orifice or an annular flow channel formed by a plug attached to the insert. The liquid pressure drop so produced has been found to improve the stability of boiler operation. Using small diameter tubes (<3/8-inch diameter) requires orifice openings of such small diameter as to be impractical. The L/D necessary to produce dry vapor for a given mass flow is related to the pitch ratio (λ/D) of the helical insert. The available potassium data is for $\lambda/D = 2.2$, which also has been used in the present design. The temperature profile for either parallel flow or counterflow has been calculated and no great difference is found for this design. For higher pressure drop units this could be a significant consideration.

Design data on the boilers are given in Table 6-4.

b. Condenser

One condenser design is illustrated in Figure 6-12. Four units are attached to the turbine discharge scroll. Turbine discharge vapor enters the inlet plenum and then passes into the converging flow passages between four conical coolant shells. These condensing passages terminate in narrow annular spaces in which the discharge phase

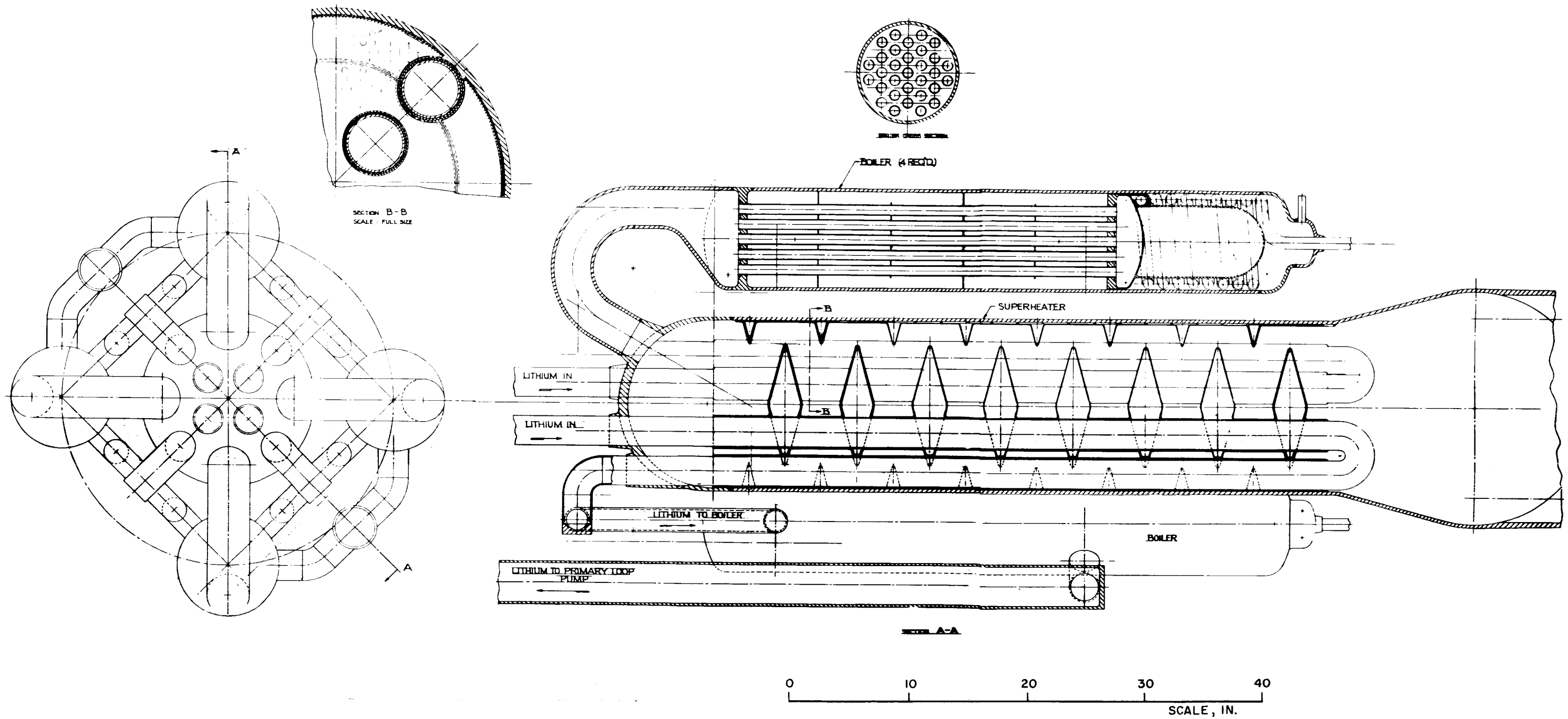

Figure 6-10. 7.6 MWt Boiler, Design "A"

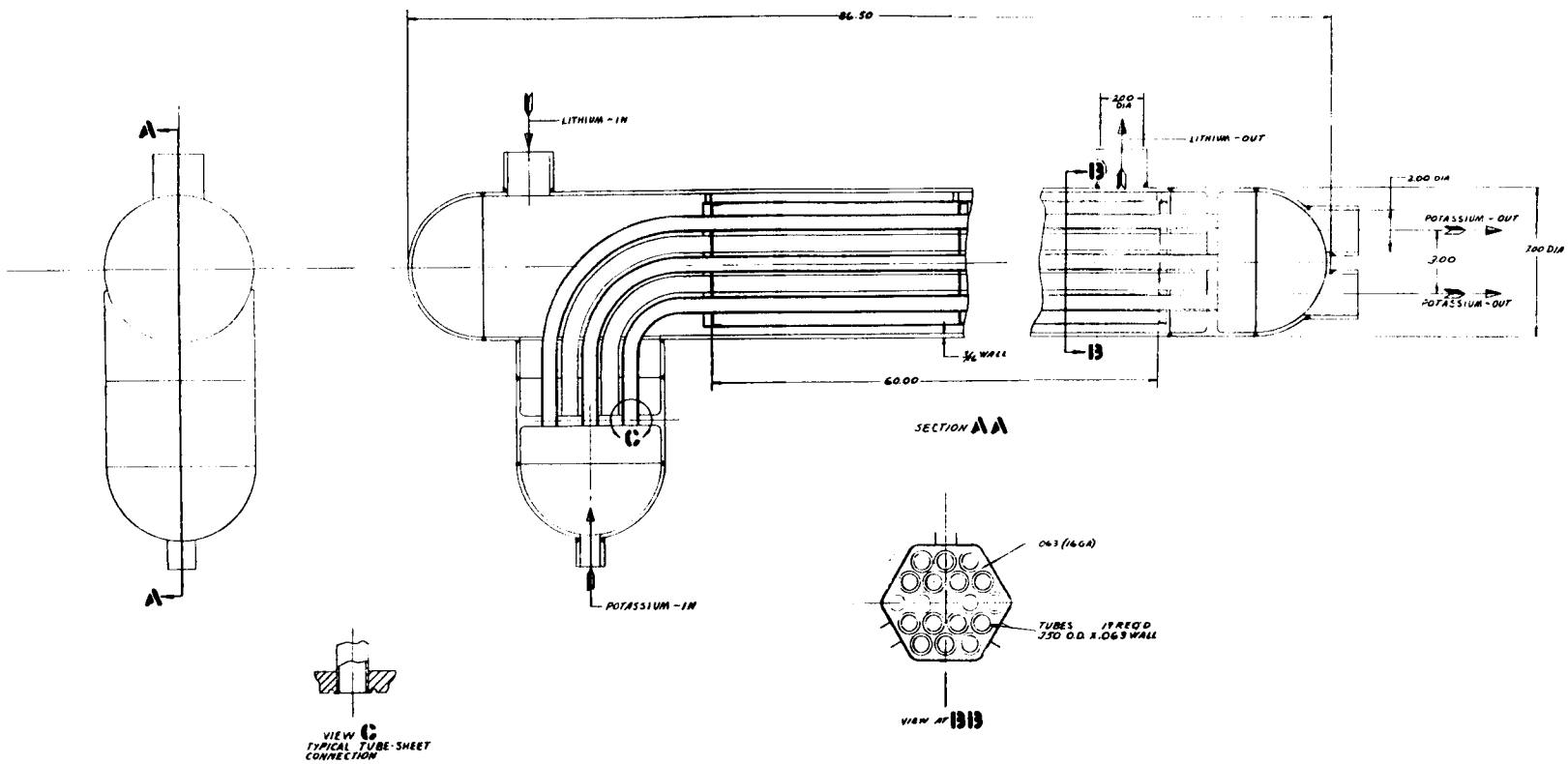

Figure 6-11. 1.9 MWt Boiler, Design "B"

TABLE 6-4. 7.6 MWt BOILER DESIGN DATA

	Lithium Side	Potassium Side
Inlet Temperature, °F	2,000	1,180
Inlet Pressure, psia	35	130
Outlet Temperature, °F	1,900	1,850
Outlet Pressure, psia	25	92
Flow Rate, lb/sec	72	7.8
	Design A (Figure 6-10)	Design B (Figure 6-11)
Total Weight, lb	800	912
Boiler		
Number	4	4
Avg. Heat Transfer Coefficient, BTU/hr-ft^2-°F	3,000	6,800
Avg. Heat Flux, BTU/hr-ft^2	300,000	257,000
Exit Quality	.85	1.00
No. Tubes/Shell	.28	19
Tube O.D., in.	.75	.75
Dryer		(not required)
Avg. Heat Flux, BTU/hr-ft^2	120,000	—

interface is stabilized by surface tension. Sufficient storage volume is provided in these interface annuli to accommodate liquid inventory shifts between boiler and condenser occurring during load changes.

Coolant liquid enters the shells at the interface end through four tubes which connect into circular manifolds. Similar manifolds are employed at the coolant discharge end of the shells. These manifolds are designed for sufficient flexibility to accommodate differential thermal expansion between the outer shell and the coolant shells.

In the event of the loss of coolant in one shell due to meteorite impact on the corresponding radiator segment, the condenser will continue to function. The shells may be

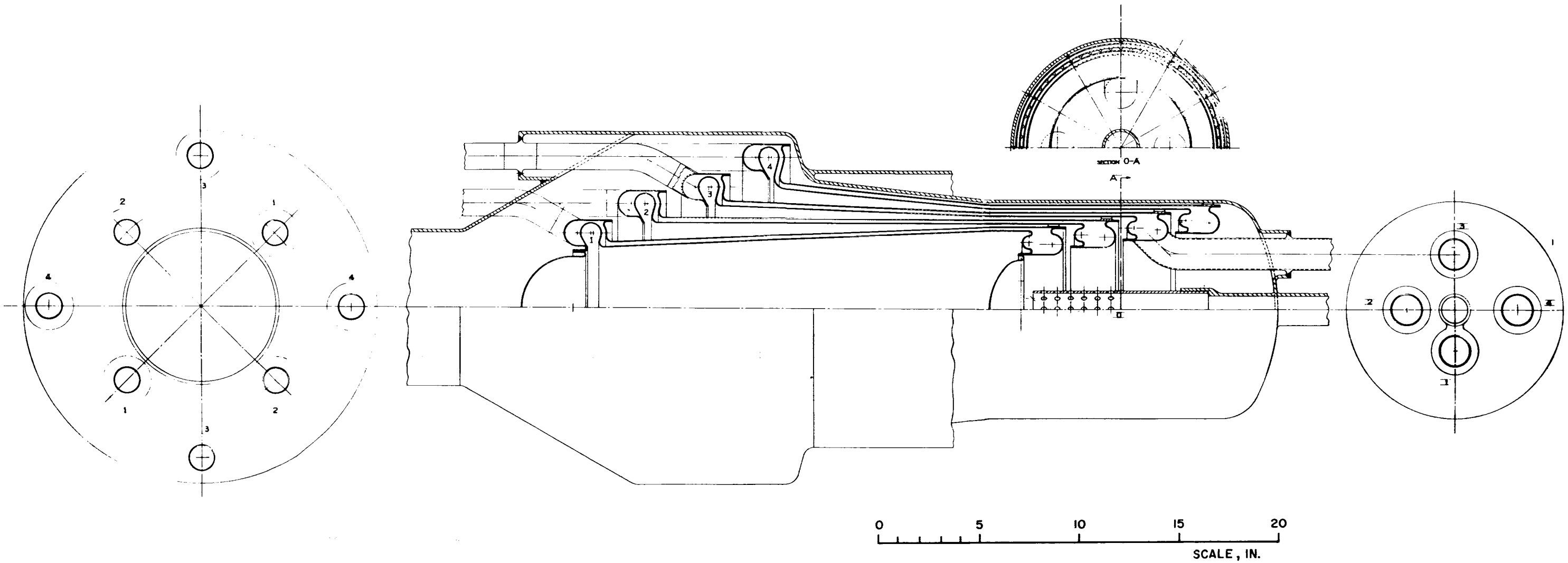

Figure 6-12. 6.2 MWt Condenser, Design "A"

designed to incorporate intercommunication between parallel condensing passages. Heat transfer in the condenser is limited on the liquid convection heat transfer side. By increasing liquid coolant flow velocity through these shells, the heat flux rate may be increased. This fact may be used to advantage in the event of failure of one or more of the radiator segments. System off-design (abnormal operating conditions) analyses will be required to resolve such questions.

An alternate condenser design based on tube and shell heat exchange construction with condensation and subcooling inside of tubes in separate shells served by different cooling loops to guard against vapor flowing to the pump inlet is shown in Figure 6-13. Eight of these units would be required, thus complicating the plumbing.

Condenser design data are summarized in Table 6-5.

TABLE 6-5. 6.2 MWt CONDENSER DESIGN DATA

	Potassium Side	NaK Side
Inlet Temperature, °F	1270.0	1130
Inlet Pressure, psia	7.4	38
Outlet Temperature, °F	1180.0	1250
Outlet Pressure, psia	7.0	32
Flow Rate, lb/sec	7.8	170
	Design A (Figure 6-12)	Design B (Figure 6-13)
Total Weight, lb	500	~500
No. of Units	4	4
Avg. Heat Flux, BTU/hr-ft^2	330,000	~ 330,000

C. SHIELD

The integrated dose that is tolerable for the payload electronics is quite difficult to estimate at the present time. In lieu of this estimate, allowable doses were assumed to be 10^6 rads of gamma rays and 10^{11} nvt of fast neutrons.

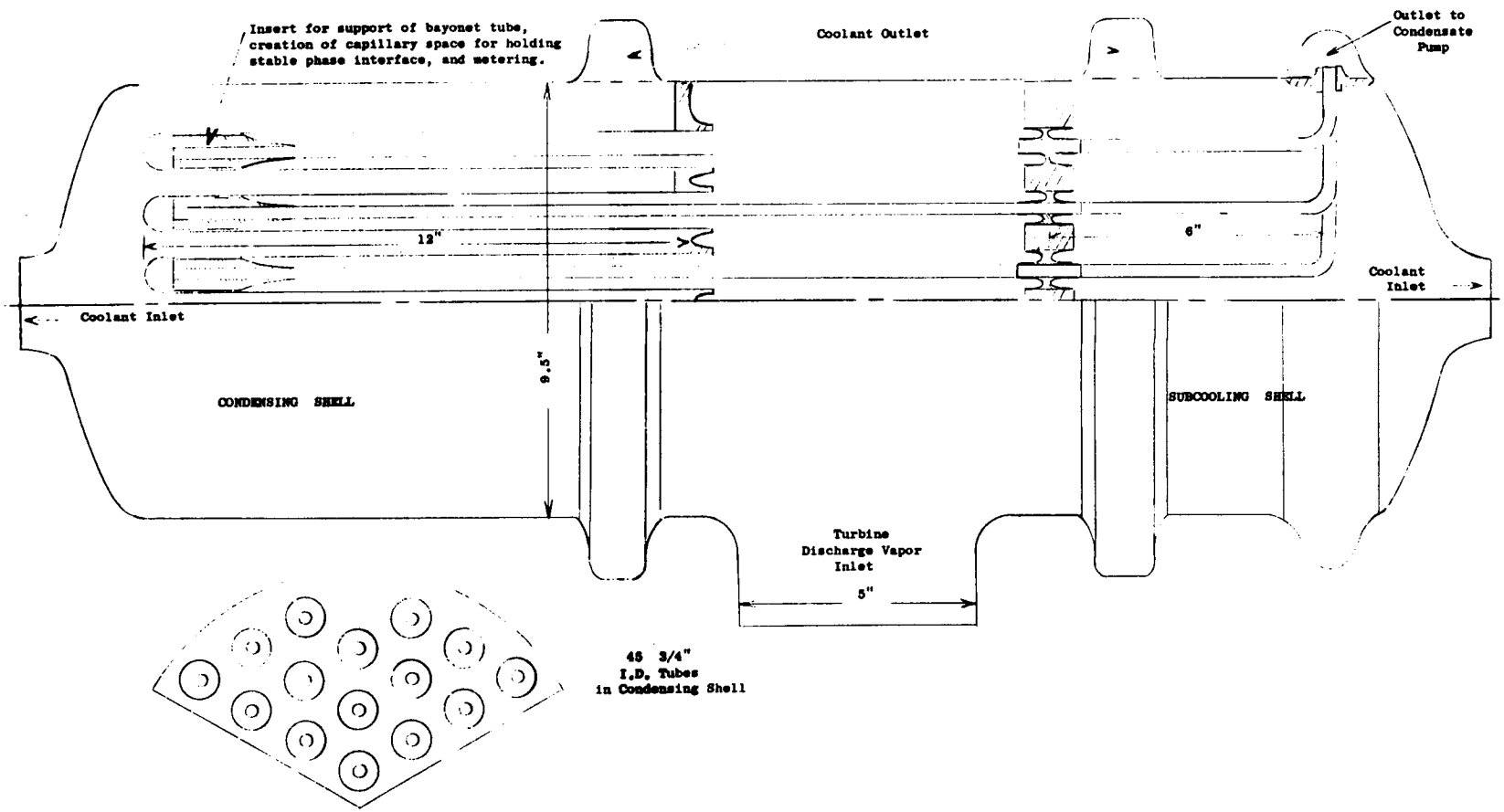

Figure 6-13. 6.2 MWt Condenser, Design "B"

The amount of shielding that must be provided in a nuclear-electric spacecraft is determined by the least radiation tolerant components in the spacecraft. In general, the electronic components in the power conditioning system and payload are the least resistant. However, careful attention must also be given to the selection of fluids for gyros of the attitude control system when these types of components are used.

In general, solid state components are preferred for the electronic subsystems because they have demonstrated long life reliability. The exclusive use of ceramic tubes and TIMMS, which have demonstrated high tolerance to radiation, would alleviate the shielding weight penalty associated with the use of solid state components. However, these components require more development and operational experience for long time at required environmental temperatures.

In determining the tolerance of solid state semiconductor components to radiation, it is necessary to measure the probability of component failure in a given radiation environment. For this analysis, failure is defined as the inability of a subsystem to perform its intended function. Failure can manifest itself in two forms: (1) catastrophic failure where the subsystem ceases to function altogether, and (2) degradation where the subsystem output drifts out of limits. The latter type of failure is most common in a radiation environment.

Most of the irradiation data for components have been presented in the literature as the change in an operating parameter as a function of integrated dose. For example, the tolerance of transistors is often given as change in transistor gain versus integrated dose. This change in gain occurs over several orders of magnitude change in integrated dose before the transistor fails completely. Therefore, it is quite difficult to speak in general terms about the radiation tolerance of components. It is first necessary to identify how the components are used in the circuits; and then, on the basis of each required operating characteristic to determine the radiation dose at which failure will occur.

A second factor is the percent failure versus integrated dose. For high reliability it is necessary to select the integrated dose at which perhaps 0.01 percent of the components fail. Here there is a real lack of irradiation data. Most irradiation testing has been based on finding the integrated doses where 50 percent or more of the components failed, with very little attention given to lower failure rates. To determine the integrated dose corresponding to 0.01 percent failure, it is necessary to make large extrapolations of the present data and this is further complicated by the very small sample sizes incorporated in the irradiation test program.

Presentations, such as shown in Figure 6-14, are often used to indicate the tolerance of materials and electronic parts to a radiation environment. This figure presents a generalization of the radiation problem but cannot be used for selection of shielding criteria. The reasons for this are:

1. The tolerance of a material or part is usually judged on change in a material characteristic or an operating parameter of an electronic part after irradiation. The characteristic or parameter chosen might not be the one of interest in the specific design.
2. In defining the radiation tolerance of parts and materials, it is necessary to select a damage threshold. This is often an arbitrary point such as a 25 percent change in the selected material characteristic or electronic part parameter. In a specific design, degradations which are more or less than those chosen for presentation may be of importance, thereby negating the value of the presented data.
3. The conditions that existed during the period of irradiation are often not specified or accurately controlled. These conditions include: temperature, electrical stress on electronic parts, the neutron spectrum, and the neutron-to-gamma ratio. Thus, it is difficult to apply the test results to a specific design.
4. The sample sizes represented are often too small to properly evaluate the accuracy of the test data.

Because of these points, data presented in a manner such as Figure 6-14 are inadequate for design purposes. One is forced to make an educated guess at the proper allowable radiation doses. Based on information available at the present time, integrated doses of 10^{11} nvt and 10^{6} rads are a reasonable limitation.

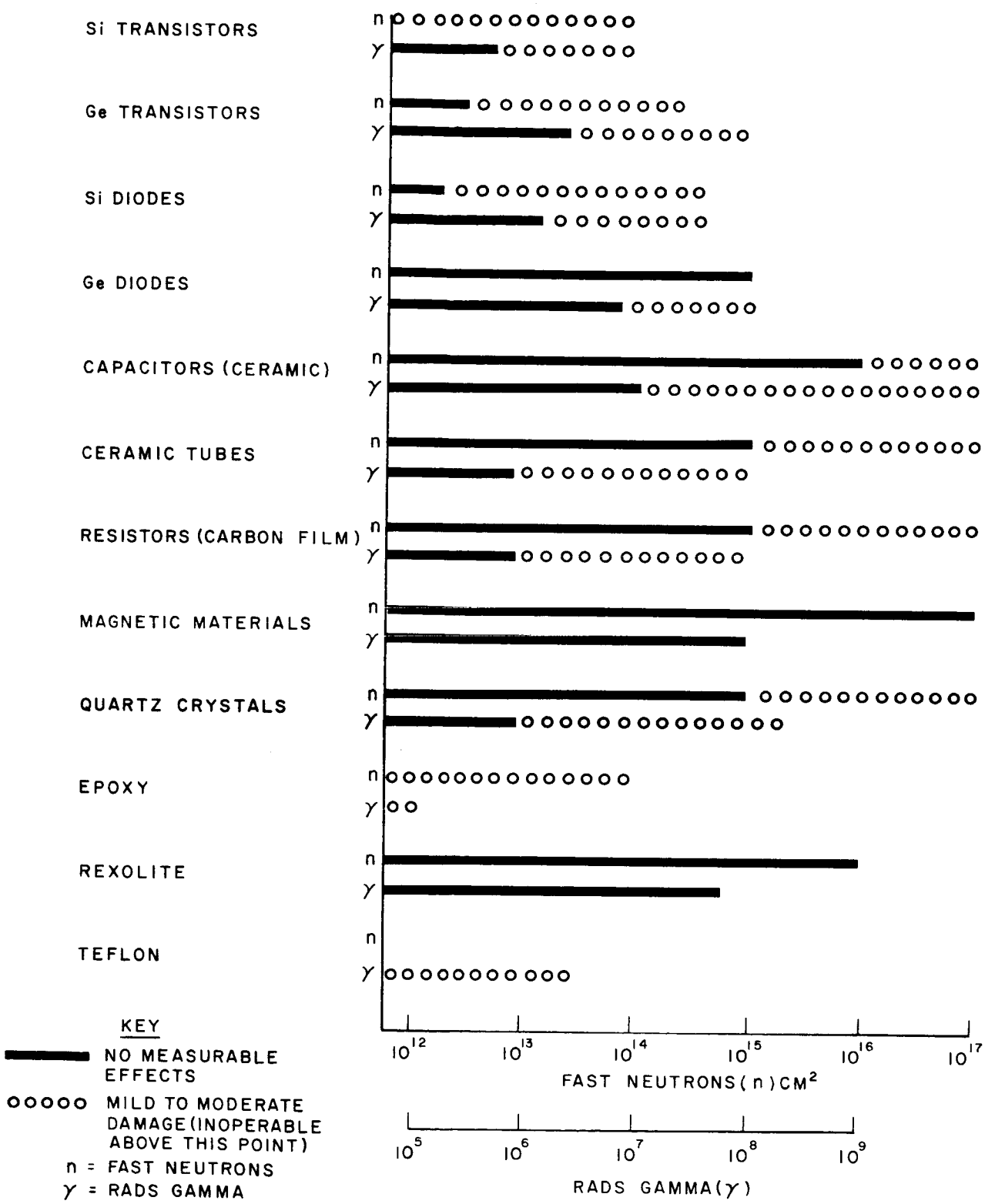

Figure 6-14. Gamma and Neutron Threshold Radiation Tolerance

The shield is generally shaped in the form of the frustum of a cone with the axis along the centerline of the spacecraft. The diameter of the shield section closest to the reactor and the shield cone angle is selected so that the payload is completely shielded from a direct view of the reactor. In this study depleted uranium (U-238) and lithium hydride (LiH) have been selected as the primary shield materials. A layer of U-238 is used as the primary shield against reactor-produced gammas. Following this is a layer consisting of a mixture of LiH and stainless steel (20 wt %), which acts as the primary neutron shield. (The stainless steel serves as structure.) An additional layer of U-238 is included behind the LiH-ss to attenuate secondary gammas produced within the previous two shield layers. A comparative study of alternative shield materials was not conducted.

A hand calculation of the shielding requirements was made for the one MWe turbo-electric spacecraft. The total shield weight has been estimated at 3410 pounds and the total shield thickness at 46 inches. Secondary gamma production in the shield is most important in the U-238 initial layer. The secondary gammas require an additional layer of U-238 on the outer edge of the lithium hydride second layer about 0.1-inch thick. The shield configuration is illustrated in Figure 6-15. The shield was sized so that the dose to the payload was evenly split between direct and scattered radiation. The power conversion equipment produces radiation shadows within which the gamma dose is reduced by a factor of 100 and the fast neutron dose is reduced by a factor of 5.

Primary gamma radiation deposits 4630 Btu per hour for each square foot of shield cross-sectional area. Sixty percent of the energy is deposited in the initial U-238 layer. The remainder is deposited in the steel and lithium hydride. Energy produced within the U-238 can be removed by radiation from the inner surface with a maximum U-238 temperature of about 1000°F.

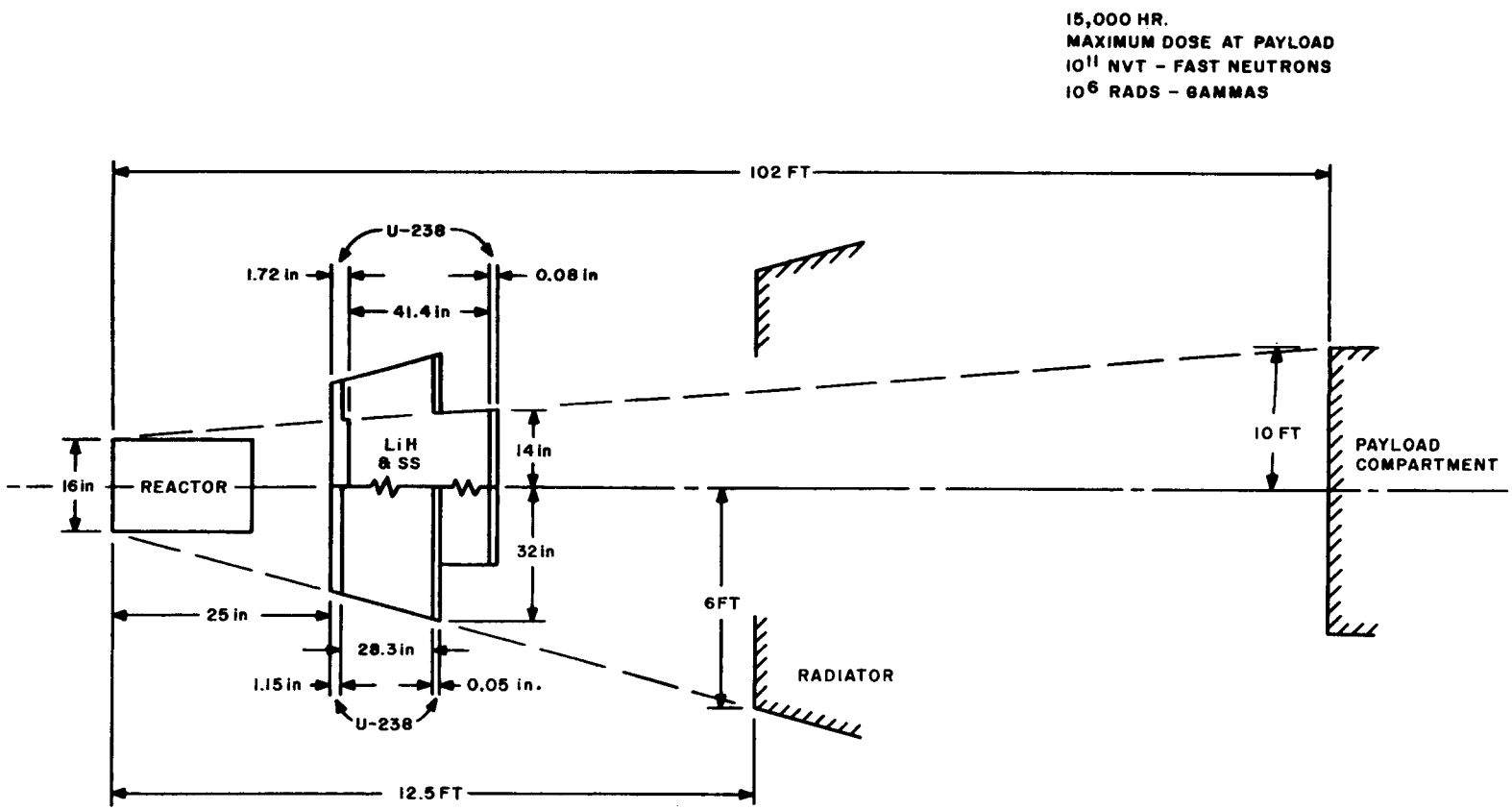

Figure 6-15. Dimensions of Shield and Separation Distances

The calculations are based on the following assumptions and data:

Gamma energy leakage rate:	2.3 mev/fission
Energy of gamma leakage photons:	5 mev/photon
Fast neutron leakage rate:	1.2 n/fission
Approximate reactor thermal power:	6670 kw
Conversion factor for a gamma flux:	9×10^5 mev/cm^2-sec = 1 r/hr
Gamma dose rate: (at payload)	66.7 r/hr
Neutron dose rate: (at payload)	1850 n/cm^2-sec

	Layer 1 (U-238)	Layer 2 (LiH-20 wt% SS)
Density	18.8 gm/cc	0.919 gm/cc
Fast neutron relaxation length (λ_n)	5.85 cm	7.37 cm
Gamma relaxation length (λ_γ)	1.155 cm	43.9 cm
d (λ_n/λ_γ)	5.06	0.168

Radiation which does not initially travel in the direction of the payload also contributes to the payload dose by virtue of scattering from the radiator section between the reactor and the payload. The payload dose from scattered radiation is significant compared to the direct dose and additional shielding is necessary between the reactor and the radiator to attenuate the scattered radiation by the required factor.

The weight of the direct radiation shield is calculated using the thickness of the three layers arranged in a configuration which shields all sections of the payload region from a direct view of the reactor. A sketch of the shield configuration is shown in Figure 6-15. The scatter shield thickness is established on the basis of attenuating the scatter dose until it equals the direct dose, which leads to a reasonable estimate of weight although this split of radiation dose may not be optimum.

In Table 6-6, the pertinent shield dimensions and weights are indicated.

TABLE 6-6. SHIELD DIMENSIONS AND WEIGHTS FOR 1.2 MWe TURBOELECTRIC POWERPLANT

Shield	Direct	Scatter
Cone Angle, deg.	6.5	21.8
Thickness, in.		
Layer 1	2.26	1.54
Layer 2	43.7	29,8
Layer 3	.147	.10
Weight, lb		
Layer 1	470	710
Layer 2	800	1210
Layer 3	90	130
	1360	2050
Total Shield Weight, lb	3410	

In addition to the direct radiation shield, additional shielding is provided by the power conversion equipment located between the reactor shield and the payload. To obtain a rough estimate of the shielding effectiveness of this equipment, it is assumed to be equivalent to an iron cylinder 38 inches in diameter and 10 inches thick with its axis along the vehicle axis. This thickness of iron will provide a fast neutron attenuation factor of 0.204 and a gamma attenuation factor of 0.011. These attenuation factors might be used to reduce the amount of neutron and gamma shielding required in the reactor shield, but before this step could be taken the effects of inelastic gamma production, scattering, and leakage through voids in the power conversion equipment would have to be evaluated.

At present, it seems preferable to allow the reactor shield dimensions, as previously computed, to remain unchanged, and to note that regions exist behind the power conversion equipment where the radiation intensity is lower than in surrounding regions. These low intensity regions may prove useful for placing equipment which is especially radiation sensitive, or for locating part of the payload equipment closer to the reactor than would otherwise be possible.

The shields for the 4.8 MWe turboelectric and 1 MWe thermionic powerplants were based on the use of the same shield thicknesses as for the 1.2 MWe turboelectric system. Corrections were not made for separation distances. The weights then varied according to reactor diameter and radiator cone angle. It is recognized that this assumption is somewhat inaccurate and that a more careful shield size estimate need be conducted during any future extension of effort on these powerplants. It is also anticipated that active cooling of these shields will be required.

7. THERMIONIC REACTOR SYSTEMS

In-core thermionic power systems were also considered for the NAVIGATOR class of missions. Details of spacecraft arrangement, radiator design, and electrical system analysis for this type of power system are included in Sections 4, 5, and 8 of this report.

A. SYSTEM SPECIFICATIONS

A heat balance and flow schematic is presented in Figure 7-1. The choice of a two-loop system is based upon the need for providing segmentation in the radiator, and the advantage of increased flexibility afforded by independent selection of working fluids in the two loops. A system of 1 MWe net output was chosen since this is close to the optimum power for a Saturn V escape launched configuration. The exact power requirement is dependent, of course, upon the powerplant specific weight that is obtained.

1. Pumps and Working Fluids

Static EM pumps are shown, although canned motor pumps could also be considered. The ac induction-type pumps are favored since these do not require conduction of current into the duct, thereby simplifying the duct structure. However, this type of pump requires a frequency convertor for its power supply. Canned motor pumps also require a frequency convertor but these pumps can deliver somewhat higher overall efficiency than EM pumps. In the reference system, however, the selection of EM pumps is based primarily upon a desire to preserve the all-static feature inherent with a thermionic powerplant.

The possible coolant fluids for an in-core thermionic system include Na, NaK, and Li. In two-loop powerplants it is possible to make an independent selection of reactor and radiator working fluids since this permits greater freedom in both core and radiator design. Lithium can be considered for both loops, if the only criteria

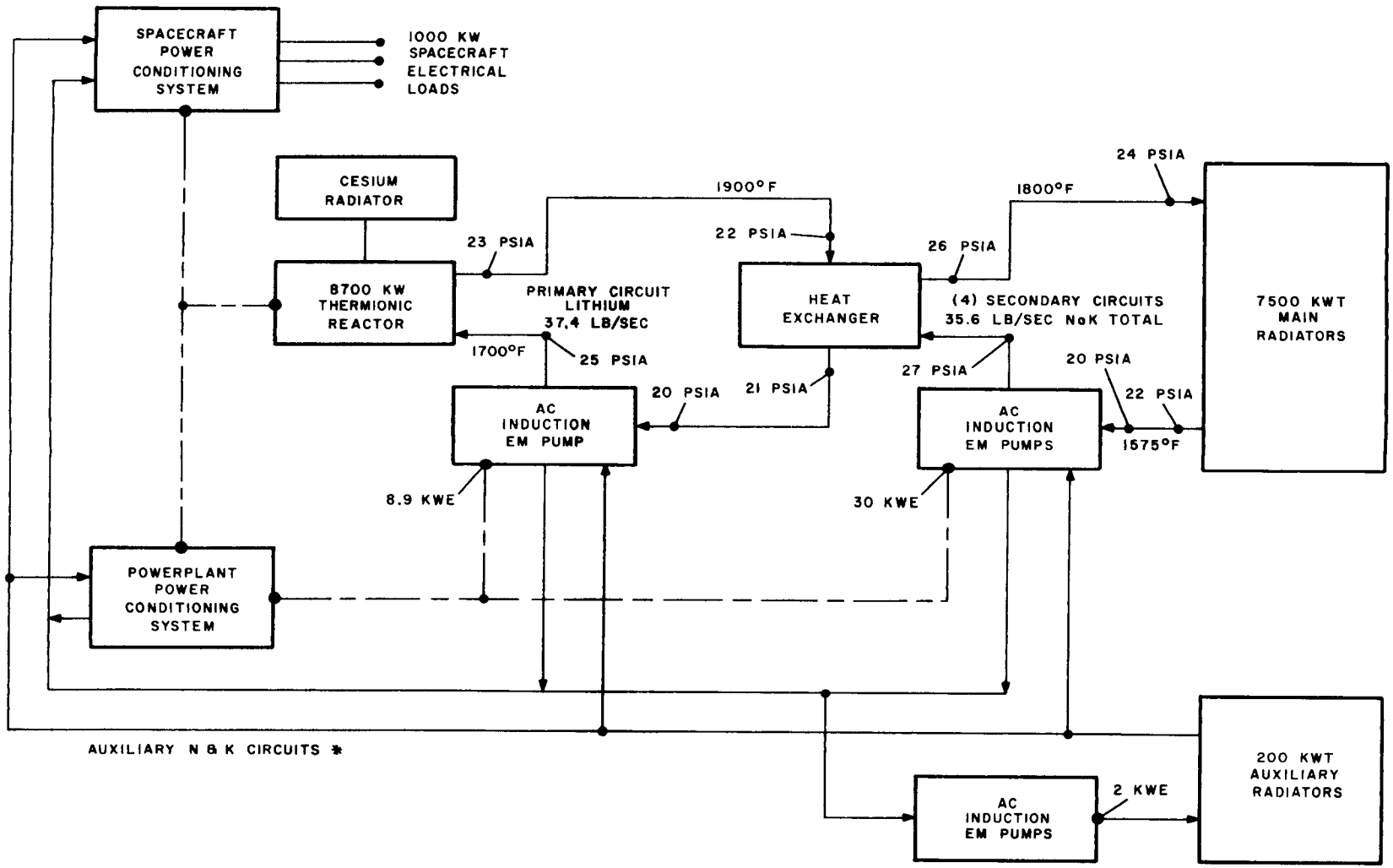

* NOTE: OPTIONS ON AUXILIARY COOLANT SYSTEM TEMPERATURES AND LOOP ARRANGEMENTS ARE GIVEN IN SECTION 8 (ELECTRICAL).

Figure 7-1. Heat Balance for the 1 MWe Thermionic Powerplant

is to be minimum pump work and/or powerplant weight. However, there are several attractive features of NaK which might overshadow any weight differences. Its low freezing point (eutectic) will greatly reduce the problem of thermal control during launch and throughout the period before startup. Also, NaK and Na are compatible with stainless steel and nickel base alloys for the lower range of temperature at which thermionic reactors may reject heat (~ 1200 to 1600°F). Another advantage of Na or NaK over Li as a primary coolant is the elimination of possible violent chemical reactions between lithium and UO_2 fuel.

Offsetting this, is the high activation of sodium which complicates the problem of payload shielding. Considering the importance of the loop activation problem, and the experience being gained under the SNAP-50 program with lithium coolant, this fluid was selected for the primary loop in the reference design. In the case of the radiator, the startup problem and the desire to avoid refractory metal construction lead to a choice of NaK.

2. Powerplant System Temperatures

The major consideration in the powerplant system design is the selection of the main radiator heat rejection temperature. Once this has been set, the flow rates and Δ T's can be determined by balancing heat exchanger and radiator weights against pumping power requirements. Although the optimum anode temperature for maximum efficiency with in-core thermionic systems occurs at about 1400-1600° F, the actual operating temperature will either be higher or lower than this value because of the discontinuity in radiator weight that occurs above the temperature where beryllium fins and armor can be used. Minimum weight systems are obtained by operating at the highest heat rejection temperature consistent with beryllium construction (1300-1400° F). However, only a small weight penalty (~ 2.0 lb/KW) is incurred by changing to a non-beryllium design operating at high temperature. This also reduces radiator area, thereby easing packaging problems. Minimum weight non-beryllium systems are found to require reactor temperatures

of about 2000° F, despite the fact that the convertor efficiency drops with increasing anode temperature. This loss in efficiency is offset by the decrease in radiator weight.

Since the beryllium radiator was covered in conjunction with the turboelectric systems, a high temperature radiator was chosen for the reference thermionic system so that data on both options would be available. For the high temperature radiator, maximum temperature was set at 1800° F to avoid the need for refractory metal construction. Below 1800° F, superalloys such as L-605 can be employed, and this material was chosen for the radiator design. It would be possible to obtain weight savings by substituting columbium or molybdenum for the radiator, due to the higher meteoroid penetration resistance parameter ($\rho^{5/6}/E^{1/3}$) for these materials. However, only with molybdenum is the advantage large enough to be considered as possible compensation for the high cost and difficult fabrication problems associated with such a large refractory metal structure.

In the third and fourth quarterly report, heat exchanger data were presented. These results have been extrapolated to the proper heat transfer rating (7.5 MWt), and to lower temperature differentials as shown in Figure 7-2. Pressure drop across the primary (shell) side of the heat exchanger is plotted in Figure 7-3. Note that as the heat exchanger gets larger, (lower ΔT between primary and secondary corresponding to lower reactor outlet temperature), the shell side pressure drop decreases rapidly. This is due to the fact that the shell side flow area increases to accommodate more tubes. Design of the heat exchanger is shown in Figure 7-4 for a cross flow system, although pure counterflow designs could also be considered.

Primary loop piping weights are given in Figure 7-5 as a function of pipe diameter. Pressure drops are also plotted for different primary loop ΔT's. If pumping power is assumed to cost 200 pounds per KW hydraulic (30 lb/KWe divided by 0.15 pump efficiency), the primary loop pipe size can be determined as in Figure 7-6. Effective weight is 170 pounds, including pumping losses, and the weight of primary piping and liquid inventory. Actual weight of piping and fluid is 140 pounds.

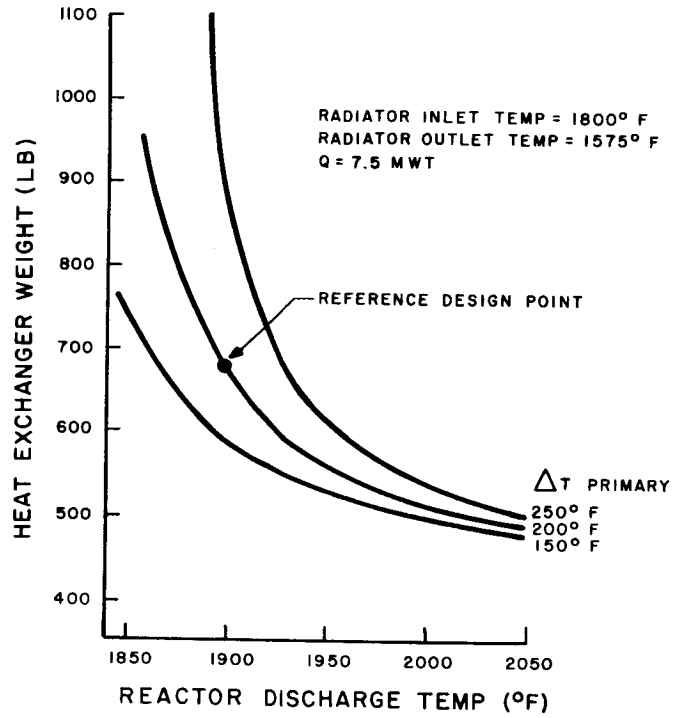

Figure 7-2. Heat Exchanger Weights

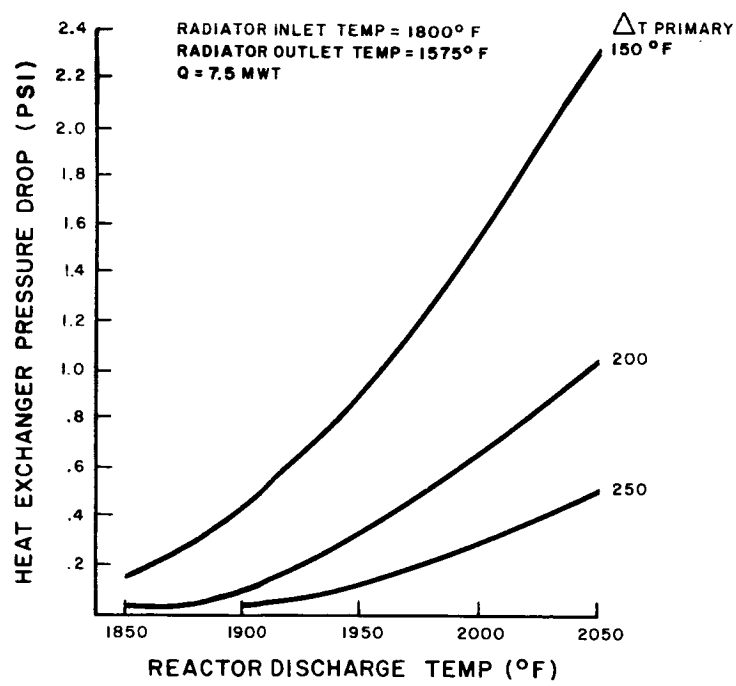

Figure 7-3. Heat Exchanger ΔP Versus Reactor Discharge Temperature

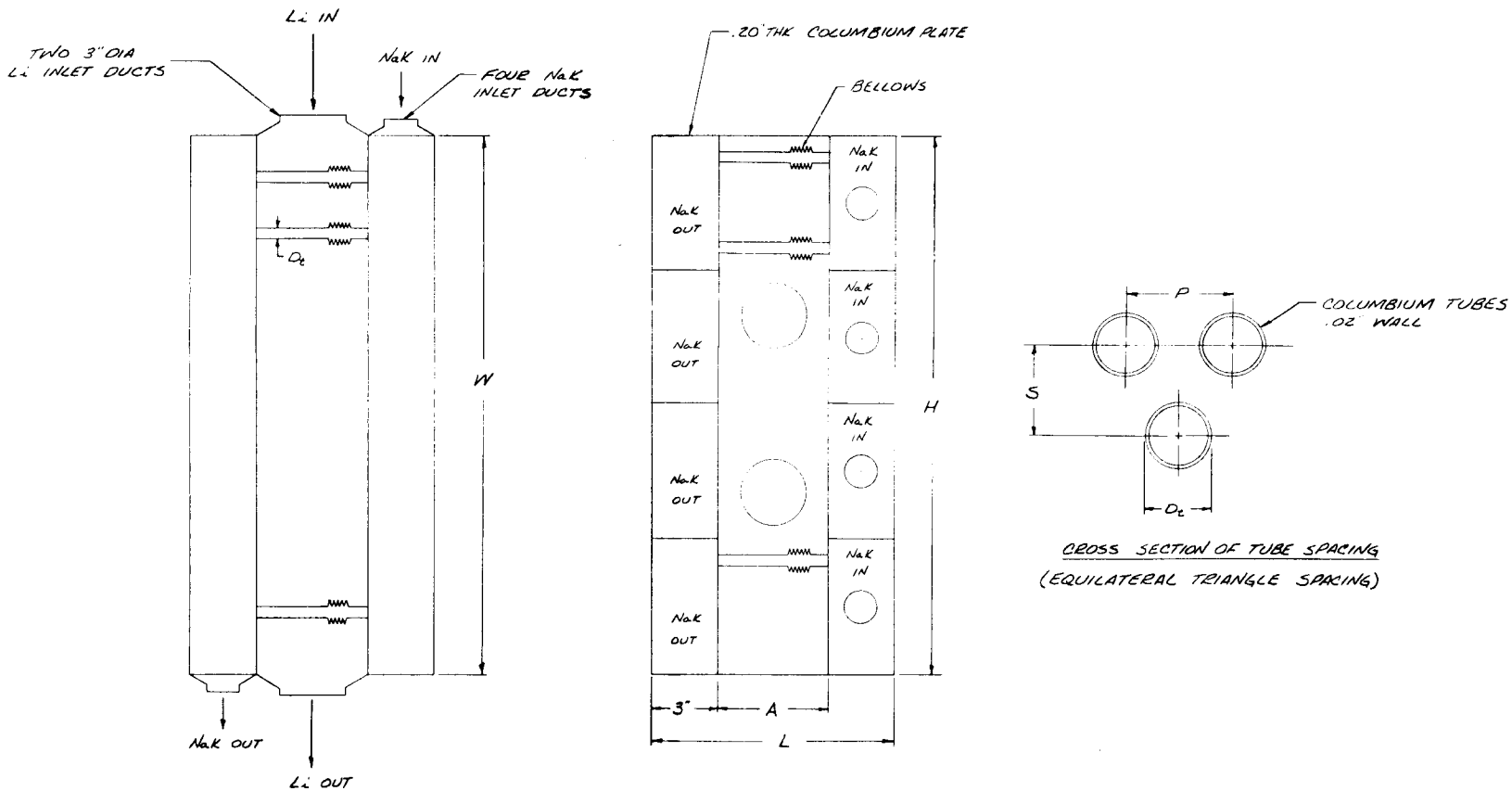

Figure 7-4. Cutaway Views of Straight Tube Heat Exchanger

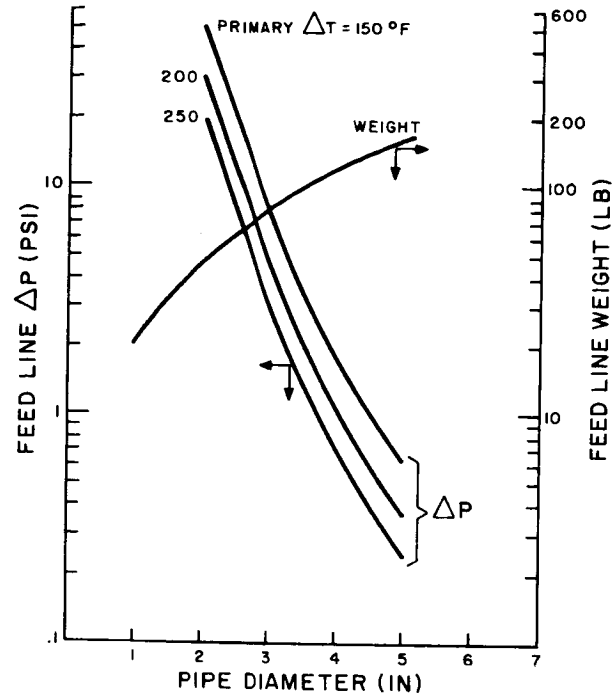

Figure 7-5. Primary Loop Piping Weight and Pressure Drop

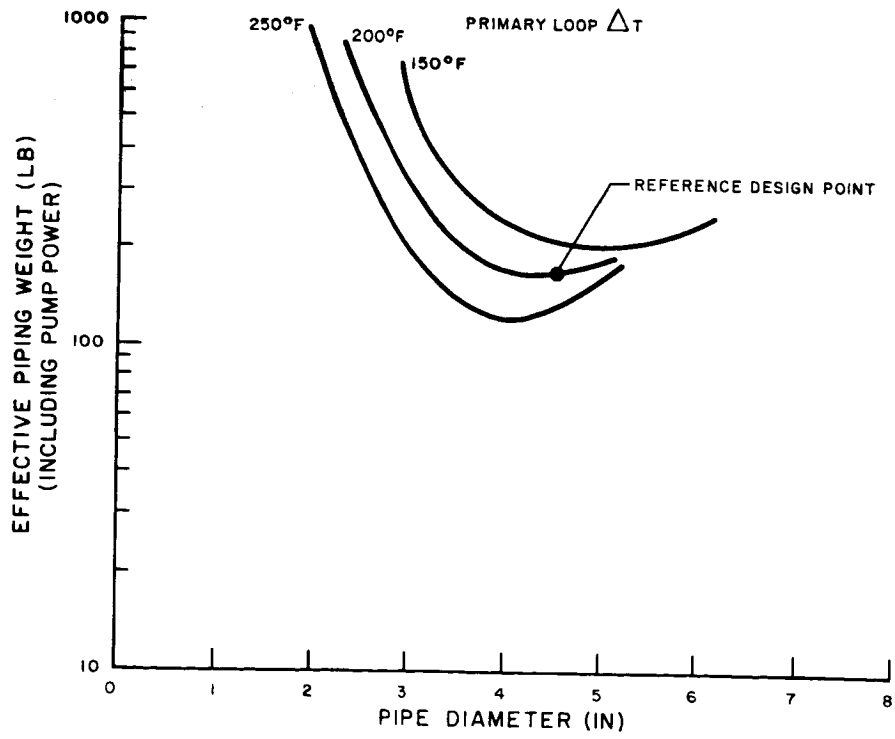

Figure 7-6. Optimization of Primary Loop Pipe Size

Figure 7-7 shows the hydraulic characteristics of the reference reactor design. These values are used to aid in the optimization of primary loop ΔT and heat exchanger ΔT (primary to secondary drop). For this optimization, it was assumed that the converter efficiency drops 0.0093 %/°F increase in average anode temperature in the range of 1600 to 2000°F. Thus, as heat exchanger ΔT is decreased, the average anode temperature drops (constant radiator inlet temperature of 1800°F), and the system efficiency improves. Radiator weight therefore decreases, and an optimum ΔT is reached when the increasing heat exchanger weight just offsets the radiator.

Figure 7-8 shows the effective weight (including pump losses) of the radiator, heat exchanger, and primary loop piping for three values of primary loop ΔT. Note that the curves are very flat over a range of heat exchanger ΔT's from 75°F to about 120°F. Moreover, the system weight is insensitive to primary loop ΔT. The reference design, indicated at 200°F loop ΔT and 100°F heat exchanger ΔT, is within 40 pounds of the minimum weight system. In practice, it is probable that a somewhat lower primary loop ΔT would be chosen to minimize variations in anode temperature within the core. These variations which were not studied in detail under this program can be expected to have some effect on the final temperature selections.

B. REACTOR AND SHIELDING

The most significant influence upon thermionic system weight is exerted by the reactor diameter since reactor weight and shield weight are both affected by this parameter.

1. Reactor Characteristics

Because of the uncertainty in predicting the ultimate performance potential for in-core thermionic diodes, it is correspondingly difficult to establish the required core dimensions for a thermionic reactor with any certainty. A set of reactor specifications has been compiled, however, to illustrate the level of performance that might eventually be achieved when this technology is fully developed and exploited. The basis for the

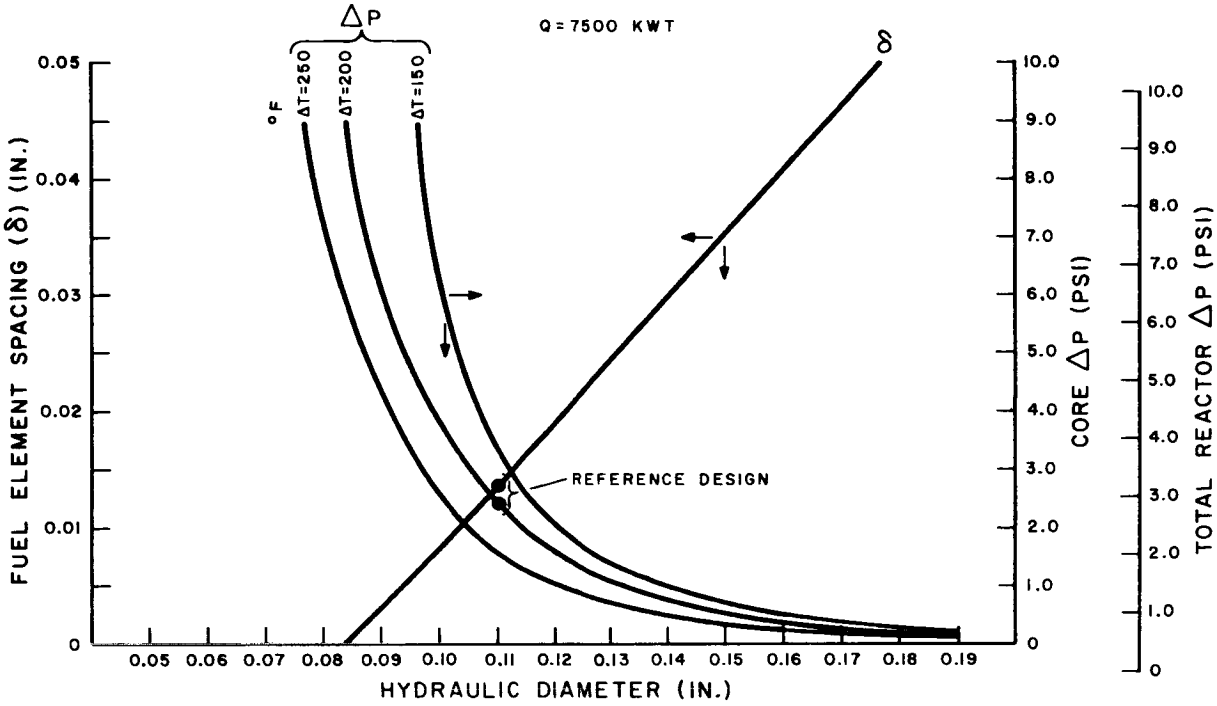

Figure 7-7. Reactor Hydraulic Characteristics

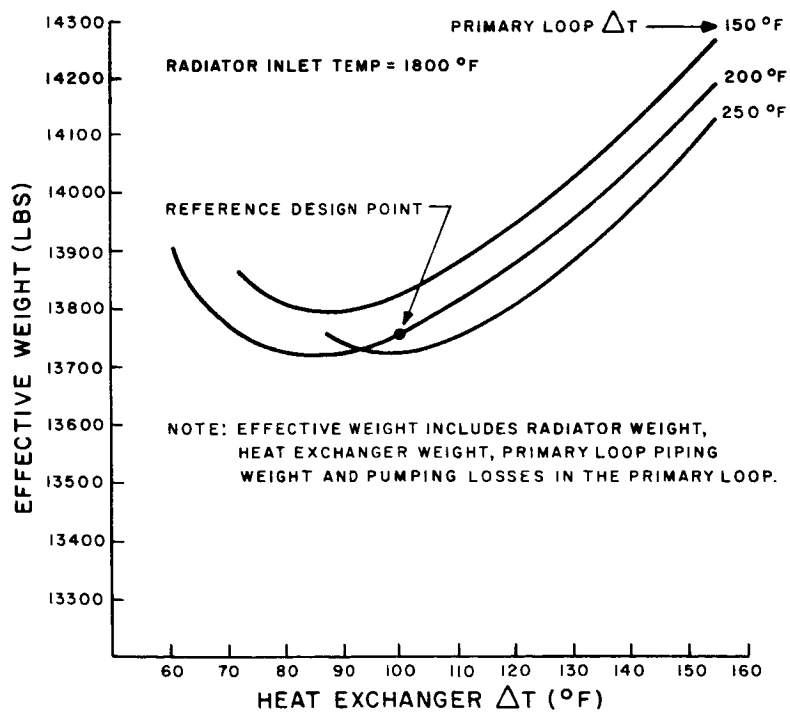

Figure 7-8. Optimization of Heat Exchanger ΔT

"reference" design reactor characteristics shown in Table 7-1 is the assumption of a converter design which is capable of operating at an emitter temperature of 2000 °K and producing an electrical power density of 15 W/cm^2 at an efficiency of 20 percent for optimum anode and cesium temperatures (single diode performance). This assumed converter would probably be optimized close to its maximum efficiency, rather than maximum power density, to achieve the above performance level.

Although there have been few converters operating at these high efficiencies, some laboratory measurements have been obtained during the past year which have demonstrated converter power densities in the 30 - 50 W/cm^2 range. A particularly dramatic improvement in power density was achieved in a thermionic converter built by Thermo Electron Engineering Corporation under an ONR-sponsored research program. This was a rhenium-moly device with a spacing of 1/2-mil which operated at a power density of 56 W/cm^2 (about 50 W/cm^2 after subtraction of lead losses) and an efficiency of approximately 20 percent at an emitter temperature of 1760 °C. The high power density was attributed to special preparation of the rhenium emitter surface as well as the close spacing of the electrodes.[1] The fact that some converters in other laboratories have also exhibited exceptional performance on occasion, lends credibility to the belief that converters with the assumed characteristics (15 W/cm^2, 20 percent efficiency at 2000 °K) will eventually be capable of manufacture on a repetitive basis with a reasonable assurance of reliability.

When one allows for the "off-optimum" average collector temperature (about 200 °C above optimum), the non-uniformities in emitter and collector temperatures due to coolant temperature variations and non-uniform fission power distributions, and the use of a common cesium reservoir temperature for thermionic fuel elements having varying electrode temperatures, the "ideal" power density and efficiency is reduced significantly. For the reference design, assuming a max./min. axial fission distribution of 1.35 and a max./min. radial fission distribution of 1.45, one obtains an overall

(1) T.E.E.Co. news release, February 26, 1964.

TABLE 7-1. 1 MWe NET THERMIONIC REACTOR REFERENCE DESIGN

Active Core dia, in.		20.0
Reflector thickness, in.		2.0
Active Core length, in.		22.4
Thermal Power, MW		8.7
Gross Elec. pwr, MW		1.24
Converter length, in.		1.5
Cathode Temperature (avg), °F		3150
Cathode Temperature (max.) °F		3450
Anode Temperature (avg), °F		1800
Power density (avg), W/cm^2		8
Converter efficiency, percent		14
Cathode area per element, cm^2		162
Number of fuel elements		960
Watts (e) per element		1300
Amps/element		135
Volts/element		9.6
Number elements in series		13
Series voltage, volts		125
Number parallel circuits		74
Number converters/element		12
Volts/converter		0.8
Total fuel weight, lbs-UO_2		880
Fuel Volume fraction		0.35
Fuel		
Reactor Weights (lb)		
Fuel	880	
Clad	300	
Anodes	300	
Cathodes	490	
Insulators, Spacers, etc.	200	
Be O Reflectors	350	
Vessel	280	
Core Support and Cesium Reservoir	150	
Control Actuators	150	
	3100 lb.	

average thermionic electrical power density of 8 W/cm^2 and an efficiency of 14 percent. To achieve this degree of power flattening, fuel concentrations must be adjusted radially and axially in fine increments. It should be emphasized that the selection of a common cesium temperature and average operating cell voltage for the series-connected diodes, should favor the maximizing of system efficiency. The reduced power density of 8 W/cm^2 would require an active core diameter of 20 inches for a net system rating of 1 MWe (8.7 MWt).

2. Shield Weights

Shielding weights depend upon not only the core diameter, but also the payload separation, allowable dose, and the shadow cone angle to be protected.

Figure 7-9 shows the relationship between these parameters with the reference design point indicated for the 20-inch diameter core and a shadow cone angle of 21 degrees. This corresponds to the vehicle layout presented in the spacecraft design section, and results in a shield weight of 8000 pounds.

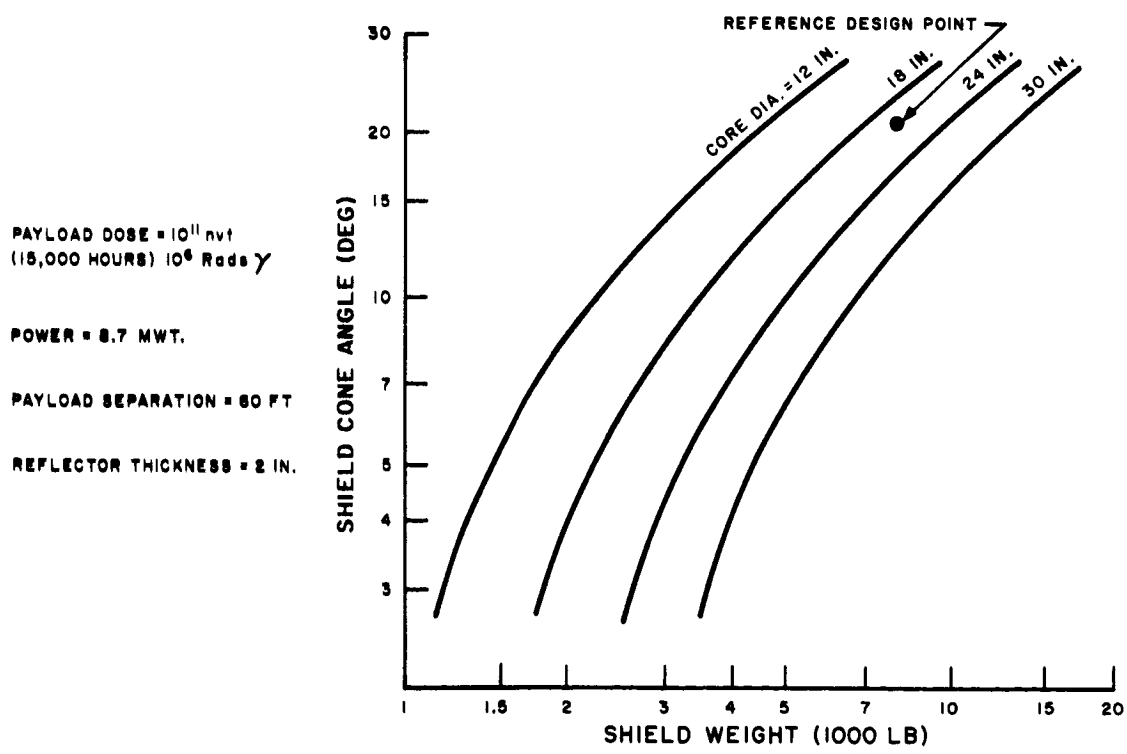

Figure 7-9. Shield Weight Parameters

8. ELECTRICAL SYSTEMS

A reasonably complete discussion of the electrical systems was presented in the third and Fourth Quarterly Report (GE Document No. 64SD700). It was not considered appropriate to rewrite this entire presentation. Instead, only the overall description of the electrical system configuration and electrical and thermal power profiles are duplicated below. Additional information is provided on the comparison of tube versus solid-state power conversion devices, and the transformer estimated weight curves are replotted for greater clarity. None of the previously published material on transmission line analysis and skin effect is included.

A. CONFIGURATION STUDY

Electrical system one-line diagrams are presented for spacecraft powered by an AC turbogenerator and a DC in-core thermionic generator in Figures 8-1 and 8-2, which include some detailed information at the nominal 1.2 and 1.0 MW reference system design levels. The turbogenerator electrical system configuration shown in Figure 8-1 is based on the fixed conical vehicle configuration fitted with ion engines, and has the following characteristics.

1. High voltage a-c transmission is desirable to minimize conductor weight for the large block power loads, such as the electric engines and the deep space communication and terminal radar transmitters.
2. Transformers and protective circuit breakers are located within the spacecraft in several modules in a configuration around the centerline of the vehicle such that balance is maintained.
3. Transformer secondary current breakers are employed.
4. Low temperature, radiation sensitive, static power conditioning components for providing power to the payload, propulsion, and spacecraft "housekeeping" equipment are located near the aft end of the vehicle in close proximity to their associated loads.
5. Fluid lines are not to cross from the main spacecraft structure to the extendable payload and propulsion module, although this eliminates the possibility of diverting a portion of the powerplant module heat load to a secondary radiator at the aft end of the vehicle.

Figure 8-3 is a somewhat more detailed schematic diagram of an electric engine power conditioning unit to illustrate the connections to an ion engine module.

Figure 8-4 is a one-line diagram of an electrical system configuration which depicts the use of multiple turbogenerator powerplant. Four turbogenerators can be connected electrically in either an isolated or a paralleled mode of operation to obtain the required total generation capacity. Paralleled generator operation will require real and reactive load division control as well as close control of the output voltages and frequencies. Real load division will likely be achieved by control of the turbine drive, while reactive load division will be achieved by controlling the generator field excitation. Isolated operation will require bus transfer and synchronization schemes to maintain and optimize partial system operation in case of system faults. The one-line diagram shown in Figure 8-4 shows the isolated operational mode with the engine loads sectionalized into three pairs of engine cluster sets and a pair of engine arrays. The three engine cluster pairs are gimballed sets for vehicle attitude control and maneuvering. The deployed-fixed (or rotatable) engine arrays provide the balance of load division for the fourth powerplant module. The recommended system approach, under normal conditions, is to isolate each generator by dividing the electrical loads into four independent parts. Power to the critical spacecraft operational subsystems is fed through a powerplant control and distribution unit. This unit in turn is connected so that electrical power can be drawn from one or a combination of the generators to satisfy the critical power requirements throughout the various mission phases and operational modes. A similar control and distribution unit provides power coordination for the spacecraft payloads in the terminal mission phase. The auxiliary power source, located in the telescoping payload assembly, provides power during the boost and start-up phases to the powerplant modules and spacecraft operational subsystems. The power from the auxiliary source to the powerplant modules is fed through the critical load power source control and distribution unit, the transmission lines, and the transformer-circuit breaker modules.

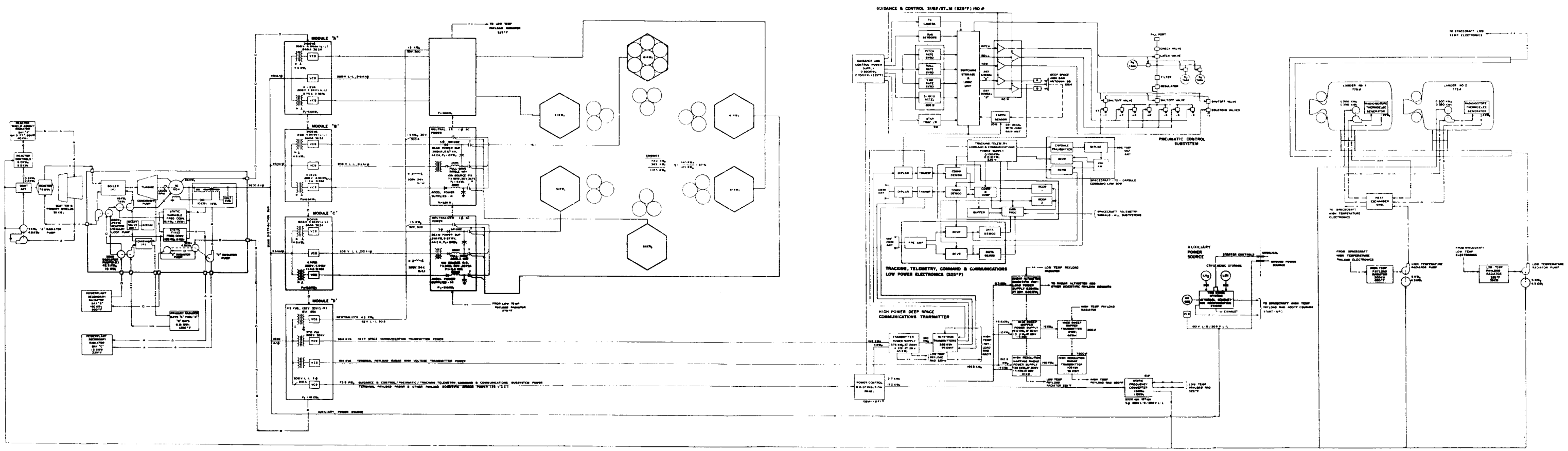

Figure 8-1. Electrical System for the 1.2 MWe Turboelectric Vehicle

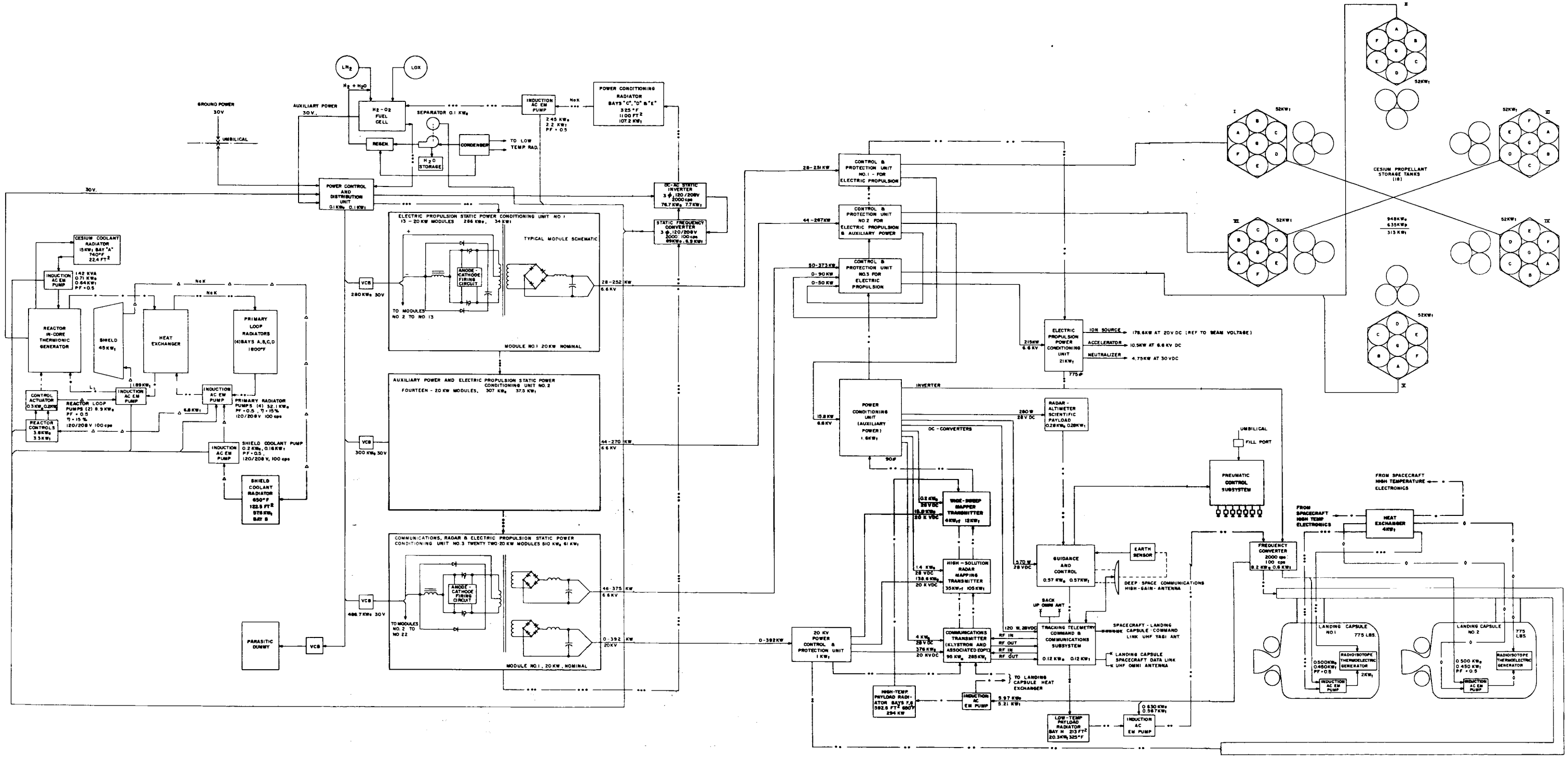

Figure 8-2. Electrical System for the 1 MWe Thermionic Vehicle

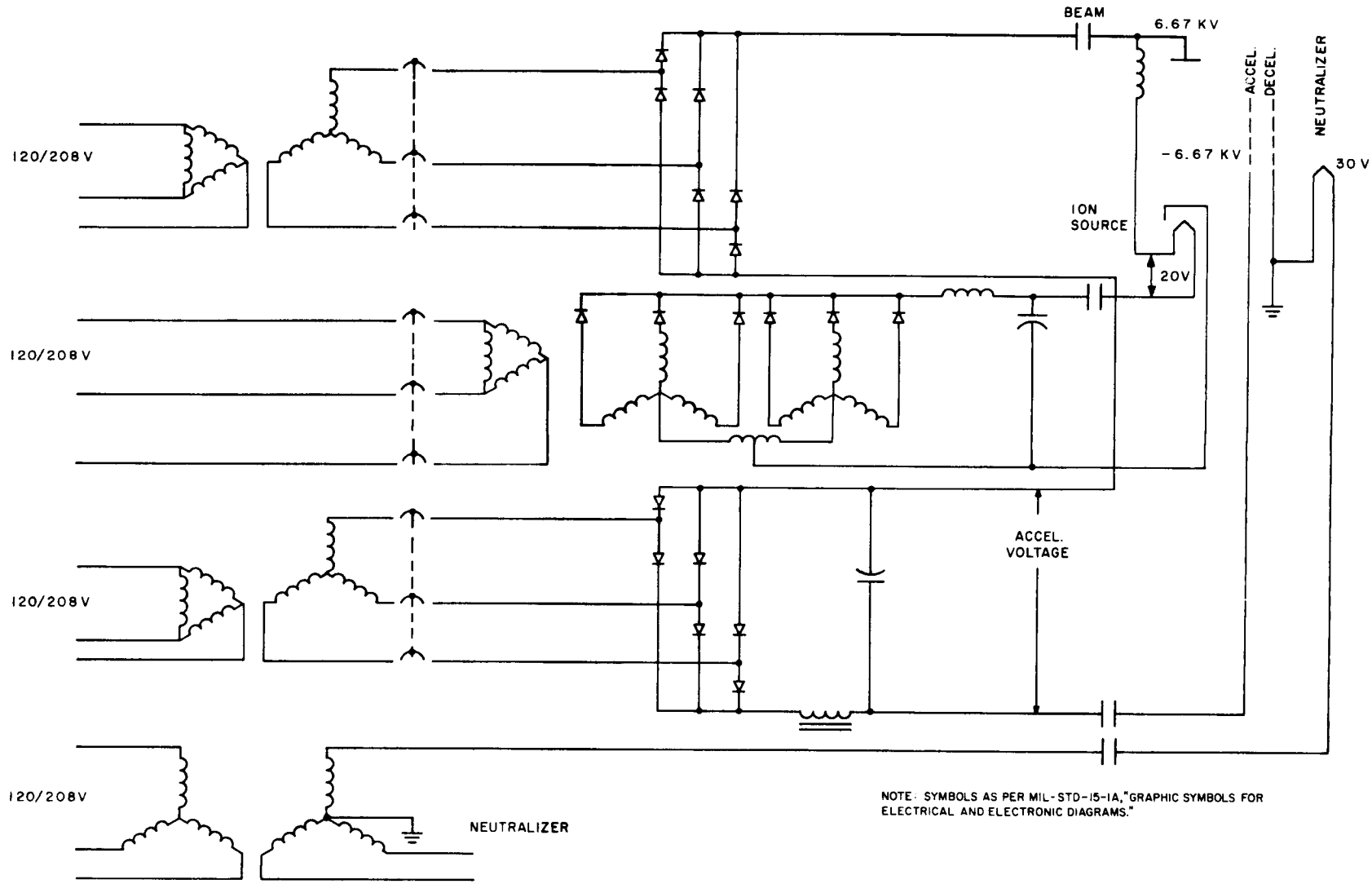

Figure 8-3. Typical Electric Engine Power Conditioning Schematic

The in-core thermionic generator electrical system configuration shown in Figure 8-2 is based on the following additional considerations:

1. The low source voltage (30V) and resultant high current, combined with high surrounding structural temperatures, leads to the requirement of large bus conductors.
2. Special integration techniques are necessary in penetrating the shield to minimize radiation leakage.
3. Running the bus connections from the reactor around the shield leads to increased power loss and radiation scatter.
4. A significant temperature gradient exists along the bus length, which introduces a heat load to the power conditioning modules.
5. Location of the power conditioning module close to the generator, results in a shorter, high current bus run, but increases the radiation level at the module, leading to a requirement for local shielding.

The bulk of power conditioning takes place near the reactor, where the 30 volt d-c output is raised to two different d-c high voltages: one to fulfill the ion engine beam power requirement, and one to match the beam power requirement of the klystrons in the communications and radar systems. The vehicle design permits the active removal of waste heat from the dc-dc converters with the placement of low temperature radiators in the forward conical section of the radiator assembly.

Three power conditioning modules are employed. The first is for high voltage beam power for two ion engine clusters. The second module supplies the beam power for two other ion engine clusters plus the power for low-voltage auxiliary equipment. The third module supplies several forms of power: for communications and radar; for ion engine beam voltage for two clusters; and ion source, neutralizer and accelerator power for all clusters. The percentage split between these forms of power is variable, to account for the needs of the various mission phases.

The liquid metal coolant pumps have been assumed to be static a-c induction pumps. The induction pumps have the advantages that: 1) there is no requirement for conduction of the current into the duct, 2) a simple duct structure can be designed in a

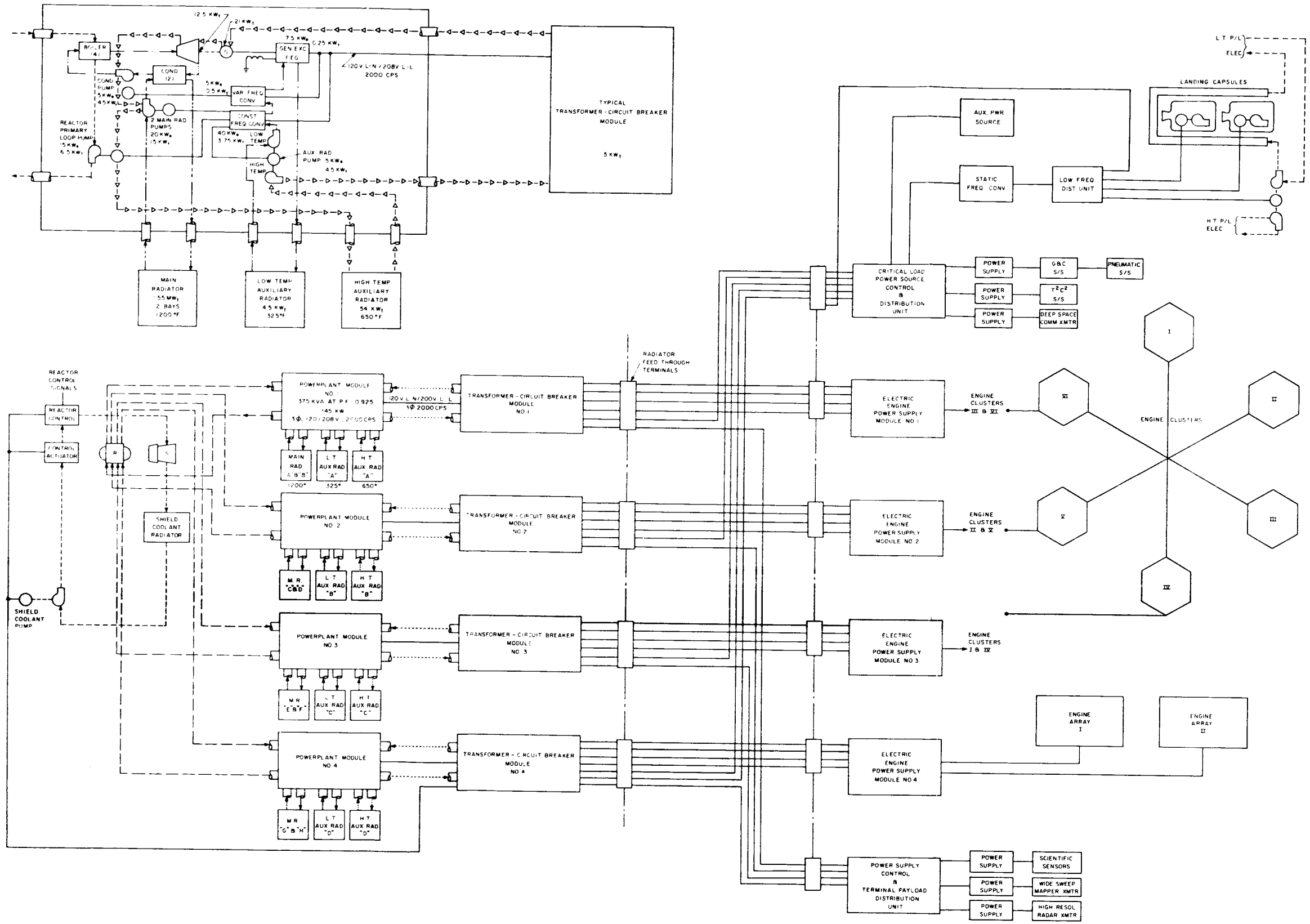

Figure 8-4. Typical Powerplant Module for 1 MW Paralleled Generator System

variety of configurations to meet system flow and pressure requirements, and 3) the pump can be wound for any convenient voltage and current level. However, disadvantages of induction pumps include the requirement of high temperature insulation for the coils, high-to-low frequency-conversion equipment, low power factor, high excitation currents, and eddy current losses. It would also be possible to employ conduction EM Pumps, either ac or dc, or to use canned-motor pumps.

The static dc-ac inverter is operated at high frequency to minimize weight. A frequency converter reduces the frequency for a-c induction pump operation. Square wave ac is provided to avoid the use of filter circuits requiring capacitors in the output circuit of the frequency converter. The harmonic content of the square wave is assumed to be absorbed by the EM induction pump where it contributes no useful work. More detailed study would have to be given to eliminating electromagnetic interference, in an actual hardware design.

The parasitic load must be integrated into the vehicle in such a manner that the power dissipated will help to minimize differential linear thermal expansion between the radiator structure and rigid bus bars if they are mounted in proximity. The parasitic load will be utilized to minimize thermal-structural stresses at strategic locations, such as the engine modules and in the primary loop radiator segments. These stresses occur during engine cutback in the coast mission phase, and in certain modes of failure. The maximum parasitic load power is established at 1 MW to allow for protection in case of total loss of load. The gradual reduction of the parasitic load, after engine load is cut back, will permit a gradual reduction of the reactor power either by a preprogrammed schedule, command, or both.

Static power conversion components were based on silicon power semiconductor devices with maximum junction temperatures at 150°C. The low source voltage makes the application of the silicon controlled rectifier (SCR) with its low forward voltage drop characteristic very attractive compared to using a high temperature gas thyratron tube with a higher forward drop. The radiation susceptibility of the

semiconductor and its comparatively low heat rejection temperature are the two main disadvantages. A comparison of the semiconductor-type forward power conditioning equipment with PCE using high temperature tubes (such as might be developed through Contract No. NAS3-2548, for the development of gas tubes for rectification at 800°C, and Contract No. NAS3-6005, for the development of vapor thyratrons at 600°C, held by the General Electric Tube Department) is presented in Table 8-1. Based upon predicted developments in high-temperature thyratrons, the tube-design exhibits a 64% radiator area savings compared with the semiconductor design, but incurs an apparent weight penalty of about 2.3 lb/kw. The smaller radiator and shield, and higher radiation tolerance with tube-type systems may, however, provide greater flexibility in packaging the converters, thereby balancing out the weight penalty.

Conductors have been sized as indicated in Table 8-2 for the 1.2 MW turboelectric vehicle, and in Table 8-3 for the 1 MW thermionic vehicle. The silicon controlled rectifiers have been shown with no connections to the gate lead. Instead, a special anode-to-cathode firing circuit is shown which should give a higher level of radiation tolerance than is attainable by gate firing. This possibility has been indicated by a limited amount of SCR radiation testing, the results of which have indicated that an anode-to-cathode firing technique will extend device operation to a radiation level one to two orders of magnitude greater than would be possible with gate firing. Alghough this technique does not completely obviate the need for local shielding at the power conditioning equipment, the integrated dose need only be attenuated one order of magnitude, from 10^{13} NVT to 10^{12} NVT.

B. ELECTRICAL AND THERMAL POWER PROFILES

The power and thermal profiles are tabulated in Tables 8-4 and 8-5 for the 1.2 MW Turbogenerator case and in Tables 8-6 and 8-7 for the 1 MW In-Core Thermionic Generator. These estimates are based on the eight different mission flight phases below.

TABLE 8-1. COMPARISON OF USE OF SEMICONDUCTORS AND HIGH TEMPERATURE TUBES IN THERMIONIC DC-DC CONVERTERS

Item	Semiconductors	Tubes
Drop in active element, volts	1.0	2.5
Net Power Output, KW	1000	1000
PCE Power Rejected Actively, KW	132.5@325°F	64KW@1500°F 61.4KW@650°F* 156KW@1100°F 12.7KW@325°F
Bus Power Loss, KW	49.0	57
Weight of Bus, lb	761	891
Weight of converter, lb	7060	13100
Weight of radiator, lb	1365	492
Approximate Shield Weight, lb (with 24-inch core)	10000	7000**
TOTAL WEIGHT, LB	19185	21,483
Radiator Area, ft^2	1445	525

* Max coolant temp. for 4 major components.
**Shield weight is reduced because of smaller shadow angle needed to protect radiators as a result of the reduction in secondary radiator area (higher temperature).

Assumptions: 1. DC-DC Converter Switching Frequency: Semiconductors 3 kc/s (optimum) Tubes 2 kc/s (apparent maximum)

2. Bus bars are stainless-steel-enclosed copper. Nickel or refractory metal would approximately quadruple bus weight for both tube and semiconductor power conditioning.

3. Weight and loss breakdown of 20-kw semiconductor power conditioning.

Element	Rating	No. Req.	Wt(lb)	Loss (kw)	Max. Temp.
SCR	200 amp 100^V PIV 1^V fwd drop $t_r = 5\ \mu s$, $t_f = 20\ \mu s$	8	8	0.758 (fwd) 0.276 (switching)	325°F
Load-sharing inductors	0.034 μh, 184 amp	8	0.0292	0.188	325°F
Transformer	22KVA (30^V:6.6 KV/ (30^V:20 KV 14KG; 50% Ni-Fe	1	10	0.45	325°F
Commutating Choke	62.5 μh, 758 amp	1	112	0.45	325°F
Commutating Capacitor	187.5 μf, 100^V	1	6.25	0.225	325°F
Rectifier Bridge	1 KV PIV, 4 amp	16/40	.32/.80	0.200	325°F
Load Sharing Resistors	50 KΩ, 10W/200 KΩ, 3W	16/40	4/10	0.1	325°F
Pump back diodes		2	1	0.06	
TOTAL per 20 KW out $\eta = \frac{20}{20 + 2.7} = 88\%$			141.6/ 148.1	2.707	2

4. Weight and loss breakdown of 20-kw tube power conditioning module:

Vapor Thyratron	250 amp 750^V PIV 2.5^V arc drop 4% switching & htr loss	10	10	2.15 (fwd) 1.03 (Switch & htg)	1100°F
Load-sharing inductors	0.1155 μh, 172 amp	10	0.11	0.215	650°F
Transformer	26KVA(30^V:6.6KV/ (30^V:20 KV) 14KG; 50% Ni-Fe	1	18	0.52	650°F
Commutating Choke	93.7 μh 866 A	1	219	0.52	650°F
Commutating Capacitor	281 μf 100^V	1	9.4	0.26	325°F
Gas Rectifier Bridge	4KV PIV 10^V arc drop 15 amp 5% htr and switch loss	4/(12)	4/(12)	1.06/(1.11)	1500°F Isolated filament supply transformer req'd for each tube
Load-Sharing Resistors	215 KΩ 50W/68 KΩ, 20W	4/(12)	0.5/(3)	0.1	1500°F
Pump-back diodes		2	2	0.12	1500°F
TOTAL per 20 KW out $\eta = \frac{20}{20 + 6.0} = 77\%$		263.01 273.51	5.98/(6.03) 263/273.5	5.98/(6.03)	

TABLE 8-2. CONDUCTOR DETAILS - 1.2 MW TURBOELECTRIC VEHICLE

From	To	Length (ft.)	Conductor Area (Circ. Mils)	Weight (lb.)
Alternator	Xformer	5	27100	1.235
Xformer	PCE (Con-O-Pak Conductor)	64.5	4100	51.8
PCE	Beam Power	8.33	9440	0.477
	Beam Power	5	5670	0.172
	Beam Power	15.5	17500	1.645
PCE	Ion Source	8.33	$.753 \times 10^6$	38.06
	Ion Source	5	$.453 \times 10^6$	13.75
	Ion Source	15.5	1.39×10^6	130.2
PCE	Accel-Decel	8.33	134	0.001
	Accel-Decel	5	80	0.002
	Accel-Decel	15.5	248	0.023
PCE	Neutralizer	8.33	15900	0.802
	Neutralizer	5	9550	0.290
	Neutralizer	15.5	29600	2.77
PCE	Communications	13.3	5740	0.290
PCE	Radar	20	2360	0.286
PCE	Lander 1 Pump	11.7	5820	0.617
	Lander 2 Pump	1.67	825	0.012
PCE	Lo-Temp Rad Pumps	20	943	0.172
	Hi-Temp Rad Pumps	67	4690	0.284
	Total			244.3

TABLE 8-3. CONDUCTOR DETAILS - 1 MW THERMIONIC VEHICLE

Conductor Endpoints	Weight (lb.)	Dissipation (KW)	Length (ft.)	Area (Circ. Mils)
Reactor to PCE				
Semiconductor Type	761	49.0	17	14.7×10^6
Tube Type	891	57	17	17.2×10^6
PCE to Rear Modules	45.6	0.89	Several conductors similar to Con-O-Pak*	
Rear Modules to Loads	194	11.6	Variously-sized conductors	
Total				
Semiconductor Type	1000.6	61.5		
Tube Type	1130.6	69.5		

*Trademark of Continental Sensing, Inc.

TABLE 8-4. POWERPLANT ELECTRICAL LOAD REQUIREMENTS FOR THE 1.2 MWe TURBOELECTRIC VEHICLE

Power Load Items	Electrical Service Requirements	Power Load Estimates, KW							
		Phase							
		A	B	C	D	E	F	G	H
I. Reactor & Shield Assembly									
Controls	28 vdc,	6.0	6.0	6.0	6.0	6.0	6.0	6.0	6.0
Circulation Pump Controls & Shield Coolant	120 vac, 167 cps	5.0	5.0	5.0	5.0	5.0	5.0	5.0	5.0
Subtotal, RSA		11.0	11.0	11.0	11.0	11.0	11.0	11.0	11.0
II. Electrical Generation Syst.									
Controls	28 vdc	0.1	0.1	0.1	0.1	0.1	0.1	0.1	0.1
Generator Excitation	120 vac, 2000 cps	10.0	10.0	10.0	10.0	10.0	10.0	10.0	10.0
Circulation Pumps									
Reactor Coolant	120 vac, 167 cps	60.0	60.0	60.0	60.0	60.0	60.0	60.0	60.0
Condensate	120 vac, 167 cps	16.0	16.0	16.0	16.0	16.0	16.0	16.0	16.0
Radiator Circuit	120 vac, 167 cps	42.5	42.5	42.5	42.5	42.5	42.5	42.5	42.5
Auxiliary Coolant	120 vac, 167 cps	5.0	5.0	5.0	5.0	5.0	5.0	5.0	5.0
Power Conditioning Equipment Losses									
Transformer		20.0	20.0	1.5	1.9	5.4	10.2	20.0	20.0
Frequency Converter	120 KW output	11.0	11.0	11.0	11.0	11.0	11.0	11.0	11.0
Subtotal, EGS		164.6	164.6	146.1	146.5	150.6	154.8	164.6	164.6
III. Power Conditioning Syst.									
Controls	28 vdc, 0.1 KW	0.1	0.1	0.1	0.1	0.1	0.1	0.1	0.1
Distribution Losses		8.6	8.9	0.8	1.2	2.9	5.6	8.9	8.9
Equipment Losses									
Transformer		4.0	4.0	0.4	0.4	0.4	0.4	2.7	2.4
Rectifier		17.4	18.0	1.7	2.3	5.4	10.2	18.0	18.0
Frequency Converter	2000:167 cps, 16 KW(e) output	1.2	1.2	1.2	1.2	1.2	1.2	1.2	1.2
Subtotal, PCS		31.3	32.2	4.2	5.2	10.0	17.5	30.9	30.6
IV. Propulsion System									
Controls	28 vdc, 1.0 KW	1.0	1.0	1.0	1.0	1.0	1.0	1.0	1.0
Propellant & Feed System	28 vdc, 1.0 KW	1.0	1.0	1.0	1.0	1.0	1.0	1.0	1.0
Ion Engines									
Beam Power	6.60 Kvdc, 878 KW	878.0	878.0	84.3	84.3	84.3	84.3	754.0	594.0
Accelerator Power	6.60 Kvdc, 12.3 KW	12.3	12.3	1.17	1.17	1.17	1.17	9.55	8.49
Ion Source	20 vdc, 208 KW	208.0	208.0	19.7	19.7	19.7	19.7	181.0	145.5
Neutralizer	30 vdc, 4.45 KW	4.45	4.45	0.54	0.54	0.54	0.54	4.56	3.01
Subtotal, PS (I_{sp} = 8.78 x 10^3 sec at full power)		1104.75	1104.75	107.71	107.71	107.71	107.71	951.11	751.00
V. Spacecraft Equipment									
Tracking, Telemetry, Command & Comm. (Deep Space) Communications	26 vac, 400 cps, 2 φ, 1.0 KW	1.0	1.0	1.0	1.0	1.0	1.0	1.0	1.0
Klystron	20 Kvdc, 376.0 KW	--	37.6	--	37.6	37.6	376.0	37.6	376.0
Electronics	28 vdc, 4.0 KW	--	4.0	--	4.0	4.0	4.0	4.0	4.0
Radar Altimeter and Scientific Sensors	28 vdc, 0.28 KW	0.28	0.28	0.28	0.28	0.28	0.28	0.28	0.28
Wide Sweep Mapper									
Klystron	20 Kvdc, 15.8 KW	--	--	--	--	15.8	15.8	15.8	15.8
Electronics	28 vdc, 0.2 KW	--	--	--	--	0.2	0.2	0.2	0.2
High Resolution Radar									
Klystron	20 Kvdc, 138.6 KW	--	--	--	--	138.6	--	138.6	--
Electronics	28 vdc, 1.4 KW	--	--	--	--	1.4	--	1.4	--
Guidance & Controls									
Electronics	28 vdc, 0.45 KW	0.45	0.45	0.45	0.45	0.45	0.45	0.45	0.45
Inertial Units	28 vac, 400 cps, 2 φ, 0.1 KW	0.10	0.10	0.10	0.10	0.10	0.10	0.10	0.10
Planet Sensors	26 vac, 400 cps, 2 φ, 0.01 KW	0.01	0.01	0.01	0.01	0.01	0.01	0.01	0.01
Coolant Circulation Pumps									
Lander No. 1	120 vac, 167 cps, 0.5 KW	0.5	0.5	0.5	0.5	0.5	0.5	0.5	0.5
Lander No. 2	120 vac, 167 cps, 0.5 KW	0.5	0.5	0.5	0.5	0.5	0.5	0.5	0.5
Radiator Circuits	120 vac, 167 cps, 10 KW	10.0	10.0	10.0	10.0	10.0	10.0	10.0	10.0
Subtotal, SE		12.85	54.45	12.85	54.45	210.45	408.85	210.45	408.85
VI. Distribution Losses		14.6	14.6	3.0	3.5	5.2	7.4	14.6	14.6
VII. Total Generator Gross Output		1339.1	1381.4	284.56	327.66	501.16	706.56	1382.46	1380.75
VIII. Total, EGS Net Ouput		1355.3	1197.4	119.56	162.26	332.26	532.86	1198.46	1196.75

TABLE 8-5. COOLING LOAD REQUIREMENTS FOR THE 1.2 MWe TURBOELECTRIC VEHICLE

Heat Load Items	Radiator Loop/ Maximum Temperature (°F)	Cooling Loads Estimates, KW							
		Phase							
		A	B	C	D	E	F	G	H
I. Reactor & Shield Assembly									
Controls	Reactor Shield Assembly Radiator "A"/650	5.5	5.5	5.5	5.5	5.5	5.5	5.5	5.5
Coolant Pump	Reactor Shield Assembly Radiator "A"/650	4.5	4.5	4.5	4.5	4.5	4.5	4.5	4.5
Shield	Reactor Shield Assembly Radiator "A"/650	30.0	30.0	30.0	30.0	30.0	30.0	30.0	30.0
Total, RSA Cooling System		40.0	40.0	40.0	40.0	40.0	40.0	40.0	40.0
II. Electrical Generation System									
Controls	Reactor Shield Assembly Radiator "A"/650	0.1	0.1	0.1	0.1	0.1	0.1	0.1	0.1
Generator	Power Plant Secondary Radiator "B"/650	85.0	85.0	24.6	27.4	39.0	57.0	85.0	85.0
Generator Excitation	Power Plant Secondary Radiator "C"/325	1.0	1.0	1.0	1.0	1.0	1.0	1.0	1.0
Circulation Pumps									
Reactor Coolant	Power Plant Secondary Radiator "B"/650	25.0	25.0	25.0	25.0	25.0	25.0	25.0	25.0
Condensate	Power Plant Secondary Radiator "B"/650	7.0	7.0	7.0	7.0	7.0	7.0	7.0	7.0
Radiator Circuit	Power Plant Secondary Radiator "B"/650	13.0	13.0	13.0	13.0	13.0	13.0	13.0	13.0
Auxiliary Coolant	Power Plant Secondary Radiator "B"/650	4.5	4.5	4.5	4.5	4.5	4.5	4.5	4.5
Power Conditioning									
Transformers	Power Plant Secondary Radiator "B"/650	29.8	29.8	1.6	1.9	5.4	10.2	29.8	29.8
Frequency Converter	Power Plant Secondary Radiator "C"/325	11.0	11.0	11.0	11.0	11.0	11.0	11.0	11.0
Total, EGS Cooling System		175.4	175.4	87.7	90.9	106.0	128.8	175.4	175.4
III. Power Conditioning System									
Controls	Low Temp. Payload Radiator/325	0.1	0.1	0.1	0.1	0.1	0.1	0.1	0.1
Equipment									
Transmitter Power Supply	Low Temp. Payload Radiator/325	--	4.0	--	4.0	4.0	4.0	4.0	4.0
High Resolution Radar Power Supply	Low Temp. Payload Radiator/325	--	--	--	--	14.0	--	14.0	--
Mapping Radar Power Supply	Low Temp. Payload Radiator/325	--	--	--	--	1.6	1.6	1.6	1.6
Propulsion Power Supply	Low Temp. Payload Radiator/325	25.8	25.8	2.5	2.5	2.5	2.5	16.7	12.1
Frequency Converter	Low Temp. Payload Radiator/325	1.2	1.2	1.2	1.2	1.2	1.2	1.2	1.2
Total, PCS Cooling System		27.1	31.1	3.8	7.8	23.4	9.4	37.5	55.0
IV. Propulsion System									
Controls	Low Temp. Payload Radiator/325	0.1	0.1	0.1	0.1	0.1	0.1	0.1	0.1
Total, PS Cooling System		0.1	0.1	0.1	0.1	0.1	0.1	0.1	0.1
V. Spacecraft Equipment									
Scientific Sensors	Low Temp. Payload Radiator/325	0.2	0.2	0.2	0.2	0.2	0.2	0.2	0.2
Tracking, Telemetry, Command & Comm.	Low Temp. Payload Radiator/325	0.1	0.1	0.1	0.1	0.1	0.1	0.1	0.1
Communications (Deep Space)									
Klystron	High Temp. Payload Radiator/650	--	28.5	--	28.5	28.5	285.0	28.5	285.0
Electronics	Low Temp. Payload Radiator/325	--	3.8	--	3.8	3.8	3.8	3.8	3.8
Radar Altimeter	Low Temp. Payload Radiator/325	--	--	--	--	0.1	0.1	0.1	0.1
Wide Sweep Mapper									
Klystron	High Temp. Payload Radiator/650	--	--	--	--	12.0	12.0	12.0	12.0
Electronics	Low Temp. Payload Radiator/325	--	--	--	--	1.6	1.6	1.6	1.6
High Resolution Radar									
Klystron	High Temp. Payload Radiator/650	--	--	--	--	105.0	--	105.0	--
Electronics	Low Temp. Payload Radiator/325	--	--	--	--	14.0	--	14.0	--
Guidance & Controls									
Electronics	Low Temp. Payload Radiator/325	0.39	0.39	0.39	0.39	0.39	0.39	0.39	0.39
Inertial Units	Low Temp. Payload Radiator/325	0.10	0.10	0.10	0.10	0.10	0.10	0.10	0.10
Guidance & Controls (Cont'd)									
Planet Sensors	Low Temp. Payload Radiator/325	0.01	0.01	0.01	0.01	0.01	0.01	0.01	0.01
Coolant Circulation Pumps									
Lander No. 1	High Temp. Payload Radiator/650	0.35	0.35	0.35	0.35	0.35	0.35	0.35	0.35
Lander No. 2	High Temp. Payload Radiator/650	0.35	0.35	0.35	0.35	0.35	0.35	0.35	0.35
Low Temp. Radiation Circuit	Low Temp. Payload Radiator/325	4.5	4.5	4.5	4.5	4.5	4.5	4.5	4.5
High Temp. Radiation Circuit	High Temp. Payload Radiator/650	4.5	4.5	4.5	4.5	4.5	4.5	4.5	4.5
Total, SE Cooling System		10.5	42.8	10.5	42.8	175.5	313.0	178.2	313.0
VI. Total, PCS + PS + SE Cooling Systems		46.5	82.8	14.4	50.7	199.0	322.5	225.6	377.9
VII. Total Active Cooling Load		256.1	289.4	142.1	181.6	345.0	491.3	432.2	584.5

TABLE 8-6. ELECTRICAL LOADS REQUIREMENTS FOR THE 1 MWe THERMIONIC VEHICLE

Power Load Items	Electrical Service Requirements	Power Loads, KW							
		Phase							
		A	B	C	D	E	F	G	H
I. Reactor & Shield Assembly									
Controls	30 vdc, 3.6 KW	3.6	3.6	3.6	3.6	3.6	3.6	3.6	3.6
Circulation Pump Controls & Shield Coolant	120/208v, 3 φ, 100 cps, 0.2 KW	0.2	0.2	0.2	0.2	0.2	0.2	0.2	0.2
Subtotal, RSA		3.8	3.8	3.8	3.8	3.8	3.8	3.8	3.8
II. Electrical Generating Syst.									
Controls	30 vdc, 0.1 KW	0.1	0.1	0.1	0.1	0.1	0.1	0.1	0.1
Circulation Pumps									
Reactor Coolant	120/208v, 3 φ, 100 cps, 8.9 KW	8.9	8.9	8.9	8.9	8.9	8.9	8.9	8.9
Radiation Circuit	120/208v, 3 φ, 100 cps, 32.1 KW	32.1	32.1	32.1	32.1	32.1	32.1	32.1	32.1
Power Conditioning Equipment Losses									
Inverter	30 vdc, 76.7 KW	7.7	7.7	7.7	7.7	7.7	7.7	7.7	7.7
Frequency Converter	120/208v, 2000 cps, 69 KW	6.9	6.9	6.9	6.9	6.9	6.9	6.9	6.9
Subtotal, EGS		55.7	55.7	55.7	55.7	55.7	55.7	55.7	55.7
III. Power Conditioning Equipment*									
dc-dc Converters for Ion Engines Radar & Communications**	30 vdc, 1030 KW	98.7	103.0	35.5	39.3	38.4	58.4	79.2	94.2
Electric Propulsion PCE	6.6 Kvdc, 215 KW	21.5	21.5	2.4	2.4	2.4	2.4	14.2	13.0
Auxiliary Power Cond. Unit	6.6 Kvdc, 15.8 KW	1.6	1.6	1.6	1.6	1.6	1.6	1.6	1.6
Frequency Converter	120/208v, 2000 cps, 8.2 KW(e)	0.6	0.6	0.6	0.6	0.6	0.6	0.6	0.6
Subtotal PCE		122.4	126.1	40.1	43.9	43.0	63.0	95.6	109.4
IV. Propulsion System									
Controls	30 vdc, 1.0 KW	1.0	1.0	1.0	1.0	1.0	1.0	1.0	1.0
Propellant & Feed System	30 vdc, 1.0 KW	1.0	1.0	1.0	1.0	1.0	1.0	1.0	1.0
Ion Engines									
Beam Power	6.60 Kvdc, 754.0 KW	754.0	754.0	84.3	84.3	84.3	84.3	624.0	456.0
Accelerator Power	-6.60 Kvdc, 10.5 KW	10.5	10.5	1.17	1.17	1.17	1.17	7.85	6.3
Ion Source	20 vdc, 178.6 KW	178.6	178.6	19.7	19.7	19.7	19.7	148.0	108.0
Neutralizer	30 vdc, 4.75 KW	4.75	4.75	0.54	0.54	0.54	0.54	3.74	2.87
Subtotal Propulsion System		949.85	949.85	107.71	107.71	107.71	107.71	785.59	573.17
(I_{sp} = 7.54 x 10^3 sec at full power)									
V. Spacecraft Equipment									
Operational									
TT&C	28 vdc, 0.1 KW	0.1	0.1	0.1	0.1	0.1	0.1	0.1	0.1
Communications									
Klystron	20 K vdc, 376 KW	--	37.6	--	37.6	37.6	376.0	37.6	376.0
Electronics	28 vdc, 4 KW	--	4.0	--	4.0	4.0	4.0	4.0	4.0
Guidance & Controls									
Electronics	28 vdc, 0.45 KW	0.45	0.45	0.45	0.45	0.45	0.45	0.45	0.45
Inertial Units	26 v, 2 φ, 400 cps, 0.11 KW	0.11	0.11	0.11	0.11	0.11	0.11	0.11	0.11
Planet Sensors	26 v, 2 φ, 400 cps, 0.01 KW	0.01	0.01	0.01	0.01	0.01	0.01	0.01	0.01
Coolant Circulation Pumps									
Lander No. 1	120 vac, 100 cps, PF = 0.5, 0.5 KW	0.5	0.5	0.5	0.5	0.5	0.5	0.5	0.5
Lander No. 2	120 vac, 100 cps, PF = 0.5, 0.5 KW	0.5	0.5	0.5	0.5	0.5	0.5	0.5	0.5
Radiator Circuit - High Temperature	120 vac, 100 cps, PF = 0.5, 5.97 KW	5.97	5.97	5.97	5.97	5.97	5.97	5.97	5.97
Radiator Circuit - Low Temperature	120 vac, 100 cps, PF = 0.5, 0.63 KW	0.63	0.63	0.63	0.63	0.63	0.63	0.63	0.63
Payload									
Scientific Sensors and Radar Altimeter	28 vdc, 0.28 KW	0.28	0.28	0.28	0.28	0.28	0.28	0.28	0.28
Wide Sweep Mapper									
Klystron	20 vdc, 15.8 KW	--	--	--	--	15.8	15.8	15.8	15.8
Electronics	28 vdc, 0.2 KW	--	---	--	--	0.2	0.2	0.2	0.2
High-Res. Radar									
Klystron	20 Kvdc, 138.6 KW	--	--	--	--	138.6	--	138.6	--
Electronics	28 vdc, 1.4 KW	--	--	--	--	1.4	--	1.4	--
Subtotal Spacecraft Equipment		8.55	50.15	8.55	50.15	206.15	404.55	206.15	404.55
Distribution Losses		58.0	61.0	11.3	14.5	21.0	34.0	58.0	58.0
Total GEN Gross Output		1198.3	1246.6	227.16	275.76	437.36	668.76	1203.84	1204.6
Total EGS Net Output		1138.8	1187.1	167.66	216.26	377.86	609.26	1144.34	1145.1

*Semiconductor
**Units Nos. 1, 2, 3 in Figure 8-2.

TABLE 8-7. COOLING LOADS ESTIMATES FOR THE 1 MWe THERMIONIC VEHICLE

Heat Load Items	Radiator Loop/Maximum (°F)	Phase							
		A	B	C	D	E	F	G	H
I. Reactor & Shield Assembly									
Controls	Shield Coolant Radiator/650	3.5	3.5	3.5	3.5	3.5	3.5	3.5	3.5
Coolant Pump	Shield Coolant Radiator/650	0.43	0.43	0.43	0.43	0.43	0.43	0.43	0.43
Shield	Shield Coolant Radiator/650	45.0	45.0	45.0	45.0	45.0	45.0	45.0	45.0
Subtotal: RSA Cooling System		48.93	48.93	48.93	48.93	48.93	48.93	48.93	48.93
II. Electrical Generating System									
Controls	Power Cond. Radiator "C", "D" & "E"/325	0.1	0.1	0.1	0.1	0.1	0.1	0.1	0.1
EM Circulation Pumps									
Reactor Coolant	Shield Coolant Radiator/650	1.89	1.89	1.89	1.89	1.89	1.89	1.89	1.89
Radiator Circuit	Shield Coolant Radiator/650	6.8	6.8	6.8	6.8	6.8	6.8	6.8	6.8
Power Conditioning Equipment Inverter	Power Cond. Radiator "C", D, & E"/325	7.7	7.7	7.7	7.7	7.7	7.7	7.7	7.7
Frequency Converter	Power Cond. Radiator "C, D, & E"/325	6.9	6.9	6.9	6.9	6.9	6.9	6.9	6.9
Subtotal EGS Cooling System		23.39	23.39	23.39	23.39	23.39	23.39	23.39	23.39
III. Power Conditioning Equipment*									
dc-dc Converter for Ion Engines, Radar, and Communications	Power Conditioning Radiator "C, D, & E"/325	103.0	132.5	35.5	39.3	38.4	58.4	79.2	94.2
Electric Propulsion PCE	Low Temp. Payload Radiator "H"/325	21.0	21.0	2.4	2.4	2.4	2.4	14.2	13.0
Auxiliary Power Cond. Unit	Low Temp. Payload Radiator "H"/325	1.6	1.6	1.6	1.6	1.6	1.6	1.6	1.6
Frequency Converter	Low Temp. Payload Radiator "H"/325	0.6	0.6	0.6	0.6	0.6	0.6	0.6	0.6
Subtotal PCE Cooling System		126.2	155.7	40.1	43.9	43.0	63.0	95.6	109.4
IV. Propulsion System Controls	Low Temp. Payload Radiator "H"/325	1.0	1.0	1.0	1.0	1.0	1.0	1.0	1.0
Subtotal Propulsion System Cooling System		1.0	1.0	1.0	1.0	1.0	1.0	1.0	1.0
V. Spacecraft Equipment									
Operational TT&C	Low Temp. Payload Radiator "H"/325	0.1	0.1	0.1	0.1	0.1	0.1	0.1	0.1
Communications Klystron	High Temp. Payload Radiator "F&G"/650	--	28.2	--	28.2	28.2	282.0	28.2	282.0
Electronics	Low Temp. Payload Radiator "H"/325	--	3.0	--	3.0	3.0	3.0	3.0	3.0
Guidance & Controls Electronics	Low Temp. Payload Radiator "H"/325	0.11	0.11	0.11	0.11	0.11	0.11	0.11	0.11
Planet Sensors	Low Temp. Payload Radiator "H"/325	0.01	0.01	0.01	0.01	0.01	0.01	0.01	0.01
Coolant Circulation Pumps									
Lander 1	High Temp. Payload Radiator "F & G"/650	0.45	0.45	0.45	0.45	0.45	0.45	0.45	0.45
Lander 2	High Temp. Payload Radiator "F & G"/650	0.45	0.45	0.45	0.45	0.45	0.45	0.45	0.45
Radiator Circuit - High Temp.	High Temp. Payload Radiator "F & G"/650	5.21	5.21	5.21	5.21	5.21	5.21	5.21	5.21
Radiator Circuit - Low Temp.	Low Temp. Payload Radiator "H"/325	0.567	0.567	0.567	0.567	0.567	0.567	0.567	0.567
Payload									
Scientific Sensors & Radar									
Altimeter	Low Temp. Payload Radiator "H"/325	0.28	0.28	0.28	0.28	0.28	0.28	0.28	0.28
Wide Sweep Radar Mapper									
Klystron	High Temp. Payload Radiator "F & G"/650	--	--	--	--	11.8	11.8	11.8	11.8
Electronics	Low Temp. Payload Radiator "H"/325	--	---	--	--	0.2	0.2	0.2	0.2
High Resolution Radar									
Klystron	High Temp. Payload Radiator "F & G"/650	--	--	--	--	104.0	--	104.0	--
Electronics	Low Temp. Payload Radiator "H"/325	--	--	--	--	1.4	--	1.4	--
Subtotal: SE Cooling System		7.63	38.83	7.63	38.83	156.23	304.63	156.23	304.63
Total PS, PCS & SE Cooling Systems		134.83	195.23	48.73	83.73	200.23	368.63	252.23	415.03
Total Active Cooling Load		207.15	267.55	121.05	190.05	272.55	440.95	324.55	487.35

*Semiconductor

Phase Designation	
A	In-Flight Propulsion
B	Propulsion and Communication
C	Mid-Course Coast
D	Mid-Course Coast and Communication
E	Terminal Coast and Radar
F	Terminal Coast, Radar and Communication
G	Terminal Orbit Correction, and Radar
H	Terminal Orbit Correction, Radar, and Communication

The launch, boost, and start-up phases are treated separately as a special case. Phase A, in-flight propulsion at full power, would apply during the initial and near-terminal phases of the heliocentric thrusting with intermittent periods of Phase B, earth-to-spacecraft communications. The communication power level in the early and intermediate flight stages would be lower than that required in the deep space flight stages of the mission. The power required for communications in Phase B would be obtained without reducing propulsion power. During mid-course (Phases C and D) the powerplant will be cut back so that only spacecraft attitude control by gimballed and switched electric engine modules, mid-course communication, and other necessary housekeeping load power requirements are provided. The actual attitude control power required will be dependent on the number of engines required in pitch, yaw, and roll to correct the disturbance of momentum unbalances. Otherwise, the power is utilized for propulsion under partial power. Phases E and F are non-propulsive phases with power level determined by attitude control plus operational payload radar with intermittent simultaneous deep space transmissions. Phases G and H are similar to Phases E and F, with the exception that a terminal maneuver or orbit correction requiring propulsive power is necessary. The thermal power profiles were estimated using the following assumptions:

1. All low voltage electronic power is completely dissipated through the low temperature radiators.
2. Engine temperature control is by passive heat rejection.

3. Klystron transmitter dissipation is proportioned as follows: 74% at high voltage (20 kv) dissipated, 25% RF transmitted and 1.0% low voltage (28 v) dissipated. The transmitter operating temperature was extrapolated to 650°F.

4. Transformer efficiencies were assumed to be 99% with an additonal 1% loss allowed for connections and breakers associated with the transformer module.

5. A 3-phase, delta-wye, fullwave bridge rectifier circuit was assumed for high voltage a-c to d-c conversion. The rectifiers were assumed to be avalanche silicon rectifier strings with a 1000 v avalanche voltage and a 1 v forward voltage drop per rectifier.

6. A three-phase, delta-double wye with interphase transformer rectifier circuit was assumed for low voltage a-c to d-c conversion with an efficiency of 94.5%.

7. Static frequency converter efficiency was assumed at 93%.

8. Static d-c to d-c converter efficiency is approximately 90% for an in-core thermionic generator source voltage level at 30 v.

9. A-c powerplant and coolant pump efficiencies are as listed in the GE document 63SD886 Sections 5 and 6.

10. Auxiliary power is provided by an H_2/O_2 internal combustion engine for the turbogenerator system and an H_2/O_2 Bacon-type fuel cell for the thermionic generator system. The heat rejection for the engine-alternator is assumed as 400°F. The heat load is handled by the high temperature payload radiator during the boost/reactor start-up phase. The fuel cell heat rejection temperature is assumed as 200°F and was allocated to the in-core thermionic spacecraft low temperature payload radiator. The engine-alternator and fuel cell electrical conversion efficiencies were taken to be 40% and 50%, respectively.

11. Liquid metal electromagnetic (EM) pumps for the power conversion loop are a-c induction type with 15% pump efficiency. Pump power factor is assumed at 0.5 lagging.

12. The weights associated with the electrical systems for both thermionic and turboelectric conversion are tabulated in Table 8-8.

C. ELECTRICAL SYSTEM COMPONENTS

Parametric design data on liquid metal cooled transformers have been generated for use in the nuclear turboelectric powerplant studies. Curves were prepared to show

TABLE 8-8. SUMMARY OF WEIGHT AND DISSIPATION OF TURBOGENERATOR AND THERMIONIC SYSTEMS

Thermionic System	Weight (lb)	Dissipation (KW)
Bus System	1000	61.5
Forward Power Conditioning Equipment (semiconductor)		
Propulsion PCE Module No. 1	1850	
Propulsion and Auxiliary Power PCE Module No. 2	2000	
Communications, Radar and Propulsion PCE Module No. 3	3210	
	7060	132.5
Rear Power Conditioning Equipment		
Engine Power Supplies	775	
Aux. Power Supply	90	
Communications and Radar Power Control Unit	10	
	875	
TOTAL	9935	

Turboelectric System	Weight (lb)	Dissipation (KW)
Bus System	244	14.6
Forward Power Conditioning Equipment		
Modules "A", "B", and "C"	830	
Module "D"	500	
	1330	29.8
Rear Power Conditioning Equipment		
Engine Power Supplies	300	
Communications Supply	100	
Radar Supplies	50	
	450	
TOTAL PCE	2024	

the variation of weight with frequency, coolant inlet temperature and efficiency. The transformers are constructed using 3-phase E-cores with a delta connected primary winding and wye connected secondaries. Assuming that the actual load is an ion engine or thruster, the low voltage output supplies power for the heaters, and the high voltage output, when rectified, supplies power to the ionizer and accelerator electrodes.

The inherent short circuit characteristics of the load present severe high voltage transient problems to the main supply transformer and its associated circuitry. Consequently, the following criteria are important:

1. The physical construction of the high voltage winding must be such as to distribute the transient electrostatic field (produced by steep-wave front transient voltages) as uniformly as possible to prevent insulation breakdown.
2. The insulation and impregnation system must keep the dielectric stress levels at a low enough value to prevent insulation deterioration from corona.
3. Interwinding capacitance must be minimized to prevent the transient voltages in the secondary windings from being reflected into the primary circuitry and causing component damage.

The results of these parametric calculations are presented in Figures 8-5 through 8-8, and represent a cross plot of the data presented in the Third and Fourth Quarterly Report, 64SD700. (Also, refer to this report for a discussion of the design approach and general assumptions.) The weights estimated by the computer program indicated that the input voltage has a negligible effect within the range of 208 to 1732 volts line-to-line. Thus, the curves, as presented, are applicable throughout this range. Also, the estimated transformer weight varies almost linearly with power and the 500 KVA data can be scaled accordingly.

The high voltage rectifier circuit will rectify the 3-phase output of the transformer, which is mounted at the generator, to provide about 180 KVA of power at 6 KV to the ion engines. Although this exact power and voltage level may not exactly match the specific requirements for the engines, the power and voltage are in the general range that will be required.

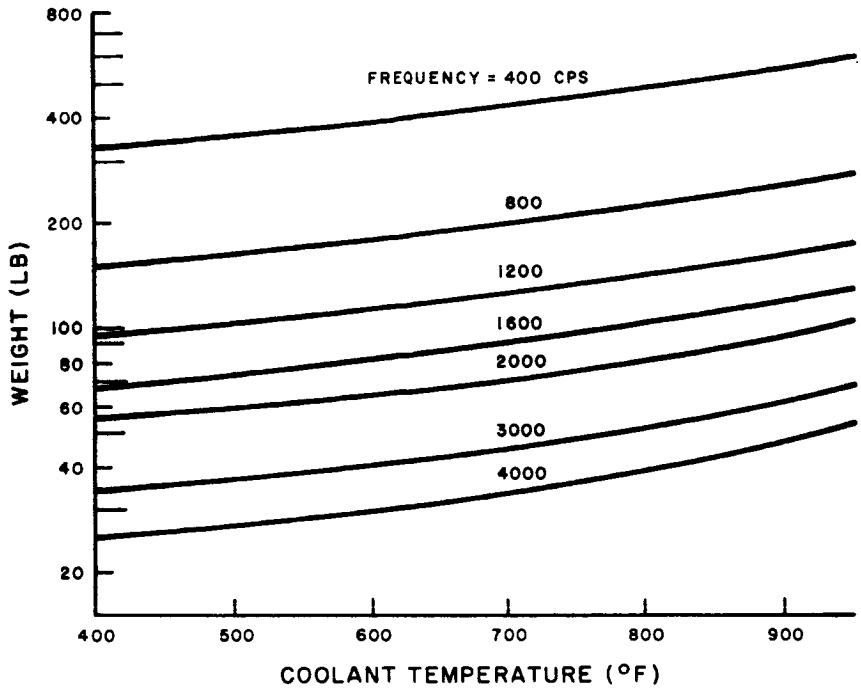

Figure 8-5. Weight of 500 KVA, 98.0% Efficient Transformer as a Function of Frequency and Coolant Temperature

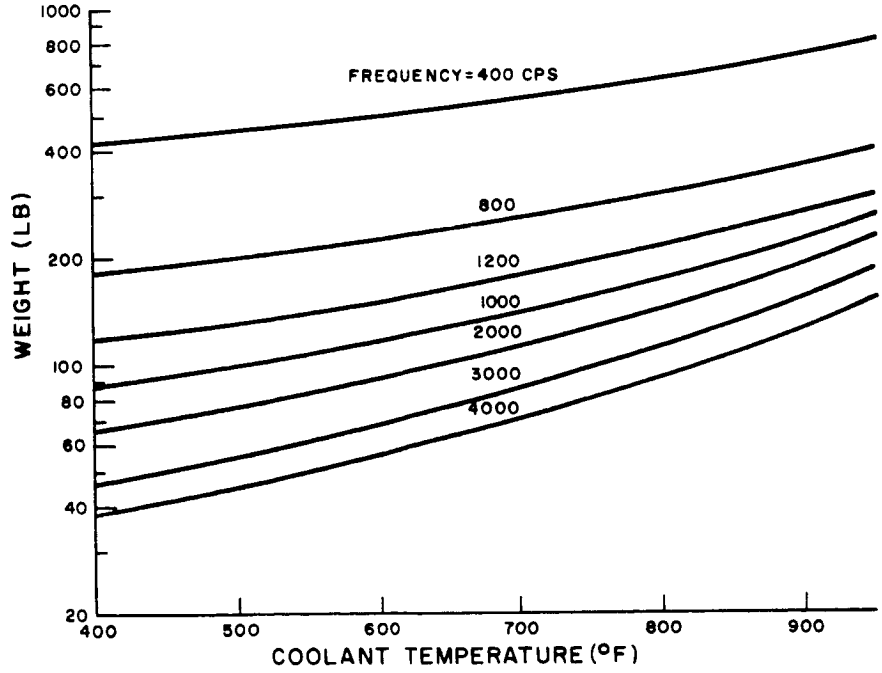

Figure 8-6. Weight of 500 KVA, 98.5% Efficient Transformer as a Function of Frequency and Coolant Temperature

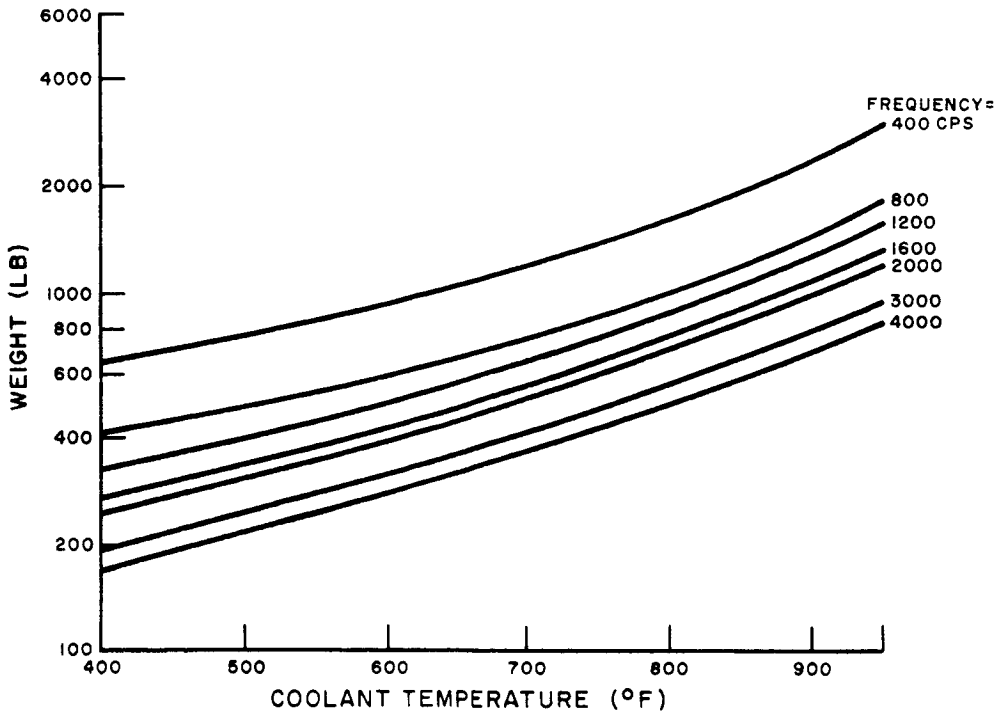

Figure 8-7. Weight of 500 KVA, 99.0% Efficient Transformer as a Function of Frequency and Coolant Temperature

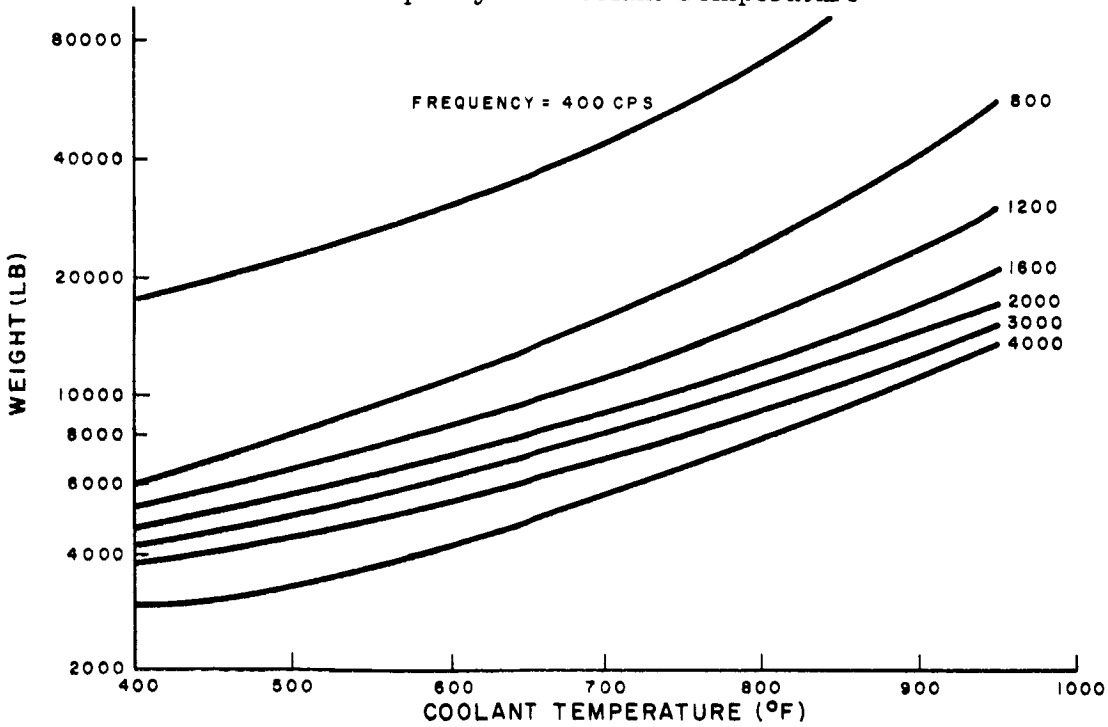

Figure 8-8. Weight of 500 KVA, 99.5% Efficient Transformer as a Function of Frequency and Coolant Temperature

The simplified rectifier circuit for a 3-phase input is the 3-phase, full-wave bridge circuit shown in Figure 8-9. This cicuit provides the most efficient use of rectifiers and transformers in this voltage range. A comparison of the many rectifier circuit discussed in the literature confirms this conclusion.

Unfortunately there are several application problems with this circuit (and most others). They can be summarixed as:

- Harmonic Distortion Induced in the A-C Source
- Radio Noise
- Reverse Recovery Time of Rectifiers
- Short Circuit Capacity.

A brief discussion of these was presented in the Third and Fourth Quarterly Report.

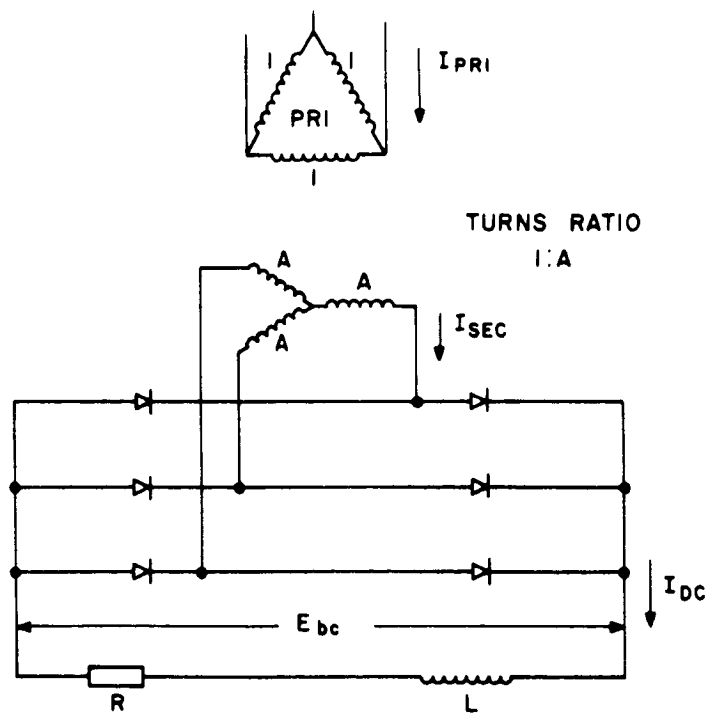

Figure 8-9. Basic Rectifier Circuit

As an example of the rectifier size and efficiency, a sample unit has been compiled.

- Sample Design

  Minimum Rectifier Repetitive Reverse Voltage = 1.05 x 6000 = 6300 volts

  For safety during generating system transients use twice minimum rating or 12,600 volts.

  Use 1N3913 as basic rectifier which is rated:

  Forward Current (I_F) = 33 amps at 100°C case

  Reverse Recovery Time (T_{RR}) = 0.2 microsecond

  Forward Voltage (V_F) = 1.0 volt max @ 150°C, 35 amps

  Peak Reverse Voltage (PRV) = 400 volts

  Reverse Current (I_R) = 10 ma max

Since 400 volts rms is the maximum available, 12,600/400 = 31.5 or 32 rectifiers will be required in each leg of the rectifier bridge circuit.

Each rectifier must be shunted with an R-C network for steady state voltage division and transient voltage division. These additional parallel components will result in a combined reverse leakage current of 35 ma.

The efficiency of the rectifier is calculated as follows:

Forward Losses = (P_R) = V_F x no. of series cells x avg current

= 2 x 1.0 x 64 x 30 = 1920 watts

Reverse Losses = Leakage current x no. of stacks x avg voltage

= 0.035 x 4 x 6000 = 840 watts

Total Losses = 1920 + 840 = 2760 watts

$$\text{Efficiency} = \frac{\text{output}}{\text{input}} = \frac{180,000}{182,760} = 98.5\%$$

The total volume of the rectifier stacks with the transient suppression network will be about 1200 cubic inches (24 by 8 by 6-1/2 inches). The size does not include the envelope, cooling components, or input-output connection. It appears that oil cooling might represent the most practical approach to cooling the individual rectifier while still mainteaining insulation to ground. An hermetically sealed assembly would be required in this event and its size would probably be about 4 inches larger in each dimension for a volume of about 3500 cu in. The maximum cooling medium temperature would be about 125°C.

- Future Needs

  1. One obvious need to reduce the size of the rectifier assembly is to have fast-recovery rectifiers with higher PRV. Discussion with GE, Hughes, and Westinghouse personnel disclosed that major problems exist in building units with higher than 400 volts PRV while still maintaining the fast recovery characteristics. This is because the narrow junction regions necessary for fast recovery do not provide high puncture levels in the silicon.

  2. The addition of the controlled avalanche feature to the fast recovery units would provide an added safety factor and perhaps reduce the total number of cells required in series.

9. ELECTRIC THRUSTORS

Electric thruster designs will be strongly influenced by the requirement for propulsion periods of one to four years. The design of the engines may be substantially different from those of the engines which have been operated in the laboratory for shorter periods of time.

The mission requirements for the unmanned interplanetary scientific probes include specific impulses for the electric thrustors in the general range of 2500 to 15,000 seconds. This range is narrowed down to between 2700 and 6200 seconds for mission attainable with 30 lb/KWe powerplants having two-year limited powerplant life. At the beginning of this program, the specific impulse requirements had been estimated in the range of 5000 to 20,000 seconds, which led to exclusion of arc-jet type engines from consideration. The entire offering of electric thrustor types will have to be reexamined as a result of this revised estimate of thrustor requirements, and as more data on the newer arc-jet concepts become available.

The prominent classifications of electric propulsion devices are electro-thermal, electro-magnetic, and electrostatic. The resistojet and arc-jet are electro-thermal types; the Hall current accelerator, crossed-field accelerator, pulsed-plasma gun, traveling-wave accelerator, radial-pinch engine and Giannina engine are electromagnetic types; and the ion engine and colloidal engine are electro-static types.

The arc-jet uses electrical resistance heating of the propellant, followed by expansion through a nozzle. As such, the specific impulse is limited by the containment vessel materials temperature limitation. Using hydrogen as a propellant, specific impulses up to 2000 seconds can be achieved at less than 50 percent efficiency. In a pure arc-jet the efficiency is limited by chemical dissociation of the hydrogen, which establishes the trends rather than absolute performance level. (See Figure 9-1.)

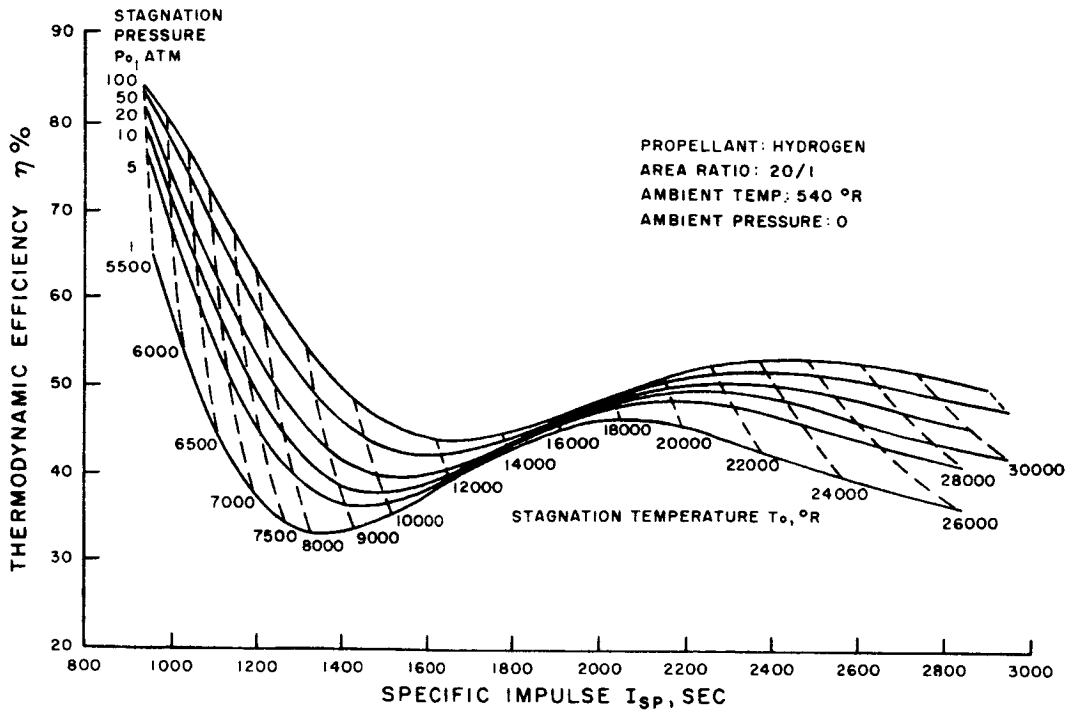

Figure 9-1. Arc-Jet Engine Thermodynamic Efficiency

In a modified version of the arc-jet engine presently under study by Giannini[1], magnetic field forces generated by the large current flow through the propellant are sufficiently large to provide the acceleration of propellant, thereby minimizing the requirement of nozzle expansion. (See Figure 9-2.) The jet velocities are not limited by containment vessel temperatures or by hydrogen disassociation. Test data from Giannini shows efficiencies of 55 percent at a 1000 second specific impulse.[2] Although the efficiency is not limited by chemical dissociation, it is affected by this factor, and to circumvent losses, non-dissociating propellants such as lithium can be used. Preliminary tests performed at EOS using lithium, have shown promising potential for this type of thrustor. The mission study results could be altered if these high

(1) AIAA paper #64-524, "Electric Propulsion in 1964 — A Status Review", by E. Stuhlinger, NASA Huntsville, presented at 1st AIAA Annual Meeting, June 29 - July 2, 1964.

(2) "Thirty-Kilowatt Arc Jet Thrustor Research," Document No. APL-TDR-64-58, March 1964.

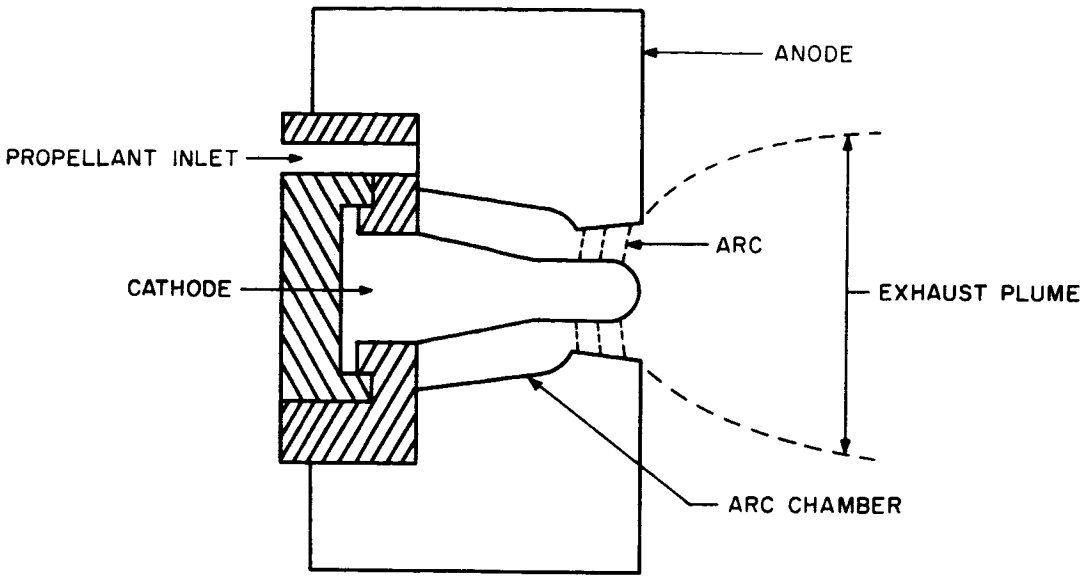

Figure 9-2. Thermo-Ionic Accelerator

efficiencies at low Isp can be obtained in a prototype engine. The tendency would be to reduce trip time by operating at higher thrust weight ratios which correspond to lower specific impulses

A number of plasma engines are in the early stages of research and offer the possibility of high efficiency operation. However, it is too early to factor these engines into mission studies. Current estimates of efficiencies tend to be confined to below 40 percent.

The electric thrustor that has demonstrated the best performance in the high specific impulse range is the electron bombardment device (Kaufman engine), a particle accelerator. The operating life of the entire engine is not yet proven. The cathode appears to be the most critical item. In August 1964, a cathode in operation at Lewis

Research Center had accumulated 4000 hours, and was still operating. Performance[3] data from the experimental program is plotted in Figure 9-3. The engine has demonstrated the highest efficiency and the lowest specific weight of any engine now under development. However, it is not adequate for performing the short duration missions investigated in this study requiring specific impulses below 5000 seconds.

The bombardment engine makes use of electron collisions with the gas in a magnetron chamber to generate a substantially ionized plasma. The crossed magnetic and electric fields in the magnetron chamber ensure long electron path lengths, and reasonably efficient utilization of the arc power. The electric field between the accel electrode and the virtual anode (formed at the edge of the plasma in the chamber) extracts the ions from the plasma and repels the electrons back into it. The necessary decelerating field, to adjust the final energy and trap neutralizing electrons, is achieved by the formation of another virtual anode surface (at neutralizer potential) in the emergent high velocity stream. The ion generation process is relatively insensitive to current density, and long life can be compatible with the results experimentally observed in the laboratory.

Contact-ionization-type particle accelerators are also under active development. However, the low efficiency of this engine[3], which is shown in Figure 9-3, is due to the ion formation loss. The electrical efficiency of this type engine could be improved significantly if the cathode heat were provided thermally rather than by an electrical resistance heater [4]. The thermal heat source could be the reactor coolant possibly boosted to higher temperature by means of a heat pump. Feasibility of incorporating this feature into the thrustor design has not been examined.

The contact engine makes use of the surface ionization of cesium on a clean refractory metal surface to generate a very large fraction of ionized propellant. The ions are

(3) Technical Note D-2172, "Status of Electrostatic Thrustors for Space Propulsion," by W.R. Mickelsen and H.R. Kaufman, NASA Lewis.

(4) IAS Paper 62-74, "Comparative Performance of Electrostatic Rocket Engines," W.R. Mickelsen, 1962.

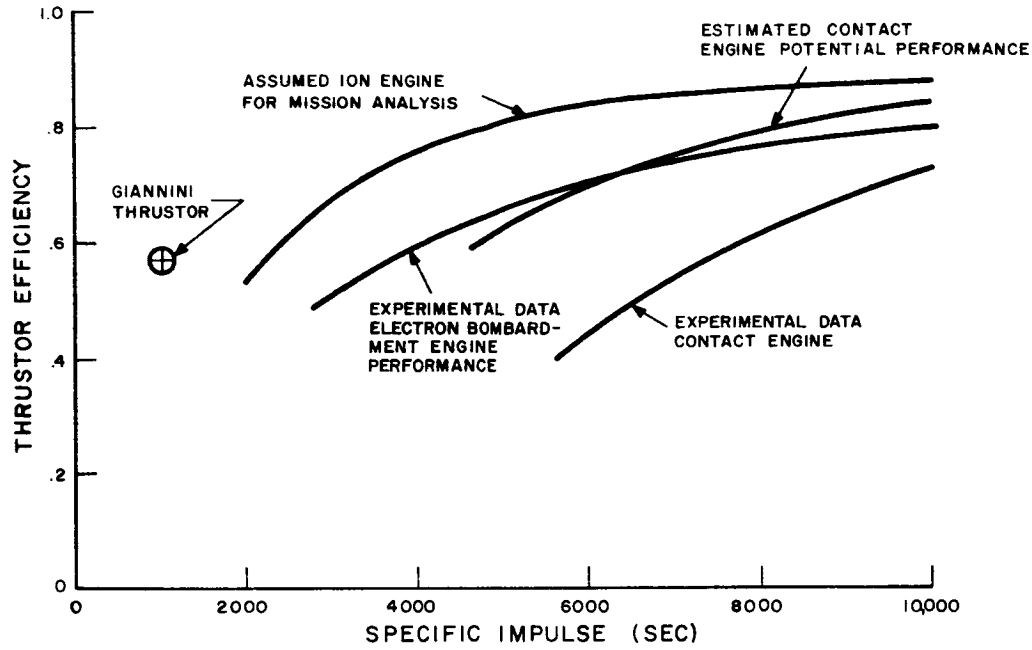

Figure 9-3. Efficiency of Candidate Thrustors

extracted from the emitter surface by a large electric field, induced by the accel electrode, and brought to their final energy as they pass through the decel electrode. Electrons are mixed into the beam, at this point, and the high velocity neutral plasma leaves the engine. Well engineered engines of this type have operated for only a few hundred hours before failure. The current densities involved in these tests are generally too high to be compatible with the long-life goals, unless a breakthrough in sintered tungsten technology (non-sintering submicron structures) can be achieved. The low current density enforced in the analysis results in rather poor engine efficiency.

Performance characteristics for both the contact ionization engine and the bombardment engine were presented in the second quarterly report. Mission studies and the designs prepared under this contract assumed an ion engine frontal area of 170 ft^2/kw and a specific mass of 1.2 lb/kw. Thrustor efficiency was determined by assuming a propellant utilization efficiency of 91 percent and an ion generation loss of 188 EV/ion.

This thrustor efficiency is compared with the experimental data on contact on electron bombardment engines in Figure 9-3. Note that the assumed efficiencies require an advance in the state-of-the-art over present experimental data.

Errata Sheet for "Research on Spacecraft and Powerplant Integration Problems" (Third and Fourth Quarterly Reports) - GE Document No. 64SD700, Contract No. NAS3-2533.

- Change Figure 4-14, "Transmissibility for m_1, Station 557" on page 4-19 to the following figure:

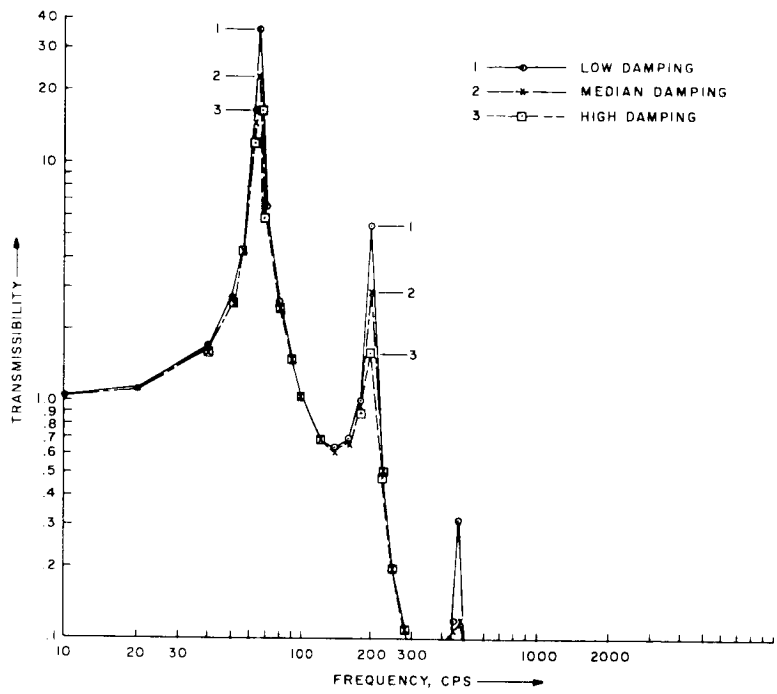

Figure 4-14. Transmissibility for m_1, Station 557

- Change equation in center of page 4-34 from:

$$t_a = K\ \alpha \left(\frac{A_v\ \tau}{-\ln P} \right)^{0.249}$$

to:

$$t_a = K \left(\alpha \frac{A_v\ \tau}{-\ln P} \right)^{0.249}$$

- Change Figure 4-26, "Effect of α , τ and P on Radiator Weight" on page 4-35 to the following figure.

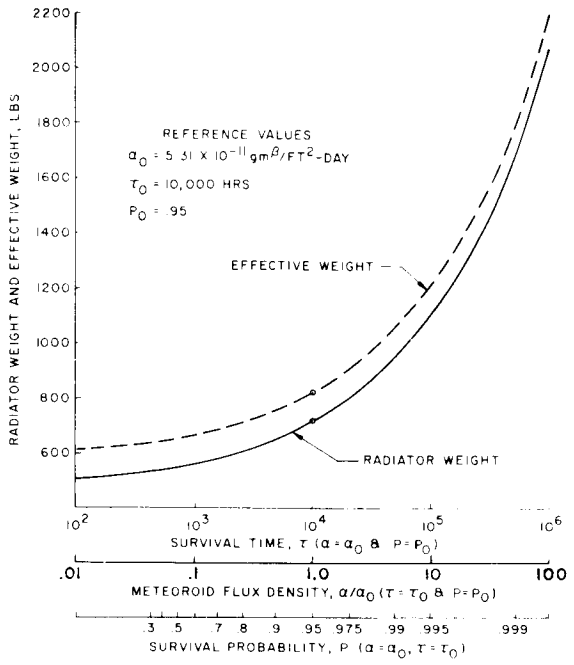

Figure 4-26. Effect of α , τ and P on Radiator Weight